SYSTEMS CONTROL, INC. (Vt)
1801 Page Mill Road
Palo Alto, California 94304

Telex: 348433

Telephone:
(415) 494-1165

NASA CONTRACTOR REPORT 158948

FLIGHT TEST DESIGN FOR CH-47 PARAMETER IDENTIFICATION

W.E. HALL, JR.
J. VINCENT

SYSTEMS CONTROL, INC. (VT)
PALO ALTO, CALIFORNIA 94304

CONTRACT NAS1 14010
DECEMBER 1978

TABLE OF CONTENTS

TABLE OF CONTENTS (Concluded)

LIST OF ILLUSTRATIONS

LIST OF ILLUSTRATIONS (Continued)

LIST OF ILLUSTRATIONS (Concluded)

LIST OF TABLES

LIST OF TABLES (Continued)

LIST OF TABLES (Concluded)

NOMENCLATURE

Symbol	
$a_{1_{MR}}$	main (fore) rotor fore-and-aft flapping displacement, positive down aft with respect to vertical shaft, rad
$a_{1_{TR}}$	tail (aft) rotor fore-and-aft flapping displacement, positive down aft with respect to vertical shaft, rad
A_c	matrix associated with state variable description of stability augmentation system
A_x, A_y, A_z	acceleration in the body x-axis, y-axis, and z-axis, respectively, m/sec^2
$b_{1_{MR}}$	main (fore) rotor lateral flapping displacement, positive down right with respect to vertical shaft, rad
$b_{1_{TR}}$	tail (aft) rotor lateral flapping displacement, positive down left with respect to vertical shaft, rad
B	control matrix used in second order matrix equation
B_c	matrix associated with state variable description of stability augmentation system
D	(1) damping matrix used in second order matrix differential equation (2) matrix associated with control inputs in measurement equation
F	stability derivative matrix for state model
F_{ij}	partitioned stability derivative matrix
F_c, F_M	matrix of instrumentation lags
F_{QS}	quasi-static stability derivative matrix derived from 10 degree-of-freedom C-81 linear derivative model
F_{C-81}	stability derivative matrix obtained from non-linear C-81 program

Symbol	
G	control derivative matrix for state model
G_i	partitioned control derivative matrix
G_1'	partitioned control derivative matrix corrected to eliminate spike anomaly occurring in C-81 (see Eq. 2.12)
G_{QS}	quasi-static control derivative matrix derived from 10 degree-of-freedom C-81 linear derivative model
G_{C-81}	control derivative matrix obtained from nonlinear C-81 program
g	acceleration due to gravity, m/sec^2
H	matrix associated with state variables in measurement equation
H_c	matrix associated with stability augmentation system equal to the identity matrix
h, h_p	altitude, m
K	stiffness matrix used in second order differential equation
K_c	gain matrix used in state variable description of stability augmentation system
K_p, K_q, K_r	roll, pitch, and yaw SAS feedback gains, respectively, m/rad/sec
K_{rp}	roll into yaw SAS feedback gain, m/rad/sec
K_v	sideslip SAS feedback gain, 1/sec
L_p, L_r	normalized rolling moment stability derivative with roll rate and yaw rate, respectively, 1/sec
L_v	normalized rolling moment stability derivative with lateral velocity, rad/(sec-m)
$L_{\delta LAT}$, $L_{\delta RUD}$	normalized rolling moment control derivatives with lateral cyclic and rudder pedal, respectively, rad/(sec^2-m)
ℓ	scale factor length used in Dryden wind gust spectrum, m

Symbol	
M	mass matrix used in second order differential equation
M_u, M_w	normalized pitching moment stability derivatives with longitudinal and vertical velocity, respectively (rad/(sec-m)
M_q	normalized pitching moment stability derivative with pitch rate, 1/sec
$M_{\delta LONG}$, $M_{\delta COLL}$	normalized pitching moment control derivates with differential collective and ganged collective inputs, respectively, rad/(sec^2-m)
N_p, N_r	normalized yawing moment stability derivates with roll rate and yaw rate, respectively, 1/sec
$N_{\delta LAT}$, $N_{\delta RUD}$	normalized yawing moment control derivatives with lateral cyclic and rudder pedal inputs, respectively, rad/(sec^2-m)
p, q, r	vehicle angular velocity about body x-axis, y-axis, and z-axis, respectively, rad/sec
R	rotor blade radius, m
s	Laplace transform operator
T_M, T_C	matrix of scale factors used in instrumentation modeling for the measurements and controls, respectively
t	time, sec
u, v, w	perturbation velocity components along body x-axis, y-axis, and z-axis, respectively, m/sec
u	(2) control input vector
u_o, w_o	trim velocity of the vehicle along body x-axis and z-axis, respectively, m/sec
u_g	longitudinal gust velocity, m/sec
u_m	control vector for instrumentation lags

Symbol	
V	vehicle airspeed, m/sec
V_o	vehicle trim airspeed, m/sec
v_Z	velocity component in inertial axis system, m/sec
$v_1, v_2, \ldots v_8$	state variables associated with the stability augmentation system
X	vector of independent variable appearing in second order differential equation
X_q	normalized X-force stability derivative with pitch rate, m/sec/rad
X_u, X_w	normalized X-force stability derivatives with longitudinal and vertical velocity, respectively, 1/sec
$X_{\delta LONG}$, $X_{\delta COLL}$	normalized X-force control derivatives with differential collective and ganged collective inputs, respectively, $m/sec^2/m$
x, y, z	orthogonal coordinates of distance in body-axis form, m
x	(2) state vector
x_1, x_2	partitioned state vector of fuselage and rotor variables, respectively
Y_p, Y_r	normalized Y-force stability derivatives with roll rate and yaw rate, respectively, m/sec/rad
Y_v	normalized Y-force stability derivative with lateral velocity, 1/sec
$Y_{\delta LAT}$, $y_{\delta LONG}$	normalized Y-force control derivatives with lateral cyclic and rudder pedals, respectively, $m/sec^2/m$
y_M	state vector for measurement lags
$Z_{B_{1S}}$	normalized Z-force control derivative with longitudinal cyclic, $m/sec^2/deg$

Symbol	
Z_q	normalized Z-force stability derivative with pitch rate, m/sec/rad
Z_u, Z_w	normalized Z-force stability derivatives with longitudinal and vertical velocity, respectively, 1/sec
$Z_{\delta LONG}$, $Z_{\delta COLL}$	normalized Z-force control derivatives with differential collective and ganged collective inputs, respectively, $m/sec^2/m$
Δ	increment
δ_{LONG}, δ_{COLL}	longitudinal (differential collective) positive forward stick and collective (ganged collective) positive up controls, respectively,cm
δ_{LAT}, δ_{RUD}	lateral cyclic, positive right stick and positive right rudder pedal (differential cyclic) controls, respectively,cm
$\zeta(t)$	white noise used in time domain version of Dryden gust model
θ, ϕ, ψ	pitch, roll, and yaw Euler angles, rad
θ_o	trim pitch angle, rad
σ_u, σ_v, σ_w	standard deviations of longitudinal, lateral, and vertical wind gust (also RMS, root mean square), respectively, m/sec
ϕ_u, ϕ_v, ϕ_w	longitudinal, lateral, and vertical Dryden power spectrum, respectively
Ω	rotor rotational speed, rad/sec
ω	frequency, rad/sec
ω_o	Dryden model cutoff frequency, rad/sec
ω_1, ω_2	frequencies of control input design, rad/sec

Subscript	
MR	main (fore) rotor
TR	tail (aft) rotor

Subscript

QS	quasi-static
C-81	*C-81 nonlinear computer program*

Superscript

$(\dot{})$	time derivative
$(\,)'$	primed quantity represents combined aerodynamic stability derivative and SAS contribution
$(\,)^T$	matrix or vector transpose
$(\,)^{-1}$	matrix inverse

Abbreviation

CPU	central processor unit
DOF	degrees of freedom
FPM	feet per minute
LRC	Langley Research Center
PADS	piloted aircraft data system
RAGS	research aircraft ground station data reduction system
SAS	stability augmentation system
SCIDNT	Systems Control, Inc. maximum likelihood identification program
TAGS	tactical aircraft guidance system
VALT	VTOL approach and landing technology program
VTOL	vertical takeoff and landing

I. SUMMARY AND INTRODUCTION

1.1 SUMMARY

The VTOL Approach and Landing Technology (VALT) program is a significant experimental research program aimed at establishing a data base for rotorcraft operation in a terminal area environment. The work described in this report was undertaken to determine helicopter math models suitable for analyzing maneuvers along a VTOL trajectory and to apply these math models to determine the flight test procedures of greatest effectiveness in establishing helicopter dynamic characteristics in this mode of operation. As the principal result of this investigation, a flight test specification is presented for the CH-47 VALT aircraft operating along the specified VTOL trajectory of the VALT program.

Simulation mathematical models are an integral part of the process that led to the recommended flight test specification. These models are used to evaluate possible error sources and to validate input design recommendations. Two CH-47 simulations were used for this study: a simulation based on CH-47 linear derivative models reported in Ref. 1 and the C-81 Rotorcraft Flight Simulation Program Ref. 5 (AGAJARMY Version). The instrumentation error models and LRC data recording system error contributions were simulated as in Ref. 3.

The principal results of this study are summarized as follows:

(1) Specification of flight test procedure for parameter identification of the CH-47 VALT Research Aircraft along a VTOL trajectory representative of VALT program requirements. This specification includes requirements for:

- Test points

- Control input shapes
- Stability augmentation system gains
- Maximum wind gust intensities for acceptable accuracy

(2) Investigation and determination of the influence on derivative identification accuracy of:

- The CH-47 force-moment characteristics along a VTOL trajectory, linear model representation, rotor degrees of freedom and SAS characteristics
- The CH-47 VALT Research Aircraft instrumentation and the LRC data recording system
- Control input design and procedures

1.2 INTRODUCTION

1.2.1 VALT Program Overview

The NASA Langley Research Center (LRC) VTOL Approach and Landing Technology (VALT) Program encompasses requirements analysis, design studies, systems development, ground simulation and flight validation of VTOL aircraft, subsystems and technology developments. The VALT research aircraft, a CH-47 tandem-rotor medium-transport helicopter, is used to provide the necessary system design evaluations and flight test validation of fully integrated system developments. A photograph of the LRC VALT CH-47 Research Aircraft is shown in Figure 1.1.

One VALT system development of significance is associated with the control system design for approach and landing conditions. Such control design is dependent on a model of the vehicle which can be used for specification of gains to improve vehicle handling qualities, stability, or overall integration with the guidance systems. To achieve such a model, the technology of system identification is to be applied to VALT CH-47 flight test data.

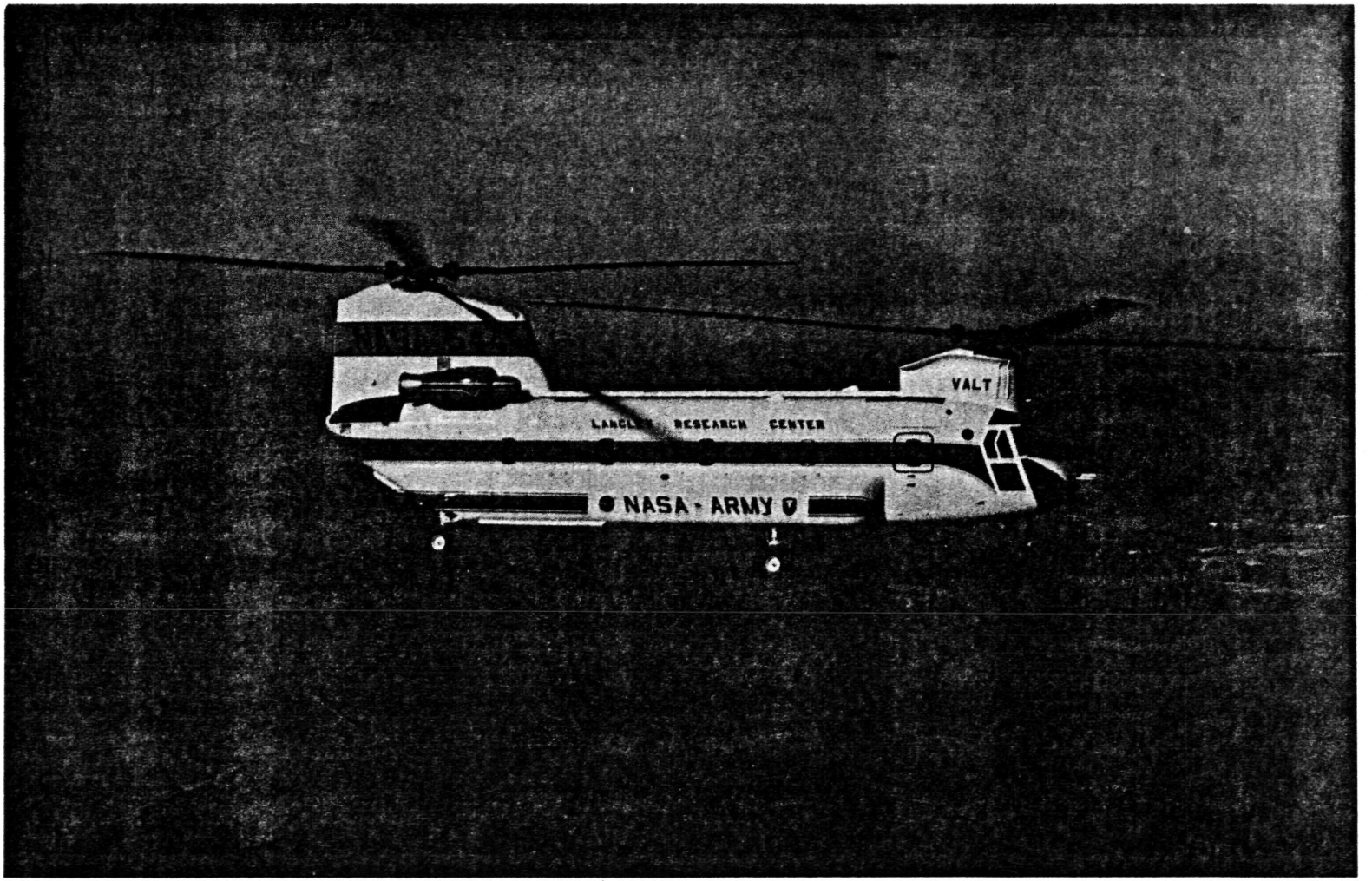

Figure 1.1 The LRC CH-47 VALT Research Aircraft

1.2.2 Study Overview

Purpose. The purpose of this investigation is to produce a flight test specification for the LRC CH-47 VALT Research Aircraft for parameter identification along the VTOL trajectory of the VALT program. In meeting this objective, specific areas of investigation are addressed in this report, which include:

(1) Selection of a nonlinear simulation program of the CH-47 and sufficient test points along the specified VTOL trajectory;

(2) Selection of an appropriate linear model representation of the CH-47 along the VTOL trajectory (e.g. test points requirements);

(3) Analysis of control input designs for parameter identification, and consideration as to the feasibility of using the CH-47 production stability augmentation system.

Scope and Limitations. The results presented in this report represent a rotorcraft parameter identification simulation study, which includes a systematic investigation of sources contributing to error in parameter identification. The results include the instrumentation error methods of Ref. 3. These results contribute to the VALT program objectives by providing the necessary analysis leading to a flight test specification for accurate CH-47 parameter identification. The CH-47 flight test specification resulting from this investigation is specifically designed for extracting the stability and control coefficients necessary for the VALT program control system design objectives.

Parameter identification accuracy is related to the quality of the control input design specification, which is dependent on the fidelity of the mathematical model used for the synthesis. Several factors influence the mathematical model selection:

(1) Degrees of freedom

(2) Significance of coupling between degrees of freedom

(3) Adequacy of a linear vehicle representation (and a nonlinear model representation).

These considerations are particularly important for rotorcraft because of their characteristic high order models (rotor and fuselage), inherent coupling between fuselage longitudinal and lateral modes in some vehicles, and the uncertain effects of aerodynamic nonlinearities under some flight conditions. The attention which must be given to each of these factors depends most importantly on the particular rotorcraft, its rotor type and its stability augmentation system. For the VALT aircraft and the objectives of the VALT study, a linear model is specified. The extent of this effort includes the following:

(1) Determine an adequate linear model approximation to the CH-47 vehicle equations of motion (based on nonlinear simulation evaluation).

(2) Design inputs for these linear models (as well as specific test points to be tested).

(3) Evaluate the anticipated accuracy obtainable from the designed inputs and specify the post-flight data processing requirements necessary to account for errors in the assumed input design model.

Approach. The technical approach is graphically outlined in Figure 1.2, and a summary of each element of the figure is discussed below. The following discussion summarizes the technical approach and the rationale leading to the procedure followed.

The CH-47 nonlinear simulation used in this analysis (indicated in Figure 1.2) is the AGAJARMY version (1975) of the C-81 Rotorcraft Flight Simulation (Ref. 5) computer program developed by Bell Helicopter Co., Fort Worth, Texas, under direction of the

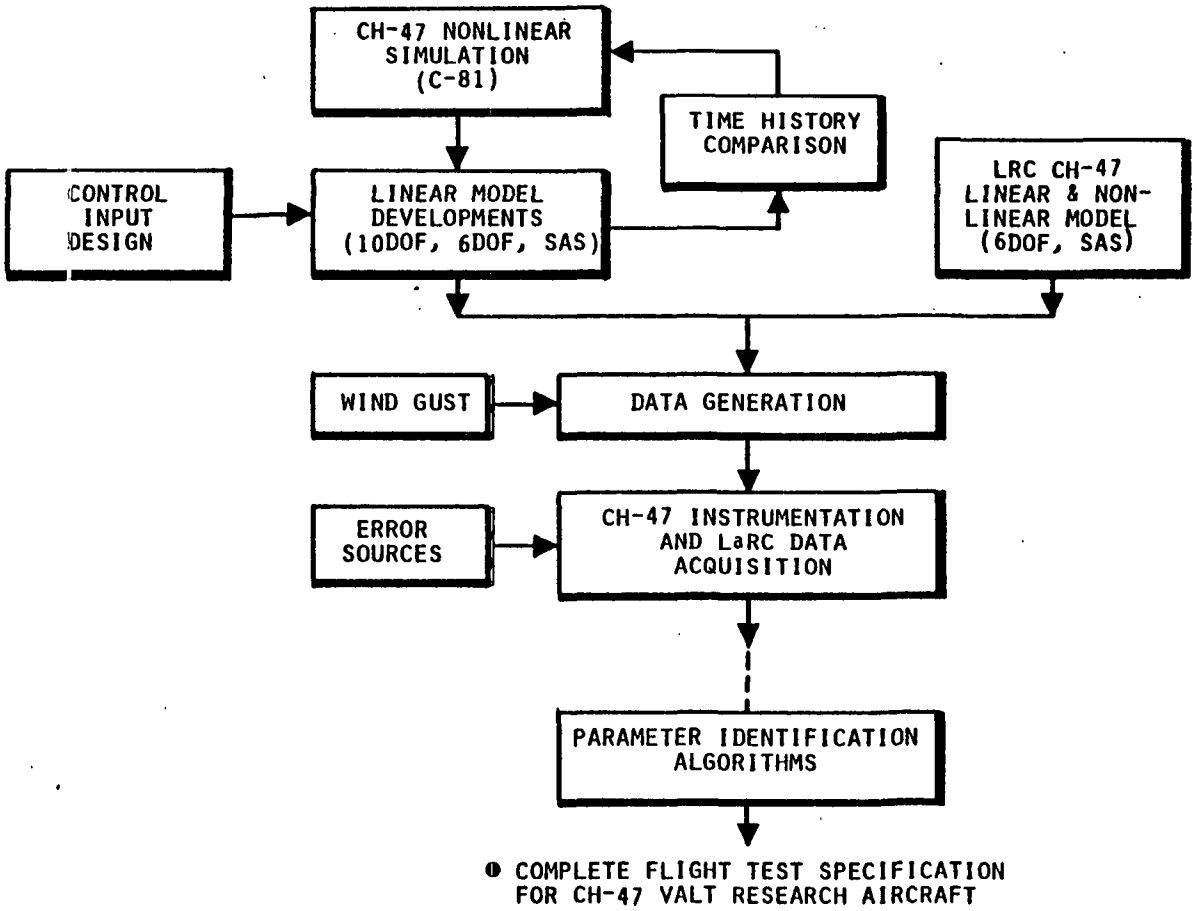

Figure 1.2 Technical Approach

Eustis Directorate, USAAMRDL, Fort Eustis, Virginia. The C-81 computer program is operational on an IBM 360/65 computer from which all of the C-81 results presented in this report were obtained.

The C-81 program is used in two modes of operation in this study: (1) in a nonlinear time history simulation mode, and (2) in a trim and stability derivative mode. The original plan for this investigation was to use the nonlinear C-81 time history simulation mode with parameter identification which would subsequently validate the linear simulation identification. The computer run time associated with a single nonlinear C-81 time history simulation was found to be prohibitive for the data lengths required for parameter identification. For example, simulating 3.5 seconds of real time data required 30 minutes of CPU time.

Since data record length requirements for identification are typically 15 seconds, this would require in excess of two hours of computer CPU time for a single maneuver. Thus, it was decided to use short time history data lengths of 0.5 second from the nonlinear simulation model for comparison purposes to the various linear models used. The linear 10 degree-of-freedom (DOF) rotor/fuselage model (obtained from the stability derivative option of C-81) was subsequently found to provide an excellent time history comparison to the nonlinear C-81 and, thus, the 10 DOF linear model was used as the baseline model throughout this investigation. The C-81 stability derivative option provides for both a 10 DOF derivative model with separate rotor flapping degrees of freedom and the conventional 6 DOF quasi-static derivative array. Both models (10 DOF and 6 DOF) are used in this study.

The linear models developed from the C-81 simulation program consist of: (1) the 10 DOF fuselage/rotor model with first harmonic rotor representation, (2) the 6 DOF quasi-static derivative model, (3) a 10 DOF fuselage/rotor model with first-order rotor representation (flap advancing mode deleted), and (4) the above models with the 8-state variable CH-47 production stability augmentation system (SAS). The C-81 stability derivative option provides derivatives in the form of a second order model (mass, spring, damper) and requires conversion to state variable form. The three aircraft models in state variable format are obtained from the computer program QUASI-STATIC, which accepts as input the C-81 second order derivative equations and provides the three models in state variable form as output, along with eigenvalues and eigenvectors for each model.

The derivative models, taken from Ref. 1, were used mainly for comparisons with the C-81 values. A detailed comparison was made and it was found that the speed-dependent derivatives (e.g. M_u, M_w, etc.) showed large discrepancies between the Ref. 1 and C-81 derivatives, and yet the damping and control derivatives showed adequate agreement. The speed-dependent derivative discrepancy was traced to the fact that the C-81 model does not contain rotor-to-rotor interference effects; whereas, the model taken from Ref. 1 does. Because of the importance to handling qualities and control system designs of the speed-dependent derivatives, it was decided that the derivative model taken from Ref. 2 is more representative of the CH-47 and should be used as the primary simulation, whereas the C-81 models should be used primarily to investigate the effects of rotor degrees of freedom on derivative identification accuracy. Thus, both simulation models are used for this study.

The control input designs indicated in Figure 1.2 are based on the integrated application of eigensystem analysis (e.g.

location of system time constants) and iterative evaluation of simulated responses of the vehicle.

The data generation and wind gust simulation indicated in Figure 1.2 use the appropriate linear model (either C-81 derived or Ref. 1 model) and the designed control inputs. A linear simulation computer program is used for this purpose. The generated data are stored on magnetic tape and provide the data base for further analysis. Wind gust is simulated using a simplified Dryden model.

The CH-47 instrumentation and LRC data acquisition system are modeled as in Ref. 3. The magnitudes of the error sources are obtained from the existing CH-47 instrumentation specification sheets, the LRC-piloted aircraft data system (PADS), and the LRC Research Aircraft Ground Station Data Reduction System (RAGS) specifications.

The parameter identification algorithm used in this investigation is the Systems Control, Inc. Maximum Likelihood Identification program (SCIDNT). This program was used in identification of open-loop stability and control coefficients with the CH-47 production SAS included as part of the model. In addition, the Optimal Subset Regression (OSR) is used for model structure determination.

The flight-test specification for the CH-47 VALT Research Aircraft is obtained after simulations using the analysis methods summarized above and indicated in Figure 1.2. Flight test points presented in Chapter IV are based upon both quantitative and qualitative results.

1.2.3 Report Organization

Subsequent chapters of this report are organized as follows. Chapter II describes the factors which influence parameter identification accuracy, with specific emphasis given to the CH-47

characteristics along the VALT trajectory. Chapter III presents the simulation results which formed the basis for the CH-47 flight test specification for parameter identification. The recommended parameter identification flight test plan is presented in Chapter IV. The conclusions and recommendations are given in Chapter V.

II. PARAMETER IDENTIFICATION ERROR SOURCE ANALYSIS

This chapter describes those factors which influence parameter identification accuracy, with specific emphasis on the CH-47 along a VALT trajectory. The physical considerations which are of fundamental importance for accurate identification are discussed. It is often assumed that an accurate parameter identification algorithm is all that is required for accurate identification. The accuracy in any parameter identification attempt is, however, closely related to knowledge of the physical characteristics of the system to be identified, the environment, the instrumentation measurement system, and the control input including constraints. These factors are discussed since they are of paramount importance to the task of defining a flight test specification. Each section in this chapter addresses in detail a major factor influencing parameter identification accuracy. These include: (1) the VALT trajectory, (2) the CH-47 characteristics and SAS, (3) the CH-47 linear model representation, (4) instrumentation and LRC data recording facilities, (5) the flight test environment, and (6) flight test inputs. Following this, the next chapter addresses the important considerations in the selection and use of parameter identification algorithms and presents pertinent theoretical developments.

2.1 THE VALT TRAJECTORY

The flight test specification resulting from this investigation for parameter identification is to be along a nominal VALT trajectory. A sufficient number of flight test points are required to permit subsequent validation and possible improvement of CH-47 simulations along this trajectory. The stability and control characteristics of helicopters in general and,

specifically , the CH-47, vary greatly over the flight envelope and are particularly dependent on velocity (longitudinal, vertical, and lateral). Thus, the particular nominal flight path along which testing is to occur will result in considerable variation of the stability and control derivatives and will also determine the degree of aerodynamic and dynamic nonlinearity at each test point. In addition, the proximity to the ground (in-ground effect) and steady wind shear profile penetration may be relevant depending on the flight paths.

Figures 2.1 and 2.2 define the nominal VALT approach trajectory which was used for this study. Important transition points are indicated by the letters A through D. The curved flight path from points A to C is flown at a constant airspeed (65 knots). Altitude is held constant at 229m ft between points A and B. At point B, a 2.54 m/sec descent rate is initiated and maintained through point D. At point C, a velocity deceleration to hover is initiated while altitude decreases from 137m to 15m.

The shape of this flight profile is dictated by the many constraints imposed on commercial transport VTOL operations in the terminal area, which are discussed in general in Ref. 9. The area of main emphasis for parameter identification is between points C and D--the terminal descent approach with decelerating velocity. This transition region, which is schematically illustrated in Figure 2.3, is the most difficult to model with analytic simulations, usually contributes the most adverse handling qualities, is the region of least stability, and is thus most demanding on control system designs and navigation in minimizing flight path dispersions.

2.2 CH-47 CHARACTERISTICS

The CH-47 is a twin-engine, tandem-rotor helicopter designed for all-weather, medium-sized transport operations. The rotors

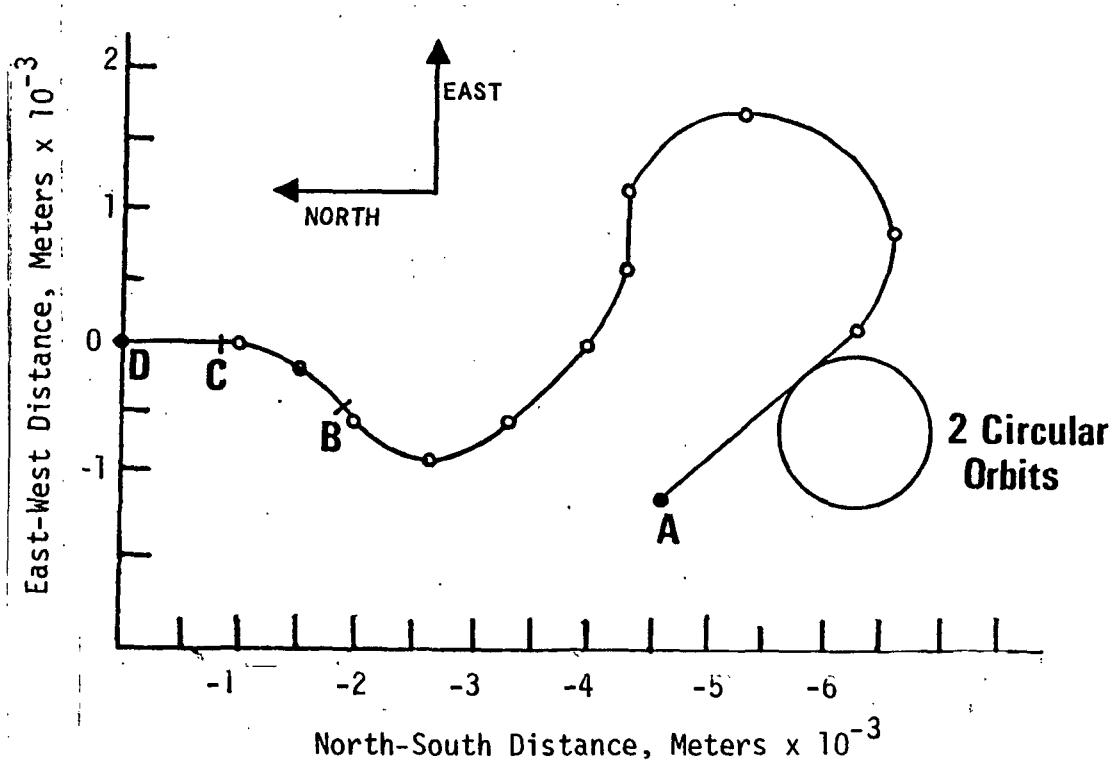

Figure 2.1 VALT Mission Ground Track

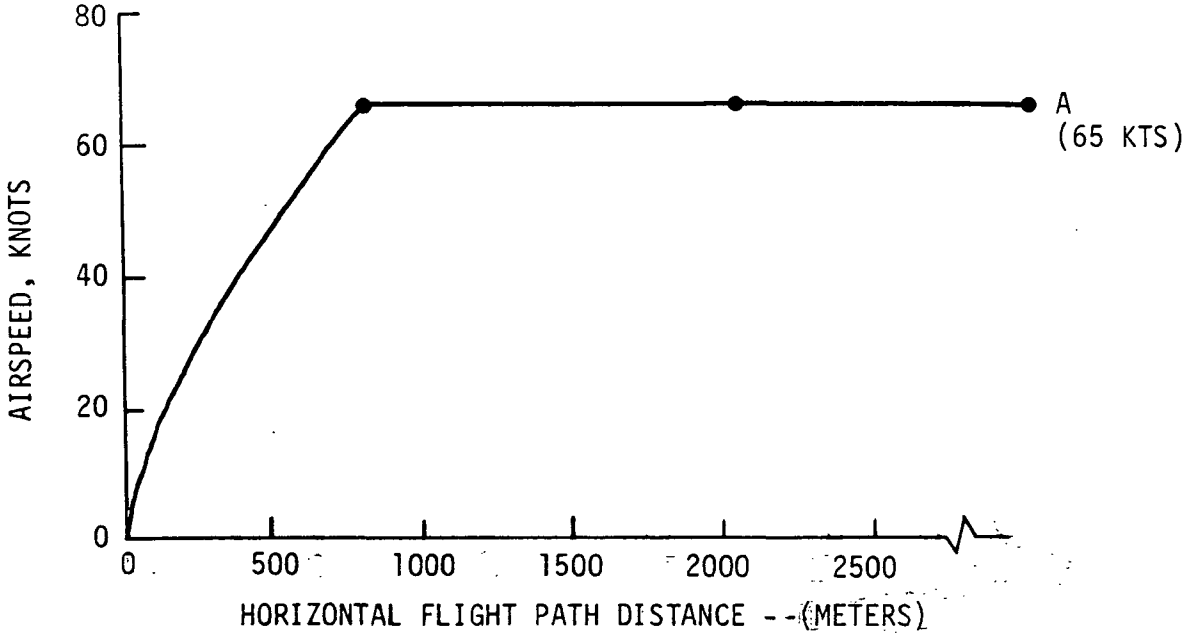

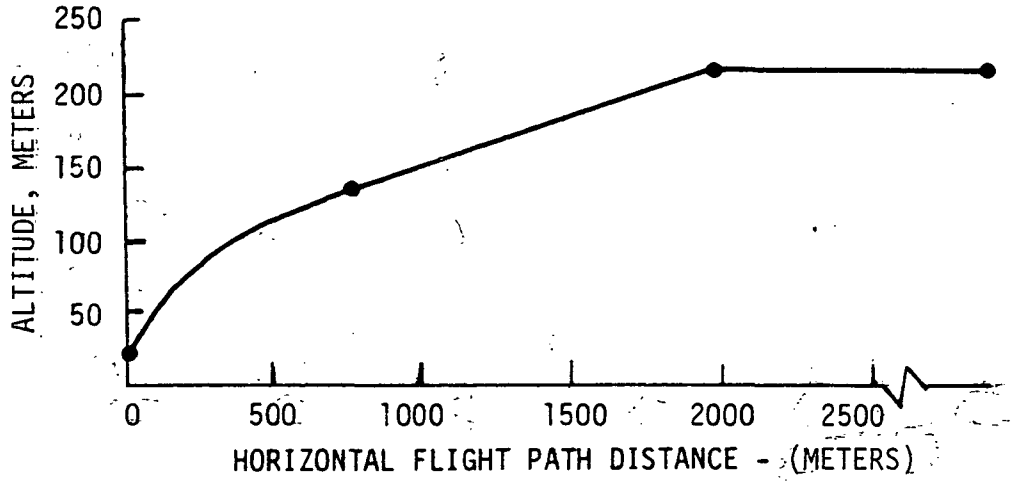

Figure 2.2 Terminal Approach Trajectory Airspeed and Altitude Profiles

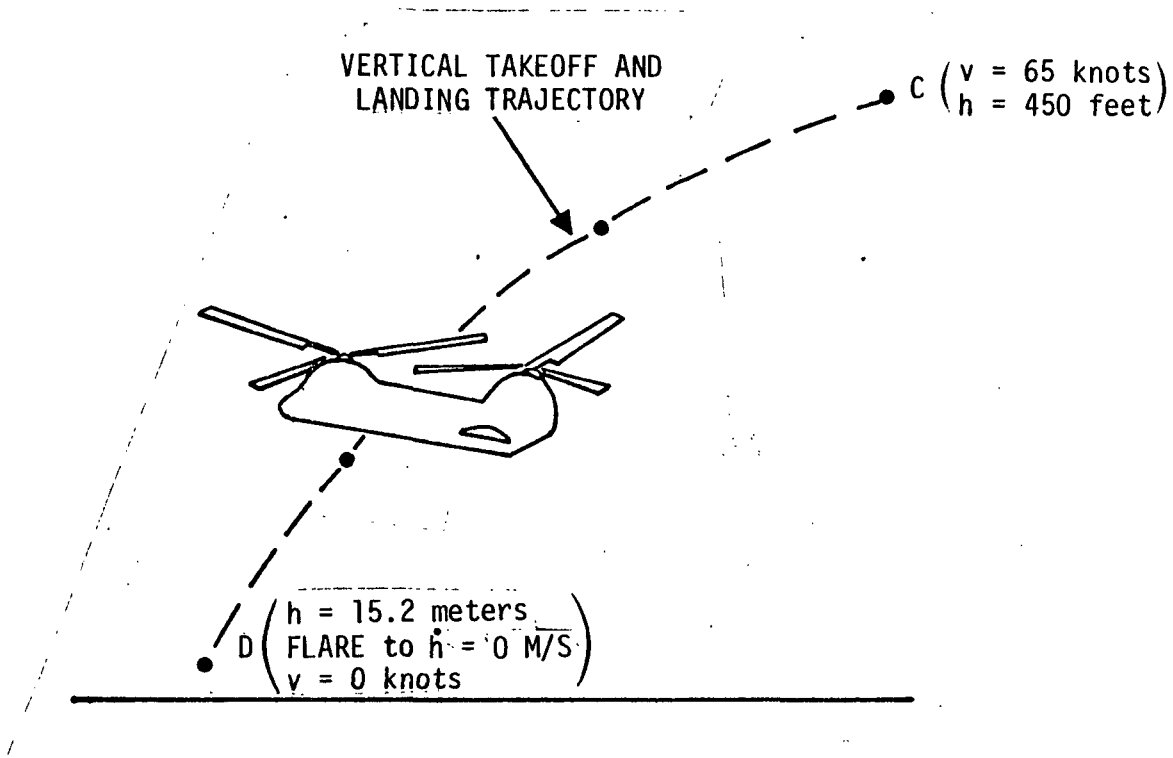

Figure 2.3 VALT Transition Flight Profile

each contain three fully articulated blades with pitch, flap, and drag hinges. The rotors are driven in opposite directions and primary helicopter control is obtained as follows: (1) longitudinal control (pitch) by differential collective, (2) vertical control by ganged collective, (3) lateral control (roll) by later cyclic, and (4) directional control (yaw) by differential lateral cyclic. This section discusses those characteristics particular to the CH-47 which are of importance to parameter identification. A general discussion of the CH-47 (Models A, B, and C) is presented in Ref. 12 with emphasis on general stability and control. Reference 13 discusses the ground-based flight simulation of the CH-47C, and Ref. 1 presents the equations and model to be used to simulate the CH-47 VALT Research Aircraft which will be flight tested for parameter identification.

2.2.1 SAS-Off Stability and Control Characteristics of the CH-47

This section discusses the basic open-loop stability and control characteristics of relevance to parameter identification. These characteristics are obtained from the various analytic models presented in Chapter III and Appendices A and B, and are introduced here to emphasize those factors influencing the flight test specification. The basic trend in stability and control characteristics of helicopters, in general, is similar for low-speed flight and the significant differences in handling qualities are a result of the magnitude of these characteristics.

Figure 2.4 presents the CH-47 characteristic root locations with SAS-off for two airspeeds (vertical descent and 40 kts) at 2.54 m/sec descent rate (obtained from the LRC-supplied CH-47 derivative model). At hover, both the Dutch roll and longitudinal long-period modes are shown to be slightly unstable and oscillatory (refer to Fig. 2.4, open triangle symbol). As airspeed increases to 40 knots, the Dutch roll remains nearly fixed, whereas the

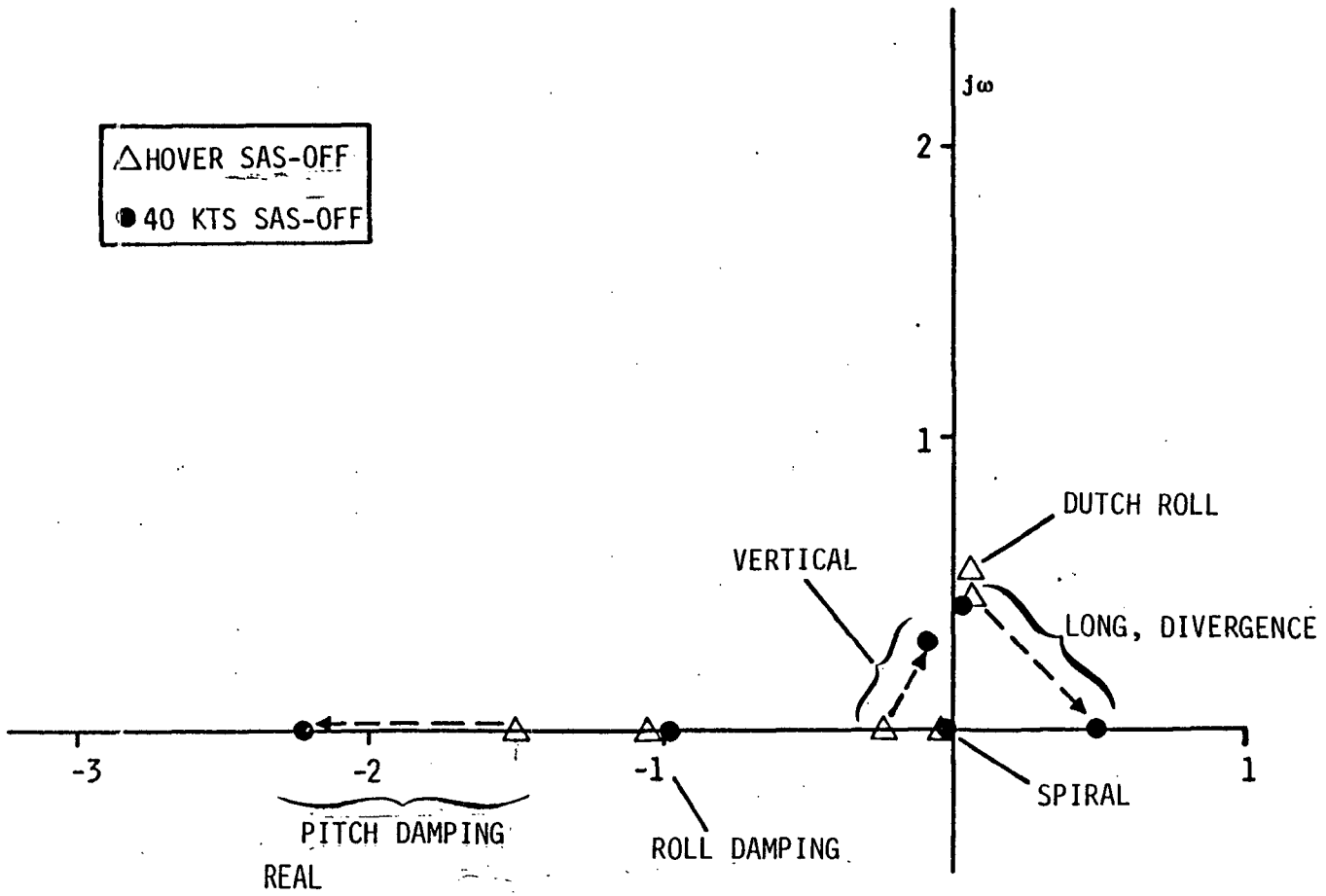

Figure 2.4 CH-47 SAS-Off Characteristic Root Location with Increasing Speed

longitudinal long-period mode migrates further toward the right half plane and is unstable and aperiodic at a value of +0.5. Figure 2.4 shows that the stability characteristics change considerably from hover to 40 knots. This variation in vehicle dynamics results from the influence that airspeed has on the stability parameters, which make up the equations of motion.

Figure 2.5 illustrates the type of nonlinear characteristics which must be considered for rotorcraft modeling beyond the linear regime. This figure presents predicted speed-dependent CH-47 derivatives M_u and M_w as a function of airspeed for three values of descent rate ($\dot{h}$ = -5.08, -2.54, 0 m/sec). The plots of M_u and M_w presented in this figure emphasize three main considerations. First, these derivatives are very nonlinear with airspeed and thus the perturbations in airspeed must be kept typically less than $\pm$5 knots. Second, these derivatives also are very nonlinear with descent rate and thus perturbations in $\dot{h}$ must also be kept small. Third, at hover and 20 knots airspeeds, in order to retain approximate linearity in M_u, vertical velocity must be maintained near its trim value (i.e. negligible or near-zero perturbation). Likewise at hover, in order to retain linearity in M_w, airspeed must not be allowed to deviate by any substantial amount from its trim condition (a $\pm$5 knot change in airspeed causes M_w to change by 0.005 at hover).

The above discussion indicates that in order to identify the approximate linear stability derivative M_u at hover and 20 knots, perturbations in $\dot{h}$ should be kept to a minimum and only airspeed should be perturbed. In an analogous manner, the identification of M_w must be done by perturbing $\dot{h}$ while maintaining nearly constant airspeed. Thus, the design of control inputs must be such that they contain state variable constraints. The reader is directed to Appendix D for a discussion that validates the qualitative conclusions of this paragraph.

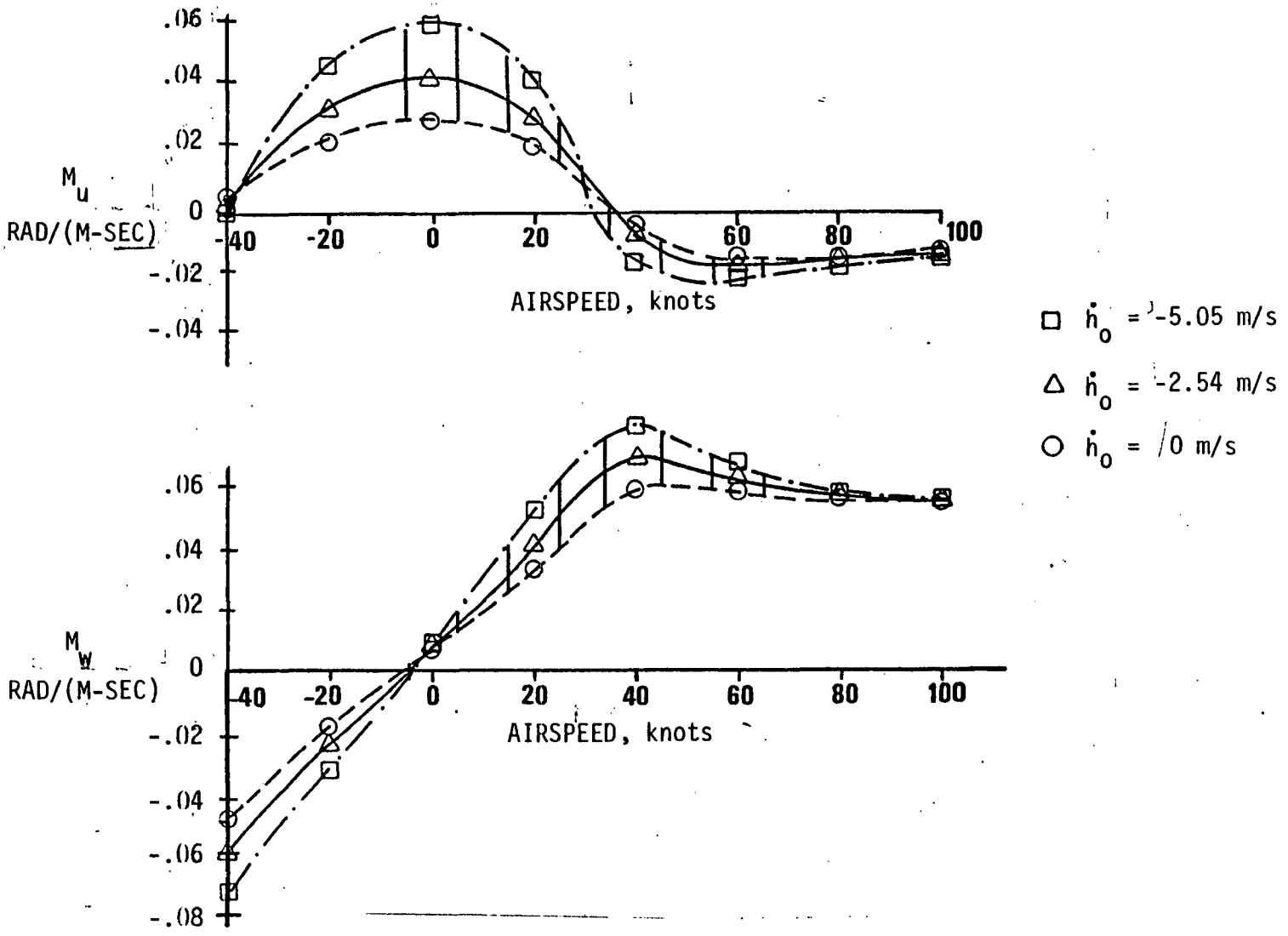

Figure 2.5 CH-47 Nonlinear Stability Characteristics at Low Speed (data from ref. [1])

2.2.2 SAS-On Dynamic Characteristics of the CH-47

The previous section reviewed those characteristics of the basic vehicle (SAS-off) which are of concern to parameter identification. Because the vehicle is unstable without a SAS, the CH-47 production SAS is investigated in this study as to its effect on parameter identification.

Figure 2.6 shows the CH-47 characteristic root location with SAS-on at hover and 40 knots airspeed and 2.54 m/sec descent rate At the hover condition, both the Dutch roll and longitudinal long-period modes are stabilized by the SAS (open triangle symbols), whereas at the 40 knot condition, only the Dutch roll is stable The longitudinal long-period root i- still unstable, although with a greater time to double amplitude. The frequency of the pitch and roll short-period modes is found to be faster with SAS (as seen by a comparison of the pitch and roll short period roots presented in Figures 2.4 and 2.6).

Before completing the discussion of SAS-on dynamic characteristics, it is necessary to briefly review the effect that the rotor degrees-of-freedom have on vehicle dynamics. Figure 2.7 shows the approximate location of basic rigid body characteristic roots both with SAS-on and SAS-off. Rotor characteristic root location for three different helicopters are on this figure to emphasize the proximity of the CH-47 rotor mode in comparison to the CH-53 and XH-59A (ABC) helicopters. The rotor root (flap regressing mode) of the CH-47 is shown to be far removed from rigid body modes. The results reported in Ref. 2 indicated the importance of the rotor degrees of freedom on identification of rigid body derivatives and presented results for the CH-53. The frequency of the CH-47 rotor flap regressing mode shown in Figure 2.7 is greater than that of the CH-53 and thus, the influence of the rotor should be correspondingly less. It should be noted that the rotor roots shown in Figure 2.7 are obtained with the SAS-off

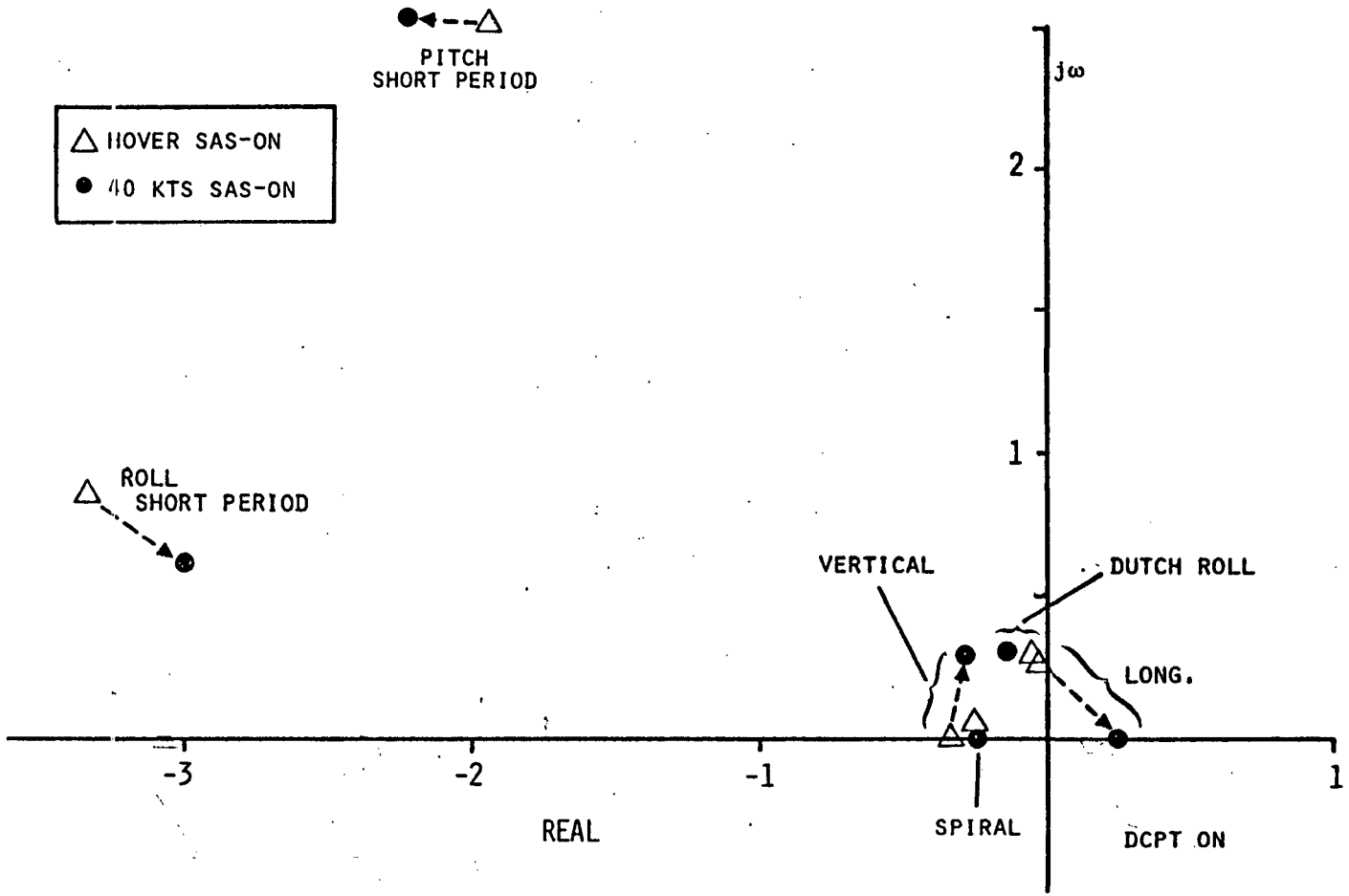

Figure 2.6 CH-47 SAS-On Characteristic Root Location with Increasing Speed

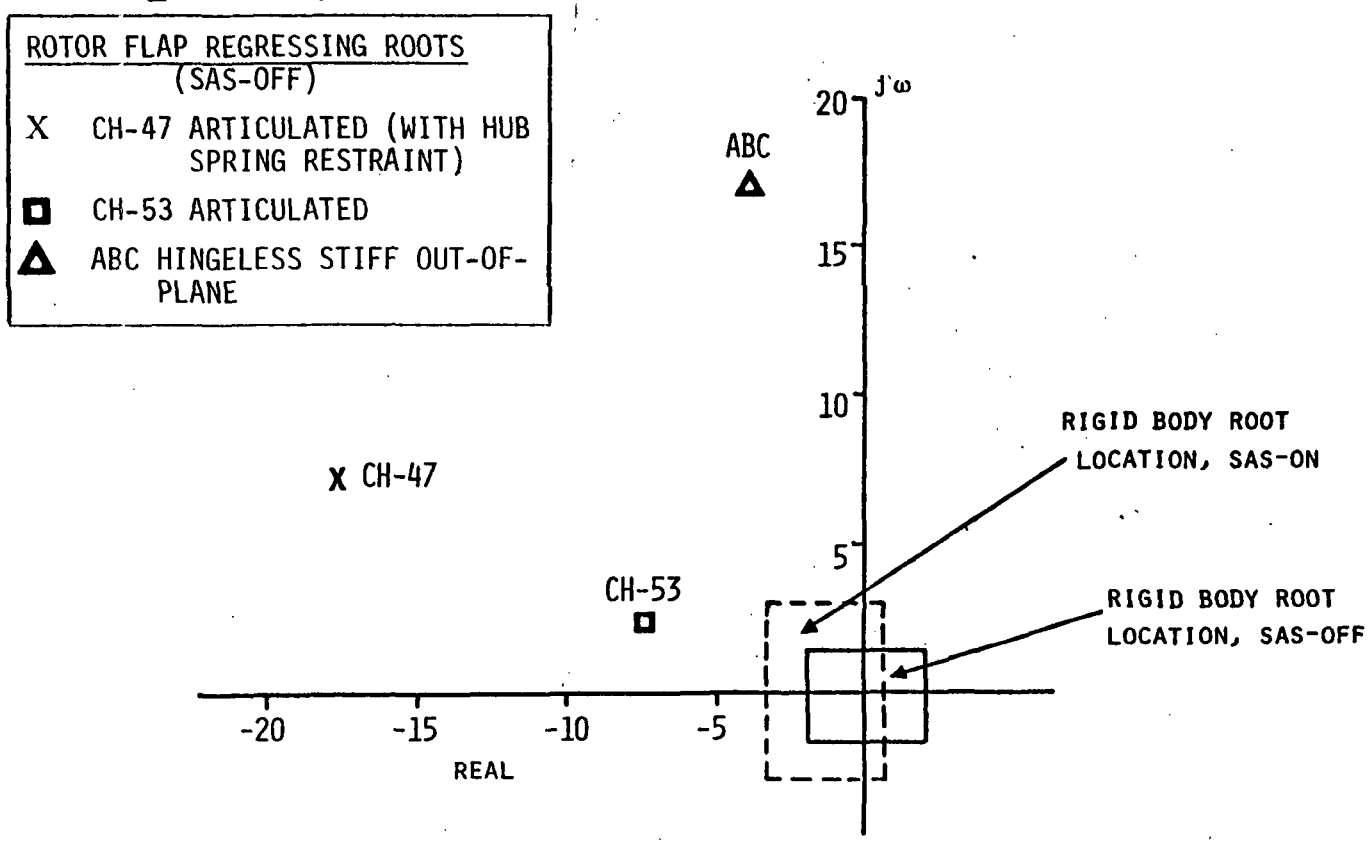

Figure 2.7 CH-47 Rotor Roots Are Far Removed from Rigid Body Modes

and, thus, ignores SAS-rotor – fuselage coupling. The CH-47 production SAS does couple with the rotor degrees-of-freedom. This coupling is shown in Figure 2.8, which shows the rotor flap regressing mode with SAS-off, CH-47 production SAS, and CH-47 production SAS with roll rate feedback gain K_p divided by two.

A reduction of the SAS roll rate feedback gain from its production value of K_p = -12.7 to = -6.35 cm/rad/sec reduces the rotor fuselage coupling as indicated by the triangle symbol of Figure 2.8. To minimize rotor-rigid body coupling, the CH-47 flight test identification should be conducted with the CH-47 production SAS operative with the roll rate feedback gain halved. The identification results presented in the chapters to follow contain this SAS modification.

The use of stability augmentation allows independent excitation of vertical velocity with collective input and independent excitation of longitudinal velocity with longitudinal stick input. The ability to perform this independent velocity excitation is a direct result of the SAS which, by nature of the control law structure, produces pole-zero cancellation. The high degree of decoupling will be shown by time history responses in a later section. This decoupling can be an advantageous feature for input design.

2.3 MATHEMATICAL MODEL STRUCTURE

This section discusses the development of the linear models from C-81 and Ref. 1 models, the linear model structure used for the simulation, the linear model structure used in the identification and the CH-47 production SAS mathematical representation. As discussed previously, the models developed from C-81 and those supplied by Ref. 1 are both used in this analysis. The analytical form and coefficient values of these models are presented in

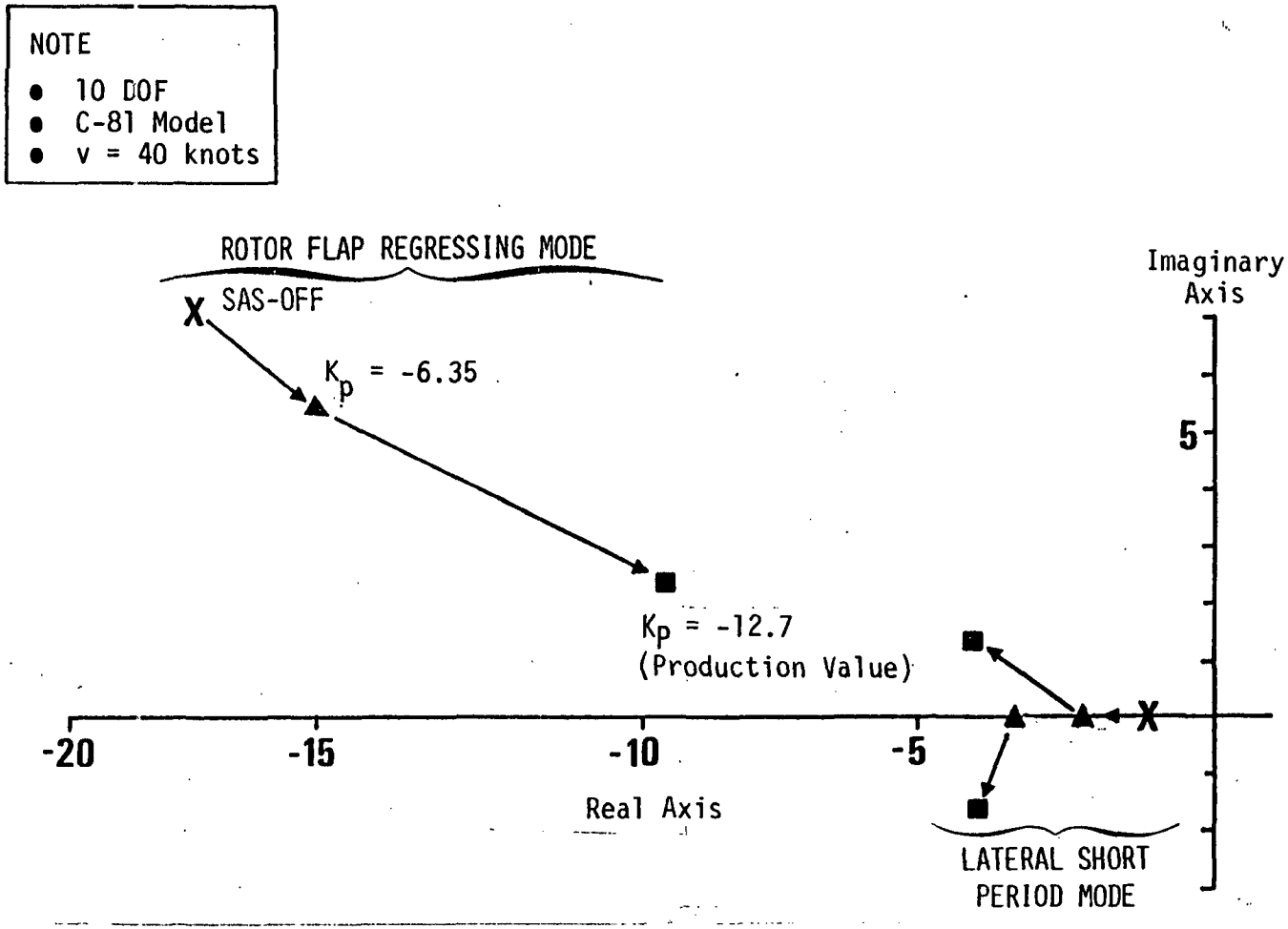

Figure 2.8 Effect of Roll Rate Feedback on Rotor-Airframe Coupling

Appendices A and B. Before discussing details of the linear models, a discussion of the results and developments from C-81 is presented which includes time history comparisons of the linear models and the nonlinear C-81 simulation.

2.3.1 Nonlinear C-81 Simulation, Linear Model Developments, and Time History Comparisons

The nonlinear C-81 simulation program is used to define trimmed conditions from which linear perturbation models can be determined or from which time histories can be generated. Both of these modes of operation are used and discussed below.

Models Derived from the Nonlinear C-81 Program. Two models are derived from the nonlinear C-81 computer program: viz, a 10 DOF model and a 6 DOF quasi-static model. The 10 DOF model is obtained from C-81 by perturbing each independent variable separately while keeping all others at their value, computing the vehicle force and moments, and dividing by the independent variable. The form of the output is that of a second-order matrix equation as

$$M\ddot{X} + D\dot{X} + KX = BU \qquad (2.1)$$

where

M = mass matrix (10 x 10)
D = damping matrix (10 x 10)
K = stiffness matrix (10 x 10)
B = control matrix (10 x 4)

The independent variables are represented by the vectors X, $\dot{X}$, and $\ddot{X}$, and the control vector by U. These are defined as

$$X = \begin{bmatrix} x \\ z \\ \theta \\ y \\ \varphi \\ \psi \\ a_{1_{MR}} \\ b_{1_{MR}} \\ a_{1_{TR}} \\ b_{1_{TR}} \end{bmatrix} \qquad \dot{X} = \begin{bmatrix} u \\ w \\ q \\ v \\ p \\ r \\ \dot{a}_{1_{MR}} \\ \dot{b}_{1_{MR}} \\ \dot{a}_{1_{TR}} \\ \dot{b}_{1_{TR}} \end{bmatrix} \qquad \ddot{X} = \begin{bmatrix} \dot{u} \\ \dot{w} \\ \dot{q} \\ \dot{v} \\ \dot{p} \\ \dot{r} \\ \ddot{a}_{1_{MR}} \\ \ddot{b}_{1_{MR}} \\ \ddot{a}_{1_{TR}} \\ \ddot{b}_{1_{TR}} \end{bmatrix} \tag{2.2}$$

The approximate 6 DOF quasi-static derivative model is obtained by perturbing only the fuselage independent variables and allowing the rotor degrees of freedom to reach steady state. The effect of the rotor is thus lumped into the fuselage resulting in quasi-static derivatives. The form of the derivative equation is the same as shown in Eq. (2.1), except that the matrices are now of dimension 6 x 6. The independent variables are defined

$$X = \begin{bmatrix} x \\ z \\ \theta \\ y \\ \varphi \\ \psi \end{bmatrix} \qquad \dot{X} = \begin{bmatrix} u \\ w \\ q \\ v \\ p \\ r \end{bmatrix} \qquad \ddot{X} = \begin{bmatrix} \dot{u} \\ \dot{w} \\ \dot{q} \\ \dot{v} \\ \dot{p} \\ \dot{r} \end{bmatrix} \tag{2.3}$$

Models Derived from the 10 DOF Linear Model. Another model is derived from the 10 DOF linear model--a 6 DOF quasi-static model. This model is developed from the 10 DOF model by first converting this model to state variable form. The state variable representation for the 10 DOF model is

$$\dot{x} = Fx + Gu \tag{2.4}$$

where

F = 17 x 17 matrix of stability derivatives
G = 17 x 14 matrix of control derivatives

and the state vector x is defined in Eq. (2.5)

$$x^T = [\theta \ \varphi \ \Psi \ u \ w \ q \ v \ p \ r \ \dot{a}_{1_{MR}} \ \dot{b}_{1_{MR}} \ \dot{a}_{1_{TR}} \ \dot{b}_{1_{TR}} \ a_{1_{MR}} \ b_{1_{MR}} \ a_{1_{TR}} \ n_{1_{TR}}] \tag{2.5}$$

$$u^T = [\delta_{COLL} \ \delta_{LONG} \ \delta_{LAT} \ \delta_{RUD}]$$

The state model Eq. (2.4) can be rewritten and partitioned for development of an approximate quasi-static model. The partitioned form is

$$\begin{bmatrix} \dot{x}_1 \\ \ddot{x}_2 \\ \dot{x}_2 \end{bmatrix} = \begin{bmatrix} F_{11} & F_{12} & F_{13} \\ F_{21} & F_{22} & F_{23} \\ \underline{0} & \underline{I} & \underline{0} \end{bmatrix} \begin{bmatrix} x_1 \\ \dot{x}_2 \\ x_2 \end{bmatrix} + \begin{bmatrix} G_1 \\ G_2 \\ \underline{0} \end{bmatrix} u \tag{2.6}$$

where

$$x_1 = \begin{bmatrix} \theta \\ \varphi \\ \psi \\ u \\ w \\ q \\ v \\ p \\ r \end{bmatrix} \quad \text{and} \quad x_2 = \begin{bmatrix} a_{1_{MR}} \\ b_{1_{MR}} \\ a_{1_{TR}} \\ b_{1_{TR}} \end{bmatrix} \tag{2.7}$$

The quasi-static condition occurs when the rotor state variables reach steady state (e.g. $\ddot{x}_2$ and $\dot{x}_2$ are zero). Making these substitutions into Eq. (2.6) and solving for x_2 results in

$$x_2 = - F_{23}^{-1} (F_{21} x_1 + G_2 u). \tag{2.8}$$

Substitution of Eq. (8) into the x_1 equation of Eq. (2.6) results in the final form for the quasi-static model as

$$\dot{x}_1 = \underbrace{(F_{11} - F_{13}F_{23}^{-1}F_{21})}_{F_{QS}} x_1 + \underbrace{(G_1 - F_{13}F_{23}^{-1}G_2)}_{G_{QS}} u \qquad (2.9)$$

Equation (2.9) defines the 6 DOF quasi-static model derived from the 10 DOF linear model. This model can be compared to the quasi-static model obtained directly from the C-81 nonlinear computer program. The state variable form for the C-81 6 DOF quasi-static model is

$$\dot{x} = F_{C-81}\, x + G_{C-81}\, u \qquad (2.10)$$

⇐ 6 DOF C-81 Model obtained by perturbation

where the notations F_{C-81} and G_{C-81} indicate that this model was obtained directly from the nonlinear C-81 program by perturbation of the nonlinear model. The derivative values for F_{C-81} are found to be of nearly the same value as F_{QS} obtained from Eq. (2.9). However, the control derivatives G_{C-81} do not agree with the values computed by Eq. (2.9). This is because G_{QS} computed from Eq. (2.9) is derived from the 10 DOF model, which was found to contain incorrect control derivatives and is in error due to a spike anomaly occurring by perturbing at t = 0 in the C-81 nonlinear computer program.

The anomalous behavior associated with the C-81 computer simulation has been observed previously. Whenever sharp edge pilot control inputs were used, spike responses occurred just as when perturbing the nonlinear model to derive the 10 DOF control derivatives. Analysis of this problem indicates that the spike results from the generation of the fuselage control derivatives of the 10 DOF

derivative model. The 10 DOF model is derived by perturbing the nonlinear model at t = 0. When this is done, spike responses result at t = 0 and, as a consequence, the t = 0 derived control derivatives are in error. This error can be corrected by using the 6 DOF C-81 quasi-static derivatives and reversing the procedure employed to develop quasi-static derivatives. The 10 DOF model used in this study and referenced in the remainder of this report is the corrected 10 DOF model.

The spike anomaly found in the C-81 program has been observed in other rotorcraft simulation programs. For example, the Sikorsky Aircraft General Helicopter Simulation program has been found to contain spike anomalies of a similar nature. Reference 15 (page 184, Figure 1) shows the stability derivative $Z_{B_{1S}}$ obtained by perturbing the nonlinear simulation. At time $t = 0$ in this figure, a large spike input exists which is an incorrect representation of the 9 DOF derivative value discussed in this reference.

The errors in the derived control derivatives G_{QS} resulting from the spike anomaly can be corrected since it is known that the 6 DOF quasi-static derivatives, G_{C-81}, obtained from C-81 are correct (since they are not obtained at $t = 0$, but after rotor transients subside). This correction follows since the control derivatives of Eq. (2.9) can be set to the C-81 values as shown in Eq. (2.12).

$$G_1 - F_{13}F_{23}^{-1}G_2 = G_{C-81} \tag{2.11}$$

Therefore, the 10 DOF control derivative values, G_1, are modified as shown in Eq. (12).

$$G_1' = G_{C-81} + F_{13}F_{23}^{-1}G_2 \tag{2.12}$$

where G_1' represents the modified correction. This corrected control derivative matrix can then be used in place of G_1 in Eq. (2.6) to yield a 10 DOF model which does not contain errors resulting from the spike anomaly from C-81. This model will then reduce to the correct 6 DOF quasi-static derivative model of Eq. (2.10).

The corrected 10 DOF linear model (i.e. with G_1') is now a consistent representation to the nonlinear C-81 simulation program. This correction is justified, since the 10 DOF must reduce to the C-81 quasi-static model. The correction thus eliminates the errors resulting from the erroneous spike and guarantees reduction to the correct quasi-static derivatives. The time histories to be shown subsequently do demonstrate this validity.

The above discussion presented the development of the 6 DOF quasi-static model from the 10 DOF (C-81 derived) linear model. The control derivatives of the 10 DOF were found to be in error and corrected in the manner discussed above.

It is of interest to compare the eigenvalues for the two models--10 DOF first harmonic rotor and 6 DOF quasi-static. Table 2.1 shows this comparison for the hover condition and excellent agreement exists for the low frequency rigid body modes. (If this agreement did not exist, then the quasi-static assumption would not be a valid approach for low frequency modeling).

C-81 Time History Comparisons (Nonlinear vs. Linear). Time history comparisons were conducted using the nonlinear C-81 computer program and results of the various linear models. As discussed previously, the computer run times associated with the nonlinear C-81 time history simulation precluded its use for derivative identification. The approach taken is to validate that the linear simulation models adequately match the

Table 2.1
Eigenvalues from the Two Linear Models (Hover)

MODE	C-81 10 DOF	REDUCED 6 DOF
Long. Divergence	.2921	.2982
Dutch Roll	.0696±j.3920	.0768±j.3850
Vert./Long.	-.1447±j.2935	-.1422±j.2973
Pitch Damping	-.9377	-.9217
Roll Damping	-.8305	-.8481
Spiral	-.4015	-.3967
Flap Regressing	-18.24±j6.381 -17.83±j7.691	
Flap Advancing	-18.20±j44.99 -18.31±j43.92	

nonlinear simulation, thus justifying their use for generating the data for use in the derivative identification.

Figure 2.9 presents the time history responses of the CH-47 at the 40 knots condition due to a 1.27 cm by 0.3 sec longitudinal pulse input (differential collective). Figure 2.9 shows pitch acceleration generated from the nonlinear C-81 simulation program. The nonlinear simulation was terminated after 0.5 sec due to the large execution time associated with the C-81 program. This amount of simulation time is sufficient for time history comparison since most of the transient discrepancies occur in the vicinity of the pulse input. The spike anomaly discussed in detail previously is shown on this figure. The simulation results of the linear 6 DOF quasi-static model and the 10 DOF fuselage

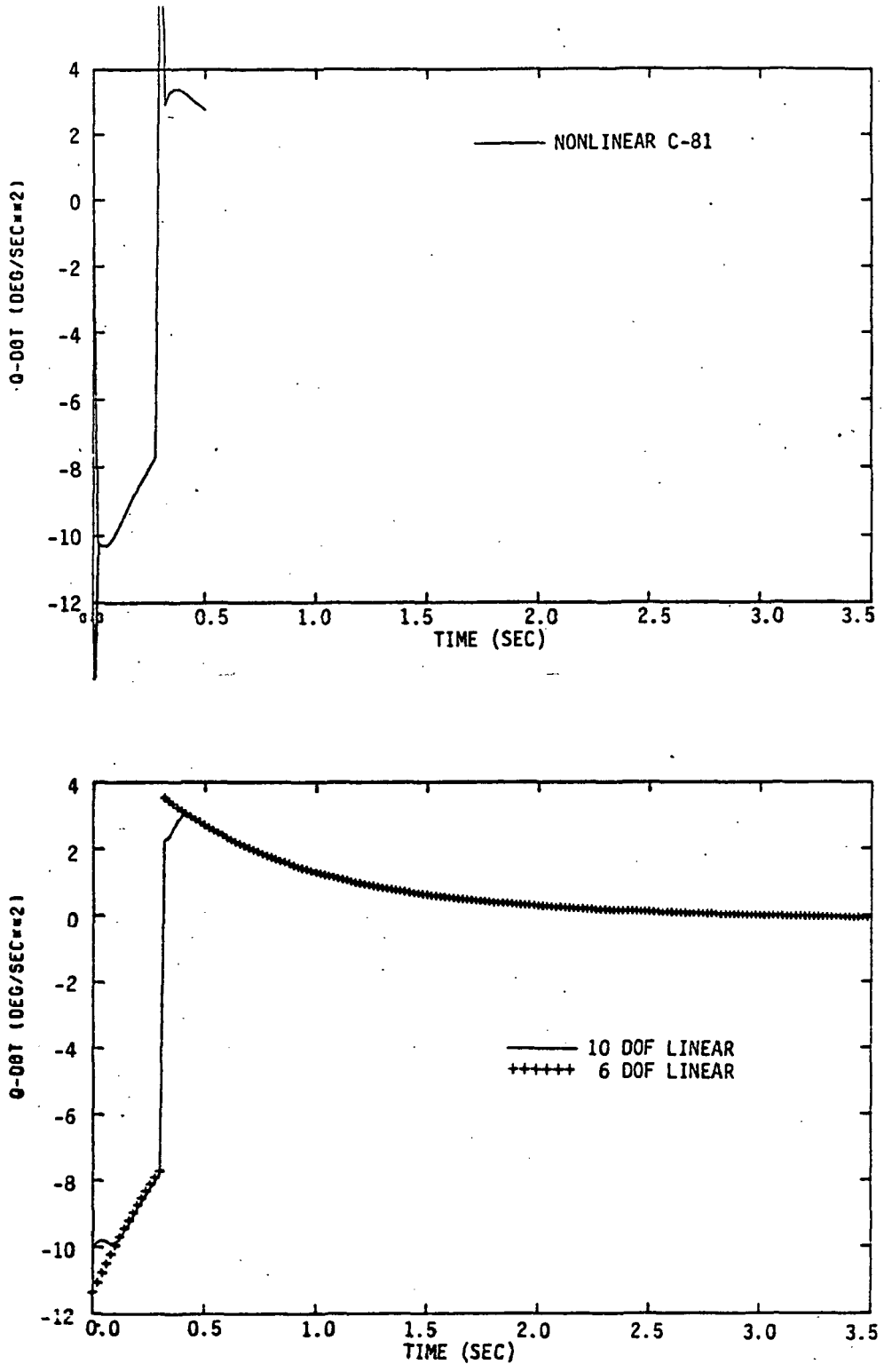

Figure 2.9 Longitudinal Time History Comparison of the Nonlinear C-81, 10 DOF, and 6 DOF, Model Response (v = 40 knots, δ_{LONG} = 0.5° for 0.3 seconds)

rotor model are also shown. The 10 DOF model is shown to represent the transients of the nonlinear response with the exception of the erroneous spike. The 6 DOF response does not model these transients; however, after the input is removed, the 10 DOF and 6 DOF show excellent comparison. The comparison between the 6 DOF and 10 DOF models is considered quite good in the vicinity of the pulse input. This is because pitch acceleration is primarily a result of differential collective and thus does not have a large time delay as would be found if pitch was produced by rotor flapping.

Figure 2.10 shows the time history response due to a 1.27 cm in by 0.3 sec lateral pulse input (lateral cyclic). Roll acceleration from the nonlinear C-81 simulation, the linear 6 DOF quasi-static, and the 10 DOF fuselage-rotor response are shown. A 0.2 sec delay is seen in Figure 2.10 due to rotor flapping. This delay is also shown in the 10 DOF linear response. The 6 DOF quasi-static response does not reproduce this delay since the rotor degrees of freedom are not included separately in this model.

Figure 2.11 shows the cross-coupling effect of the lateral cyclic input on pitch acceleration from the nonlinear C-81 simulation. The response of the 10 DOF and 6 DOF linear models due to the lateral input is shown in Figure 2.11. The linear 10 DOF cross-coupled response is shown to accurately represent the nonlinear C-81 model. The 6 DOF quasi-static response, however, does not represent the cross-coupling response.

The comparisons presented in this report are representative of the remaining time history comparisons which have not been shown. The comparisons shown in Figures 2.9 through 2.11 are presented since these time histories demonstrate the main features of the various models which are used in this study.

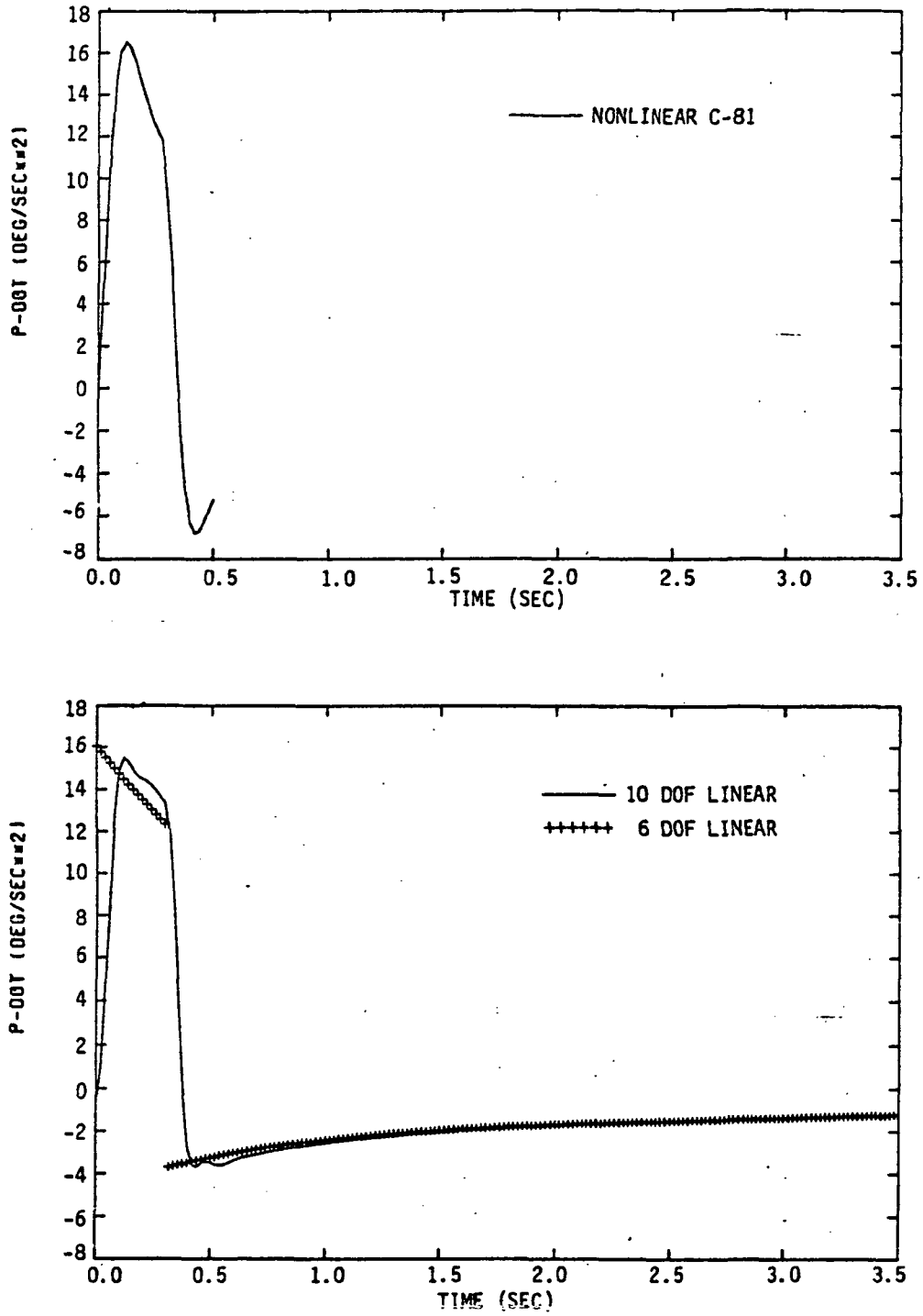

Figure 2.10 Lateral Time History Comparison of the Nonlinear C-81, 10 DOF, and 6 DOF Model Responses (v = 40 knots, $\delta_{LAT} = 0.5°$ for 0.3 seconds)

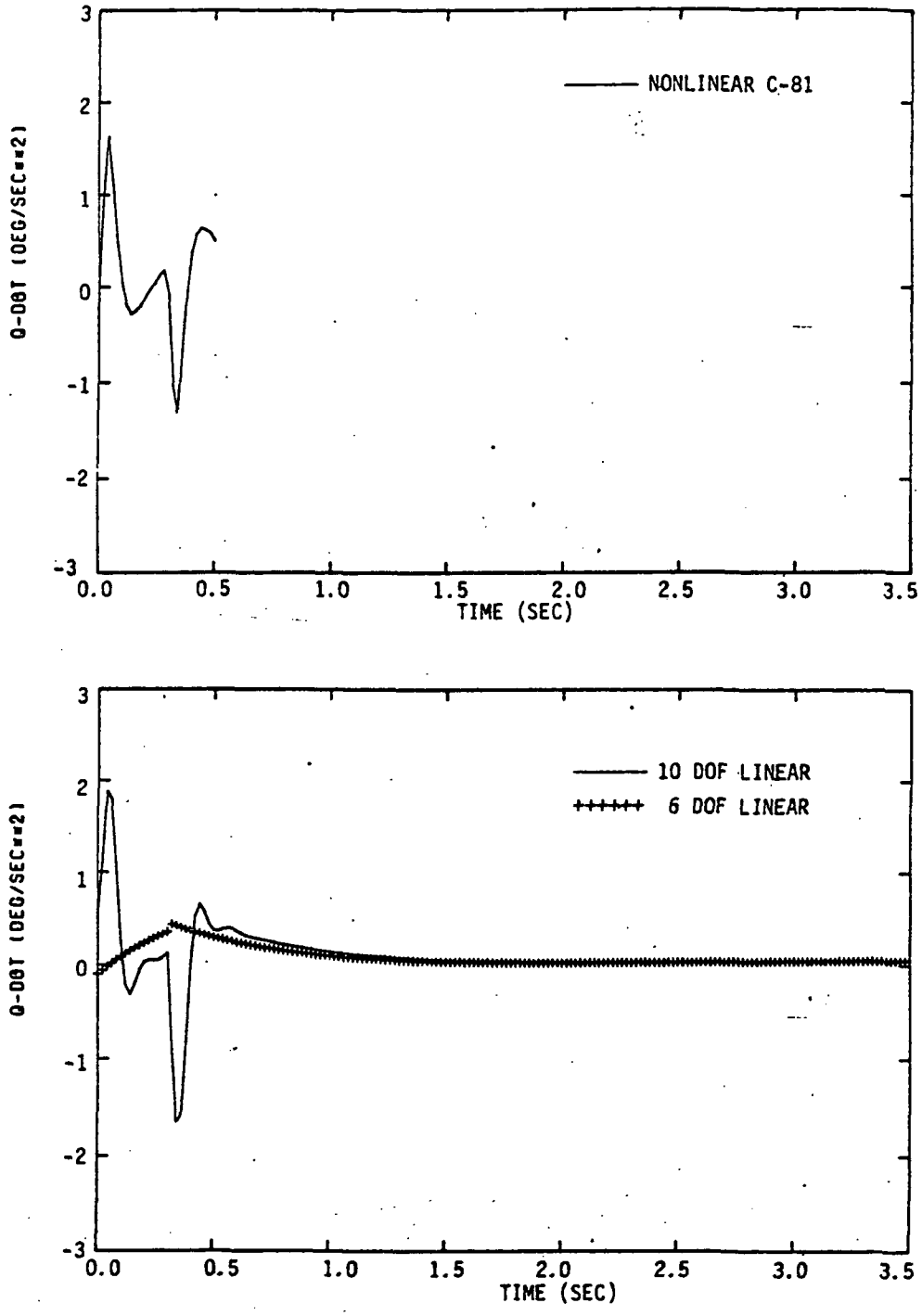

Figure 2.11 Cross-Coupled Time History Comparison of the Nonlinear C-81, 10 DOF, and 6 DOF Responses (v = 40 knots, δ_{LAT} = 0.5° for 0.3 seconds)

The treatment of nonlinearities due to large state variable perturbations from trim was discussed in the previous section (SAS-off stability and control characteristics of the CH-47). The nonlinear trend due to speed effects obtained from the C-81 program is not representative of the actual vehicle due to the lack of inter-rotor interference modeling in this program. Thus, nonlinear effects are treated based upon the Ref. 1 models and C-81 derived models were used primarily for assessing the influence of rotor degrees of freedom.

Reference 1 CH-47 Derivative Models and Comparison to C-81. The CH-47 derivative models employed in this study were obtained from the NASA Langley Research Center and are discussed in detail in Ref. 1. Numerical values of the 6 DOF derivatives are presented in the appendix of Ref. 1 at various forward velocity trim conditions and descent rates. The Ref. 1 derivative models used in this identification effort are presented in Appendix B.

The C-81 derivatives discussed in the previous section are compared with those taken from Ref. 1. This was done for three speeds: hover, 20 knots, and 40 knots. Table 2.2 presents a detailed comparison of the 40-knot condition. Those derivatives usually considered important are noted with an asterisk. The remaining derivatives are cross-coupling derivatives or contribute a negligible influence on vehicle response for small perturbations and thus large differences may exist but they are of negligible consequence.

The derivative correlation at hover and 20 knots airspeed is equally good with the exception of M_u and M_w. These derivatives are of importance to low speed helicopter flight and C-81 shows a considerable discrepancy to the Ref. 1 values. Table 2.3 presents M_u and M_w for the three conditions.

Table 2.2 CH-47 Derivative Comparison (Ref. 1 and C-81)
(V = 40 Knots, $\dot{h}$ = -2.54 m/s)

	u	w	q	v	p	r	δ_{COLL}	δ_{LONG}	δ_{LAT}	δ_{PED}
X	-.00932* -.00869	.0385 .0607	---	-.00016 .00855	.0008 .0413	-.0334 -.1222	6.6072 9.5604	-1.2504* 2.9484	.00108 -.00636	.00084 -.29280
Z	-.1341 -.1170	-.4154* -.6565	---	.01077 -.0439	.1306 -.0312	.3585 -.1397	-100.128* -135.240	-5.1192 8.5380	-.01356 -.00744	.00444 .66564
M	-.00761* -.00705	.06801* .01214	-1.608* -1.329	.00059 .00377	.06559 .13047	.02728 -.1629	3.92323 2.08819	-13.94567* -15.5906	.00039 -.13071	.00984 .08858
Y	-.00042 -.00034	.00463 .00082	-.11863 -.3921	-.06418* -.04275	---	---	.50388 .04896	-.8712 -1.0860	13.428 13.032	-.5004 -.660
L	-.00072 -.00151	.00653 .00469	-.01289 -.3213	-.01709* -.02398	-.82699* -.83710	-.06756 -.07788	-.3583 -1.4095	-.25945 -2.1496	15.9370* 21.9095	-5.1811* -5.2441
N	.00085 .000348	-.08467 .03148	-.08467 .03148	.00072* -.00620	-.01420 -.1075	-.03928* -.05625	.14685 1.5158	-1.1614 -.8465	.37677* .35394	7.7520* 7.5906

*Indicates an important derivative

1st number - LRC Derivative
2nd number - C-81

Table 2.3
Comparison of M_u and M_w from Ref. 1 and C-81

AIRSPEED	M_u		M_w	
	LRC	C-81	LRC	C-81
Hover	.01356	-.000457	.00285	.000104
20 Kts	.00965	-.00117	.01226	.00162
40 Kts	-.00232	-.00215	.02073	.00370

The general conclusions concerning the correlation of derivatives from C-81 and the Ref. 1 program are that for the most part, good agreement exists for the two programs with the important exception of M_u at low speeds (20 knots and below) and M_w. At 40 knots airspeed, the two programs can be considered to show reasonable correlation (although M_w differs by a factor of six) and thus at this speed the C-81 model is used throughout this study to investigate the importance of rotor degrees of freedom on derivative identification. It is questionable whether the C-81 model is representative at speeds below 40 knots and thus the Ref. 1 models are used at these conditions. However, the importance of rotor degrees of freedom must be assessed in the post-flight identification processing before pursuing identificaion with the six degree of freedom Ref. 1 derivative model.

2.3.2 CH-47 Production SAS Models

The CH-47 SAS used throughout this investigation was supplied by LRC and is discussed in Ref. 12. The form of this SAS was supplied as a transfer function feedback which requires conversion to state variable representation. The procedure for accomplishing this and the resulting state variable representation is presented.

The SAS used throughout this investigation in transfer function form is presented in Eqs. (2.13) through (2.18).

Pitch SAS

$$\frac{\delta_{LONG}}{q} = K_q \frac{17.9s}{(17.9s+1)} \cdot \frac{1.98s+1}{(.364s+1)(4.22s+1)} ,$$

$$K_q = -.439 \text{ m/sec} \quad (17.3 \text{ in/sec}) \qquad (2.13)$$

Roll SAS

$$\frac{\delta_{LAT}}{p} = \frac{K_p}{(.047s+1)} , \quad K_p = -.127 \text{ m/sec} \quad (-5.0 \text{ in/sec}) \qquad (2.14)$$

Yaw SAS

$$\frac{\delta_{RUD}}{r} = K_r \frac{3.2s}{(3.2s+1)} \cdot \frac{1}{(.098s+1)} , \qquad (2.15)$$

Velocity > 40 kts $\quad K_r = -.262$ m/sec (-10.32 in/sec)

Roll Into Yaw

$$\frac{\delta_{RUD}}{p} = K_{rp} \frac{1}{(4.11s+1)} , \quad K_{rp} = 16.4 \text{ cm/rad/sec} \quad (6.47 \text{ in/rad/sec}) \qquad (2.16)$$

Sideslip SAS (converted to lateral velocity at 40 kts)

$$\frac{\delta_{RUD}}{v} = +K_v \frac{1}{(.174s+1)} , \quad K_v = .00272 \text{ m/m/sec} \quad (.0326 \text{ in/fps}) \qquad (2.17)$$

DCPT SAS (NOTE: Not implemented on LRC CH-47)

$$\frac{\delta_{LONG}}{u} = +.0111 \qquad (2.18)$$

Conversion of the transfer functions Eqs. (2.13) through (2.18) to state variable form is complicated by the presence of zeros in the numerator. Standard techniques are available and appear in many references (c.f. Ref. 16) for this type of conversion (i.e. with the presence of zeros in the numerator). This conversion is not unique and depends primarily on the type of representation desired. The standard canonical form was selected for the structure of the transformation and is of the form shown in Eq. (2.19).

$$\begin{bmatrix} \dot{v}_1 \\ \dot{v}_2 \\ \vdots \\ \dot{v}_{n-1} \\ \dot{v}_n \end{bmatrix} = \begin{bmatrix} 0 & 1 & 0 & \cdots & 0 \\ 0 & 0 & 1 & \cdots & 0 \\ \cdots & \cdots & \cdots & \cdots & \cdots \\ 0 & 0 & 0 & \cdots & 1 \\ -a_o & -a_1 & -a_2 & \cdots & -a_{n-1} \end{bmatrix} \begin{bmatrix} v_1 \\ v_2 \\ \vdots \\ v_{n-1} \\ v_n \end{bmatrix} + \begin{bmatrix} 0 \\ 0 \\ 0 \\ \vdots \\ b_{n-m} \\ \vdots \\ b_{n-1} \\ b_b \end{bmatrix} u$$

$$y = [1 \quad 0 \quad 0 \quad \cdots\cdots\cdots]v \tag{2.19}$$

where

n = order of denominator
m = order of numerator
$v_{i(i=1,2,...)}$ = canonical states
y = output vector of transfer function state mode

Complete details of this technique can be found in Ref. 16 (pp. 182-190).

The state variable form for the CH-47 SAS presented in Eqs. (2.13) through (2.18) is shown in Eqs. (2.20) through (2.24).

Pitch SAS

$$\begin{bmatrix} \dot{v}_1 \\ \dot{v}_2 \\ \dot{v}_3 \end{bmatrix} = \begin{bmatrix} 0 & 1 & 0 \\ 0 & 0 & 1 \\ -.0364 & -.8179 & -3.041 \end{bmatrix} \begin{bmatrix} v_1 \\ v_2 \\ v_3 \end{bmatrix} + \begin{bmatrix} 1.289 \\ -3.2688 \\ 8.8863 \end{bmatrix} K_q \cdot q$$

$$\delta_{LONG} = v_1 \tag{2.20}$$

Roll SAS

$$\dot{v}_4 = -21.28\, v_4 + 21.28\, K_p \cdot p$$

$$\delta_{LAT} = v_4 \tag{2.21}$$

Yaw SAS

$$\begin{bmatrix} \dot{v}_5 \\ \dot{v}_6 \end{bmatrix} = \begin{bmatrix} 0 & 1 \\ -3.189 & -10.517 \end{bmatrix} \begin{bmatrix} v_5 \\ v_6 \end{bmatrix} + \begin{bmatrix} 10.2 \\ -107.29 \end{bmatrix} K_r \cdot r$$

$$\delta_{RUD} = v_5 \tag{2.22}$$

Roll Into Yaw

$$\dot{v}_7 = -.2435\, v_7 + .2435\, K_{rp} \cdot p$$

$$\delta_{RUD} = v_7 \tag{2.23}$$

Sideslip SAS (Lateral Velocity)

$$\dot{v}_8 = -5.75\, v_8 + 5.75\, K_v \cdot v$$

$$\delta_{RUD} = v_8 \tag{2.24}$$

DCPT SAS (V = 40 kts)

$$\delta_{LONG} = +.0111\, u \tag{2.25}$$

The complete closed-loop model with SAS can be written in state variable form as shown in Eq. (2.26).

$$\begin{bmatrix} \dot{x} \\ \dot{v} \end{bmatrix} = \begin{bmatrix} F & GH_C \\ B_C K_C & A_C \end{bmatrix} \begin{bmatrix} x \\ v \end{bmatrix} + \begin{bmatrix} G \\ 0 \end{bmatrix} u \qquad (2.26)$$

where x represents the open-loop state vector of the appropriate model (10 DOF or 6 DOF) and v represents the state vector of the SAS (8 state variables).

Appendices A and B present the model structure of the combined state vector models augmented by the SAS in state variable form (i.e., Eq. (2.26)) used throughout this study.

2.3.3 Input Control Design Models

Two basic approaches available for input design at this time are based on linear models. These are:

(1) Utilization of specialized algorithms which extremize the information on the parameters of interest (Ref. 8);

(2) Eigenstructure (e.g. eigenvalues and eigenvectors) of the system;

The model analysis of the previous sections presents a challenging problem for input design because of the high order of the coupled dynamics models and the presence of significant effects of nonlinear aerodynamic and dynamic interactions. The approach to this CH-47 input design was therefore accomplished by the following method.

(1) Evaluation of the inputs against the closed-loop eigensystem corresponding to the 10 DOF (SAS-on) system to determine frequencies and phases of the inputs;

(2) Simulation evaluation of the inputs on 10 DOF simulated data to further optimize the identification of the desired parameters and to evaluate the magnitude of vehicle responses (which should not be "excessive").

This approach concentrates on input designs which will enhance the uncoupled 3 DOF model parameters, and is evaluated upon 3 DOF and 10 DOF (coupled) responses. It should be noted that this approach does not imply that cross-coupled derivatives are not identifiable from the subsequent flight test data, nor should only 3 DOF models be used for post-flight processing.

Based upon the discussion above, the procedure employed for parameter identification is outlined in Figure 2.12.

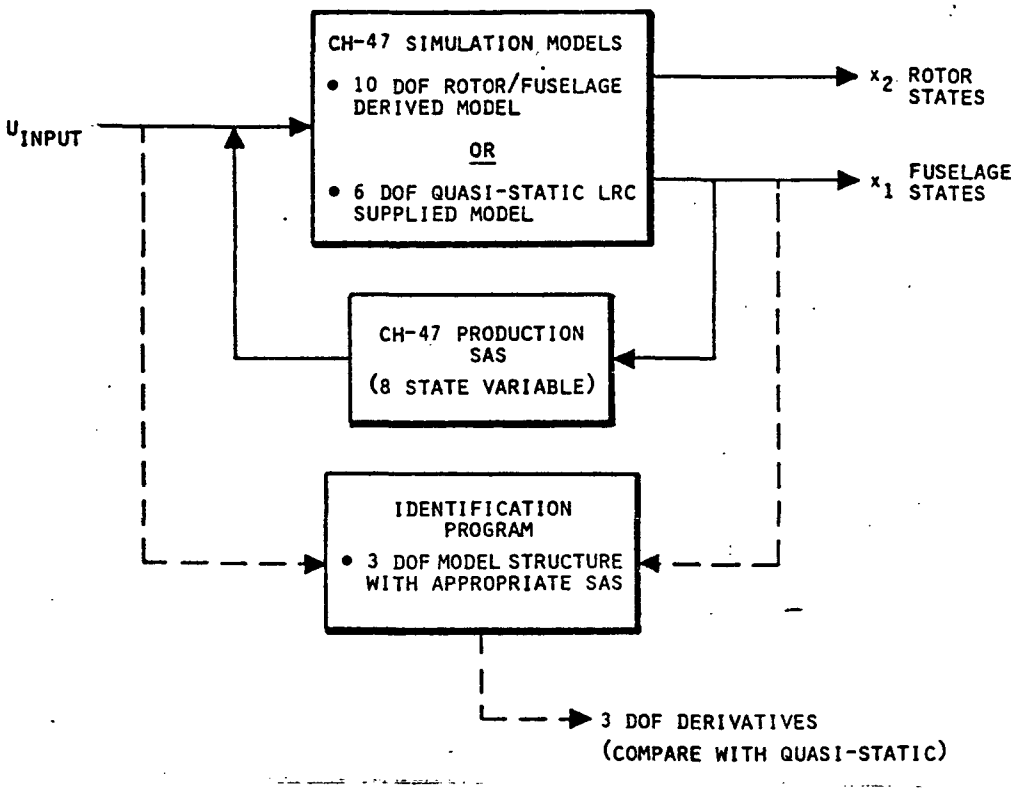

Figure 2.12 Simulation Procedure Employed for Identification of Uncoupled 3 DOF CH-47 Derivatives

The 3 DOF model structure used in the identification procedure including the appropriate SAS is presented in Eq. (2.27) for the longitudinal case and the baseline measurement equation is shown in Eq. (2.28).

$$\begin{bmatrix} \dot{u} \\ \dot{w} \\ \dot{q} \\ \dot{\theta} \\ \dot{v}_1 \\ \dot{v}_2 \\ \dot{v}_3 \end{bmatrix} = \begin{bmatrix} X_u & X_w & X_q - w_o & -g\cos\theta_o & X_{\delta_{LONG}} & 0 & 0 \\ Z_u & Z_w & Z_q + u_o & -g\sin\theta_o & Z_{\delta_{LONG}} & 0 & 0 \\ M_u & M_w & M_q & 0 & M_{\delta_{LONG}} & 0 & 0 \\ 0 & 0 & 1.0 & 0 & 0 & 0 & 0 \\ 0 & 0 & -22.3 & 0 & 0 & 1.0 & 0 \\ 0 & 0 & +56.55 & 0 & 0 & 0 & 1.0 \\ 0 & 0 & -133.73 & 0 & -.0364 & -.8179 & -3.041 \end{bmatrix} \begin{bmatrix} u \\ w \\ q \\ \theta \\ v_1 \\ v_2 \\ v_3 \end{bmatrix} + \begin{bmatrix} X_{\delta_c} & X_{\delta_{LONG}} \\ Z_{\delta_c} & Z_{\delta_{LONG}} \\ M_{\delta_c} & M_{\delta_{LONG}} \\ 0 & 0 \\ 0 & 0 \\ 0 & 0 \end{bmatrix} \begin{bmatrix} \delta_{COLL} \\ \delta_{LONG} \end{bmatrix} \tag{2.27}$$

$$\begin{bmatrix} q \\ \theta \\ A_z \\ A_x \end{bmatrix} = \begin{bmatrix} 0 & 0 & 1.0 & 0 & 0 & 0 & 0 \\ 0 & 0 & 0 & 1.0 & 0 & 0 & 0 \\ Z_u & Z_w & Z_q & 0 & Z_{\delta_{LONG}} & 0 & 0 \\ X_u & X_w & X_q & 0 & X_{\delta_{LONG}} & 0 & 0 \end{bmatrix} \begin{bmatrix} u \\ w \\ q \\ \theta \\ v_1 \\ v_2 \\ v_3 \end{bmatrix} + \begin{bmatrix} 0 & 0 \\ 0 & 0 \\ Z_{\delta_c} & Z_{\delta_{LONG}} \\ X_{\delta_c} & X_{\delta_{LONG}} \end{bmatrix} \begin{bmatrix} \delta_{COLL} \\ \delta_{LONG} \end{bmatrix} \tag{2.28}$$

The lateral model structure is shown in Eq. (2.29) and the baseline measurement equation in Eq. (2.30).

$$\begin{bmatrix} \dot{v} \\ \dot{p} \\ \dot{r} \\ \dot{\varphi} \\ \dot{v}_5 \\ \dot{v}_7 \end{bmatrix} = \begin{bmatrix} Y'_v & Y'_p + w_o & Y'_r - u_o & +g\cos\theta_o & Y_{\delta_{RUD}} & Y_{\delta_{RUD}} \\ L'_v & L'_p & L'_r & 0 & L_{\delta_{RUD}} & L_{\delta_{RUD}} \\ N'_v & N'_p & N'_r & 0 & N_{\delta_{RUD}} & N_{\delta_{RUD}} \\ 0 & 1.0 & \tan\theta_o & 0 & 0 & 0 \\ 0 & 0 & +3.225 & 0 & -.3125 & 0 \\ 0 & 1.5754 & 0 & 0 & 0 & -0.2435 \end{bmatrix} \begin{bmatrix} v \\ p \\ r \\ \varphi \\ v_5 \\ v_7 \end{bmatrix} + \begin{bmatrix} Y_{\delta_{LAT}} & Y_{\delta_{RUD}} \\ L_{\delta_{LAT}} & L_{\delta_{RUD}} \\ N_{\delta_{LAT}} & N_{\delta_{RUD}} \\ 0 & 0 \\ 0 & 0 \\ 0 & 0 \end{bmatrix} \begin{bmatrix} \delta_{LAT} \\ \delta_{RUD} \end{bmatrix} \tag{2.29}$$

where

$$Y'_v = Y_v + K_v Y_{\delta_{RUD}},\quad Y'_p = Y_p + K_p Y_{\delta_{LAT}},\quad Y'_r = Y_r + K_r Y_{\delta_{RUD}}$$

$$L'_v = L_v + K_v L_{\delta_{RUD}},\quad L'_p = L_p + K_p L_{\delta_{LAT}},\quad L'_r = L_r + K_r L_{\delta_{RUD}}$$

$$N'_v = N_v + K_v N_{\delta_{RUD}},\quad N'_p = N_p + K_p N_{\delta_{LAT}},\quad N'_r = N_r + K_r N_{\delta_{RUD}}$$

$$\begin{bmatrix} p \\ r \\ \varphi \\ A_y \end{bmatrix} = \begin{bmatrix} 0 & 1.0 & 0 & 0 & 0 & 0 \\ 0 & 0 & 1.0 & 0 & 0 & 0 \\ 0 & 0 & 0 & 1.0 & 0 & 0 \\ Y'_v & Y'_p & Y'_r & 0 & Y\delta_{RUD} & Y\delta_{RUD} \end{bmatrix} \begin{bmatrix} v \\ p \\ r \\ \varphi \\ v_5 \\ v_7 \end{bmatrix} + \begin{bmatrix} 0 & 0 \\ 0 & 0 \\ 0 & 0 \\ Y\delta_{LAT} & Y\delta_{RUD} \end{bmatrix} \begin{bmatrix} \delta_{LAT} \\ \delta_{RUD} \end{bmatrix} \qquad (2.30)$$

The longitudinal model includes the complete pitch SAS, whereas the lateral SAS, which contains 5 state variables, was reduced to the 2 state-variable SAS as shown in Eq. (2.29). This is justified since the frequency associated with the SAS state variables which are deleted is very high. The three SAS variables deleted are roll rate feedback (v_4), yaw rate feedback (v_6), and sideslip (v_8), with time constants of 0.047, 0.098, and 0.174 respectively. It should be noted that the roll and yaw SAS time constants are in the vicinity of the rotor modes and, since the rotor is not modeled in this analysis, these SAS state variables are deleted.

The effect of the reduced SAS in the lateral equations (Eq. (2.29)) is to modify the open-loop derivatives as indicated by the primed derivative values (e.g., $Y'_v = Y_v + K_v\, Y\delta_{RUD}$). The primed values are the parameters to be identified and the open-loop values are then derived (e.g., $Y_v = Y'_v - K_v\, Y\delta_{RUD}$).

2.4 INSTRUMENTATION AND DATA ACQUISITION

Instrumentation and the aircraft data recording facilities constitute one of the factors influencing parameter identification accuracy. An extensive analysis of this factor is documented in Ref. 3, with further investigations published in Refs. 18 and 19. The modeling of the instrumentation of the VALT Research Aircraft and LRC data recording facilities follows the procedures and conclusions presented in Ref. 3.

Figure 2.13 presents an overall diagram of the instrumentation modeling procedure used in this investigation. The CH-47 is shown with SAS operative, and the vehicle sensors and LRC data recording system models are shown in this figure. The models indicated in Figure 2.13 include dynamic lags, scale factor matrices, random error, and bias errors on both system measurements and control measurements.

The baseline values used to represent the sources of error indicated in Figure 2.13 are presented in Table 2.4. These values were obtained by examination of the individual error specification sheets associated with the instrumentation of the CH-47 VALT Program Research Aircraft, the PADS (Piloted Aircraft Data System), and the RAGS (Research Aircraft Ground Station Data Reduction System) data systems. Although these specification sheets present essentially overall system upper bound accuracy limits which are not representative of Gaussian standard deviations (1σ), the values presented in Table 2.4 were selected based upon best estimates which take into account those considerations addressed in Ref. 3.

In addition to the baseline (nominal) error magnitudes presented in Table 2.4, both larger and smaller error magnitudes were investigated in this study. These error magnitudes will be further discussed and presented in the section which gives results of the simulation study (Section 3.1.1).

2.5 FLIGHT ENVIRONMENT

The flight test environment constitutes an important factor in the identification of aircraft stability and control derivatives. Its importance to helicopter identification is a result of low speed, low altitude flight and the high level of vehicle sensitivity to wind gust due to the speed dependent stability derivatives (e.g., M_u and M_w). The flight test environment

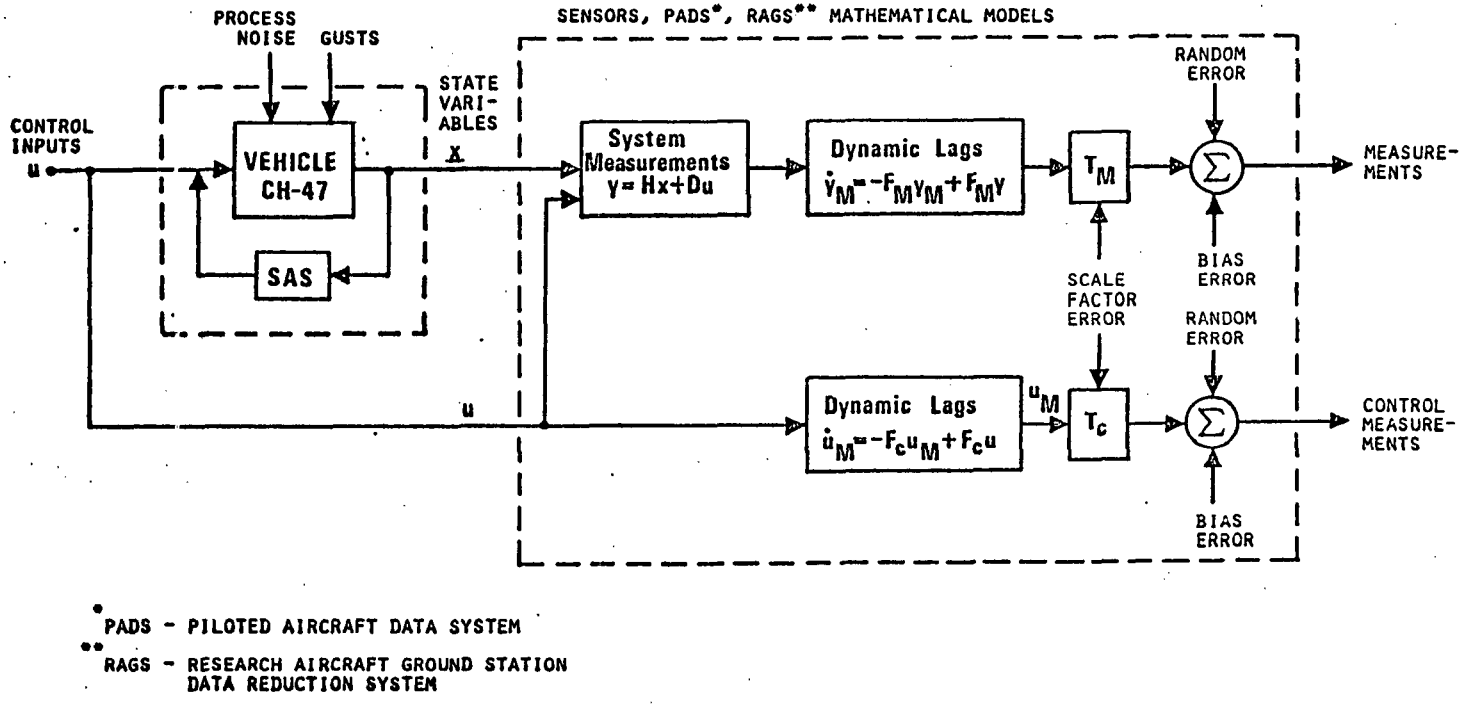

Figure 2.13 Instrumentation and Data Recording Mathematical Model Errors

Table 2.4 Nominal CH-47 VALT Flight Instrumentation Measurement Errors

MEASUREMENT	UNITS	RANGE	NATURAL[1] FREQ. Hz	RANDOM[2] NOISE 1σ	RANDOM BIAS 1σ	SCALE FACTOR % FS
Rate Gyros: p, q, r	deg/sec	±80	10-25	.033	.033	.2
Attitude Gyros: θ, φ, ψ	deg	±80	---	.066	.066	.2
Linear Accel.: A_x, A_y, A_z	g's	±.5 .5 to 1.5	High Freq. Type	.0033	.0033	.1
Control Inputs: δ_{LONG}, δ_{COLL}, δ_{LAT}, δ_{RUD}	cm	25.4	---	.127	.127	.5
Radar: $\dot{x}$, $\dot{y}$, $\dot{z}$	m/sec		---	.305	---	---

[1] Instrument lags and data filters > 10 Hz, thus ignored

[2] Misalignment and mass unbalance included

important to identification accuracy can be considered to consist of three elements: random turbulence, wind shear, and ground effects. Each of these are discussed in the following.

Random Turbulence. The random turbulence model used in this study is based upon theoretical and experimental information. The nature of random turbulence in the general case is such that present theoretical and experimental analysis techniques only approximate the actual random characteristics. The simplest model for wind gust is the well known Dryden model of atmospheric turbulence. Extensions and developments are continually being researched to improve upon this characterization [20]. Among those included are modeling effects directed toward the non-Gaussian nature of turbulence (in particular, "patchiness"), spatial and time variability, and nonisotropic representation. Although each of these modeling areas represents an improvement in the actual characterization of random turbulence, it is not the intent of this investigation to model wind gust, but to assess the influence of random wind disturbances on parameter identification accuracy. For this reason, the Dryden model is chosen. The following three assumptions are made in regard to the wind turbulence model used in this investigation:

- Isotropic (i.e., equal scale lengths and zero cross-spectra)
- The turbulence field is "frozen" (i.e., time and spatial frequencies are related by the relative tip airspeed of the rotor)
- The power spectral density for the horizontal velocity component is used for the lateral and vertical components

The last assumption is believed to have no consequence on the general conclusions of this study. The vertical and lateral Dryden model spectrums differ slightly in comparison to the longitudinal axis, thus modifying the distribution of energy in the low frequency region.

Equation (2.31) presents the Dryden gust spectral representation (Ref. 20).

$$\phi_u(\omega) = \frac{\sigma_u^2}{\omega_o \pi} \frac{2}{[1+(\omega/\omega_o)^2]} = \underbrace{\phi_v = \phi_w}_{\text{assumed for this study}} \qquad (2.31)$$

where,

$\omega_o = (\Omega R + V)/\ell$

Ω = rotor rotational speed, not the spatial frequency

The turbulence scale length, ℓ, is set to 122 meters. The spectral break frequency ω_o is a function of airspeed, rotor tip speed, and correlation distance. (Rotor tip speed is used to modify airspeed since at hover, the break frequency goes to zero and, as computed in Ref. 12, gives an improved representation based upon simulation analysis.)

Equation (2.32) presents the time domain version of the longitudinal gust model and is used throughout this investigation for modeling all three axes as discussed above.

$$\dot{u}_g = -\omega_o u_g + \omega_o \zeta(t) \qquad (2.32)$$

At hover, $\omega_o = 1.8$ rad/sec and $\zeta(t)$ represents random white Gaussian noise with standard deviations selected such that the output of Eq. (2.32) has standard deviations of σ_u.

Table 2.5 summarizes definitions of the turbulence level assumed for this investigation.

Mean Wind Profile (Wind Shear). In addition to random turbulence, parameter identification accuracy may also be affected by the presence of a wind shear. This is particularly true in a landing approach where the wind shear effect is most pronounced. As the vehicle descends in the presence of a wind shear, the wind velocity decreases and this changes the relationship between

Table 2.5
Definitions of Turbulence Level

1σ GUST VELOCITY M/SEC	TURBULENCE LEVEL
0 - .91	CALM AIR
.91 - 1.82	LIGHT
1.82 - 2.44	MODERATE
> 2.44	HEAVY

the inertial and airmass relative velocity vectors. Depending upon how a pilot handles the helicopter in the wind shear (i.e., does he hold Θ, v_T, $\dot{h}$?) and the vehicle's inertial properties, the measured accelerations will vary due to the wind shear. Parameter identification accuracy is, thus, dependent upon knowing the relationship between the inertial and relative velocity vectors.

For this study, a detailed quantitative appraisal of wind shear effects on parameter identification accuracy is not made. Because of this, the proposed flight test plan is premised on testing only when significant shears are not present.

Ground Effect. Ground effect is usually modeled as a correction to thrust coefficient as a function of hub altitude from the ground and hub velocity. This correction is typically insignificant above altitudes one-half to three-fourths of the rotor diameter. Above approximately 15 meter altitude, the CH-47 can be expected to be out-of-ground effect. The procedure recommended for determining the influence of ground effect is to test the flight vehicle at two conditions--in-ground effect (below 50 meters) and out-of-ground effect (above 15 meters). Parameters identified at each condition can be compared and differences in parameter values attributed to the proximity of the ground.

2.6 FLIGHT TEST INPUT DESIGN CONSIDERATIONS

The design of flight test control inputs is complicated for rotorcraft due to the many constraints imposed upon the design. These constraints include simplicity for practical implementation, good excitation of modes for good identifiability, frequency constraints to avoid excessive rotor excitation, state variable constraints to retain linearity, and pilot stabilization at various flight test conditions. In addition, the presence of a dynamic state variable SAS required for additional stability complicates any analytic design procedure since it is desired to identify open-loop derivatives with the SAS operative. Figure 2.14 summarizes those considerations important to rotorcraft input design for parameter identification including the various constraints imposed for the CH-47. The nominal flight test input design used in this effort is of the shape shown in this figure. Details of the actual inputs recommended will be presented in the next chapter.

- GOOD EXCITATION OF DESIRED MODES: (GOOD IDENTIFIABILITY)

$$\delta = A_1 \sin \omega_1 t + A_2 \sin \omega_2 t \quad ; \text{ SINGLE CYCLE FOR PRACTICAL IMPLEMENTATION}$$

(ω_1: SHORT PERIOD MODE; ω_2: LONG PERIOD MODE)

- FREQUENCY CONSTRAINT TO PREVENT EXCITATION OF ROTOR MODES
- STATE CONSTRAINTS TO RETAIN LINEARITY:
  - EXCITATION OF LONG. VELOCITY, VERTICAL VELOCITY FIXED
  - EXCITATION OF VERTICAL VELOCITY, LONG. VELOCITY FIXED
- PILOT STABILIZATION REQUIRED 40 TO 60 KTS

NOMINAL FLIGHT TEST INPUT DESIGN

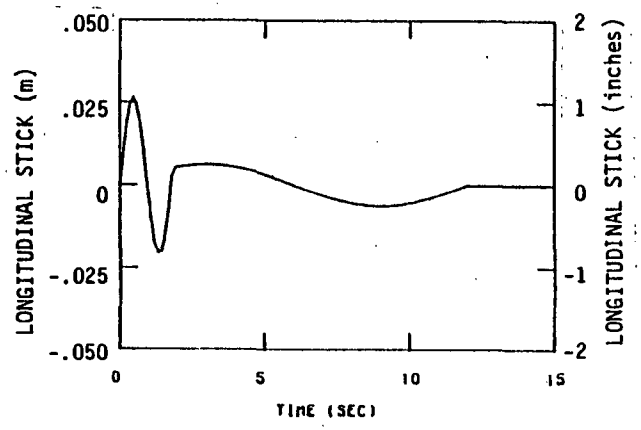

	DECOUPLING THROUGH SAS	PILOT STABILIZATION REQUIRED
HOVER	✓	
20 KTS	✓	
40 KTS	✓	✓
60 KTS	✓	✓

Figure 2.14 Flight Test Input Design

III. IDENTIFICATION RESULTS USING CH-47 SIMULATION

This chapter presents the simulation results upon which the CH-47 flight test design is based. All simulation runs include the CH-47 production SAS with the roll rate feedback gain divided by a factor of two (except where noted) to eliminate fuselage/rotor coupling as discussed in detail in Chapter II (Section 2.2.2). The procedure employed in the simulation studies follows the Technical Approach outlined in Figure 1.2.

Table 3.1 provides a summary of the simulation conditions investigated in this study. The models employed at the 40 kt and 60 kt conditions are derived from the C-81 simulation program and the models used for the hover condition were supplied by LRC. The conditions indicated by the check (✓) represent actual computer simulations. The previously mentioned computational problems with C-81 precluded a detailed evaluation of all test points.

3.1 LONGITUDINAL IDENTIFICATION RESULTS AT THE 40 KT CONDITION

This section presents the longitudinal identification results at the 40 kt condition. This analysis is generated from the 10 DOF, 6 DOF, or 3 DOF models shown in Appendix A; and control inputs consist of either a longitudinal input (differential collective) applied separately or in combination with a collective input. This section summarizes the various control inputs investigated and presents the final input designs recommended for flight test.

Table 3.1

Simulation Conditions Examined Leading to Flight Test Specification

EFFECT ON DERIVATIVE IDENTIFICATION ACCURACY OF:	40 KTS (C-81 MODELS)	HOVER (REF. 1 MODELS)	60 KTS SPIRAL (C-81 MODELS)
1. COUPLING, ROTOR DOF, NONLINEARITIES			
3 DOF	✓	✓	
6 DOF	✓	✓	✓ (Linear & Non-linear Simulation)
10 DOF	✓		
Model Structure Determination	✓		
Aerodynamic Nonlinearities	— Qualitative, See Chapter 2 —		✓
SAS Redesign	✓	✓	
2. CONTROL INPUTS			
Longitudinal:			
o δ_{LONG}, Multicycle	✓		
o δ_{LONG}, Single Cycle	✓		✓
o δ_{LONG} and δ_{COLL}	✓		
o δ_{LONG} - Long./Pitch Excitation		✓	
o δ_{COLL} - Vert. Excitation		✓	
Lateral:			✓
o δ_{LAT} and δ_{RUD}	✓		
o δ_{LAT} - Sideslip/Roll Excitation		✓	
o δ_{RUD} - Yaw Excitation		✓	

Table 3.1
(Concluded)

EFFECT ON DERIVATIVE IDENTIFICATION ACCURACY OF:	40 KTS (C-81 MODELS)	HOVER (REF. 1 MODELS)	60 KTS SPIRAL (C-81 MODELS)
3. INSTRUMENTATION ERRORS			
• Random Noise, Meas.	✓	✓	
• Bias Error; Meas., Controls		✓	
• Scale Factor		✓	
• Process Noise		✓	
• Radar			
• Airspeed			
• Sample Rate, Record Length Lags, IC's	---	REF. 3	---
4. ENVIRONMENT			
• Wind Gust			
• Long. u_g		✓	
w_g		✓	
v_g		✓	
• Lat. v_g		✓	
• Rotor/Fuselage	✓		
• Wind Shear	— Qualitative, see Chapter 2 —		
• Ground Effect	— Qualitative, see Chapter 2 —		

3.1.1 Control Input Design Procedure and Simulation Results

The 3 DOF closed-loop model representing the CH-47 at the 40 kt condition was used for designing inputs. The characteristic roots of the closed-loop system, natural frequency, damping, and period are presented below.

Table 3.2
CH-47 Closed-Loop Characteristic Roots (40 Kts)

	EIGENVALUE	ω_n	ζ	T (SECS)
Pitch Damping + SAS:	$-1.977 \pm j2.80$	3.43	.572	1.83
Vertical/Long.:	$-.517 \pm j.09348$	.525	.984	12.0
Long. Divergent + SAS:	$-.000092 \pm j.0859$	.0859	.0107	73.0
SAS:	-.0468	0	---	---

The longitudinal input shown in Eq. (3.1) was initially selected such that the three frequencies were chosen to be those of the closed-loop natural frequencies.

$$\delta_{LONG} = 10.2 \sin 3.43t + 2.5 \sin .525t + 2.5 \sin .0859t \text{ (cm)} \quad (3.1)$$

Application of this input to the closed-loop CH-47 model resulted in state variable responses of very large magnitudes; considerably greater than the small perturbations of the linear model. After several simulation attempts with different control inputs, the input design shown in Eq. (3.2) was found to produce acceptable state response:

$$\delta_{LONG} = A_1 \sin 3.43t + A_2 \sin .424t \text{ (cm)} \quad (3.2)$$

where, based on simulation in response evaluation,

$$A_1 = \begin{cases} 2.5 & t < 7.32 \text{ sec} \\ 0.0 & t \geq 7.32 \end{cases}$$

$$A_2 = \begin{cases} .64 & t < 12.0 \\ 0 & t \geq 12.0 \text{ sec} \end{cases}$$

The input used in Eq. (3.2) is such that four complete cycles occur at the frequency 3.43 rad/sec, and one complete cycle at the frequency 0.525 rad/sec. This input excites all of the longitudinal state variables with good amplitude, yet the perturbations are within the linear model assumptions.

The input design of Eq. (3.2) was used to generate data for use in the identification phase. The data were contaminated with random noise and the length of data used was 15 sec, sampled at 0.04 sec increments.

The longitudinal model of Eqs. (2.27) and (2.28) was used to assess the effects of random noise on derivative prediction accuracy. This investigation also determines if it is possible to obtain accurate identification using only the measurements of Eq. (2.28). Random noise was added to the measurements and was chosen to be that used in the previous instrumentation requirements study of Ref. 3. The random noise was selected to be the large noise case and is shown in Eq. (3.3).

$$\begin{aligned} \sigma_q &= .0017 \text{ rad/sec} \\ \sigma_\theta &= .0034 \text{ rad} \\ \sigma_{A_Z} &= .01 \text{ g's} \\ \sigma_{A_X} &= .01 \text{ g's} \end{aligned} \qquad (3.3)$$

The data base generated using the 3 DOF model shown in Eqs. (2.27) and (2.28) was used to identify the open-loop stability and control derivatives. The level of measurement noise used is as shown in Eq. (3.3) and the control input used is shown in Eq. (3.2). The maximum likelihood identification program (SCIDNT) was modified to accommodate the model structure shown in Eqs. (2.27) and (2.28).

Table 3.3 summarizes the results of the identification and presents the parameter start-up used, maximum likelihood estimated parameters and a 1σ band, and the actual error.

Table 3.3

Results of Longitudinal 3 DOF Maximum Likelihood Identification (V = 40 Kts, High Noise Case)

IDENTIFIED PARAMETER	ASSUMED TRUE PARAMETER VALUE	INITIAL GUESS	ML ESTIMATED PARAMETER	ML EST. 1σ	(ABS) ACTUAL PAR. ERROR	ACTUAL % ERROR
X_u	-.0087	-.01	-.00399	.00244	.00742	54.1
Z_u	-. 117	.0	-.1148	.00805	.0096	1.9
M_u	-.00705	.0	.00761	.0001716	.00056	7.9
X_w	.06069	.0	.09664	.01308	.03595	59.0
Z_w	-.6566	-.5	-.6248	.01949	.0318	4.84
M_w	.0121	.003	.01236	.000814	.00020	1.62
M_q	-1.329	-1.0	-1,3225	.006045	.0065	.49
$X_{\delta_{LONG}}$	2.9484	.0	2.14896	.45276	.79944	27.1
$Z_{\delta_{LONG}}$	8.5380	2.4	8.4324	.57684	.1056	1.24
$M_{\delta_{LONG}}$	-15.5906	-11.811	-1.29941	-15.5929134	.02362	.0151

Examination of the actual error in the estimated derivatives of Table 3.3 reveals that all derivatives are identified with less than 10% error with the exception of X_u, X_w, and $X_{\delta_{LONG}}$. These derivatives all occur in the X-force equation. The longitudinal acceleration A_x provides most of the information regarding these derivatives and the level of random noise used on the A_x measurement is nearly as large as the signal level. This accounts for the poor accuracy on the X-force derivatives. Also, it should be noted that the level of noise chosen for the A_x measurement (0.01 g's) represents the high noise case. Reduction of this noise level to be more representative of light data can improve the accuracy further.

In developing a control input for actual implementation, it is desirable to have simplicity in the shape of the input, yet retain good accuracy in identified parameters. The effect of simplifying the shape of the input shown in Eq. (3.2) is presented below, along with the effect of noise level, lateral-to-longitudinal coupling, and rotor degrees of freedom.

The time history response data is generated from the 3 DOF, 6 DOF, and 10 DOF linear C-81 derivative model at the 40 kt condition. In each case, the complete CH-47 SAS is included. Table 3.4 summarizes the various sets of data generated for use

Table 3.4

Summary of Time History Data Generated for Use with SCIDNT (CH-47C C-81 Models, 40 Kts)

MODEL USED IN DATA GENERATION (SAS-ON)	MULTIPLE CYCLE INPUT			1 CYCLE INPUT
	NEGLIGIBLE NOISE	NOMINAL NOISE	HIGH NOISE	LOW NOISE
3 DOF	✓	✓	✓	✓
6 DOF			✓	
10 DOF		✓	✓	✓

in the parameter identification program (SCIDNT). Table 3.5 summarizes the noise levels used for the cases described in Table 3.4.

Table 3.5
Noise Levels Used in Data Simulation

TIME HISTORY MEASUREMENT	NOISE LEVEL STANDARD DEVIATIONS		
	NEGLIGIBLE[1]	NOMINAL[2]	HIGH
q rad/sec	.0000173	.00054	.00173
θ rad	.0000173	.0011	.0034
A_x g's	.0001	.0033	.01
A_z g's	.0001	.0033	.01

[1] Negligible noise = $\sigma_{High} \div 100$

[2] Nominal noise = $\sigma_{High} \div 3$

Two different longitudinal control inputs (differential collective) were investigated: (1) a multiple cycle input, and (2) a single cycle input. These inputs are shown below.

Multiple Cycle Input

$$\delta_{LONG} = \overbrace{A_1 \sin 3.43t}^{4 \text{ cycles}} + \overbrace{A_2 \sin .525t}^{1 \text{ cycle}} \quad \text{cm} \qquad (3.4)$$

$$A_1 = \begin{cases} 2.54 & t < 7.32 \text{ sec} \\ 0.0 & t \geq 7.32 \text{ sec} \end{cases}$$

$$A_2 = \begin{cases} 0.635 & t < 12.0 \text{ sec} \\ 0.0 & t \geq 12.0 \text{ sec} \end{cases}$$

Single Cycle Input

$$\delta_{LONG} = \overbrace{A_1 \sin 3.43t}^{1 \text{ cycle}} + \overbrace{A_2 \sin .525t}^{1 \text{ cycle}} \quad \text{cm} \qquad (3.5)$$

$$A_1 = \begin{cases} 2.54 & t < 1.8 \text{ sec} \\ 0.0 & t \geq 1.8 \text{ sec} \end{cases}$$

$$A_2 = \begin{cases} 0.635 & t < 12.0 \text{ sec} \\ 0.0 & t \geq 12.0 \text{ sec} \end{cases}$$

These inputs contain two frequencies ($\omega_1 = 3.43$, $\omega_2 = .525$ rad/sec) which were chosen to be equal to the natural frequencies of the closed-loop system. The multiple frequency input of Eq. (3.4) contains 4 complete cycles of high frequency, which is designed to excite the short period mode of the closed-loop system. The low frequency input contains 1 cycle and is designed to excite the longitudinal/vertical coupled mode and long period mode.

The single cycle input shown in Eq. (3.5) is used in this study to assess whether accuracy in derivative identification is impaired as compared to the multiple cycle input. The single cycle input is preferred in a flight test program due to its simplicity (essentially a doublet) and if accuracy is not degraded, is the recommended input for implementation.

SCIDNT was used to assess the effects on derivative identification accuracy of: (1) noise level, (2) longitudinal-to-lateral coupling, (3) rotor degrees-of-freedom, and (4) control input simplification. In each case, the model structure programmed in SCIDNT contains only the longitudinal 3 DOF derivative model with longitudinal SAS. The form of the equation used in SCIDNT is presented in Eqs. (2.27) and (2.28). The influence of: (1) noise

level, (2) longitudinal-to-lateral coupling, (3) rotor degrees-of-freedom, and control input simplification, are determined. (Refer to Table 3.4 for a summary of the cases investigated.)

Effect of Noise Level on Derivative Identification Accuracy

The effect of noise level on derivative identification accuracy is summarized in Table 3.6. Data are generated from the 3 DOF longitudinal model for the three cases—negligible noise, nominal noise, and high noise. For each case, the identified derivative values and error in the estimate are presented. As shown in Table 3.6, all derivatives are identified with less than 10% error (excellent accuracy) for the nominal noise case. The high noise case causes further degradation in the accuracy of the derivatives X_u, X_w and $X_{\delta_{LONG}}$. The reason for this is that the term $(g \cos \theta_o)\theta$ contributes significantly to the u time history; thus, the derivatives X_u, X_w, and $X_{\delta_{LONG}}$ are difficult to identify when noise is high. The results of Table 3.6 indicate that for the noise levels typical of flight data (nominal noise case), accuracy will be excellent.

Effect of Longitudinal-to-Lateral Coupling on Derivative Identification Accuracy

The effects of lateral coupling on longitudinal identification accuracy were determined by generating time history data using the 6 DOF coupled longitudinal and lateral model (with complete SAS) and attempting to identify only the 3 DOF longitudinal derivatives. Again, the 3 DOF (with SAS) model was used in SCIDNT. Table 3.7 summarizes the identification results for the high noise case and shows identified derivatives from data generated by the 3 DOF simulation and the 6 DOF simulation.

A comparison of 3 DOF and 6 DOF results (Table 3.7) reveals that lateral coupling altered the prediction accuracy in X_u

Table 3.6

Effect of Noise Level on Derivative Identification Accuracy
(Data Generation from 3 DOF Model with SAS, CH-47C, 40 KTS)

PARAMETER	C-81 TRUE PARAMETER VALUE	NEGLIGIBLE NOISE		NOMINAL NOISE		HIGH NOISE	
		MAXIMUM LIKELIHOOD ESTIMATED PARAMETER	% ERROR	MAXIMUM LIKELIHOOD ESTIMATED PARAMETER	% ERROR	MAXIMUM LIKELIHOOD ESTIMATED PARAMETER	% ERROR
X_u	-.01141	-.01218	6.7	-.0107	5.3	-.00399	65.0
Z_u	-.1244	-.1186	4.7	-.1182	5.0	-.1148	7.7
M_u	.00705	.00761	7.9	.00735	4.7	.00761	7.9
X_w	.06069	.0595	2.0	.05309	12.5	.0966	59.0
Z_w	-.6566	-.6501	0.1	-.6366	3.0	-.6248	4.8
M_w	.0121	.0128	5.4	.0112	8.1	.01234	1.6
M_q	-1.329	-1.325	0.3	-1.318	1.0	-1.322	0.5
$X_{\delta_{Long}}$	2.9484	2.9652	0.6	3.2508	10.3	2.1492	27.1
$Z_{\delta_{Long}}$	8.5380	8.4516	1.0	8.2656	3.2	8.4324	1.2
$M_{\delta_{Long}}$	-15.5906	-15.6220	0.2	-15.5748	0.1	-15.5929	0.01

LOW NOISE = $\sigma_{HIGH} \div 100$

NOMINAL NOISE = $\sigma_{HIGH} \div 3$

Table 3.7

Effect of Lateral Coupling and Rotor DOF on Longitudinal Derivative Identification Accuracy (High Noise Case)

PARAMETER	C-81 TRUE PARAMETER VALUE	DATA FROM 3 DOF SIMULATION		DATA FROM 6 DOF SIMULATION		DATA FROM 10 DOF SIMULATION	
		MAXIMUM LIKELIHOOD ESTIMATED PARAMETER	% ERROR	MAXIMUM LIKELIHOOD ESTIMATED PARAMETER	% ERROR	MAXIMUM LIKELIHOOD ESTIMATED PARAMETER	% ERROR
X_u	-.01141	-.00399	65.9	-.01066	6.6	-.01192	4.5
Z_u	-.1244	-.1148	7.7	-.1186	4.7	-.12715	2.2
M_u	.00705	.00761	7.9	.00696	1.4	.00650	7.9
X_w	.06069	.0966	59.0	.03508	42.2	.02093	65.5
Z_w	-.6566	-.6248	4.8	-.6199	5.6	-.6200	5.6
M_w	.0121	.01234	1.6	.00869	28.4	.0046	61.1
M_q	-1.329	-1.322	0.5	-1.318	0.8	-1.195	10.1
$X_{\delta_{Long}}$	2.9484	2.1492	27.1	3.9048	32.4	4.2300	43.5
$Z_{\delta_{Long}}$	8.5380	8.4324	1.2	7.9704	6.7	7.6524	10.4
$M_{\delta_{Long}}$	-15.5906	-15.59291	0.01	-15.5945	0.03	-15.2638	2.1

Errors Due to Random Noise

Errors Due to Random Noise + Lat. Coupling

Errors Due to Random Noise + Lat. Coupling + Rotor DOF

and M_w and that the accuracy in other derivatives is essentially the same. The derivative M_w is affected by coupling because its contribution to the q time history is very small at this condition (40 kts) using the C-81 derivative model. (Note that the C-81 value for M_w is .0037, whereas the Ref. 1 derivative for M_w is .0207; five times as large.) The finding that lateral coupling has a negligible effect on longitudinal derivative identification is due to two factors: (1) longitudinal inputs do not excite the lateral-directional degrees of freedom, and (2) lateral-directional motions are suppressed by the stability augmentation system.

Effect of Rotor Degrees-of-Freedom on Derivative Identification Accuracy

The effect of rotor DOF on derivative identification accuracy was determined by generating time history data using the 10 DOF fuselage-flap derivative model (with complete SAS) and identifying only the 3 DOF longitudinal derivatives. Table 3.7 summarizes the identification results for the high noise case and shows the results when using 3 DOF, 6 DOF and 10 DOF simulation data (SAS-on). Notice that there is further degradation of M_w (61.1% error), M_q is now at 10.1% error, and the X-force derivative (X_w and $X_{\delta_{LONG}}$) errors are a combined result of high noise level, lateral coupling, and rotor DOF.

Table 3.8 summarizes the effect of both lateral coupling and rotor degrees-of-freedom on derivative identification accuracy for the nominal noise case. Identification results from the 10 DOF simulation shows the degradation due to lateral coupling and rotor DOF. Again, M_w is identified to 48.7% error; part of this error due to lateral coupling and part due to rotor DOF. The X-force derivatives X_w and $X_{\delta_{LONG}}$ are identified to 36.7% and 20.8% error, respectively, and these errors

Table 3.8

Effect of Lateral Coupline and Rotor DOF on Derivative Accuracy (Nominal Noise Case)

PARAMETER	C-81 TRUE PARAMETER VALUE	DATA FROM 3 DOF SIMULATION		DATA FROM 10 DOF SIMULATION	
		MAXIMUM LIKELIHOOD ESTIMATED PARAMETER	% ERROR	MAXIMUM LIKELIHOOD ESTIMATED PARAMETER	% ERROR
X_u	-.01141	-.01078	5.3	-.0121	6.7
Z_u	-.1244	-.1182	5.0	-.1203	3.3
M_u	.00705	.00735	4.7	.00676	4.2
X_w	.06069	.0531	12.5	.03837	36.7
Z_w	-.6566	-.6366	3.0	-.6356	3.2
M_w	.0121	.0112	8.1	.00630	48.7
M_q	-1.329	-1.318	1.0	-1.202	9.6
$X_{\delta_{Long}}$	2.9484	3.2508	10.3	3.5592	20.8
$Z_{\delta_{Long}}$	8.5380	8.2656	3.2	7.9392	7.0
$M_{\delta_{Long}}$	-15.5906	-15.5748	0.1	-15.2953	1.9

Errors Due to Random Noise

Errors Due to Random Noise + Lat. Coupling + Rotor DOF

result because of the small influence these derivatives have in the X-force equation. In summary, the prediction trends for the 3 DOF and 10 DOF results are similar for both noise levels investigated.

Effect of Control Input Simplification on Derivative Identification Accuracy

Two different control inputs were investigated for the differential collective control (δ_{LONG}): (1) a multiple cycle input, and (2) a single cycle input. The precise form of the inputs used are shown in Eqs. (3.4) and (3.5). Table 3.9 summarizes the identification results and accuracies obtained for the two inputs using both the 3 DOF simulation and the 10 DOF simulation. The results using the 3 DOF simulation data indicate that the single cycle input yields results nearly as good as the multiple cycle (4 cycles) input. The results using the 10 DOF simulation also indicate that a single cycle input is satisfactory.

Table 3.10 summarizes the eigenvalues from the identified derivatives for the nominal noise case with the single cycle input. Eigenvalues are shown from derivatives identified using the 3 DOF simulation and the 10 DOF simulation and compared with the Ref. 1 3 DOF values. Table 3.10 also shows that the eigenvalues from the identified derivatives using the 3 DOF and 10 DOF simulations are similar and that their agreement with the "true" values is excellent.

An important element of the overall identification is the standard deviations for parameters and measurement noise. Estimated parameters from flight data are themselves incomplete since their usefulness is limited without accuracy confidence bands. Table 3.11 shows the estimated 1σ confidence bands, as determined via the maximum likelihood information matrix. In all cases, except M_u of Table 3.11, the actual errors are represented by either 1σ or 2σ bands. A 2σ band is an upper bound on the errors.

Table 3.12 shows 3σ confidence bands for the nominal case where derivatives were identified using the 10 DOF simulation data. The effects of lateral coupling and rotor DOF degrade the accuracy

Table 3.9

Effect of Control Input Simplification on Derivative Identification Accuracy
(Nominal Noise Case, 40 Knots)

PARAMETER	C-81 TRUE PARAMETER VALUE	USING 3 DOF SIMULATION				USING 10 DOF SIMULATION			
		MULTIPLE CYCLE INPUT		SINGLE CYCLE INPUT		MULTIPLE CYCLE INPUT		SINGLE CYCLE INPUT	
		MAXIMUM LIKELIHOOD ESTIMATED PARAMETER	% ERROR	MAXIMUM LIKELIHOOD ESTIMATED PARAMETER	% ERROR	MAXIMUM LIKELIHOOD ESTIMATED PARAMETER	% ERROR	MAXIMUM LIKELIHOOD ESTIMATED PARAMETER	% ERROR
X_u	-.01141	-.01078	5.3	-.01009	11.6	-.01217	6.7	-.0181	58.5
Z_u	-.1244	-.1182	5.0	-.1155	7.1	-.1203	3.3	-.1211	2.7
M_u	.00705	.00732	4.7	.00745	5.6	.00676	4.2	.00686	2.8
X_w	.06069	.05309	12.5	.0597	1.6	.03837	36.7	.05226	13.9
Z_w	-.6566	-.6366	3.0	-.6401	1.3	-.6356	3.2	-.6378	2.9
M_w	.0121	.0112	8.1	.0118	0.5	.00630	48.7	.00650	45.5
M_q	-1.329	-1.318	1.0	-1.323	0.4	-1.2021	9.6	-1.2148	8.6
$X_{\delta Long}$	2.9484	3.2508	10.3	3.1524	6.9	3.5592	20.8	3.2796	11.3
$Z_{\delta Long}$	8.5380	1.0656	3.2	8.2236	3.7	7.9380	7.0	7.9368	7.0
$M_{\delta Long}$	-15.5906	-15.5748	0.1	-15.6102	0.1	-15.2953	1.9	-15.2913	1.9

Table 3.10

Eigenvalues from Identified Derivatives, Nominal Noise, 1 Cycle Input

	C-81 TRUE EIGENVALUES	USING DERIVATIVES IDENTIFIED FROM 3 DOF SIMULATION	USING DERIVATIVES IDENTIFIED FROM 10 DOF SIMULATION
PITCH DAMPING	$-1.977 \pm j\ 2.804$	$-1.974 \pm j\ 2.806$	$-1.904 \pm j\ 2.775$
VERTICAL/LONGITUDINAL	$-.5174 \pm j\ .0935$	$-.5101 \pm j\ .0966$	$-.524 \pm j\ .0451$
LONGITUDINAL DIVERGENCE	$-.00092 \pm j\ .0859$	$-.00027 \pm j\ .0904$	$.00063 \pm j\ .0929$
SAS	-.0468	-.0468	-.0473

Table 3.11

Parameter Standard Deviations for the Nominal Noise Case, 1 Cycle Input (Derivatives Identified from 3 DOF Simulation Data, 40 Knots)

PARAMETER	C-81 TRUE PARAMETER VALUE	MAX. LIKELIHOOD ESTIMATED		ACTUAL ERROR |ABS.|
		PARAMETER ESTIMATE	1σ*	
X_u	-.01141	-.01009	.0009	.0013
Z_u	-.1244	-.1155	.0034	.0089
M_u	.00705	.00745	.000082	.00039
X_w	.06069	.05970	.0057	.001
Z_w	-.6566	-.6501	.0083	.0165
M_w	.0121	.01207	.00043	.00007
M_q	-1.329	-1.323	.0053	.0054
$X_{\delta_{Long}}$	2.9484	3.1524	.276	.204
$Z_{\delta_{Long}}$	8.5380	8.2236	.3204	.312
$M_{\delta_{Long}}$	-15.5906	-15.6102	.02480	.01966

of the confidence bands. A 3σ to 6σ confidence band more accurately reflects the actual errors in the derivatives when using the 10 DOF simulated data.

Table 3.12

Parameter Standard Deviations for the Nominal Noise Case, 1 Cycle Input (Derivatives Identified from the 10 DOF Simulation Data, 40 Knots)

PARAMETER	C-81 TRUE PARAMETER VALUE	MAX. LIKELIHOOD ESTIMATED		ACTUAL ERROR |ABS.|
		PARAMETER ESTIMATE	3σ*	
X_u	-.01141	-.01809	.003	.0067
Z_u	-.1244	-.12108	.013	.0033
M_u	.00705	.00686	.00020	.00020
X_w	.06069	.05226	.018	.0084
Z_w	-.6566	-.6378	.024	.0187
M_w	.0121	.00650	.0013	.0056
M_q	-1.329	-1.2148	.016	.114
$X_{\delta_{Long}}$	2.9484	3.2796	.864	.3324
$Z_{\delta_{Long}}$	8.5380	7.9368	.936	.6012
$M_{\delta_{Long}}$	-15.5906	-15.2913	.0748	.2992

*3σ bands shown accurately represent only 6 out of 10 actual parameter errors

The measurement noise covariance is estimated in the maximum likelihood program (SCIDNT) and the values for the nominal noise case, 1 cycle input are shown in Table 3.13. As shown in Table 3.13, those obtained using the 3 DOF simulation data and those obtained using the 10 DOF simulation are accurately identified.

Table 3.13

Measurement Noise Standard Deviations Estimated From SCIDNT, Nominal Noise Case, 1 Cycle Input

MEASUREMENT NOISE	TRUE* STANDARD DEVIATION	ESTIMATED STANDARD DEVIATION	
		3 DOF SIMULATION CASE	10 DOF SIMULATION CASE
σ_q rad/sec	.00058	.00073	.00082
σ_θ rad	.00115	.00133	.00134
σA_z g's	.0033	.0032	.0032
σA_x g's	.0033	.0033	.0035

*Used in the simulation

3.1.2 Application of Model Structure Determination

The procedure used throughout this contract is to treat the decoupled problem (i.e., longitudinal separate from lateral). The results of the studies to-date indicate that the presence of lateral coupling provides very little effect on longitudinal identification accuracy. However, the CH-47 flight test vehicle could possibly contain greater coupling than the analytic simulation models and, thus, it would be desirable to determine the degree of coupling in the flight data itself. Also, the question of identification of the cross-coupling derivatives is raised.

Since one of the objectives of this effort is to provide stability and control derivatives for flight control systems design, one consideration is to accurately identify the longitudinal and lateral decoupled derivative arrays. In addition to this, it is required to: (1) determine from the flight data the degree of lateral coupling, and (2) identify the required cross-coupled

derivatives if coupling is found to be significant. The assessment of the amount of lateral coupling can be accomplished through the use of a model structure determination program.

A model structure determination program was applied to the 6 DOF model (with SAS) for a multiple cycle input case [i.e., Eq. (3.4)]. The model structure determination technique operates on the state variables and accelerations of the system and produces the "best model" (i.e., simplest model) required to explain the data. This model building procedure is based upon a step-wise regression procedure which tests the significance of each possible derivative term, adds or deletes the terms from the model, and provides regression estimates of those derivatives found to be significant. The output of this procedure is a reduced order model which explains almost all of the variation occurring in the time history data (e.g., 99% of the variation).

Application of the model structure determination program to time history data from the 6 DOF model (with the 8-state variable SAS) resulted in the model shown in Eq. (3.6).

$$\begin{bmatrix} \dot{u} \\ \dot{w} \\ \dot{q} \\ \dot{\theta} \\ \dot{v}_1 \\ \dot{v}_2 \\ \dot{v}_3 \end{bmatrix} = \begin{bmatrix} X_u & X_w & X_q - w_o & -g\cos\theta_o & X_{\delta_{LONG}} & 0 & 0 \\ Z_u & Z_w & Z_q + u_o & -g\sin\theta_o & Z_{\delta_{LONG}} & 0 & 0 \\ M_u & M_w & M_q & 0 & M_{\delta_{LONG}} & 0 & 0 \\ 0 & 0 & 1.0 & 0 & 0 & 0 & 0 \\ 0 & 0 & -22.3 & 0 & 0 & 1.0 & 0 \\ 0 & 0 & +56.66 & 0 & 0 & 0 & 1.0 \\ 0 & 0 & -153.73 & 0 & -.0364 & -.8179 & -3.041 \end{bmatrix} \begin{bmatrix} u \\ w \\ q \\ \theta \\ v_1 \\ v_2 \\ v_3 \end{bmatrix} + \begin{bmatrix} X_{\delta_{LONG}} \\ Z_{\delta_{LONG}} \\ M_{\delta_{LONG}} \\ 0 \\ 0 \\ 0 \\ 0 \end{bmatrix} \left[\delta_{LONG}\right] \qquad (3.6)$$

The derivative terms provided the following explanation of the time history data:

	REQUIRED DERIVATIVE TERMS	% CONTRIBUTION to X, Z, or $\dot{q}$
X-Force:	X_u, X_w, X_q, $X_{\delta_{LONG}}$	98.82
Z-Force:	Z_u, Z_w, Z_q, $Z_{\delta_{LONG}}$	99.95
$\dot{q}$-Equation:*	M_u, M_q, $M_{\delta_{LONG}}$	99.75

*M_w was found to provide a negligible contribution to the $\dot{q}$ time history.

The lateral terms are thus shown to provide a very small contribution to the longitudinal motion for the control input used. Notice that for the q-equation, the derivatives M_u, M_q, and $M_{\delta_{LONG}}$ contribute 99.75% and M_w contributes a very small amount. This is probably the reason that the identification accuracy of M_w deteriorates when lateral degrees-of-freedom and rotor degrees-of-freedom are present (see Tables 3.7 and 3.8). Also, the M_w in Eq. (3.6) is from C-81 and is one-fifth the size of the LRC derivatives discussed earlier.

This example demonstrates a viable procedure for examination of actual flight data to assess the degree of coupling in any time history response and the derivatives required for identification.

Identification of Cross-Coupling Derivatives

Although the simulation results clearly indicate that the SAS decouples the longitudinal and lateral response, it may be desirable to attempt identification of the cross-coupled derivatives. The procedure recommended for accomplishing this includes the following steps:

(1) Generate one maneuver of data using longitudinal inputs.

(2) Generate one maneuver of data using lateral inputs.

(3) Apply model structure determination program to determine the significant derivatives for each maneuver.

The longitudinal input (step 1) will provide information primarily for the longitudinal uncoupled derivatives. The lateral input (step 2) will provide information primarily for the lateral uncoupled derivatives. These derivative arrays can be identified using SCIDNT. Once these arrays are identified, then the longitudinal input maneuvers (step 1) can be

used with the lateral (uncoupled) derivatives identified from step 2 and the longitudinal-to-lateral coupled derivatives identified. Likewise, the lateral-to-longitudinal (coupled) derivatives can be identified from the maneuver of step 2 using the longitudinal derivatives identified in step 1.

This procedure reduces the problem of overparameterization, reduces the number of parameters required for each SCIDNT run, and should yield all the information required for flight control system design.

3.1.3 Final Control Input Design and Simulation Results

The control input designs of the previous sections are based upon a differential collective input (δ_{LONG}) only. This section presents the results of identification where control inputs for both longitudinal and collective stick are applied simultaneously in the maneuver. The results show improvement in derivative identification accuracy over the one input designs, and represent the final recommended inputs for the 40 kt longitudinal case. This section also presents the time history response for the 40 kt longitudinal case.

Figure 3.1 shows the time history response due to a combined longitudinal (δ_{LONG}) and collective (δ_{COLL}) control input. Each input contains two frequencies representing the short and long period modes of the closed-loop system as discussed previously. The solid line response shown in Figure 3.1 is from the 10 DOF rotor/fuselage/SAS model shown in Appendix A and the plus (+) symbols are from the 3 DOF decoupled longitudinal model (with longitudinal SAS) also shown in Appendix A. The 3 DOF response is shown to accurately duplicate the 10 DOF response, thus indicating that a 3 DOF model would be sufficient for derivative identification purposes (rotor DOF and lateral coupling are shown to have a negligible effect for the control inputs

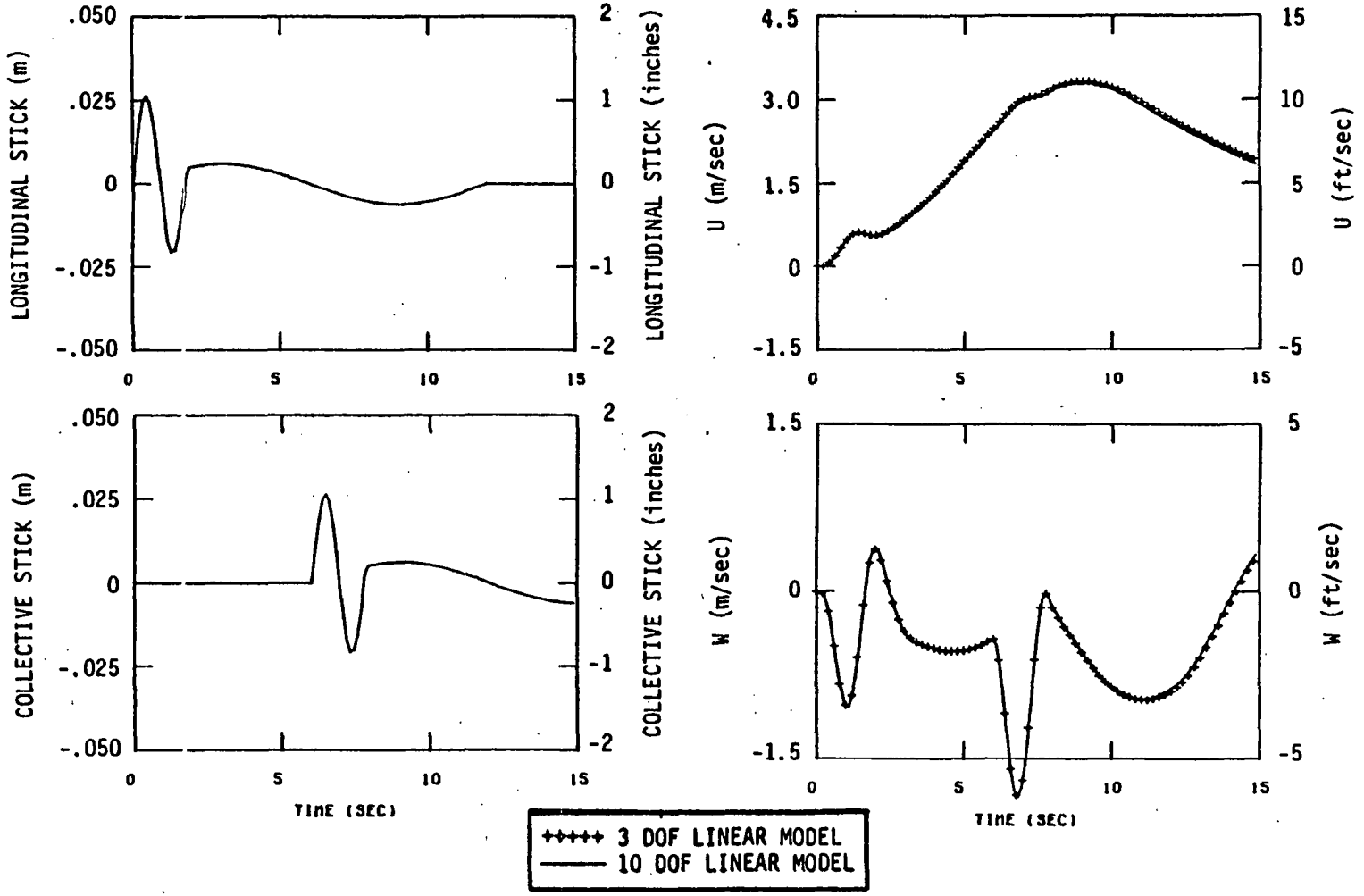

Figure 3.1 Time History Response from the 10 DOF Linear C-81 Model Due to a Combined Longitudinal and Collective Control Input (40 KTS)

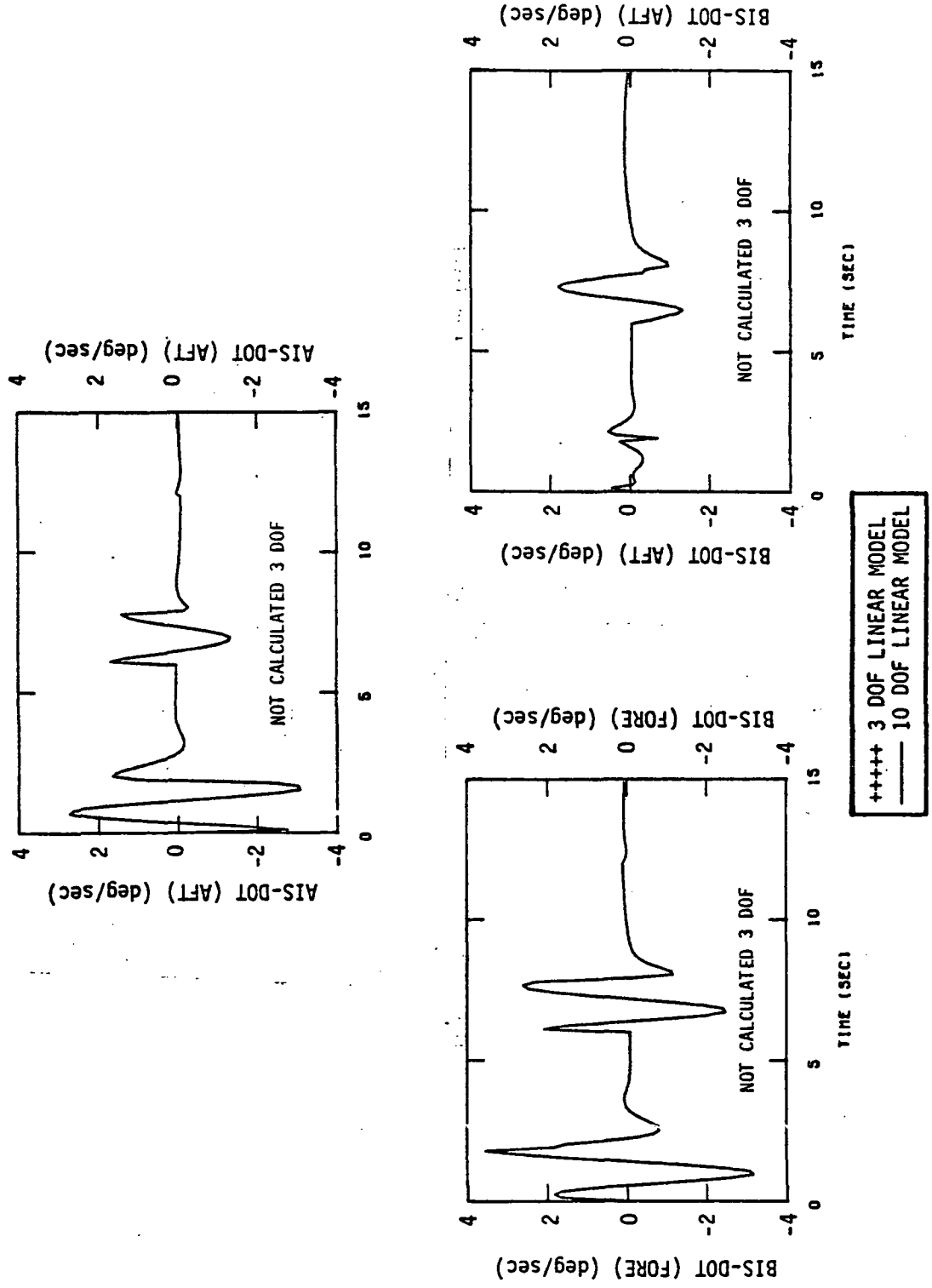

Figure 3.1 (Continued)

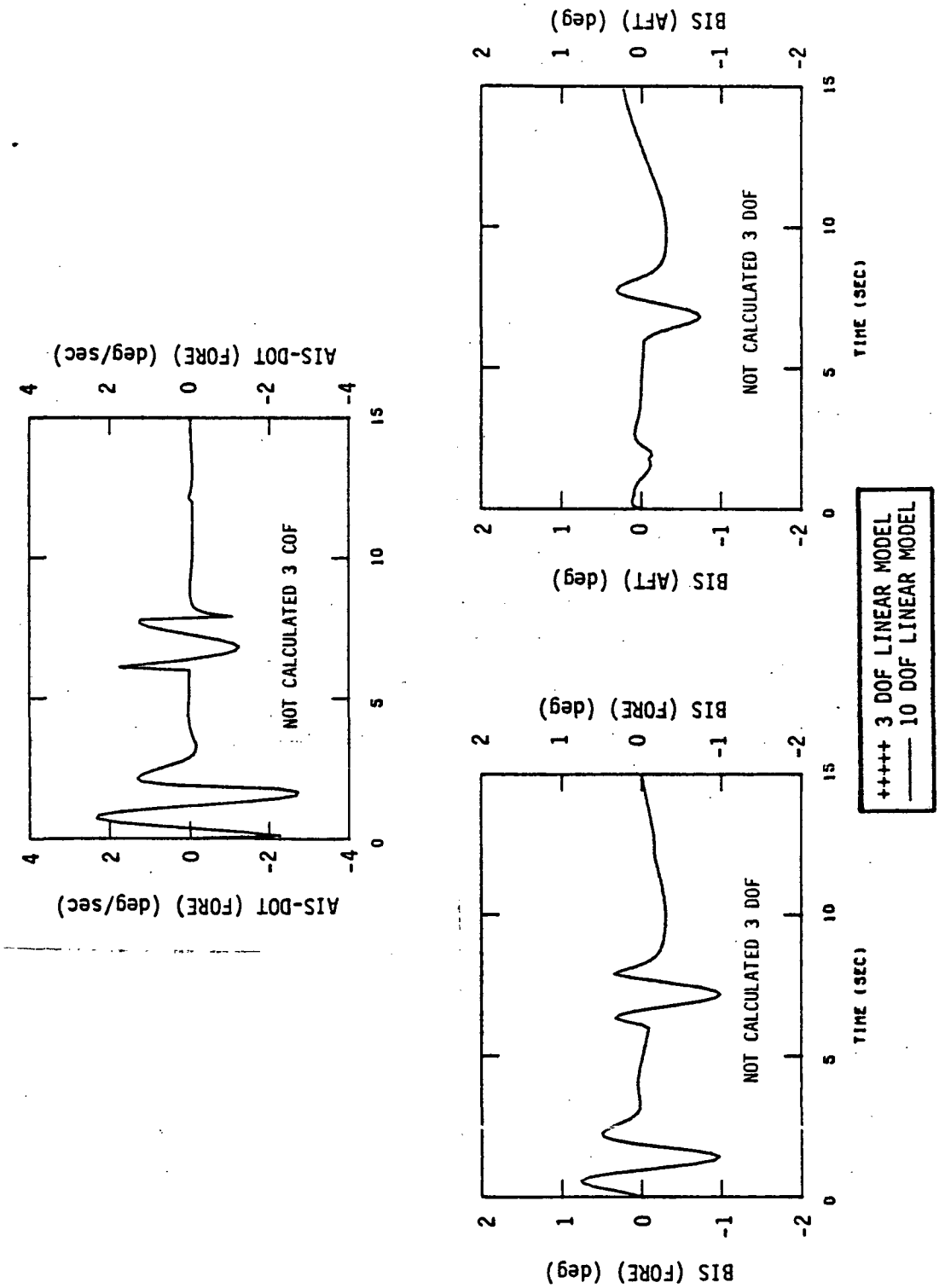

Figure 3.1 (Continued)

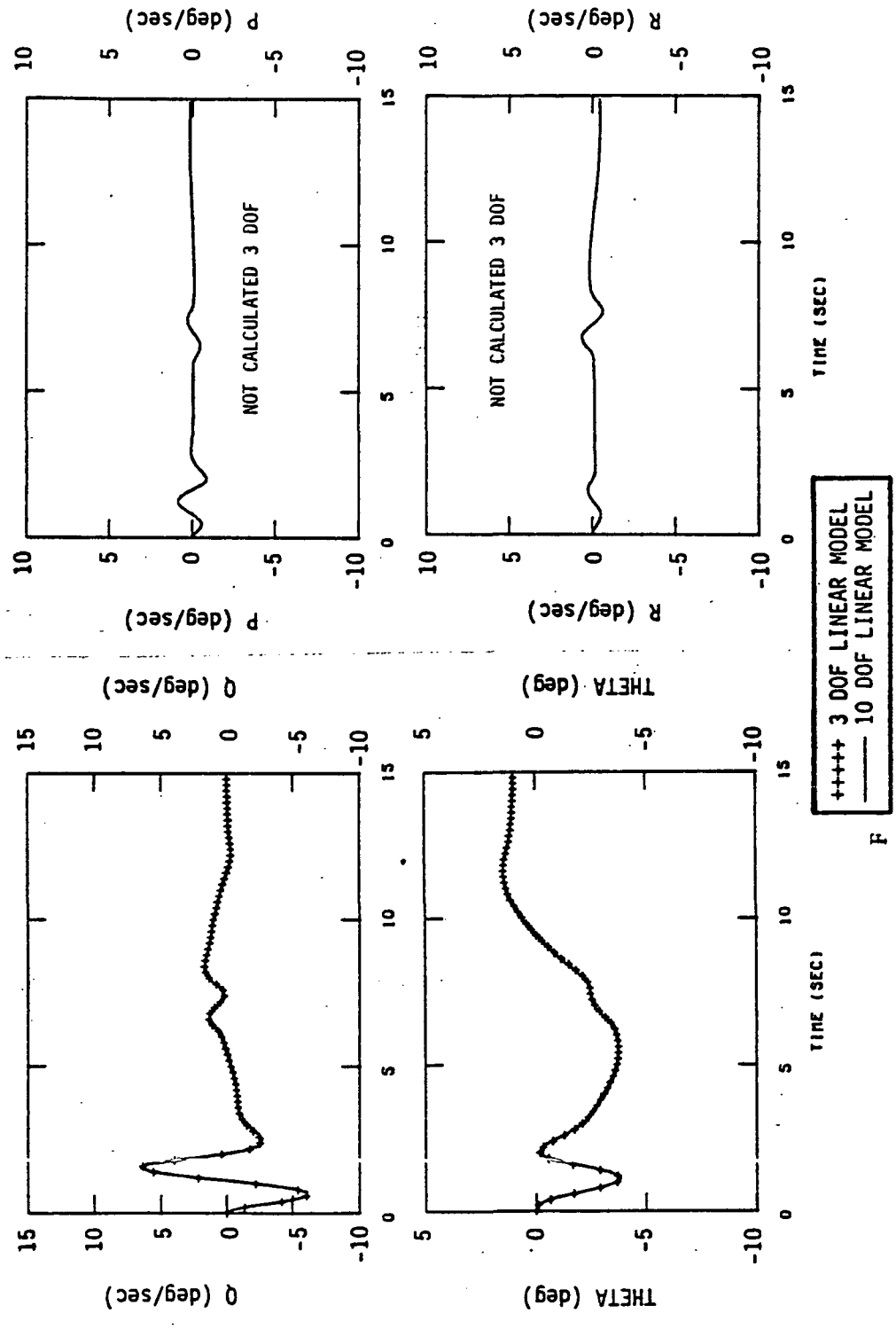

F

Figure 3.1 (Continued)

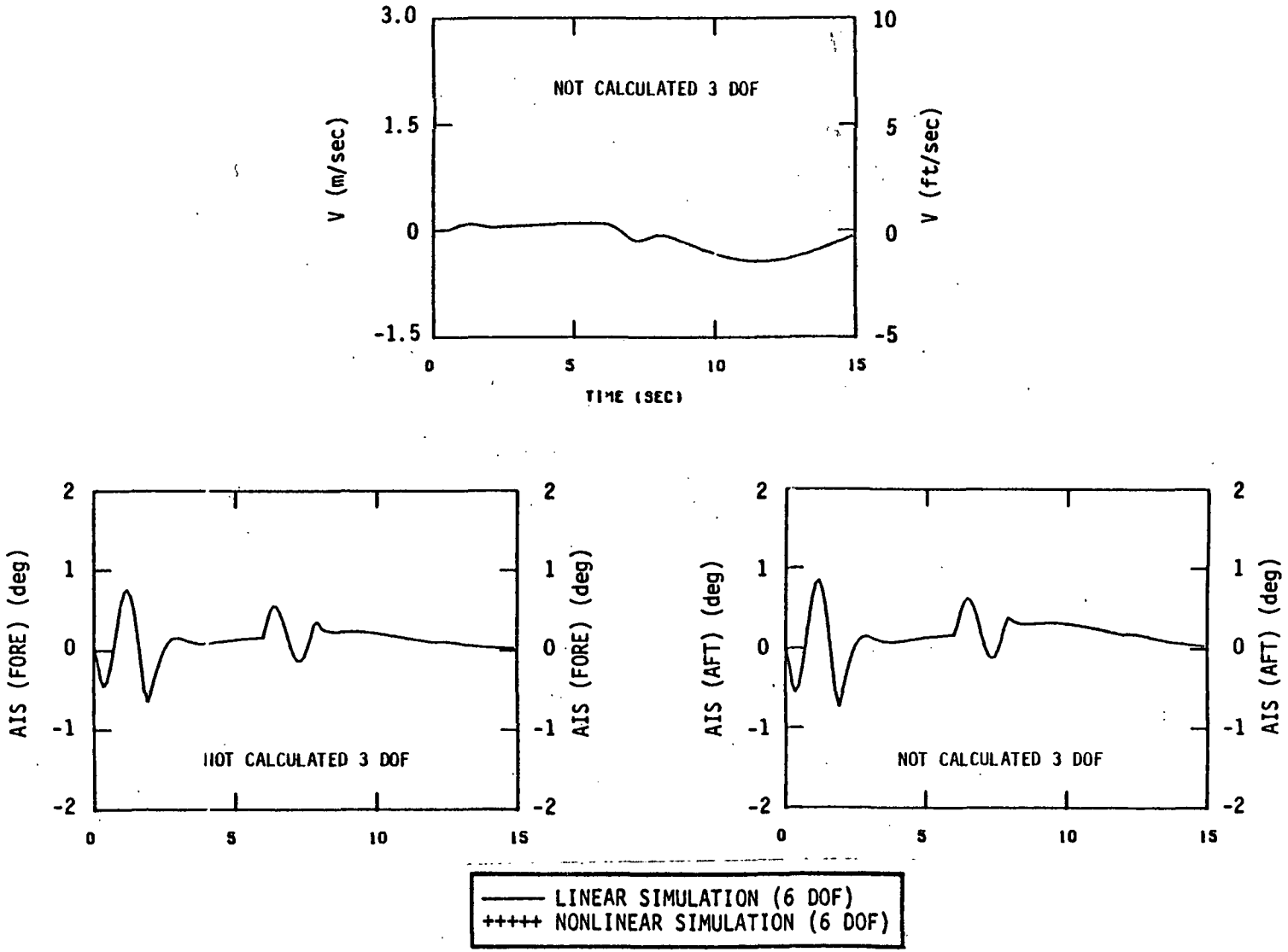

Figure 3.1 (Concluded)

employed). The lateral state variables have a negligible response demonstrating the effectiveness of the SAS in providing decoupled motion.

Both the 10 DOF and 3 DOF simulation data of Figure 3.1 were contaminated with the nominal random noise level and derivatives identified. The dual input identification results are shown in Table 3.14. The identified parameters using the 10 DOF simulation data show accuracy levels only slightly different compared with the results from the 3 DOF simulation data. These results are clearly superior to those obtained from the single input maneuvers (δ_{LONG}) which were shown in Table 3.8. In particular, the derivative M_w shows only 18% error compared to 48.7% error for the single input maneuver.

Figure 3.2 shows the time history comparison of the 3 DOF identified derivative model of Table 3.14 and the 10 DOF simulation data with random noise contamination. Although most derivatives in Table 3.14 are identified to less than 10% error, M_u and M_w are identified with 18% error and are primarily responsible for the diverging fit shown occurring after 10 sec in Figure 3.2. This discrepancy in the time history match occurs because the long period root is nearly neutrally stable and M_u and M_w have the most direct influence on this characteristic mode. As a result, the time response of the identified derivative model is very sensitive to small errors in M_u and M_w. The eigenvalues for the simulation model, and identified derivative model using 3 DOF and 10 DOF simulation data, are shown in Table 3.15.

3.2 LATERAL DIRECTIONAL IDENTIFICATION RESULTS AT 40 KTS

Based upon the results obtained for the longitudinal 40 kt condition, the lateral-directional input design was chosen in a

Table 3.14

Effect of Lateral Coupling and Rotor DOF on Derivative Accuracy – Two Control Inputs (40 KTS, Nominal Noise Case)

PARAMETER	C-81 TRUE PARAMETER VALUE	DATA FROM 3 DOF SIMULATION		DATA FROM 10 DOF SIMULATION	
		MAXIMUM LIKELIHOOD ESTIMATED PARAMETER	% ERROR	MAXIMUM LIKELIHOOD ESTIMATED PARAMETER	% ERROR
X_u	-.01141	-.01123	1.6	-.01172	2.7
Z_u	-.1244	-.1058	14.9	-.1058	14.95
M_u	.00705	.00807	14.4	.00833	18.3
X_w	.06069	.0615	1.4	.0615	1.4
Z_w	-.6566	-.649	1.1	-.6608	.64
M_w	.0121	.0112	8.7	..00994	18.0
M_q	-1.329	-1.319	0.8	-1.243	6.5
$X_{\delta LONG}$	2.9484	3.2412	9.9	3.2292	9.5
$Z_{\delta LONG}$	8.5380	8.6448	1.3	8.6256	1.0
$M_{\delta LONG}$	-15.5906	-15.5945	0.03	-15.3858	1.3
$X_{\delta COLL}$	9.5592	9.3036	2.7	9.4284	1.4
$Z_{\delta COLL}$	-135.24	-135.36	0.13	-136.08	.62
$M_{\delta COLL}$	2.0866	1.9567	1.1	1.7441	16.5

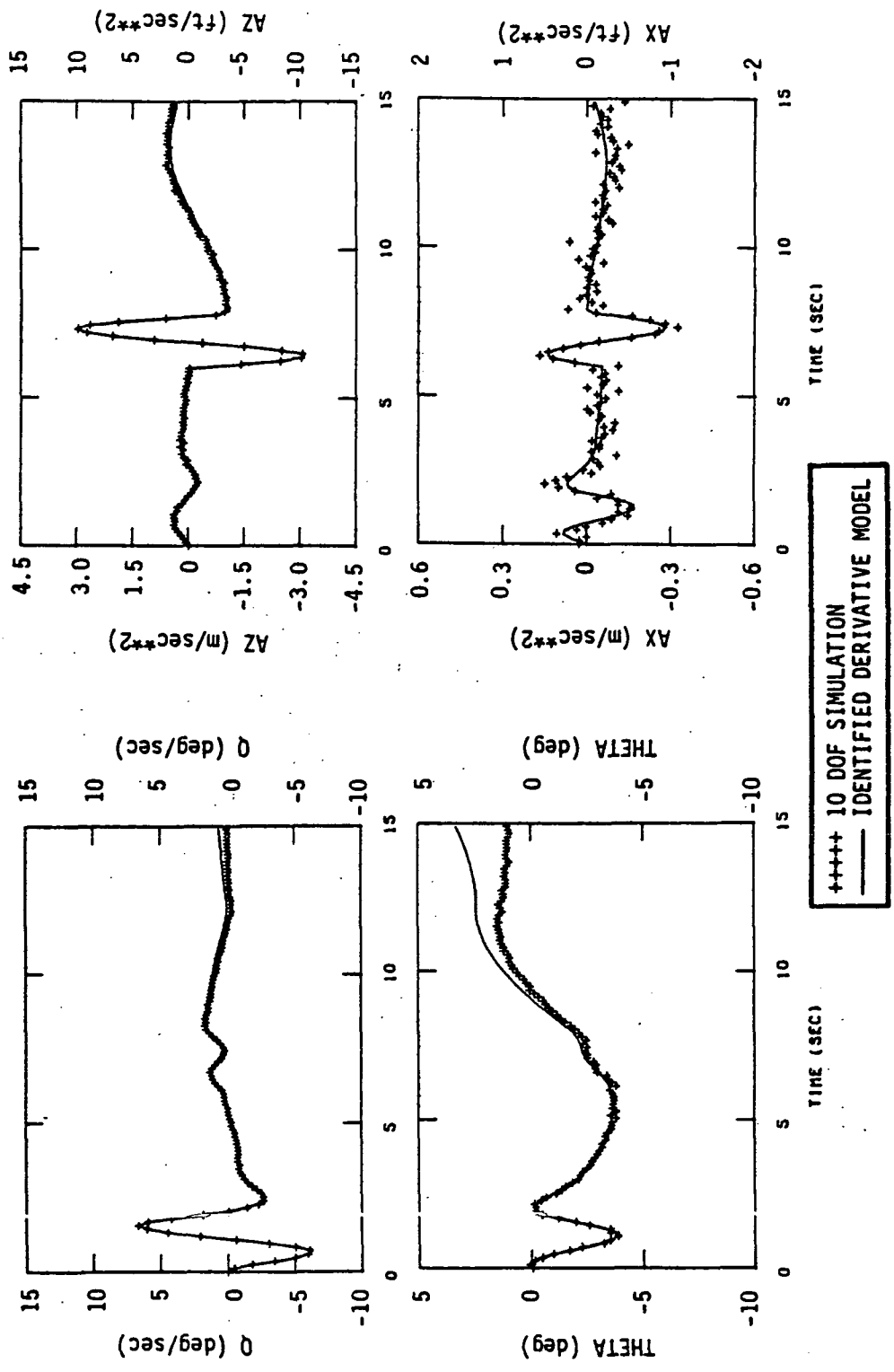

Figure 3.2 Time History Match of Identified Derivative Model Vs. 10 DOF Simulation Data (40 KTS, δ_{LONG}, δ_{COLL} Inputs, Nominal Noise)

Table 3.15

Eigenvalues of Identified Derivatives, 40 Knots
Nominal Noise, Two Control Inputs

	C-81 TRUE EIGENVALUES	USING DERIVATIVES IDENTIFIED FROM 3 DOF SIMULATION	USING DERIVATIVES IDENTIFIED FROM 10 DOF SIMULATION
Pitch Damping	-1.977 ± j 2.804	-1.969 ± j 2.807	-1.926 ± j 2.779
Vertical/Longitudinal	-.5174 ± j .0935	-.5166 ± j .0822	-.526 ± j .0691
Longitudinal Divergence	-.00092 ± j .0859	-.00073 ± j .0976	-.00142 ± j .1016
SAS	-.0468	-.0478	-.0483

similar manner. A lateral (δ_{LAT}) and a pedal (δ_{RUD}) input were chosen with two frequencies which occur at the short period and long period (Dutch roll) modes of motion. The amplitudes of the control inputs were chosen in an analogous manner to the longitudinal and were chosen such that the state variable response contains good excitation yet remains in a linear regime. Equations (3.7) and (3.8) present the control input selected for the 40 kt lateral-directional identification condition.

$$\delta_{LAT} = A_1 \sin 3.5t + A_2 \sin .319t \quad \text{(cm)} \tag{3.7}$$

$$A_1 = \begin{cases} 3.81 & t < 1.8 \\ 0.0 & t \geq 1.8 \end{cases}$$

$$A_2 = .25$$

$$\delta_{RUD} = B_1 \sin 3.5t + B_2 \sin 0.319t \quad \text{(cm) ies)} \tag{3.8}$$

$$B_1 = \begin{cases} -3.81 & t > 6 \quad \text{and} \quad t < 7.8 \\ 0.0 & t < 6 \quad \text{and} \quad t > 7.8 \end{cases}$$

$$B_2 = \begin{cases} -.25 & t > 6 \\ 0.0 & t < 6 \end{cases}$$

An earlier chapter discussed the problem of rotor-fuselage-SAS coupling as determined from the C-81 linear 10 DOF derivative model with the production SAS. This coupling was illustrated in Figure 2.8 which showed that both the rotor root locations and lateral short period root locations change when the CH-47 production SAS is included. It was also shown that this coupling could be essentially eliminated by reducing the CH-47 production SAS roll rate feedback gain by a factor of two. Table 3.16 presents the eigenvalues of the various linear models derived from the C-81 nonlinear simulation program at the 40 knot condition (SAS-off). The effect of the CH-47 production SAS on the eigenvalues of the various models is shown in Table 3.17. Included in Table 3.17 are the eigenvalues with the roll rate feedback gain (K_p) divided by a factor of two. This SAS modification is shown to reduce the rotor coupling and place the lateral short period roots on the real axis as was illustrated in Figure 2.8.

The lateral identification for the 40 knot condition in each case uses the 3 DOF lateral model with complex lateral SAS (5-state SAS), shown in Appendix A. The model structure used in the identification is as shown in Eq. (2.29) and contains two state variables for the SAS and assumes constant feedback gains for the remaining three states, as discussed in Chapter II. Identification results are presented for two cases: (1) simulation data employing the CH-47 production SAS and (2) simulation data generated with the CH-47 production SAS with the roll rate feedback gain K_p divided by a factor of two.

Table 3.18 presents the identified parameters for the lateral case where the data was generated from the 3 DOF lateral model with the 5-state variable CH-47 production SAS ($K_p = -5.0$). Those parameter values of Table 3.18 denoted with the prime represent the combined open-loop derivatives plus the constant feedback SAS contribution as shown in Eq. (2.29). The level of

Table 3.16

Eigenvalues of the Various Linear Open-Loop Models Derived from C-81 (40 Kts)

MODE	3 DOF UNCOUPLED	6 DOF	10 DOF
Pitch Damping	-1.605	-1.535	-1.517
Vert./Long.	-.320±j.211	-.310±j.261	-.3101±j.261
Long. Divergence	.2512	.2370	.2377
Roll Damping	---	-1.145	-1.186
Dutch Roll	---	+.0905±j.4198	.0877±j.4159
Spiral	---	-.04816	-.04828
Flap Regressing	--- ---	--- ---	-18.08±j7.115 -17.86±j7.256
Flap Advancing	--- ---	--- ---	-18.134±j43.53 -18.093±j43.44

Table 3.17

Eigenvalues of the Various Linear Models Derived from C-81 with CH-47 Production SAS (40 Kts, Including DCPT Feedback)

MODE	3 DOF UNCOUPLED (PRODUCTION SAS)	6 DOF (PRODUCTION SAS)	10 DOF (PRODUCTION SAS)	10 DOF $K_p \div 2$
Pitch Damping	-1.977±j2.804	-1.974±j2.817	-1.914±j2.845	-1.9138±j2.837
Vert./Long.	-.5174±j.09348	-.5202±j.0923	-.5199±j.0914	-.527±j.0873
Long. Divergence	-.009214±j.0859	-.000111±j.08517	-.000183±j.0874	.000866±j.0873
Roll Damping	-3.490±j.2385	-3.491±j.2391	-4.187±j1.369	-2.774, -1.156
Dutch Roll	-.1158±j.3012	-.11067±j.2998	-.1122±j.2992	-.2095±j.393
Spiral	-.00124	-.00255	-.00255	-.0241
Flap Regressing	--- ---	--- ---	-9.66±j2.34 -18.7±j6.49	-15.7±j5.43 -19.4±j6.75
Flap Advancing	--- ---	--- ---	-18.18±j43.53 -18.33±j43.61	-18.2±j43.57 -18.1±j43.5

Table 3.18

Identified Derivatives from the Lateral Simulation with CH-47 Production SAS (40 Kts, Nominal Noise)

PARAMETER	C-81 TRUE PARAMETER VALUE	MAXIMUM LIKELIHOOD ESTIMATED PARAMETER	% ERROR
Y'^{*}_{v}	-.044544	-.046323	4.0
L'^{*}_{v}	-.030272	-.034268	13.2
N'^{*}_{v}	.013891	.0139501	.43
Y'^{*}_{p}	-2.074	-2.3472	13.2
L'^{*}_{p}	-3.6416	-4.0625	11.6
N'_{p}	-.37475	-.57287	52.9
Y'_{r}	-.30727	-.21590	29.7
L'_{r}	.529015	.73681	39.3
N'_{r}	-1.99723	-2.2939	14.9
$Y_{\delta_{LAT}}$	21.660	14.9004	31.2
$L_{\delta_{LAT}}{}^{*}$	22.0827	25.02244	13.3
$N_{\delta_{LAT}}$	2.10433	3.151496	49.8
$Y_{\delta_{RUD}}$	-.66036	-1.094640	65.8
$L_{\delta_{RUD}}$	-2.3150	-3.262008	40.9
$N_{\delta_{RUD}}{}^{*}$	7.40472	8.82008	19.1

random noise contamination on the measurements of Eq. (2.30) represents the nominal case shown in Table 2.4.

Figure 3.3 shows the time history responses of the identified derivative model of Table 3.18 and the simulated 3 DOF model. The time history match is shown to be an excellent fit even though a number of the identified derivatives (Table 3.18) are identified with large errors. Those derivatives of Table 3.18 denoted with an asterisk are considered primary and contribute most to the time response, thus resulting in good accuracy (<20% error). The remaining derivatives contribute little to the response and, thus, are difficult to identify.

The lateral simulation model used for generating the time history data was then modified by dividing the roll rate feedback gain (K_p) by a factor of two. For this case, the time histories used in the identification were not contaminated by random noise to assess whether the derivative prediction accuracy could be improved. Table 3.19 shows large percent errors are still found for the secondary derivatives. Since zero noise contamination is used, these errors most likely are a result of using the approximate representation to the CH-47 SAS (i.e., the 2-state variable of Eq. (2.29) model rather than the 5-state variable model used in the simulation shown in Appendix A).

Table 3.20 presents the identified open-loop aerodynamic derivatives which are computed from Table 3.19 using Eq. (3.9).

$$
\begin{aligned}
Y_v &= Y'_v - K_v\, Y_{\delta_{RUD}} && \text{(a)}\\
L_v &= L'_v - K_v\, L_{\delta_{RUD}} && \text{(b)}\\
N_v &= N'_v - K_v\, N_{\delta_{RUD}} && \text{(c)}\\
Y_p &= Y'_p - K_p\, Y_{\delta_{LAT}} && \text{(d)}\\
L_p &= L'_p - K_p\, L_{\delta_{LAT}} && \text{(e)}
\end{aligned}
\qquad (3.9)
$$

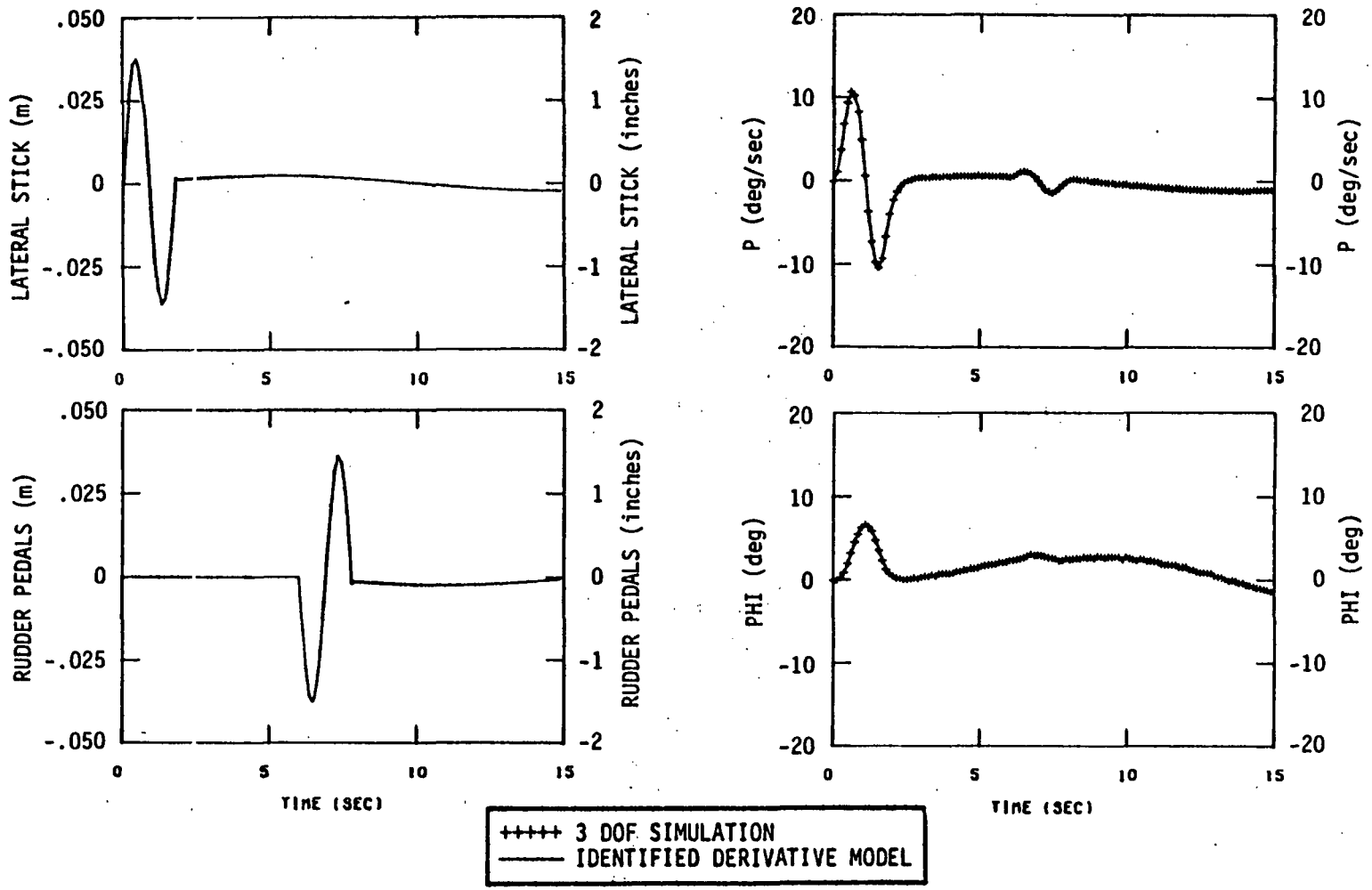

Figure 3.3 Time History Comparison of the Identified Lateral Derivative Model with the Simulation Data (40 Kts, K_p = -5.0, Nominal Noise)

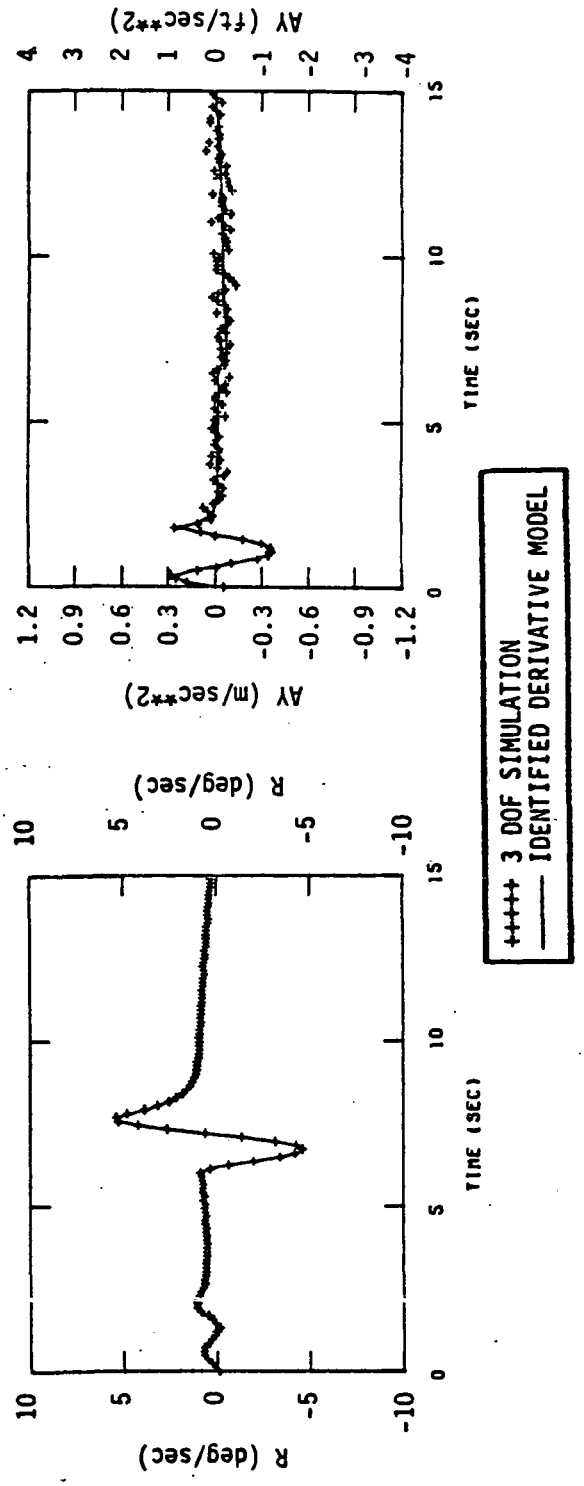

Figure 3.3 (Concluded)

Table 3.19

Identified Derivatives from the Lateral Simulation with CH-47 Production SAS with Roll Rate Feedback Gain Divided by a Factor of Two (40 Kts) (No Measurement Noise)

PARAMETER	C-81 TRUE PARAMETER VALUE	MAXIMUM LIKELIHOOD ESTIMATED PARAMETER	% ERROR
Y'_v	-.044544	-.045790	2.8
L'_v	-.030272	-.0328068	8.4
N'_v	.013891	.0139692	0.5
Y'_p	-1.2474	-1.3207	5.87
L'_p	-2.2394	-2.3370	4.35
N'_p	-.24113	-.35453	47.0
Y'_r	-.30727	-.24610	19.9
L'_r	.529015	.68495	29.46
N'_r	-1.99723	-2.2303	11.7
$Y_{\delta_{LAT}}$	21.660	13.8720	36.0
$L_{\delta_{LAT}}$	22.0827	23.35472	5.76
$N_{\delta_{LAT}}$	2.10433	2.83925	34.9
$Y_{\delta_{RUD}}$	-.66036	-.948276	43.6
$L_{\delta_{RUD}}$	2.3150	-2.993032	29.3
$N_{\delta_{RUD}}$	7.40472	8.74173	18.0

$$N_p = N'_p - K_p N_{\delta_{LAT}} \quad (f)$$

$$Y_r = Y'_r - K_r Y_{\delta_{RUD}} \quad (g)$$

$$L_r = L'_r - K_r L_{\delta_{RUD}} \quad (h)$$

$$N_r = N'_r - K_r N_{\delta_{RUD}} \quad (i)$$

$$K_v = .00272 \text{ m/m/sec}$$
$$K_p = -.0635 \text{ m/sec} \quad (3.9)$$
$$K_r = -.262 \text{ m/sec}$$

Table 3.20

Lateral Aerodynamic Derivatives Obtained from Equation (3.9) using Identified Values of Table 3.19 (40 Knots)

PARAMETER	C-81 TRUE PARAMETER VALUE	MAXIMUM LIKELIHOOD ESTIMATED VALUE*
Y_v	-.04275	-.04321
L_v	-.02398	-.02467
N_v	-.006224	-.00978
Y_p	-.42	-.440
L_p	-.8371	-.8539
N_p	-.1075	-.1742
Y_r	-.480	-.495
L_r	-.0778	-.0996
N_r	-.05025	.06115

*Derived from Eq. (3.9).

Figure 3.4 presents the time history comparison of the identified derivative model of Table 3.19 and the simulation data ($K_p \div 2$ in the production SAS). The time history fit is

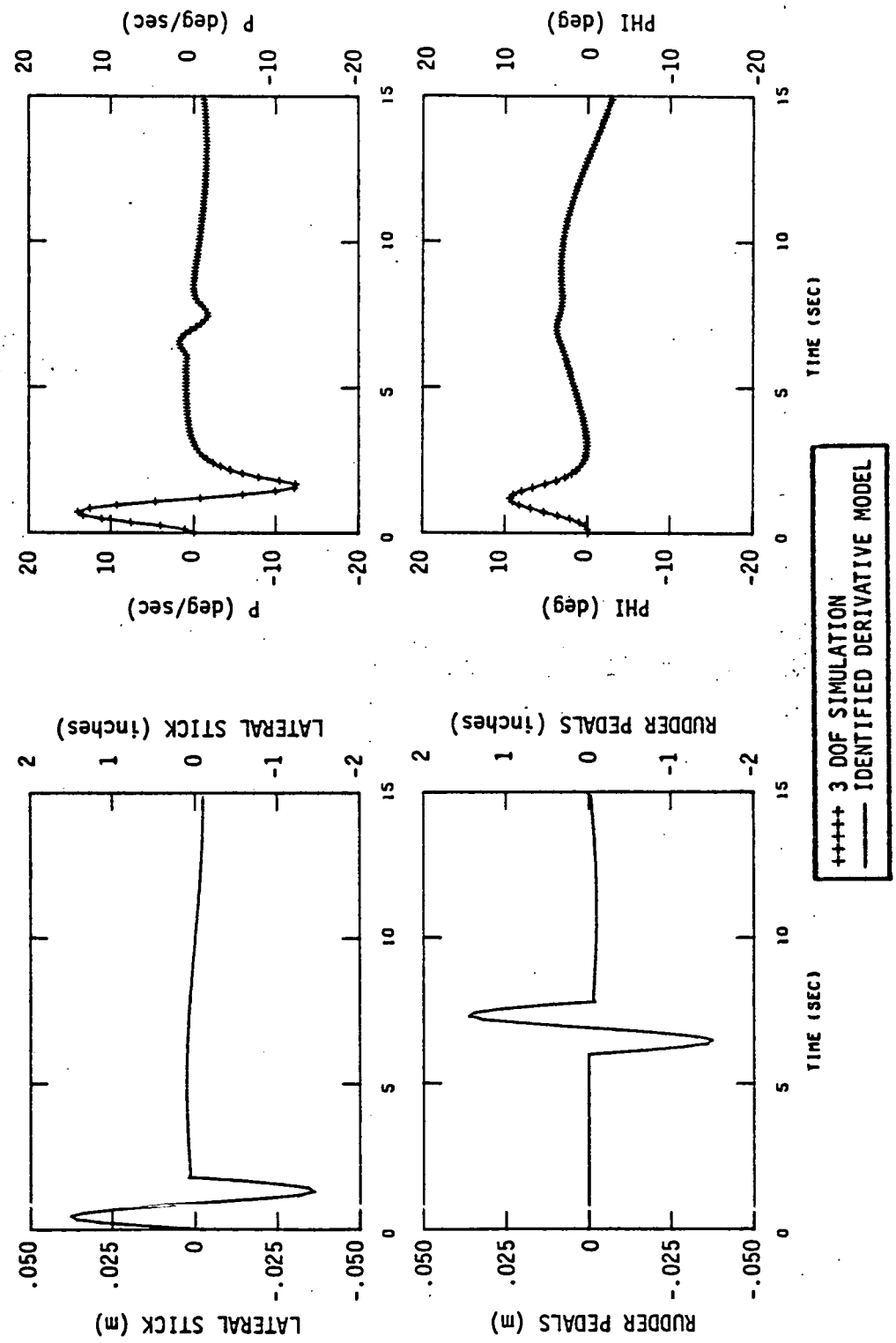

Figure 3.4 Time History Comparison of the Identified Lateral Derivative Model with the Simulation Data (40 Kts, CH-47 Production SAS Gain $K_p \div 2$)

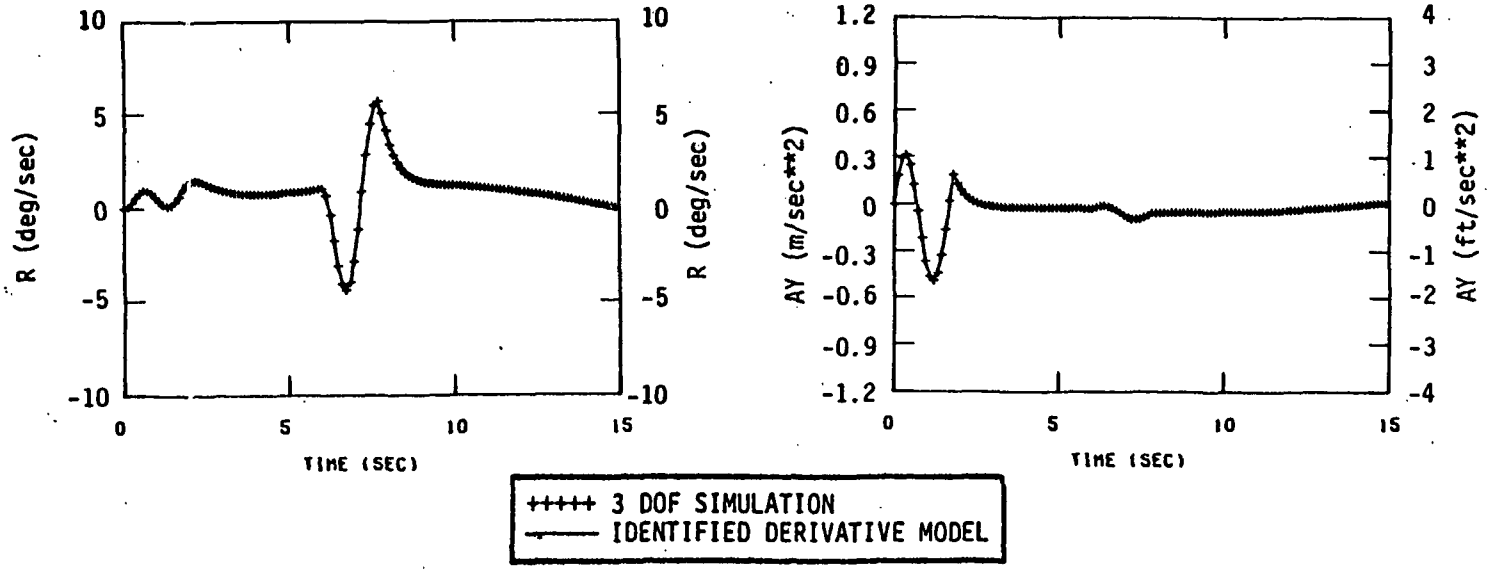

Figure 3.4 (Concluded)

near perfect which further demonstrates that the derivatives of Table 3.19 identified with large errors have a negligible influence on the response. The effect of reducing the CH-47 production SAS roll rate feedback gain and, thus, the rotor-to-airframe coupling is best seen by a comparison of the lateral acceleration responses (a_y) in Figures 3.3 and 3.4. Reducing the gain improves the match between the 3 DOF simulation and the identified derivation model a_y responses.

3.3 LONGITUDINAL IDENTIFICATION RESULTS AT THE HOVER CONDITION

This section presents the results of the simulation studies for the longitudinal hover condition. The control input designs for the hover case employ single-axis inputs to constrain the appropriate state variables (either u or w) to retain linearity. This requirement was discussed earlier and is required due to the nonlinear variation at hover of the velocity derivatives M_u and M_w, as shown in Figure 2.5. In addition to the above, the effect of data sample length and random wind gust on identification accuracy is presented.

3.3.1 Longitudinal Control Input Identification Results--Zero Turbulence

The identification procedure followed throughout the longitudinal hover simulations is as follows: (1) identify derivatives associated with longitudinal velocity, pitch rate, and longitudinal control, with excitation provided by a longitudinal control input δ_{LONG} and (2) identify the remaining vertical velocity and collective control derivatives, with excitation provided by a collective control input. Independent excitation of longitudinal velocity with vertical velocity fixed is required to avoid nonlinearity in the derivatives, as discussed in Section 2.2. This independent state excitation is possible at hover primarily because the SAS stabilizes the vehicle and essentially decouples

airspeed and pitch from vertical motion. Also, many of the coupling effects in the longitudinal equations are small at low speeds (particularly at hover and 20 knots). The degree to which this decoupling is achieved is best seen by examination of a time history response.

Figure 3.5 shows the time history response from the 6 DOF hover derivative model supplied by LRC with complete CH-47 production SAS included (with $K_p \div 2$). The longitudinal control input (δ_{LONG}) is designed in an analogous manner to the 40 knot case with two differences. First, the amplitude of both the low frequency and high frequency part was determined by trial runs such that good excitation resulted in u and q. Secondly, the low and high frequencies were not designed exactly at the long and short period modes, but slightly removed to assess whether this difference deteriorates identification accuracy. The time history response of Figure 3.5 shows excellent longitudinal velocity and pitch rate response, while the vertical velocity response is less than 2 ft/sec. This decoupling also reflects itself in the accuracy with which the u and q derivatives are identified. Also, notice that excellent decoupling exists between the lateral and longitudinal motions (the decoupling again a result of the SAS).

The simulation data shown in Figure 3.5 was used to identify the u, q, and δ_{LONG} derivatives appearing in the longitudinal equation [Eq. (2.27)]. The data used in the identification is first contaminated with the nominal random noise, scale factor errors, and bias errors of Table 2.4. The identified derivatives are shown in Table 3.21, with those denoted by an asterisk held fixed to zero. The percent errors shown in Table 3.21 indicate the excellent accuracy attainable in the identified derivatives with the exception of Z_w and M_q. Z_w is identified to 11% error in the δ_{COLL} maneuver described next; and the nonlinear analysis, Appendix D, shows that reducing the data sample length also improved the prediction of Z_w and

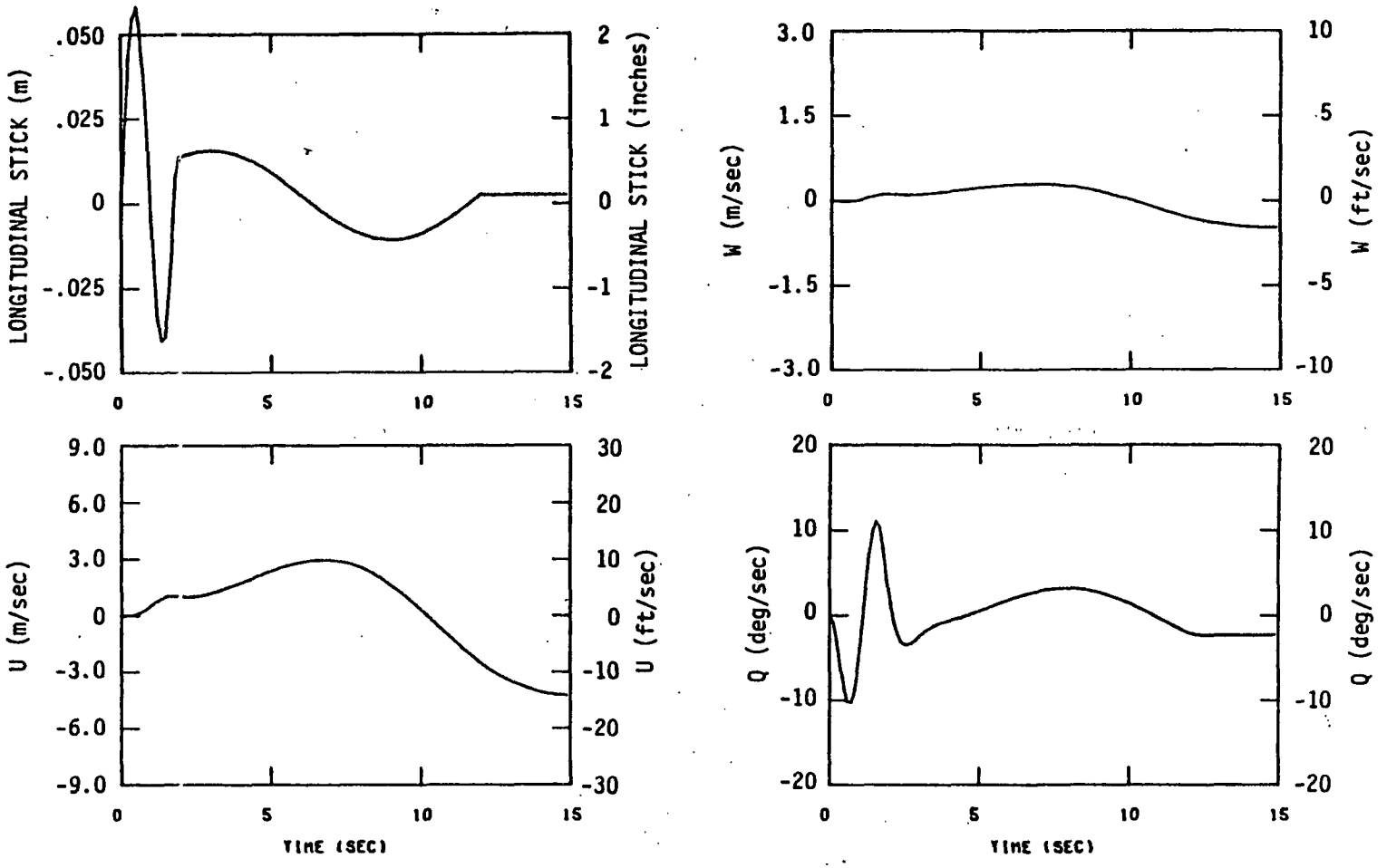

Figure 3.5 Time History Response of the 6 DOF LRC Derivative Model with CH-47 Production SAS ($K_p \div 2$) Generated for Derivative Identification (Hover, δ_{LONG} Input)

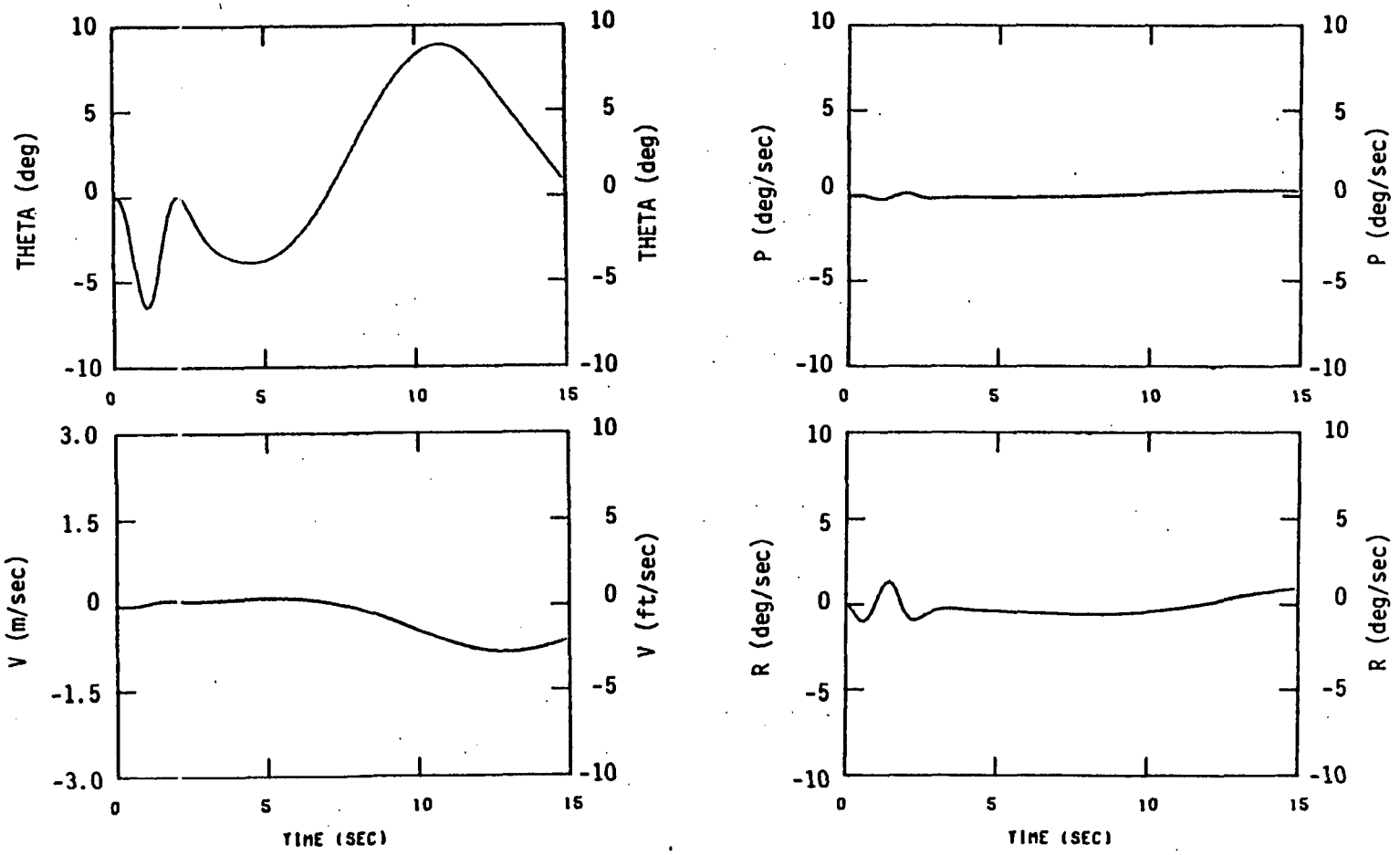

Figure 3.5 (Concluded)

Table 3.21

Longitudinal Derivative Identification Results at Hover from δ_{LONG} Input Maneuver (6 DOF LRC Simulation, Random Noise, Bias, and Scale Factor Errors Included)

PARAMETER	TRUE PARAMETER VALUE	IDENTIFIED PARAMETER	% ERROR
X_u	-.01857	-.01599	13.9
Z_u	.02097	*	--
M_u	.04449	.04698	5.7
X_w	.02894	*	--
Z_w	-.2598	-.0734	71.7
M_w	.00935	*	--
M_q	-1.3422	-1.536	14.5
$X_{\delta_{LONG}}$	-1.3092	-1.3788	5.3
$Z_{\delta_{LONG}}$	-.37776	-.4248	12.6
$M_{\delta_{LONG}}$	-12.58189	-12.2008	3.0
$X_{\delta_{COLL}}$	11.2452	*	--
$Z_{\delta_{COLL}}$	-96.612	*	--
$M_{\delta_{COLL}}$	.69449	*	--

*Held fixed to zero

M_q. The time history comparisons using the identified derivative model and the simulation data are shown in Figure 3.6. The fit is excellent (note that the simulation data contains random, scale factor, and bias errors) and, as indicated previously, the vertical mode (A_z) shows negligible response and the simulation response contains mostly noise.

3.3.2 Collective Control Input Identification Results--Zero Turbulence

In an analogous manner to the longitudinal input maneuvers of the last section, the collective control input was designed and used with the hover 6 DOF LRC simulation. The time history response of the 6 DOF simulation due to the collective control input is shown in Figure 3.7. The vertical velocity responds considerably, whereas longitudinal velocity and pitch rate show negligible excitation. Also, the lateral time histories show near-zero response.

The identified derivatives are shown in Table 3.22 resulting from the δ_{COLL} input maneuvers, which include the w and δ_{COLL} derivatives. The derivatives previously identified from the δ_{LONG} input maneuver are shown repeated in Table 3.22 and were held fixed to their previously identified values (except Z_w). The w and δ_{COLL} derivatives are identified with adequate accuracy even with random, bias, and scale factor noise contamination. The uncoupled vertical from longitudinal motion is, thus, proved to be a viable procedure for identification of the linear longitudinal derivatives, even though the derivatives are highly nonlinear with u and w as exhibited by Figure 2.5.

Figure 3.8 shows the time history comparisons using the identified derivative model from the δ_{COLL} input maneuver and the simulation data of Figure 3.7. The fit is excellent and, as indicated previously, only the vertical motion (A_z) is

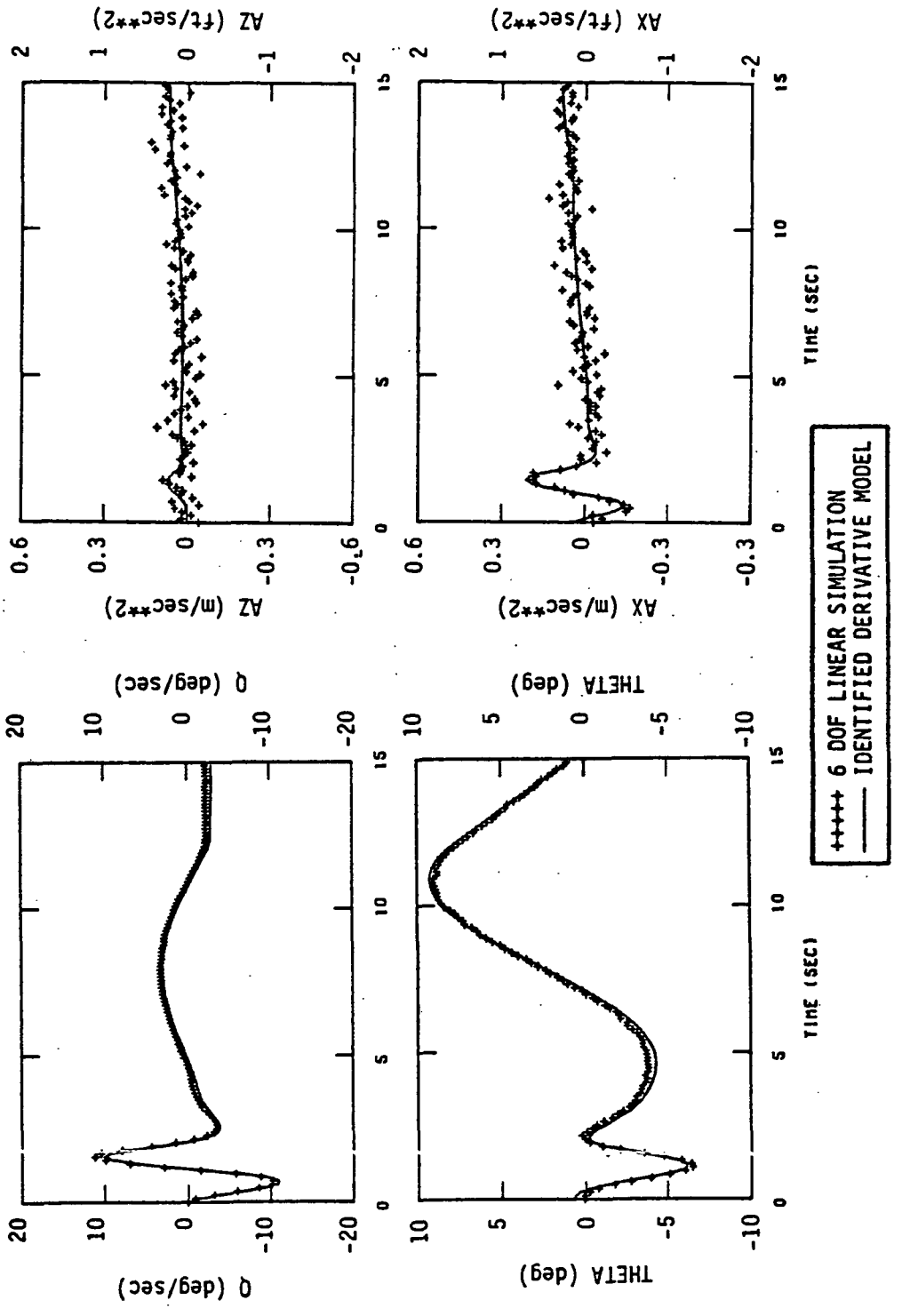

Figure 3.6 Longitudinal Time History Match of Identified Derivative Model and 6 DOF LRC Derivative Noise Contaminated Simulation Data (Hover, δ_{LONG} Input, Random Noise, Bias, and Scale Factor Errors)

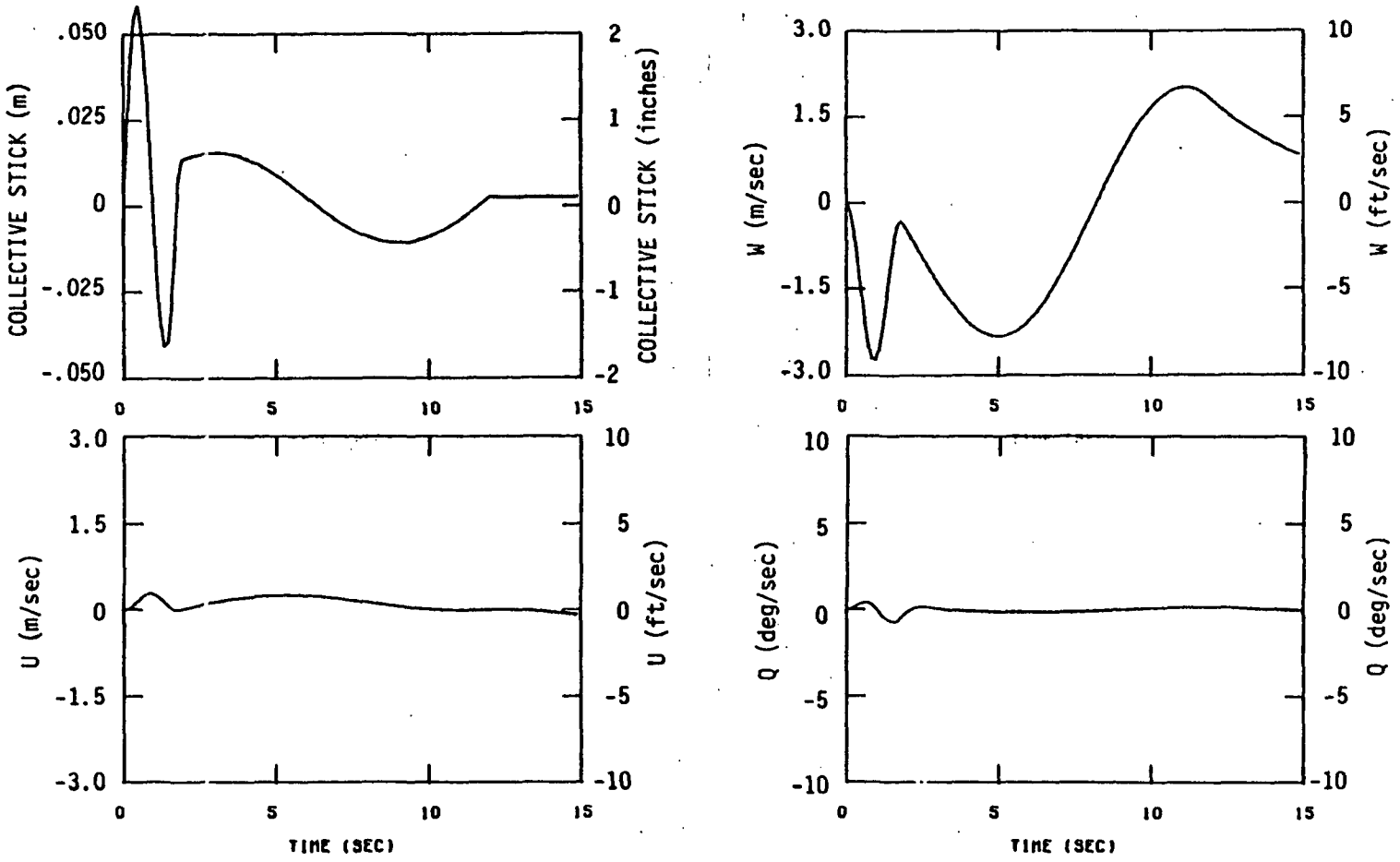

Figure 3.7 Time History Response of the 6 DOF LRC Derivative Model with CH-47 Production SAS ($K_p \div 2$) Generated for Derivative Identification (Hover, δ_{COLL} Input)

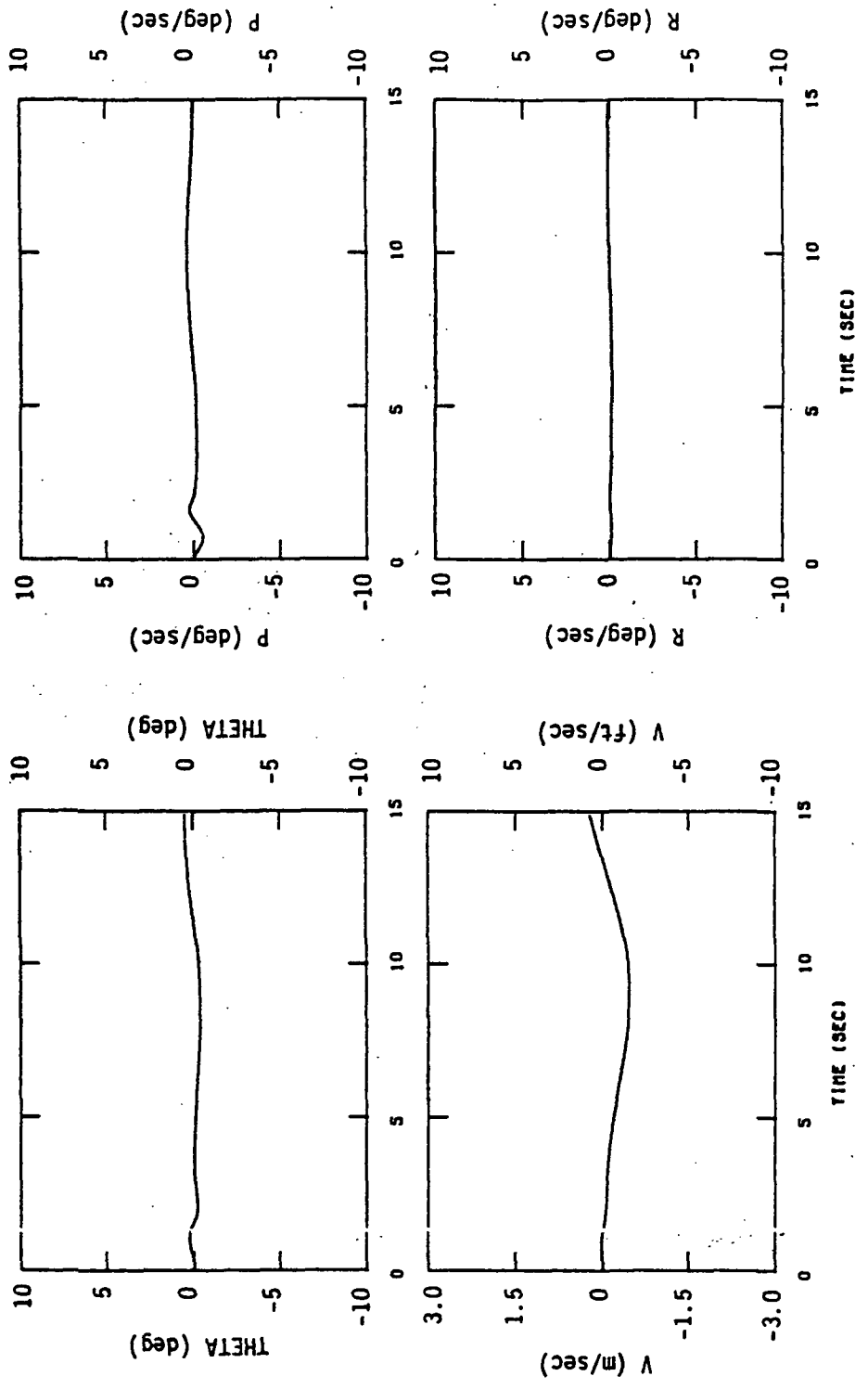

Figure 3.7 (Concluded)

Table 3.22

Longitudinal Derivative Identification Results at Hover from δ_{COLL} Input Maneuver (Random Noise, Bias, Scale Factor Errors, 6 DOF LRC Simulation)

PARAMETER	REF. 1 TRUE PARAMETER VALUE	δ_{LONG} INPUT MANEUVER		δ_{COLL} INPUT MANEUVER	
		IDENTIFIED PARAMETER	% ERROR	IDENTIFIED PARAMETER	% ERROR
X_u	-.01857	-.01599	13.9	**	--
Z_u	.02097	--	--	--	--
M_u	.04449	.04698	5.7	**	--
X_w	.02894	*	--	.0295	2.1
Z_w	-.2598	-.0734	71.7	-.2887	11.1
M_w	.00935	*	--	.00997	6.8
M_q	-1.3422	-1.536	14.5	**	--
$X_{\delta_{LONG}}$	-1.3092	-1.3788	5.3	**	--
$Z_{\delta_{LONG}}$	-.37776	-.4248	12.6	**	--
$M_{\delta_{LONG}}$	-12.58189	-12.2008	3.0	**	--
$X_{\delta_{COLL}}$	11.2452	*	--	10.9680	2.5
$Z_{\delta_{COLL}}$	-96.612	*	--	-97.056	.46
$M_{\delta_{COLL}}$	.69450	*	--	.69016	.58

*Held fixed to zero
**Held fixed to values identified from δ_{LONG} maneuver

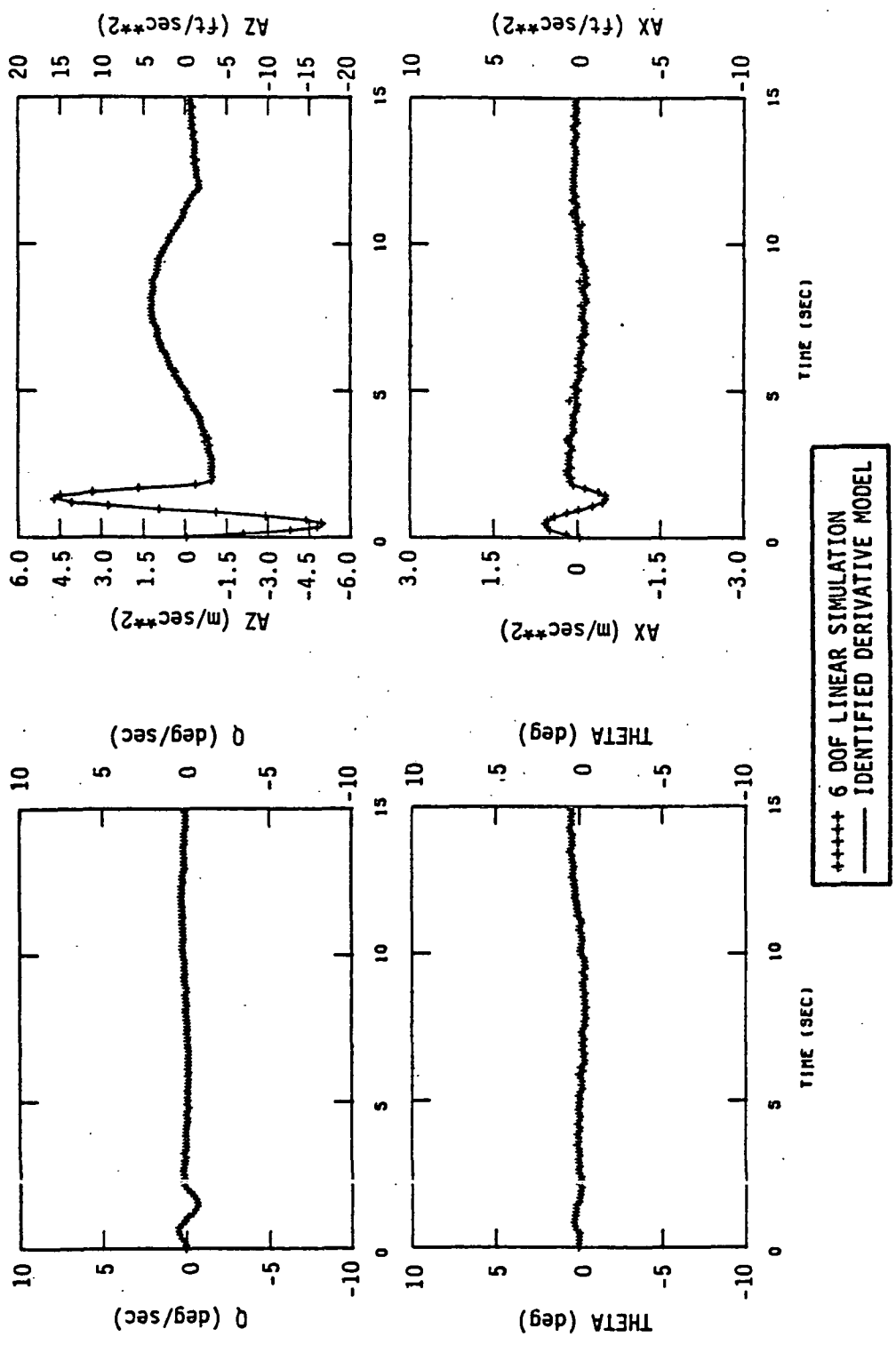

Figure 3.8 Longitudinal Time History Match of Identified Derivative Model and 6 DOF LRC Derivative Noise Contaminated Simulated Data (Hover δ_{COLL} Input, Random Noise, Bias, and Scale Factor Errors)

excited. The excitation of A_x is mainly due to the control derivative $X_{\delta COLL}$ which is identified for this maneuver.

3.3.3 Collective Input Maneuver Identification Results with Gust Disturbance

This section presents the identification results with random gust disturbance included in the simulation. The simulation, control input used, and procedure are identical to those of the last section with the exception of the addition of the gust disturbance to the simulation. The identification program does not account for gust in the model structure and, as such, the results presented show under what conditions random gust deteriorates parameter identification accuracy. The results of this section establish the magnitude of gust tolerable during the flight test, such that good identification accuracy is achieved.

Moderate and Light Longitudinal Gust. Figure 3.9 shows the hover 6 DOF (Ref. 1) derivative model time history response due to a collective input with moderate random longitudinal gust excitation (σ_u = 2.13 m/sec). Comparison of this figure with Figure 3.7 reveals the sensitivity of the response to moderate turbulence level. As shown in Figure 3.9, both the u and q responses are affected by the presence of the gust. The effect on derivative identification accuracy is seen by referring to Table 3.23 which shows that for the moderate turbulence level (σ_u = 2.13 m/sec) identified parameter accuracy is degraded and significantly degraded for M_w and $M_{\delta COLL}$. Also shown in Table 3.23 is separate identification results where the random gust in the simulation was reduced to an RMS value of .91m/sec, which corresponds to light-to-calm air. The identified parameters shown in Table 3.23 are only slightly changed relative to the no-turbulence case (Table 3.22) and are of totally acceptable accuracy.

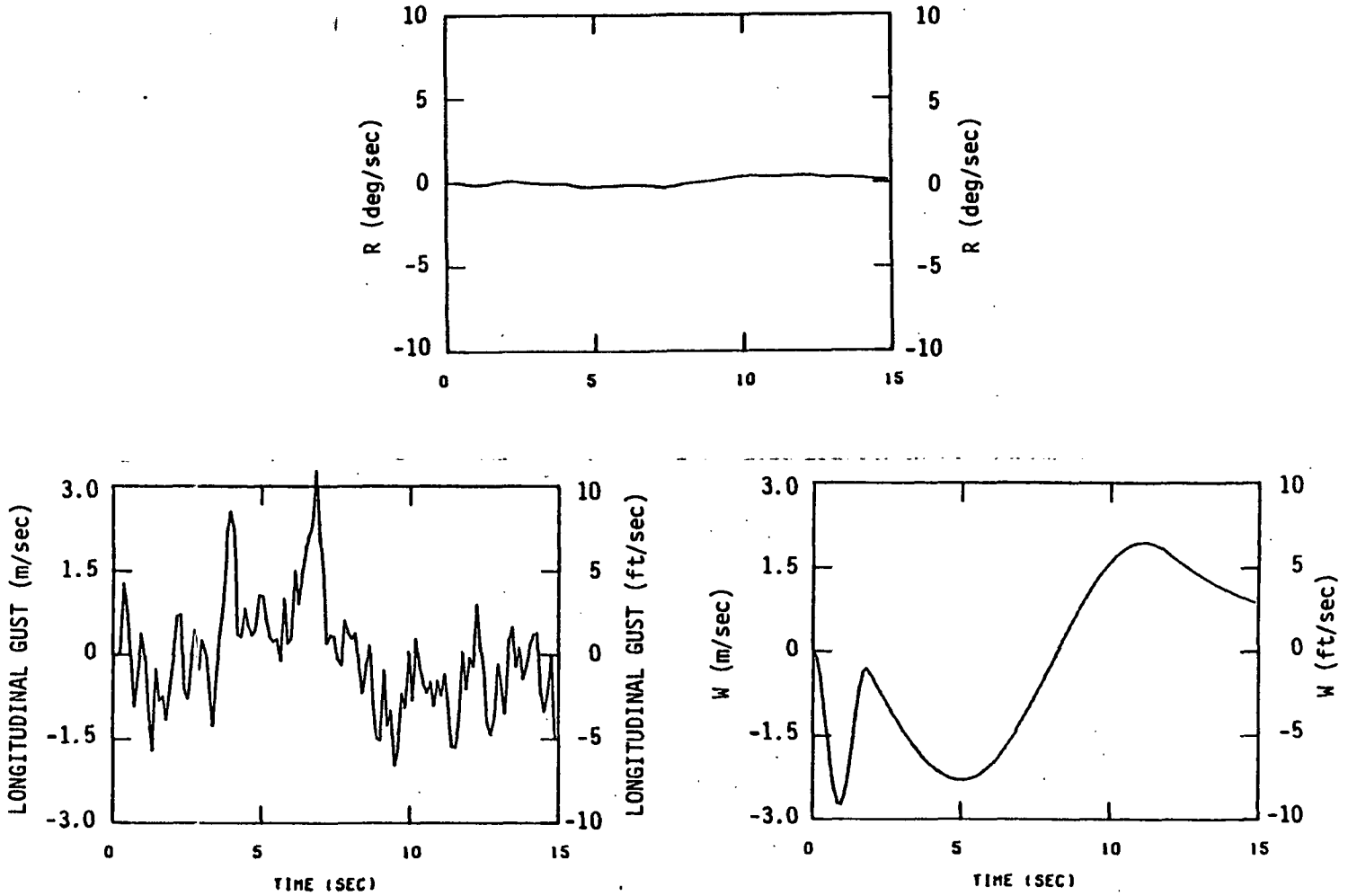

Figure 3.9 Time History Response of the 6 DOF LRC Derivative Model with CH-47 Production SAS ($K_p \div 2$) with Moderate Longitudinal Random Wind Gust Disturbance ($\sigma_u = 2.13$ m/sec)

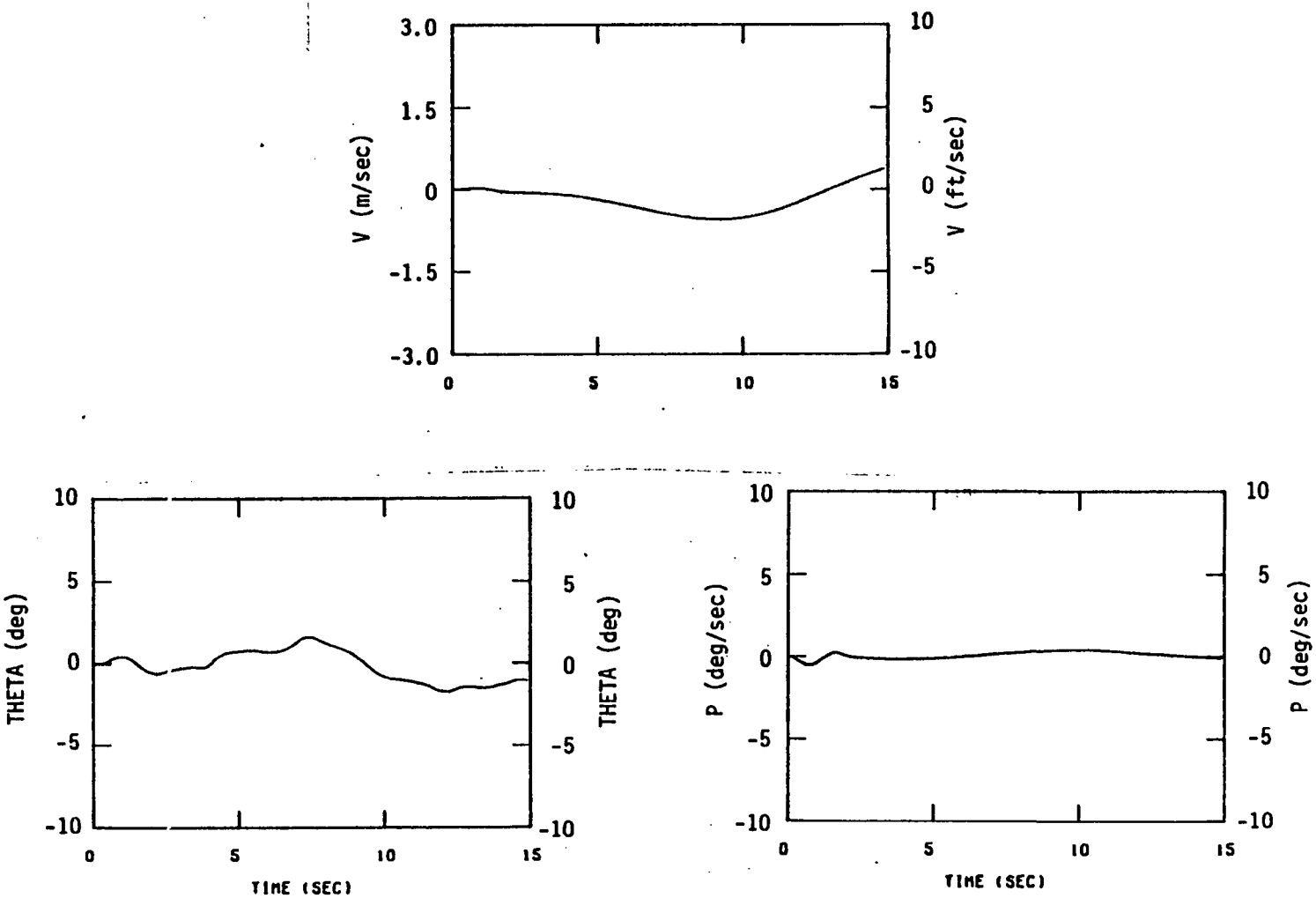

Figure 3.9 (Continued)

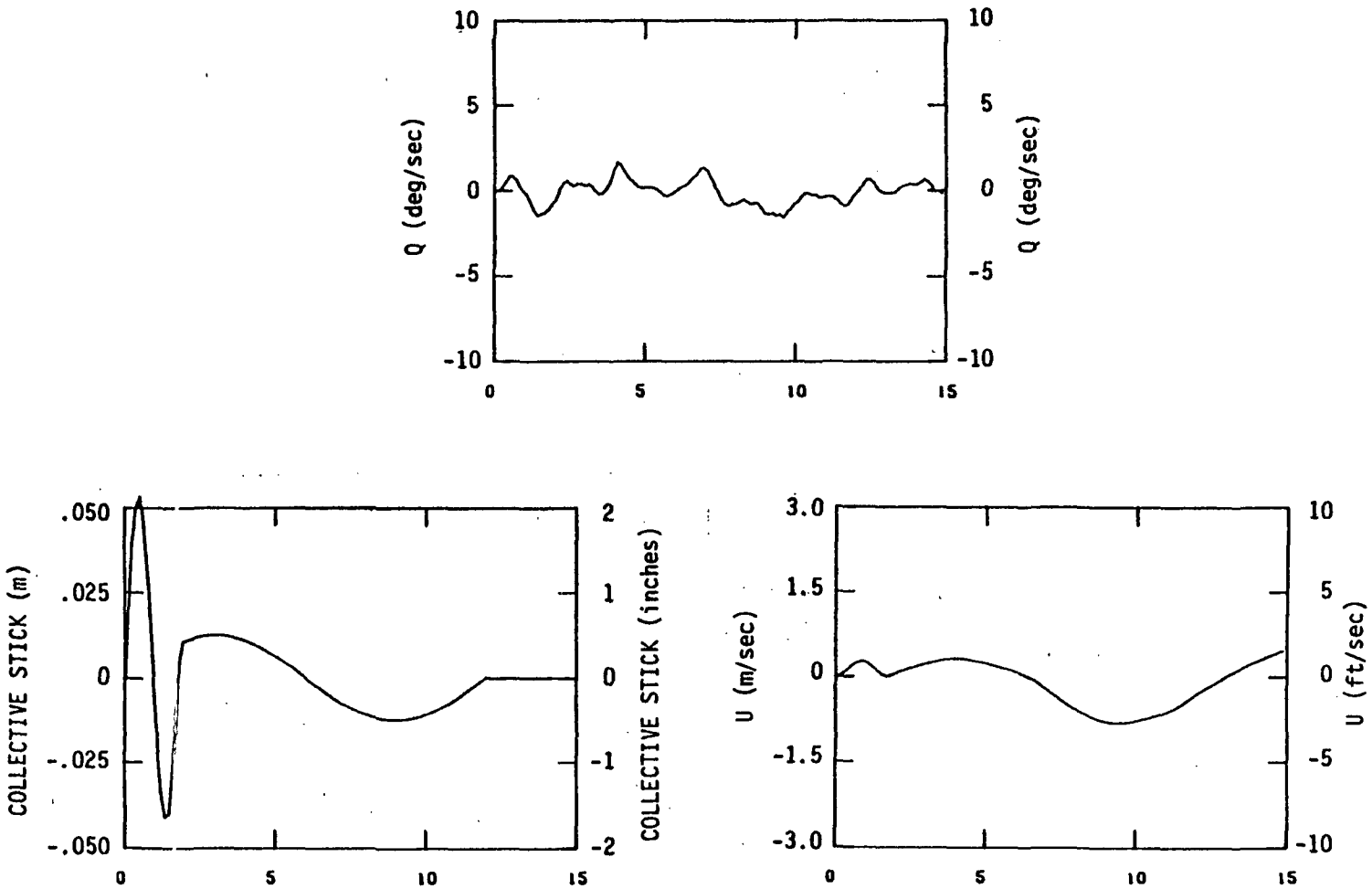

Figure 3.9 (Concluded)

Table 3.23

Longitudinal Derivative Identification Results at Hover from δ_{COLL} Input Maneuver with Longitudinal Wind Gust Disturbance (Random Noise, Bias, Scale Factor Errors, 6 DOF Simulation)

PARAMETER	[REF. 1] TRUE PARAMETER VALUE	MODERATE LONGITUDINAL TURBULENCE (σ_u = 2.13 m/sec)		LIGHT LONGITUDINAL TURBULENCE (σ_u = .91 m/sec)	
		IDENTIFIED PARAMETER	% ERROR	IDENTIFIED PARAMETER	% ERROR
X_u	-.01857	*	--	*	--
Z_u	.02097	*	--	*	--
M_u	.04449	*	--	*	--
X_w	.02894	.0346	19.8	.0252	12.9
Z_w	-.2598	-.2957	13.8	-.2943	13.3
M_w	.00935	-.004852	151.9	.00636	31.8
M_q	-1.3422	*	--	*	--
$X_{\delta_{LONG}}$	-1.3092	*	--	*	--
$Z_{\delta_{LONG}}$	-.37776	*	--	*	--
$M_{\delta_{LONG}}$	-12.58189	*	--	*	--
$X_{\delta_{COLL}}$	11.2452	11.0184	2.0	10.9632	2.5
$Z_{\delta_{COLL}}$	-96.612	-96.684	.08	-97.032	.44
$M_{\delta_{COLL}}$	.69449	.13031	81.2	.6575	5.1

*Held fixed to values identified from δ_{LONG} maneuver

The time history comparisons with the simulation data of the identified derivative models for both the moderate and light turbulence levels are shown in Figure 3.10 and 3.11, respectively. The degraded accuracy of the moderate turbulence case is reflected in the poor fit of Figure 3.10 and the excessive response in q and θ. The time history match for the light turbulence case is shown to be quite good, as was reflected in the good accuracy in identified parameters.

Vertical and Lateral Gust (Heavy Turbulence Level). The results just presented demonstrated the effect of longitudinal gust on identified derivative accuracy for the collective input maneuver. In a similar manner, this section presents the results where a vertical gust and then a lateral gust disturbance are included in the simulation.

Table 3.24 shows the identified derivative values for these two cases: (1) a vertical gust with heavy turbulence, σ_w = 3.05 m/sec and (2) a lateral gust with heavy turbulence, σ_v = 3.05 m/sec. The vertical gust is shown in degrade accuracy in the identified stability derivatives X_w, Z_w, and M_w unacceptably, whereas the control derivatives $X_{\delta COLL}$ and $Z_{\delta COLL}$ retain good accuracy. The lateral gust is shown to have a negligible effect on the identified derivative accuracy over the no-gust condition and thus flight testing in a cross wind would be an acceptable testing procedure. The time history comparison of the simulation model and the identified derivative model for both the vertical gust case and the lateral gust case is shown in Figures 3.12 and 3.13, respectively. The degree of time history match is, thus, as expected based upon the identified derivative accuracies of Table 3.24.

3.4 LATERAL-DIRECTIONAL RESULTS AT THE HOVER CONDITION

This section presents the identification results for the lateral-directional hover condition. The simulation model in

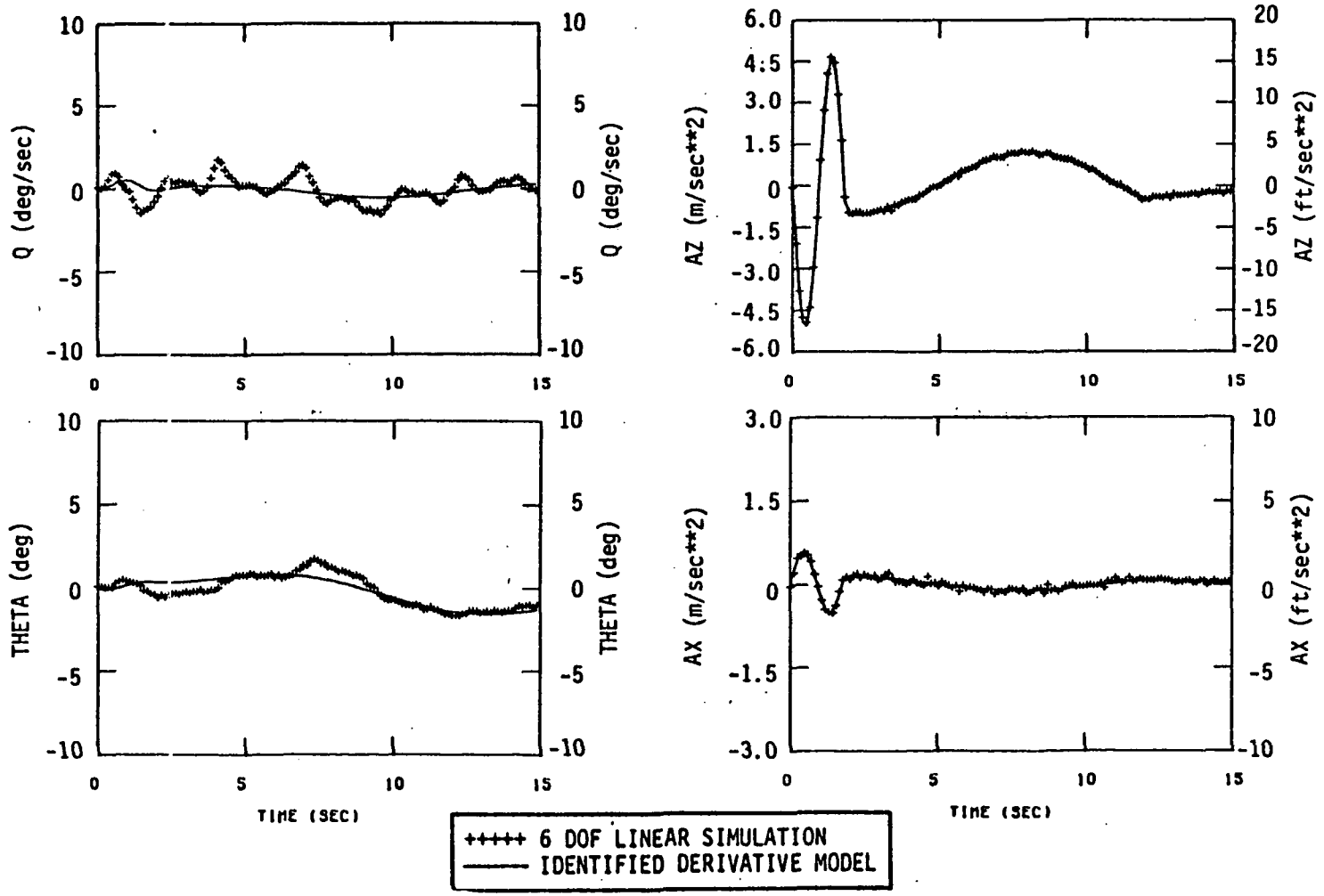

Figure 3.10 Longitudinal Time History Match of Identified Derivative Model and 6 DOF LRC Derivative Noise Contaminated Simulated Data with Moderate Longitudinal Random Wind Gust Disturbance (σ_u = 2.13 m/sec, Hover

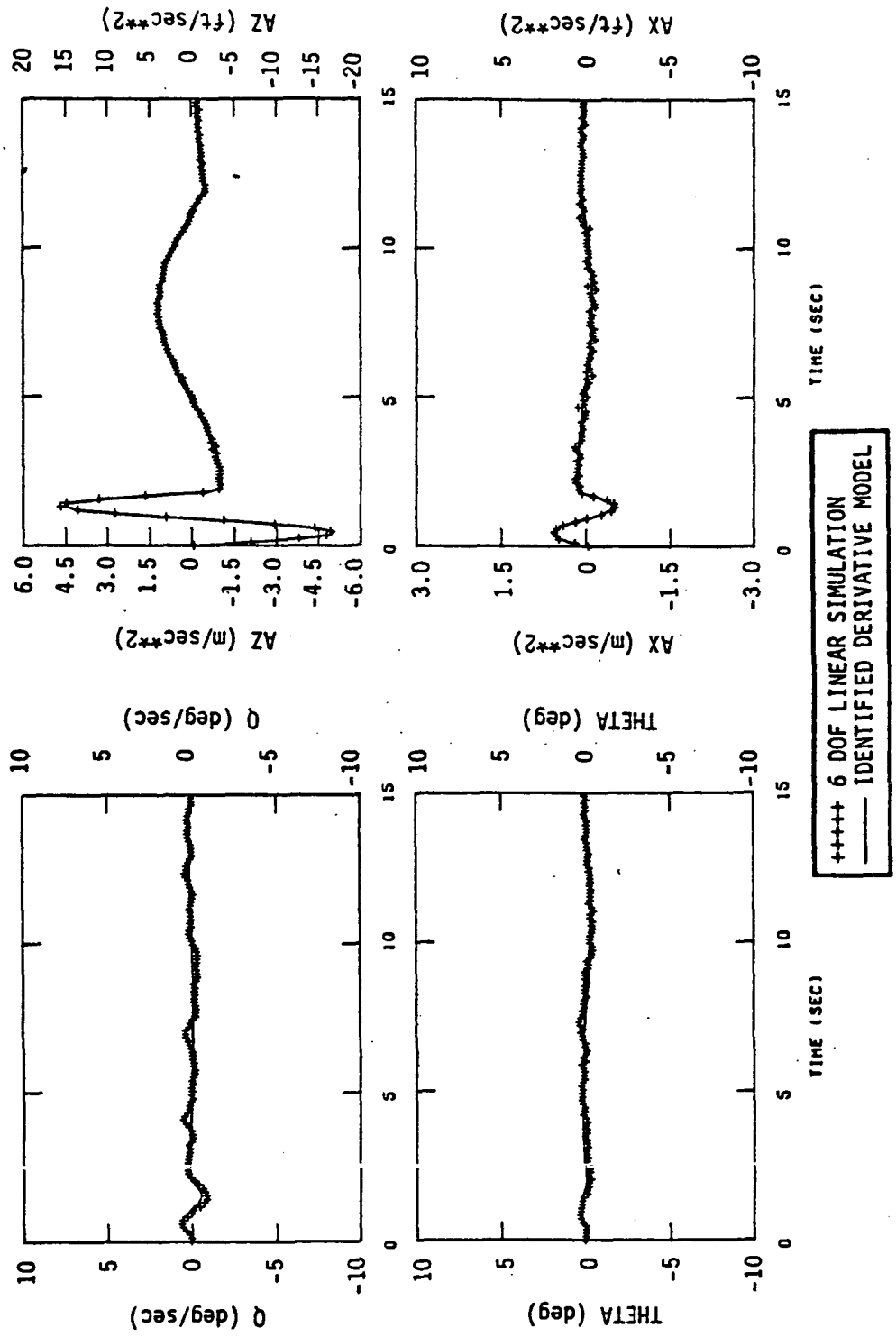

Figure 3.11 Longitudinal Time History Match of Identified Derivative Model and 6 DOF LRC Derivative Noise Contaminated Simulated Data with Light Longitudinal Random Wind Gust Disturbance (σ_u = .91 m/sec, Hover)

Table 3.24

Longitudinal Derivative Identification Results at Hover from a δ_{COLL} Input Maneuver with Vertical and Lateral Turbulence (Random Noise, Bias, Scale Factor Errors, 6 DOF Simulation)

PARAMETER	REF. 1 TRUE PARAMETER VALUE	HEAVY VERTICAL TURBULENCE (σ_w = 3.05 m/sec)		HEAVY LATERAL TURBULENCE (σ_v = 3.05 M/SEC)	
		IDENTIFIED PARAMETER	% ERROR	IDENTIFIED PARAMETER	% ERROR
X_u	-.01857	*	--	*	--
Z_u	.02097	--	--	--	--
M_u	.04449	*	--	*	--
X_w	.02894	-.0248	185.8	.0289	.13
Z_w	-.2598	.01075	104.1	-.3021	16.3
M_w	.00935	.000433	95.3	.00971	3.5
M_q	-1.3422	*	--	*	--
$X_{\delta_{LONG}}$	-1.3092	*	--	*	--
$Z_{\delta_{LONG}}$	-.37776	*	--	*	--
$M_{\delta_{LONG}}$	-12.58189	*	--	*	--
$X_{\delta_{COLL}}$	11.2452	10.6824	5.0	5.0244	1.9
$Z_{\delta_{COLL}}$	-96.612	-86.844	10.2	-97.500	.91
$M_{\delta_{COLL}}$	.69449	.14606	78.9	.69134	.45

*Held fixed to values identified from δ_{LONG} maneuver

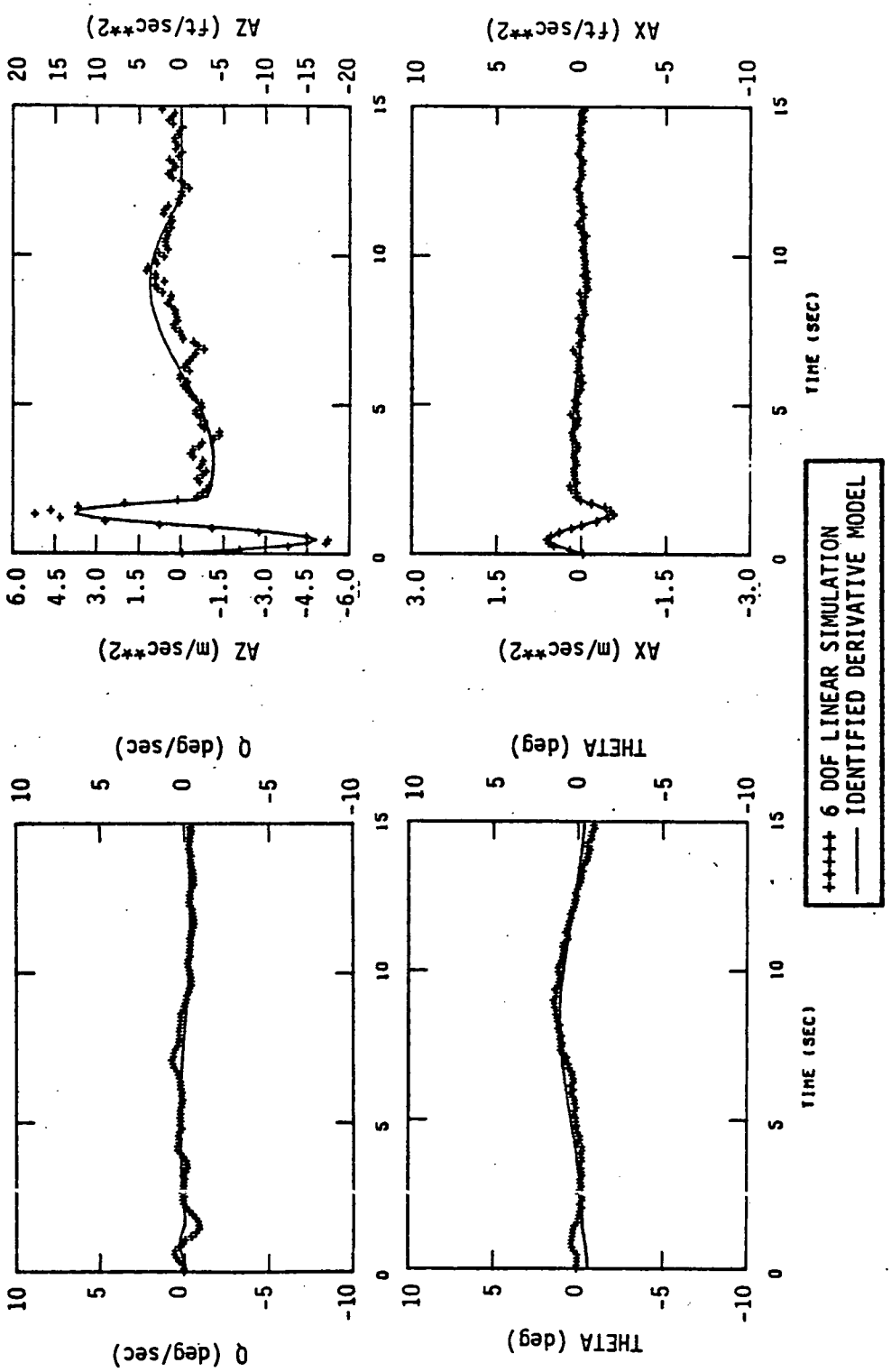

Figure 3.12 Longitudinal Time History Match of Identified Derivative Model and 6 DOF LRC Derivative Noise Contaminated Simulated Data with Heavy Vertical Random Wind Gust (σ_w = 3.05 m/sec, Hover)

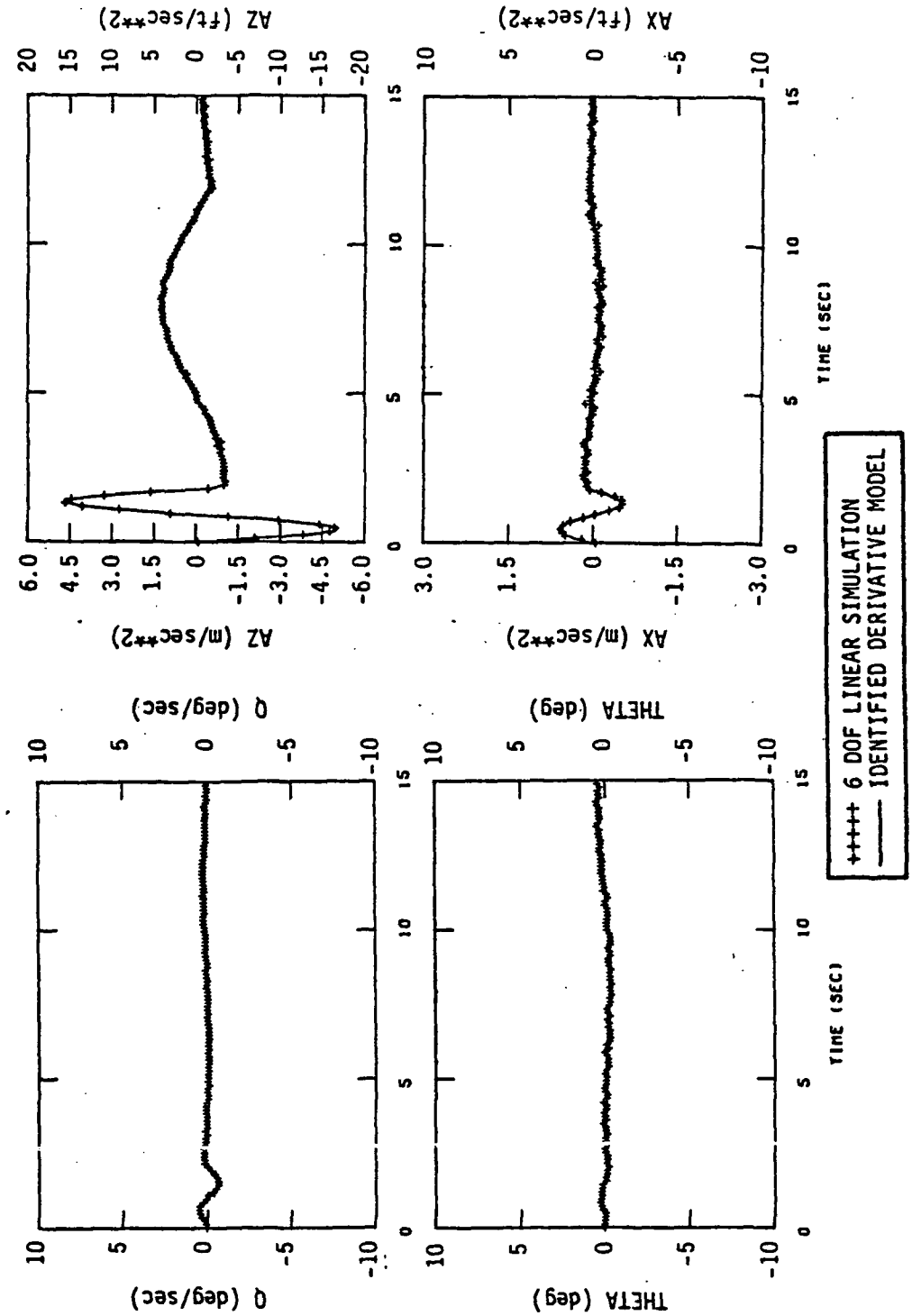

Figure 3.13 Longitudinal Time History Match of Identified Derivative Model and 6 DOF LRC Derivative Noise Contaminated Simulated Data with Heavy Lateral Random Wind Gust (σ_v = 3.05 m/sec, Hover)

each case is the 6 DOF LRC derivative model with the CH-47 production SAS (with $K_p \div 2$) shown in Appendix B. The procedures used are essentially identical to those employed for the longitudinal case. Random noise, bias, and scale factor errors are used and the nominal values employed are shown in Table 2.4, and implemented as shown in Figure 2.13. Single input excitations are employed as in the longitudinal case and designed to contain frequencies at the natural system modes. The procedure employed first identifies derivatives using a lateral input maneuver and then the remaining derivatives are identified using a rudder (lateral cyclic) input. In addition, the effect of random wind gust on identification accuracy is presented.

3.4.1 Lateral and Rudder Input Maneuver Results--Zero Turbulence

Table 3.25 presents the identified lateral parameter values for both the lateral control input (δ_{LAT}) maneuver and the rudder pedal input (δ_{RUD}) maneuver. The resulting accuracy for most of the derivatives is shown to be very good with the exception of those derivatives contributing negligibly to the time response. Figure 3.14 shows the time history fit using the derivatives identified from the lateral control input (δ_{LAT}) maneuver and Figure 3.15 shows the time response comparison for the rudder pedal input (δ_{RUD}) maneuver. The time history fits are shown to be excellent for each maneuver reflecting the accuracy levels shown in Table 3.25.

As discussed previously, the lateral model employs constant feedback gains in the structure; thus, the primed derivatives shown in Table 3.25 include the effects of the roll and yaw SAS. Table 3.26 shows the aerodynamic derivatives without the SAS as determined from Eq. (3.9). The lateral velocity derivatives are not affected for the hover case since there is no sideslip feedback at hover.

Table 3.25

Lateral Derivative Identification Results at Hover for Both A δ_{LAT} and δ_{RUD} Maneuver (Random Noise, Bias Scale Factors, 6 DOF Simulation)

PARAMETER	REF. 1 TRUE PARAMETER VALUE	δ_{LAT} INPUT MANEUVER		δ_{RUD} INPUT MANEUVER	
		IDENTIFIED PARAMETER	% ERROR	IDENTIFIED PARAMETER	% ERROR
Y_v	-.1317	-.1328	.78	**	--
L_v	-.02044	-.02175	7.2	**	--
N_v	-.00338	-.002175	35.5	**	--
Y'_p	-1.383	-1.463	5.8	**	--
L'_p	-1.834	-1.960	6.9	**	--
N'_p	-.1653	-.0972	41.2	**	--
Y'_r	-.1180	*	--	.1743	218.1
L'_r	.5517	*	--	.7403	34.2
N'_r	-2.098	*	--	-2.53	20.7
$Y_{\delta LAT}$	13.884	15.132	9.0	**	--
$L_{\delta LAT}$	16.9961	18.2638	7.5	**	--
$N_{\delta LAT}$	1.66496	1.1732	29.3	**	--
$Y_{\delta RUD}$	-.66072	-1.80060	172.5	-.9348	41.5
$L_{\delta RUD}$	-2.36496	-4.38976	81.4	-3.1378	32.4
$N_{\delta RUD}$	7.8268	3.82717	51.1	9.6614	23.4

*Held fixed to zero
**Held fixed to values identified from δ_{LAT} maneuver

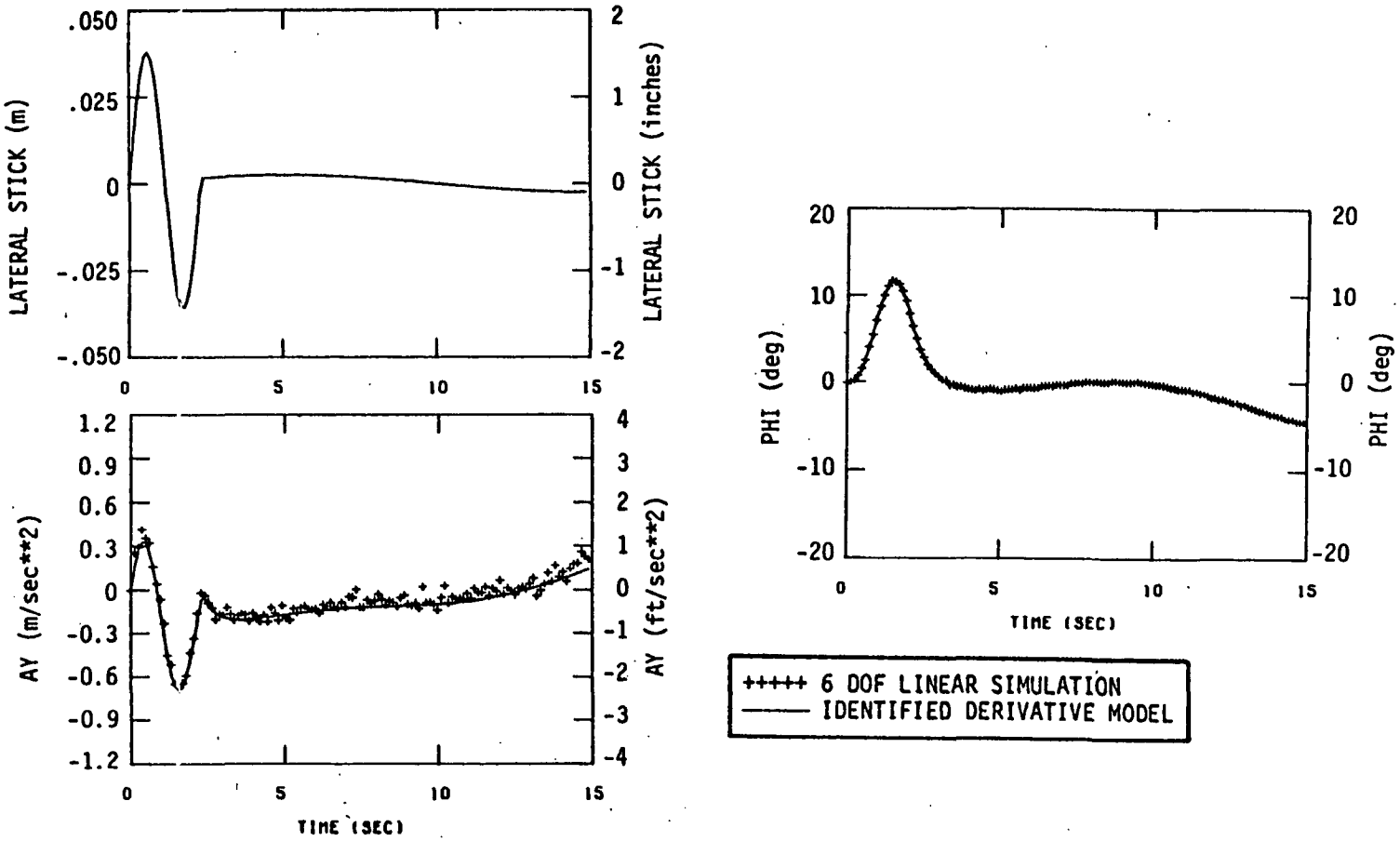

Figure 3.14 Lateral Time History Comparison of Identified Derivative Model and 6 DOF LRC Derivative Noise Contaminated Simulated Data (Hover, δ_{LAT} Input, Random Noise, Bias, and Scale Factor Errors)

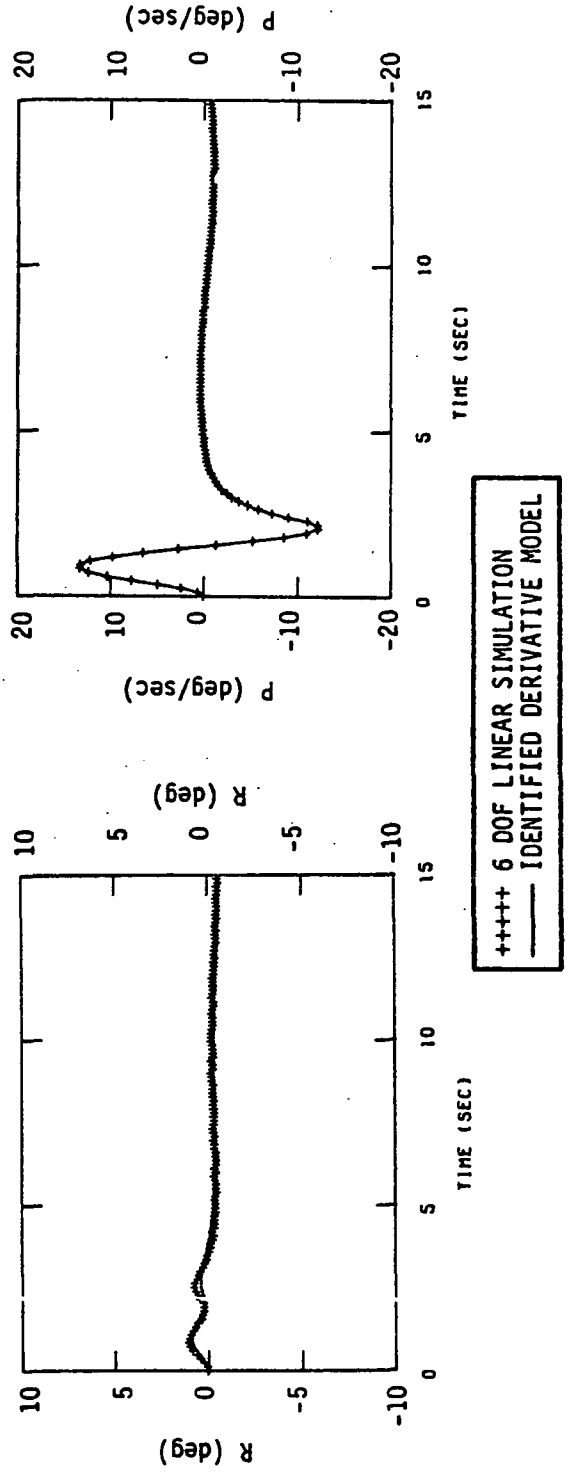

Figure 3.14 (Concluded)

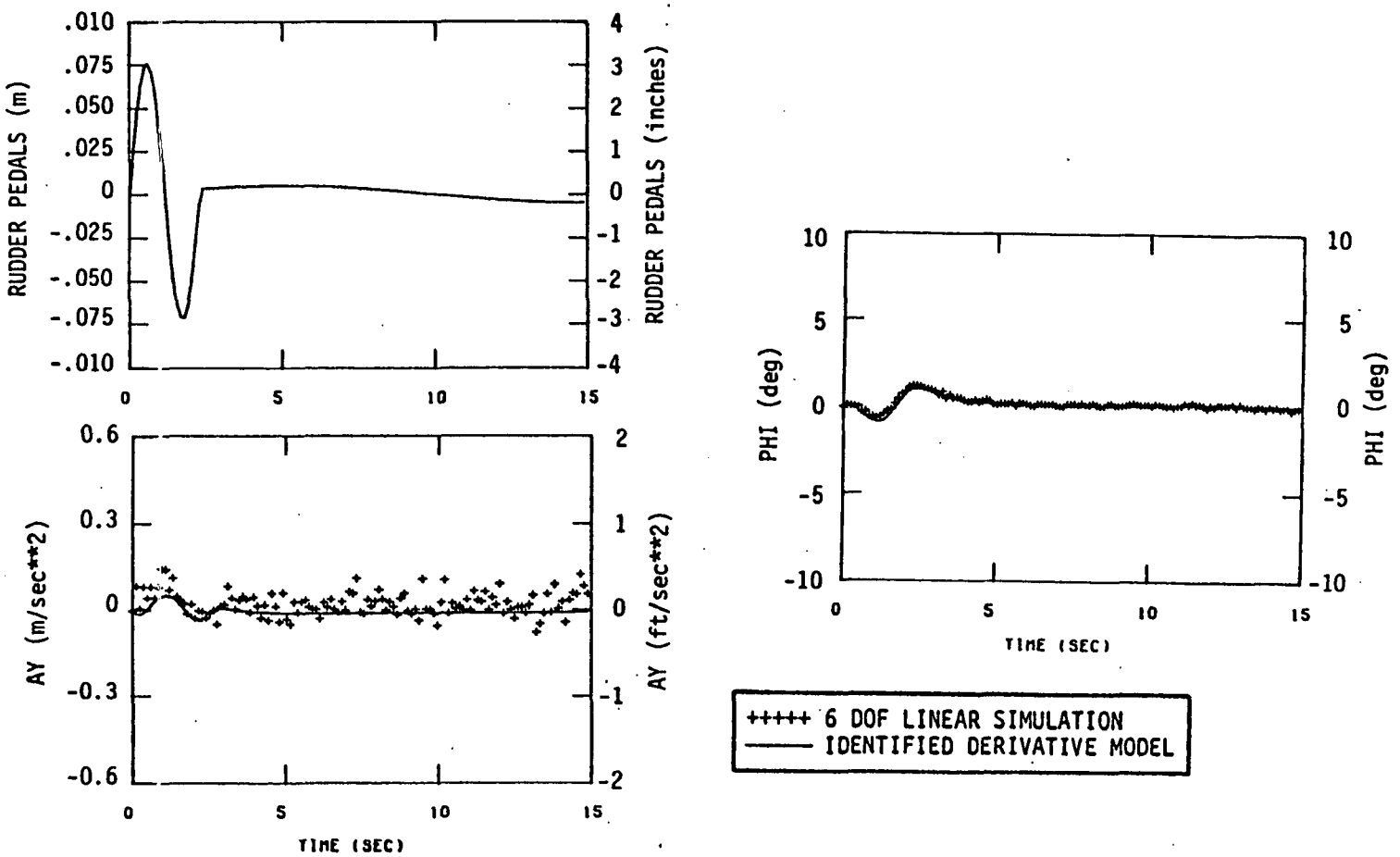

Figure 3.15 Lateral Time History Comparison of Identified Derivative Model and 6 DOF LRC Derivative Noise Contaminated Simulated Data (Hover, δ_{RUD} Input, Random Noise, Bias and Scale Factor Errors)

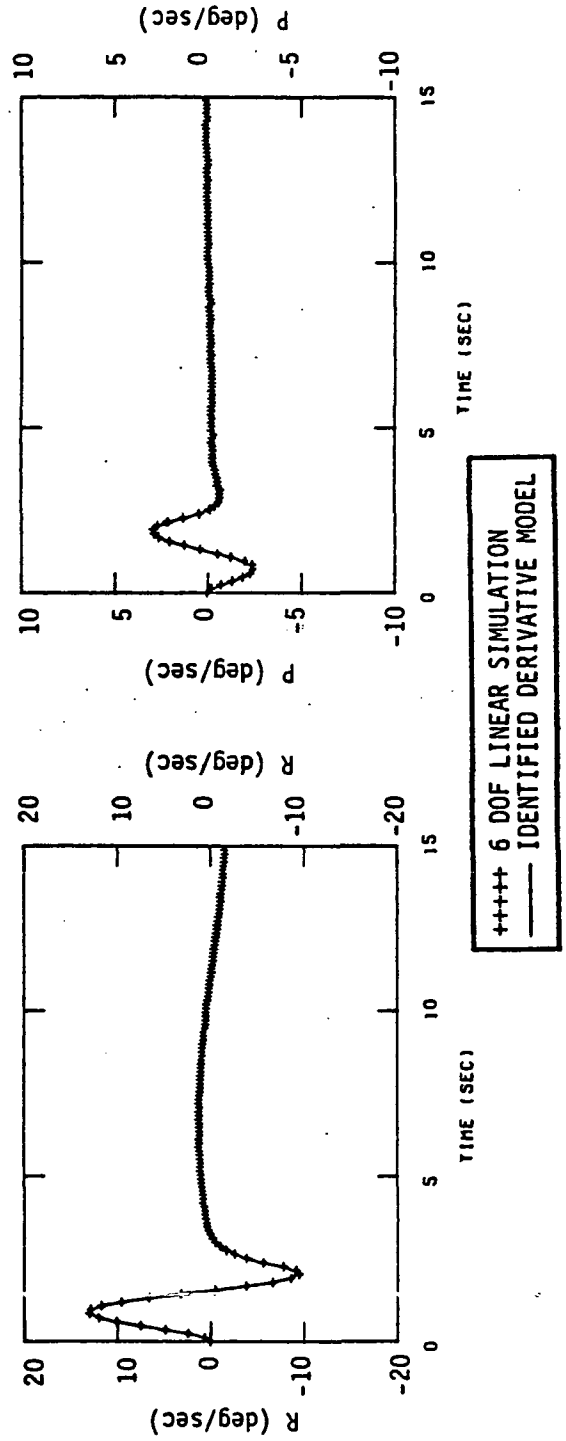

Figure 3.15 (Concluded)

Table 3.26

Lateral Aerodynamic Derivatives without the SAS Contribution from Equation (41) using Identified Values of Table 3.25 (Hover)

PARAMETER	Ref. 1 TRUE PARAMETER VALUE	MAXIMUM LIKELIHOOD ESTIMATED VALUE*	% ERROR
Y_p	-.501	-.502	0.24
L_p	-.7547	-.800	6.0
N_p	-.0595	-.0227	61.8
Y_r	-.0552	-.1057	91.4
L_r	-.0753	-.0822	9.1
N_r	-.0465	-.00047	98.9

*Derived from Eq. (55): K_p = -.064, K_r = -.262

3.4.2 Lateral Results – Heavy Turbulence

The lateral control input (δ_{LAT}) maneuver was repeated with heavy turbulence (σ_v = 3.05 m/sec) in the lateral axis. The identified parameter values are shown in Table 3.27 and, for the most part, have been degraded appreciably over the zero gust case. The lateral input control derivatives $Y_{\delta_{LAT}}$, $L_{\delta_{LAT}}$, and $N_{\delta_{LAT}}$ are shown to be of fair accuracy and the stability derivative N_v is of good accuracy. Gust, in general, is found to have the smallest degradation in accuracy of the control derivatives and the excellent accuracy in N_v of Table 3.27 is most likely due to the large excitation in lateral velocity as a result of the gust, thus causing good identifiability. The time history responses (Figure 3.16) show a reasonable fit between the identified derivative and simulation models.

Table 3.27

Lateral Derivative Identification Results at Hover for δ_{LAT} Input with Heavy Lateral Turbulence (Random Noise, Bias, Scale Factors, 6 DOF Simulation)

PARAMETER	REF. 1 TRUE PARAMETER VALUE	δ_{LAT} INPUT MANEUVER	
		IDENTIFIED PARAMETER	% ERROR
Y_v	-.1317	-.2533	92.2
L_v	-.00623	-.01086	74.3
N_v	-.00103	-.00109	6.5
Y_p	-4.537	-8.79	93.9
L_p	-1.834	-2.157	17.6
N_p	-.1653	-.1123	32.0
Y_r	-.3870	*	--
L_r	.5517	*	--
N_r	-2.098	*	--
$Y_{\delta LAT}$	1.157	1.609	39.1
$L_{\delta LAT}$	.4317	.4769	10.5
$N_{\delta LAT}$	.04229	.0315	25.4
$Y_{\delta RUD}$	-.05506	--	--
$L_{\delta RUD}$	-.06007	--	--
$N_{\delta RUD}$	.1988	--	--

*Held fixed to zero

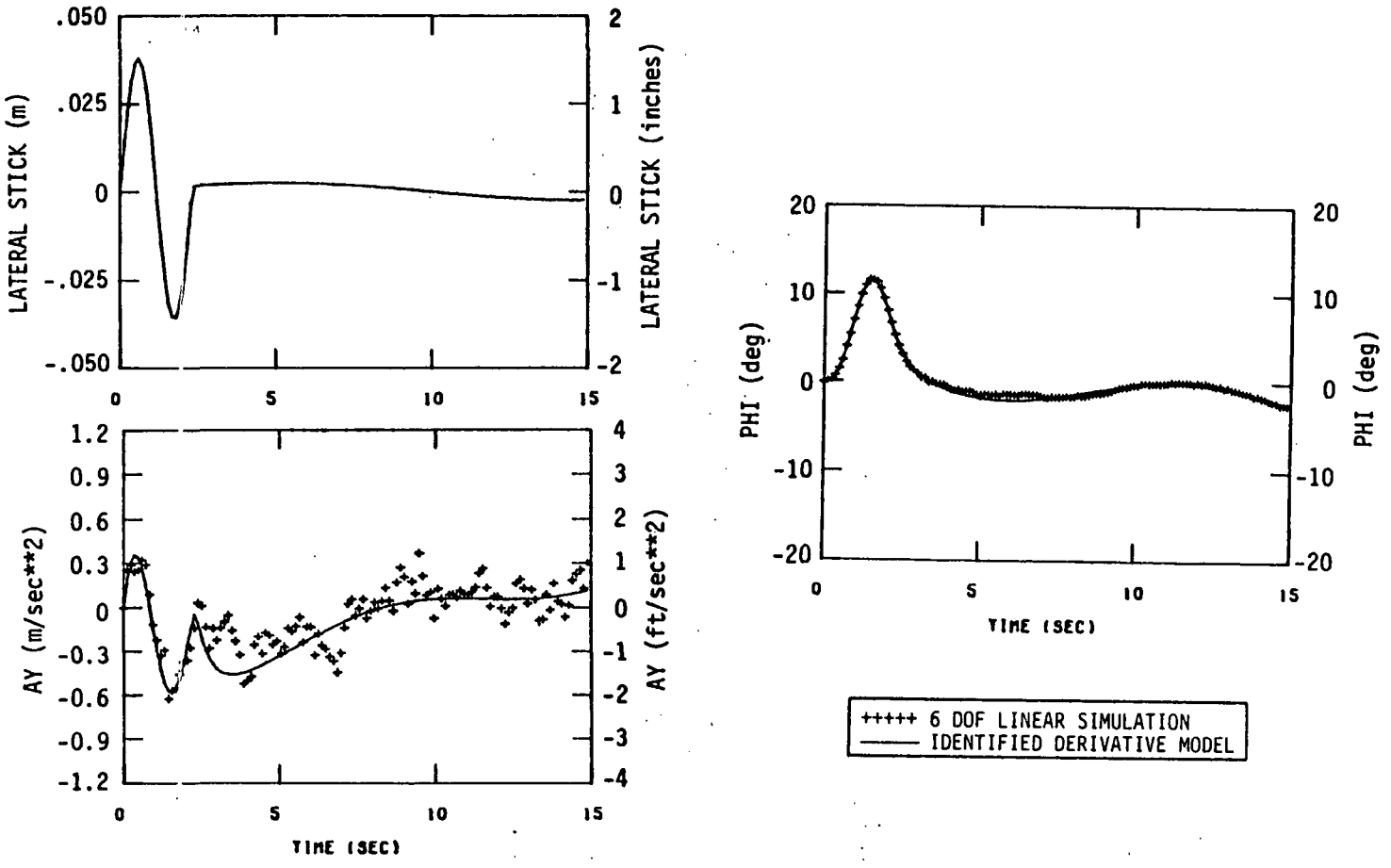

Figure 3.16 Lateral Time History Comparison of Identified Derivative Model and 6 DOF LRC Derivative Noise Contaminated Simulated Data with Heavy Lateral Turbulence (σ_v = 3.05 m/sec, Hover)

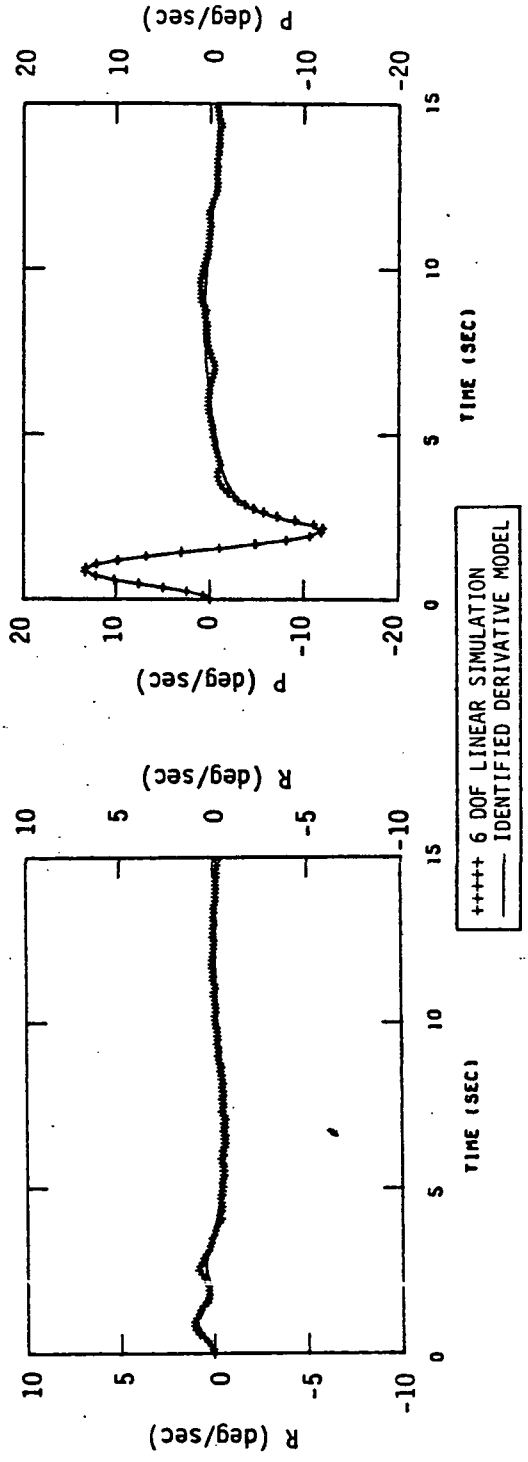

Figure 3.16 (Concluded)

3.5 IDENTIFICATION RESULTS AT THE 60 KNOT SPIRAL DESCENT CONDITION

The 60 knot spiral descent flight derivatives from Ref. 1 were used to generate a nonlinear simulation model. A nonlinear model was used in order to correctly represent the kinematics of turning flight. Control inputs were designed similar to the 40 knot case previously discussed. The results of the 60 knot spiral descent flight condition are summarized below for the longitudinal and lateral maneuvers; the simulation model is shown in Appendix C.

3.5.1 Longitudinal Identification Results

The longitudinal inputs designed for the 40 knot condition were also used for 60 knots. Eigenvalues were obtained from the LRC derivatives at the 60 knot spiral descent flight condition with and without the CH-47 production SAS. This condition was found to be the most unstable of the three airspeeds analyzed (due to longitudinal divergent root); thus, the control inputs caused excessive divergence in the response for both longitudinal and lateral input maneuvers. The open- and closed-loop eigenvalues are shown in Table 3.28.

The longitudinal input maneuver used for the 40 knot condition was used with the 60 knot simulation program. This input was clearly unsatisfactory due to the large degree of instability even with SAS-on. After several input redesign attempts, it was found that by setting to zero the first one-half cycle of the low frequency input, the response in pitch remained within acceptable response limits. The resulting input used for the longitudinal maneuver is shown in Eq. (3.10) and is within the TAGS rate authority.

Table 3.28

Eigenvalues for the 60 Knot Spiral Descent Flight Condition with and without the CH-47 Production SAS

	SAS-OFF	CH-47 PRODUCTION SAS-ON $K_p \div 2$
Long./Vert.	$-.112 \pm j\ .281$	$-.328 \pm j\ .298$
Long. Divergent	.5025	.220
Pitch Damping	-2.607	$-2.336 \pm j\ 2.637$
Dutch Roll	$.08 \pm j\ .379$	$-.218 \pm j\ .3734$
Roll Damping	-1.07	$-2.24 \pm j\ .3512$
Spiral	-.0406	-.00185

$$\delta_{LONG} = A_1 \sin 3.43t + A_2 \sin .525t \quad \sim \text{cm}$$

$$A_1 = \begin{cases} 3.6 & t < 1.8 \\ 0.0 & t \geq 1.8 \end{cases}$$

$$A_2 = \begin{cases} .90 & 6 < t < 12 \\ 0.0 & t < 6 \\ 0.0 & t > 12 \end{cases}$$

$$\delta_{COLL} = B_1 \sin 3.43t + B_2 \sin .525t \quad \sim \text{cm} \qquad (3.10)$$

$$B_1 = \begin{cases} 3.6 & 6 < t < 7.8 \\ 0.0 & t < 6 \\ 0.0 & t > 7.8 \end{cases}$$

$$B_2 = \begin{cases} .90 & t > 6 \\ 0.0 & t < 6 \end{cases}$$

The time history response for the longitudinal input of Eq. (3.10) for the 60 knot spiral descent condition is shown in Figure 3.17 using both the linear and nonlinear simulation. The δ_{LONG} input is shown to consist of one-half cycle of the low frequency input to prevent divergence of the pitch response due to the highly unstable pitch divergent eigenvalues. Also, the δ_{COLL} input employs the reduced value for the high frequency input so that saturation of the TAGS actuator is prevented.

The longitudinal derivatives are identified with reasonable accuracy using either the linear or nonlinear simulation data. The results are shown in Table 3.29.

The time history match of the identified derivatives and nonlinear simulation data is shown in Figure 3.18 for the spiral descent condition. The excellent match further reflects the accuracy in the identified derivatives. Table 3.30 presents the identified derivatives, standard deviations, and F-ratios for this condition.

3.5.2 Lateral Identification Results

Lateral inputs were designed similar to the 40 knot condition and resulted in large divergence in the pitch mode 9.0 m/sec longitudinal velocity change]. The cross-coupling was determined to be very weak and the longitudinal divergence is a result of the pitch longitudinal divergent root. Since under actual flight conditions the pilot normally stabilizes this divergence, it was decisded that a pilot math model should be used to simulate this situation. Although the math model representation is only an approximation to pilot response, it should be adequate for the purposes of this study (i.e. to keep the pitch mode from diverging). It was assumed that a pilot model which corrected for pitch changes would be acceptable for stabilizing the divergent root.

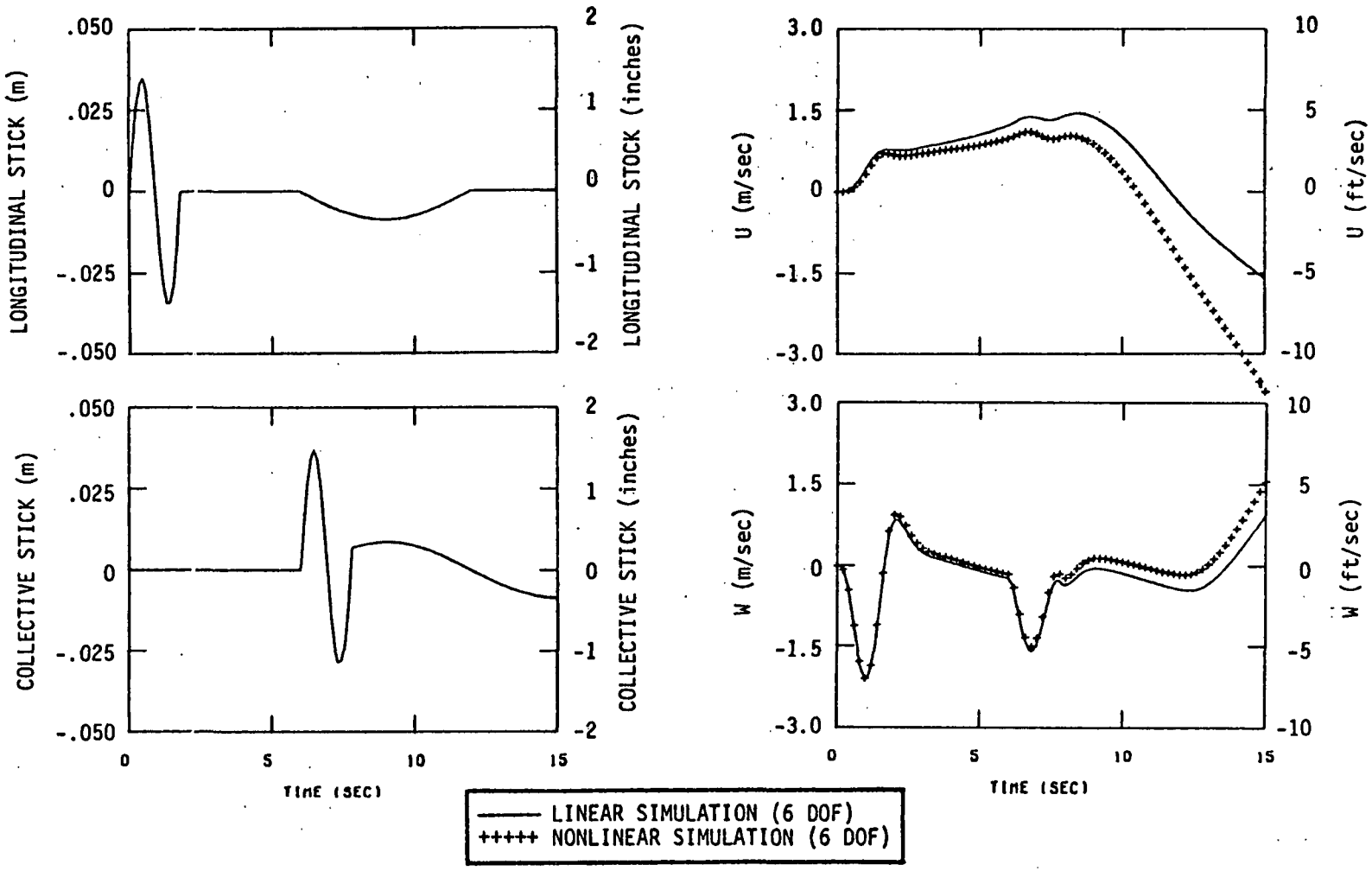

Figure 3.17 Time History Comparison of the 6 DOF Nonlinear and Linear Simulation for the Longitudinal 60 KT Spiral Descent Condition (Hover)

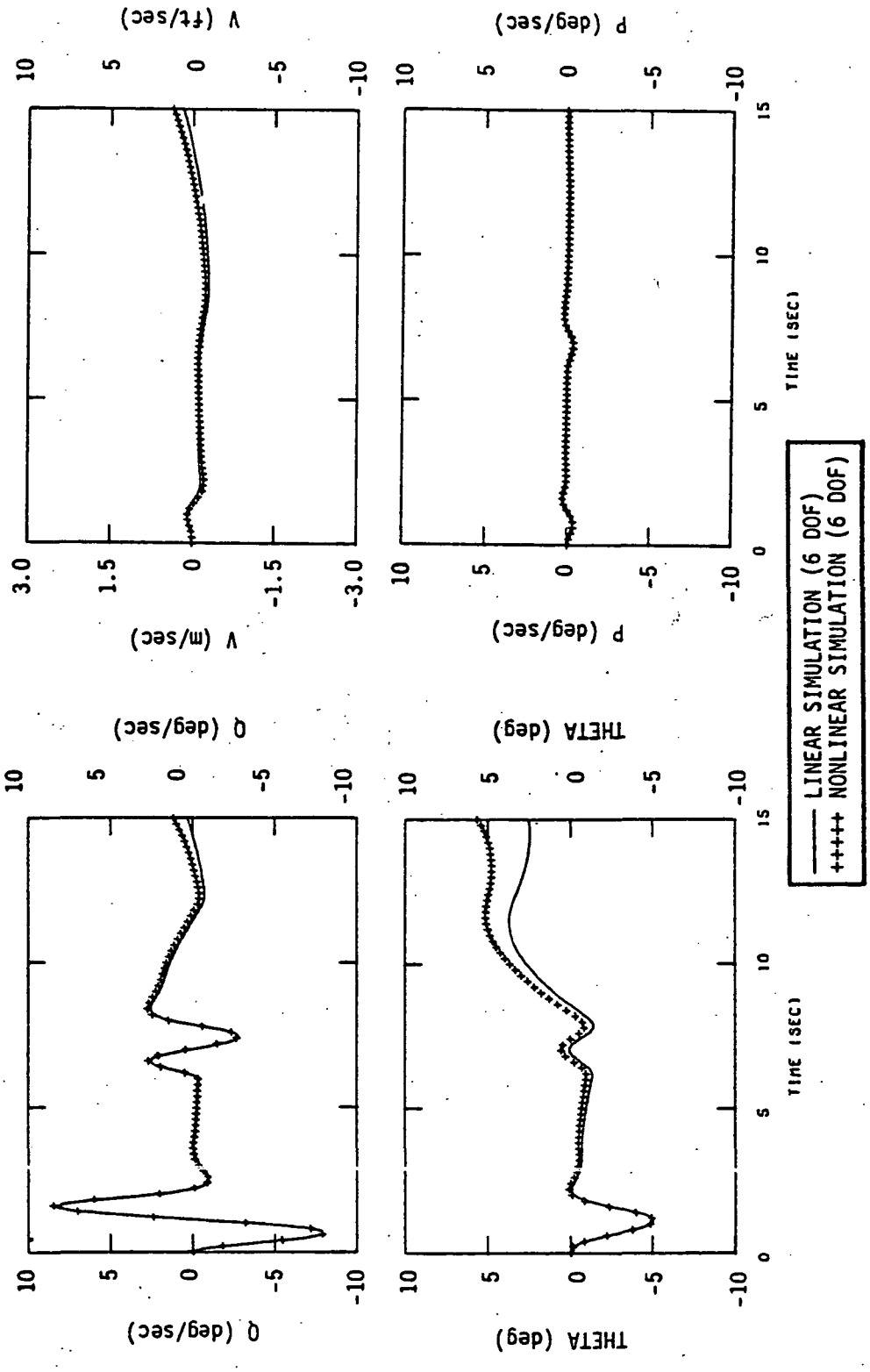

Figure 3.17 (Continued)

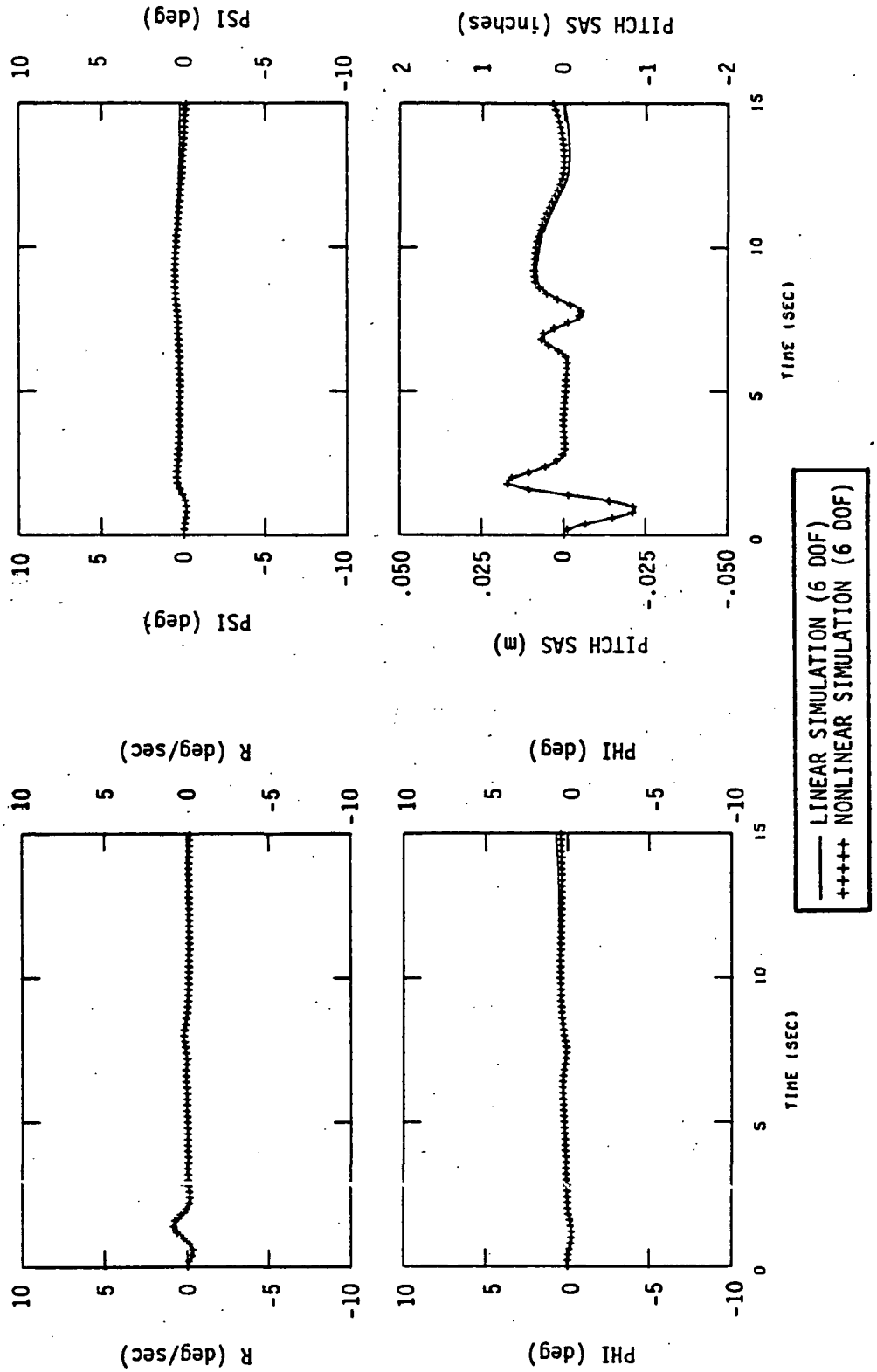

Figure 3.17 (Continued)

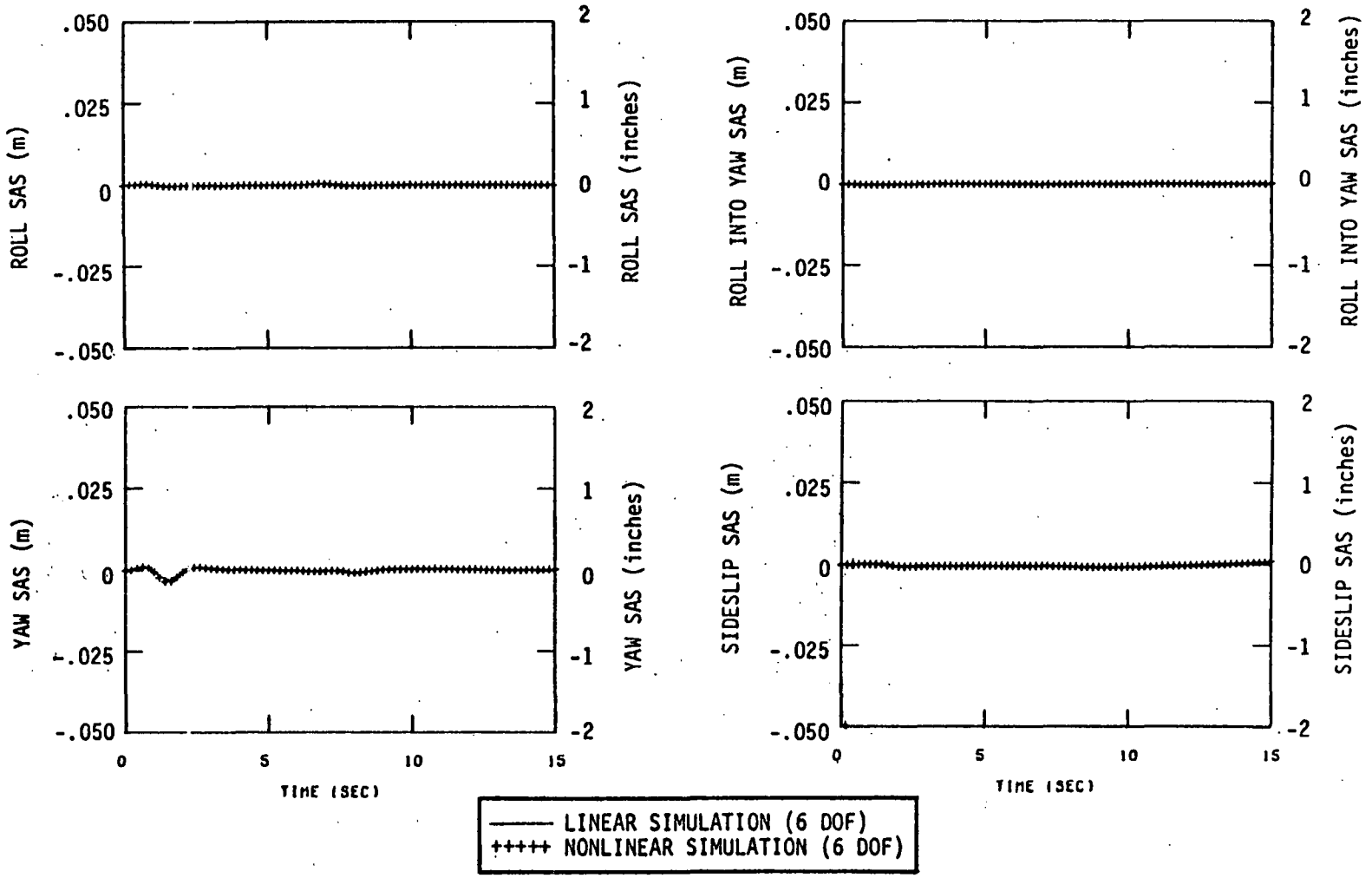

Figure 3.17 (Concluded)

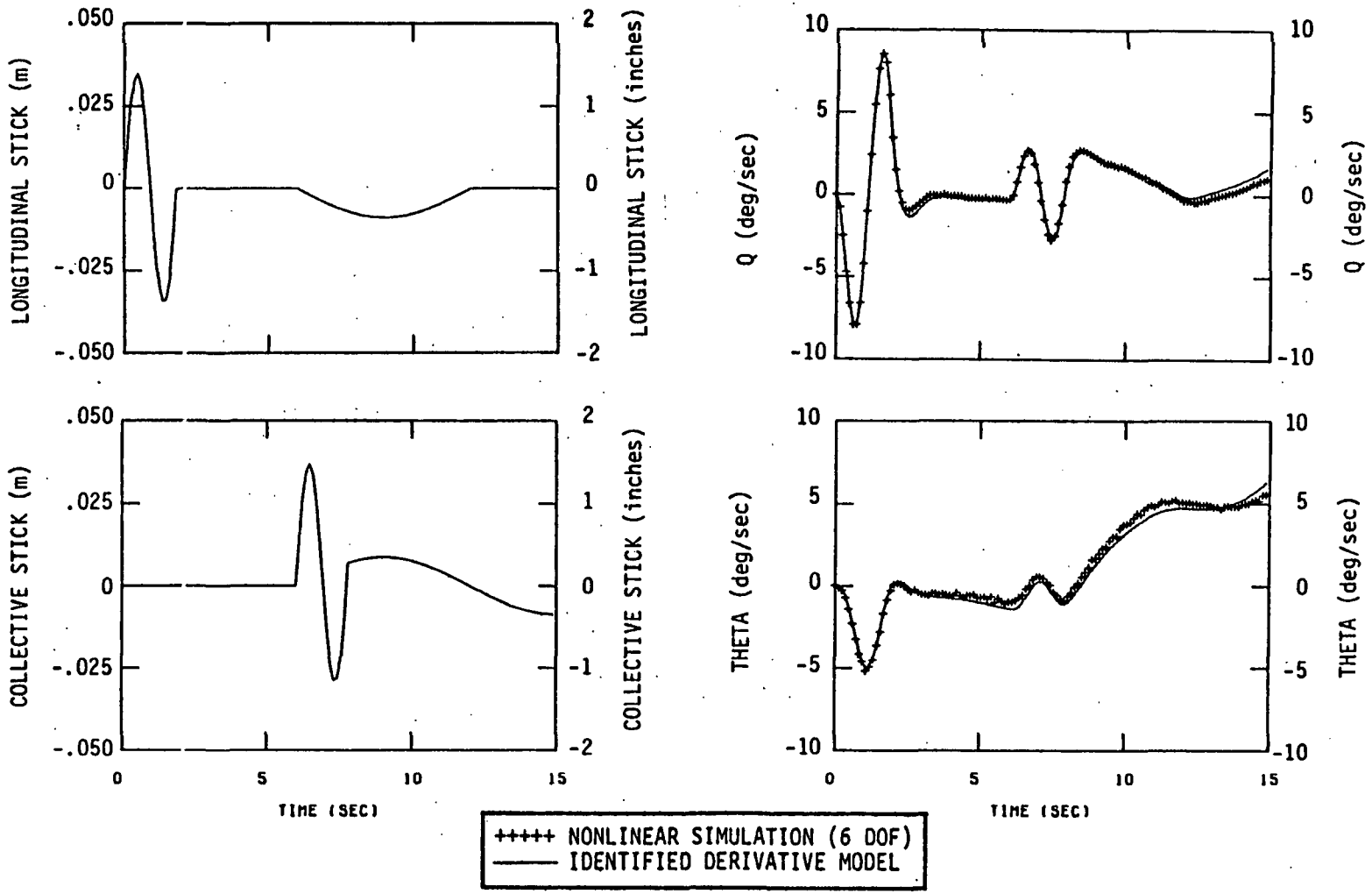

Figure 3.18 Longitudinal Time History Match of Identified Derivative Model and 6 DOF Nonlinear Noise Contaminated Simulation Data (60 KT Spiral Descent)

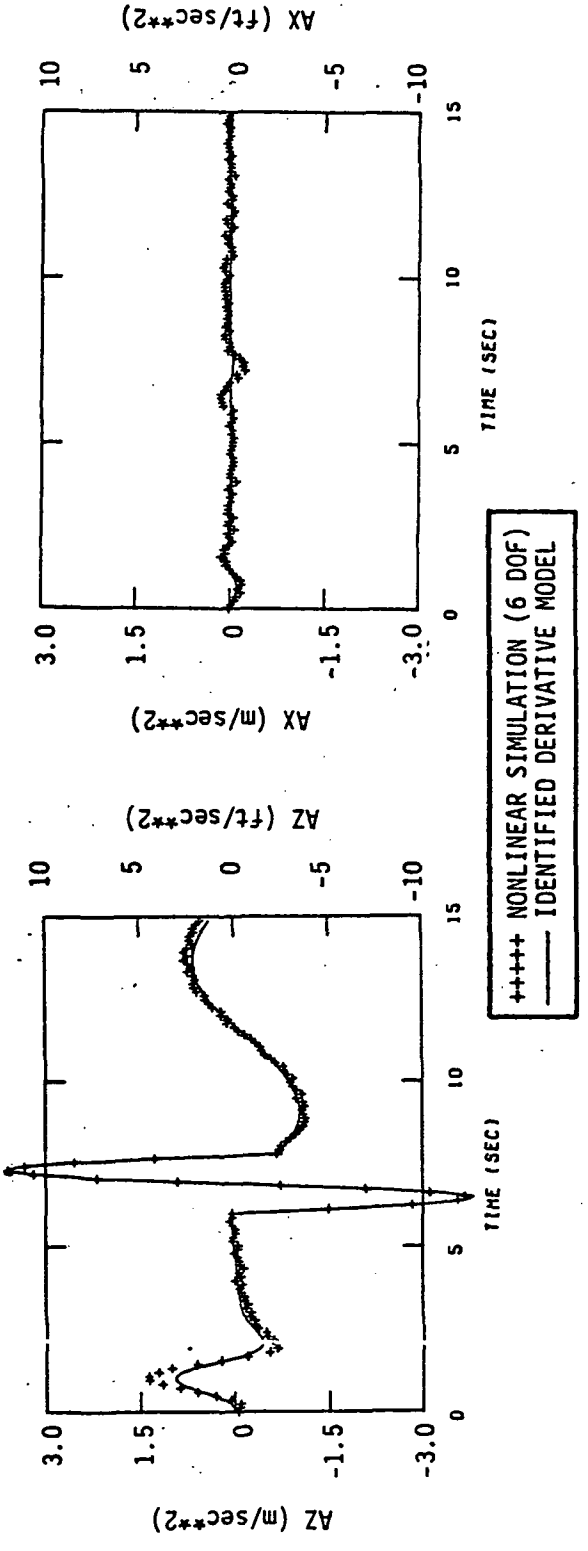

Figure 3.18 (Concluded)

Table 3.29

Longitudinal Identification Results for the 60 Knot Spiral Descent Flight Condition

PARAMETER	REF. 1 TRUE PARAMETER VALUE	DATA FROM 6 DOF LINEAR SIMULATION	DATA FROM 6 DOF NONLINEAR SIMULATION
		MAXIMUM LIKELIHOOD ESTIMATED PARAMETER	MAXIMUM LIKELIHOOD ESTIMATED PARAMETER
X_u	-.01916	-.00873	-.00988
Z_u	-.0740	-.1017	-.0536
M_u	-.01637	-.01814	-.01644
X_w	.03956	.01310	.0102
Z_w	-.5395	-.5302	-.4479
M_w	.06089	.04974	.03835
M_q	-1.701	-1.447	-1.393
$X_{\delta_{LONG}}$	-1.4880	-.1656	-.4236
$Z_{\delta_{LONG}}$	-6.1572	.02748	-.2508
$M_{\delta_{LONG}}$	-15.4685	-14.8268	14.5512
$X_{\delta_{COLL}}$	5.6532	4.8132	-.0876
$Z_{\delta_{COLL}}$	-110.196	-113.856	-115.38
$M_{\delta_{COLL}}$	6.5118	7.4803	6.0866

Table 3.30

Longitudinal Identification Results for the 60 kt Spiral Descent Flight Condition Using the Nonlinear Simulation

PARAMETER	REF. 1 TRUE PARAMETER VALUE	MAXIMUM LIKELIHOOD		
		IDENTIFIED PARAMETER	STANDARD DEVIATION	PARAMETER F-RATIO
X_u	-.01916	-.00988	.00275	12.9
Z_u	-.0740	-.0536	.00855	39.3
M_u	-.01637	-.01644	.00066	628.3
X_w	.03956	.0102	.00556	3.36
Z_w	-.5395	-.4479	.01101	1654.
M_w	.06089	.03835	.00144	697.
M_q	-1.701	-1.393	.0228	3704.
$X_{\delta_{LONG}}$	-1.4880	-.4236	.34404	1.51
$Z_{\delta_{LONG}}$	-6.1572	-.2508	.70536	.127
$M_{\delta_{LONG}}$	-15.4685	-14.5512	.10158	20463.
$X_{\delta_{COLL}}$	5.6532	-.0876	.34956	.0639
$Z_{\delta_{COLL}}$	-110.196	-115.68	.72444	25534.
$M_{\delta_{COLL}}$	6.5118	6.0866	.09724	3894.

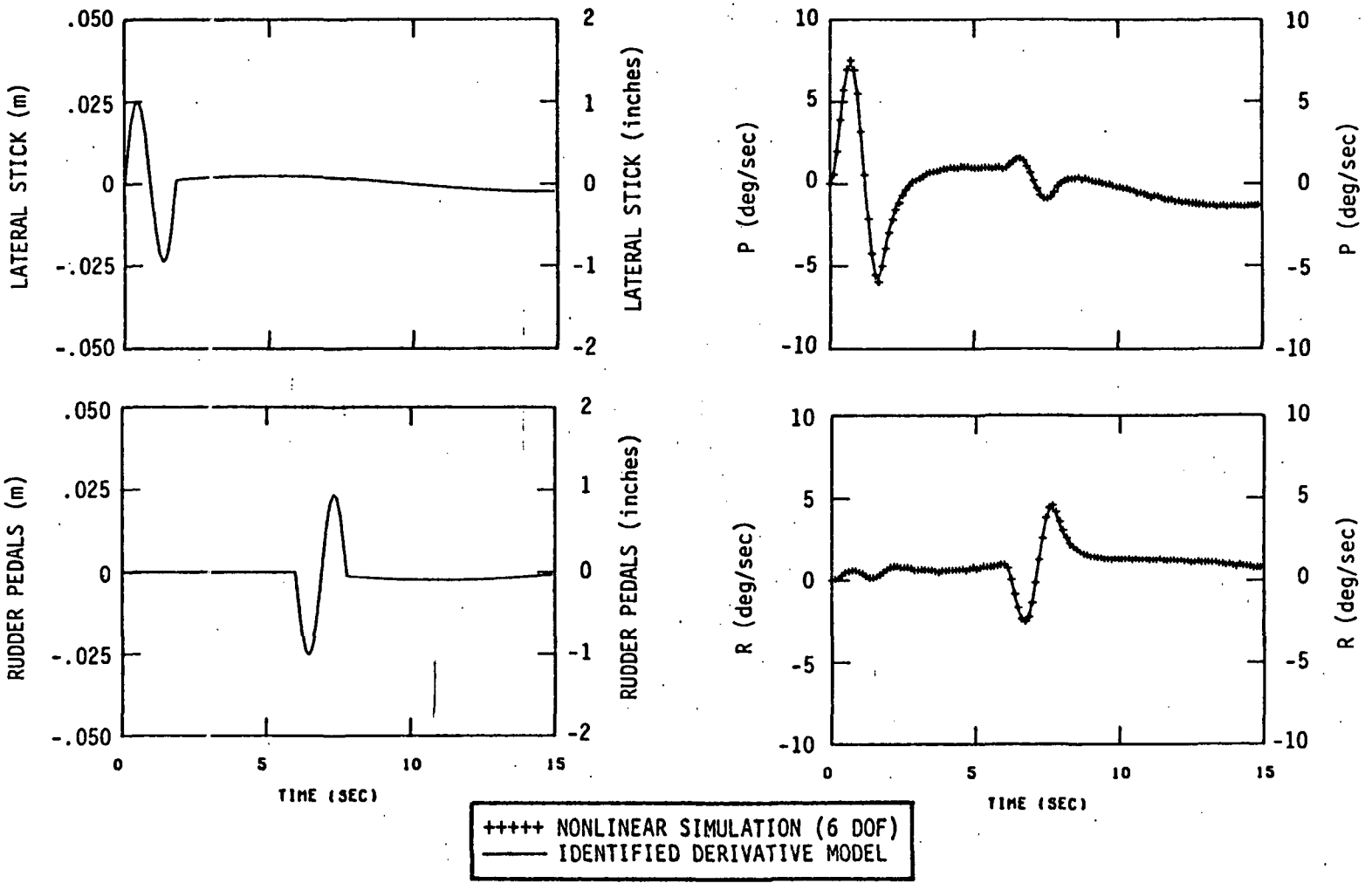

Figure 3.19 Lateral Time History Match of Identified Derivative Model and 6 DOF Nonlinear Noise Contaminated Simulation Data (60 KT Spiral Descent)

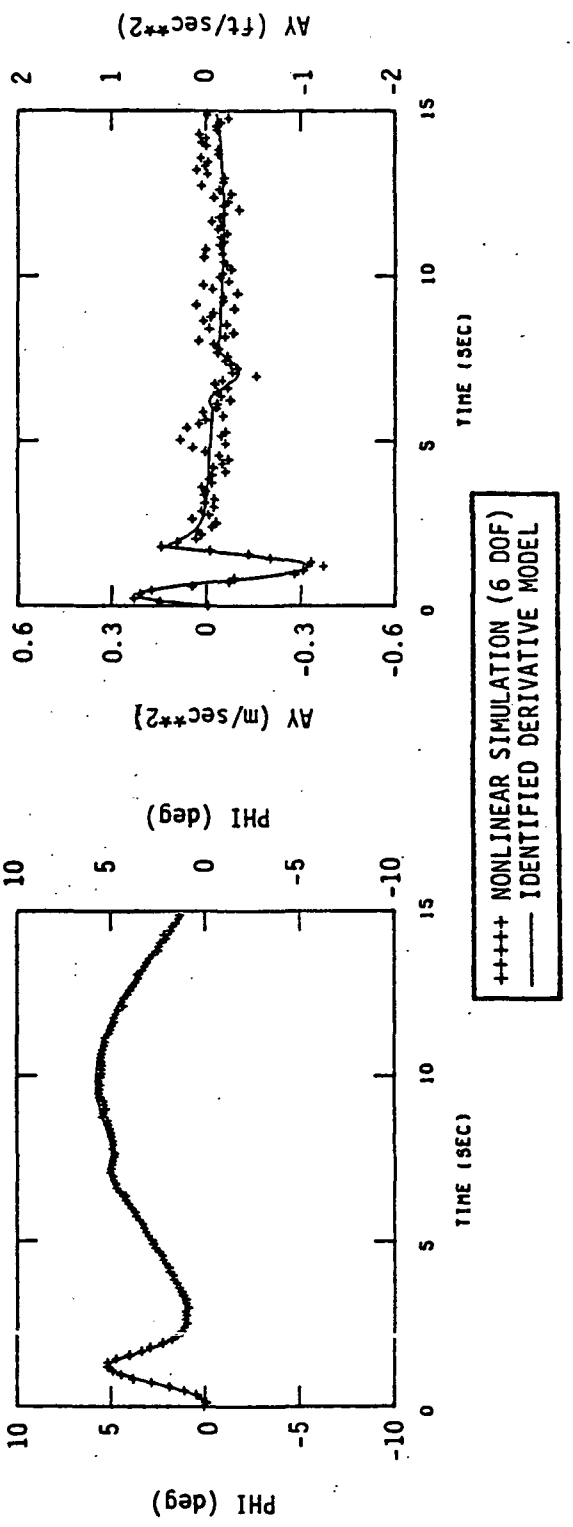

Figure 3.19 (Concluded)

Identification results for the lateral inputs are shown in Table 3.31, with the pilot model incorporated in the simulation to stabilize divergent pitch mode. The time history match to the non-linear simulation is shown in Figure 3.19.

Table 3.31

Lateral Identification Results from the Nonlinear Simulation Including the Pilot Model (60 Knot Sprial)

PARAMETER	REF. 1 TRUE PARAMETER VALUE	MAXIMUM LIKELIHOOD[1]		
		ESTIMATED PARAMETER	STANDARD DEVIATION	F-RATIO
Y_v	-.07208	-.05207	.00273	361.
L_v	-.23648	-.020085	.000446	2014.
N_v	.02093	.019423	.000584	1105.
Y_p	-1.517	-1.697	.068	620.
L_p	-1.943	-2.070	.00960	46453.
N_p	-.1797	-.2692	.0128	440.
Y_r	.1188	---	---	---
L_r	.53176	.8437	.0191	1934.
N_r	-1.9906	-2.329	.0249	8729.
$Y_{\delta_{LAT}}$	13.128	13.992	.3528	1567.
$L_{\delta_{LAT}}$	16.3307	16.8780	.05472	96012.
$N_{\delta_{LAT}}$	1.5906	2.2283	.08228	729.
$Y_{\delta_{RUD}}$	-.73008	-1.5204	.3192	22.7
$L_{\delta_{RUD}}$	-2.3740	-3.7047	.06417	3318.
$N_{\delta_{RUD}}$	7.4370	9.1535	.08819	10732.

[1]With pilot model used in simulation data

The next chapter presents the flight test plan for the CH-47 VALT research aircraft for parameter identification based on the results presented in this chapter.

IV. FLIGHT TEST PLAN FOR CH-47 PARAMETER IDENTIFICATION

The flight test plan presented in this chapter is based on the operational requirements of the VALT mission and the results of the previously described analytical identification study. The recommended flight test plan is based on a number of separate test points which have been selected for the task of CH-47 parameter identification along the VALT trajectory. These test points are described, and the required pilot input are specified in separate sections.

4.1 FLIGHT TEST CONDITIONS

Table 4.1 provides an overview of the recommended flight test plan and each test point is described in the following paragraphs.

Flight Test Point (1): Flight test point (1) is at a hover condition at 200 ft altitude. This condition is selected to familiarize the pilot with the recommended testing procedures. This point serves as a useful starting point for the remainder of the test by providing a "bench mark" evaluation of atmospheric conditions, "feel of the aircraft," and instrumentation calibration. In addition, the CH-47 is out-of-ground effect and is stable with the SAS on.

Four uncoupled inputs are applied at this point. These are:

(1) differential collective for excitation of the longitudinal mode (δ_{LONG});

(2) collective for excitation of the vertical mode (δ_{COLL});

(3) lateral cyclic for excitation of the primary roll modes (δ_{LAT}); and

TABLE 4.1

Summary Table of Flight Test Conditions Recommended for Testing (Zero Sideslip Except Where Noted)

FLIGHT TEST POINT	FLT. TEST SEQ. NO.	AIRSPEED (KTS)	VERTICAL SPEED (M/SEC)	ALTITUDE (M)	CONTROL INPUT	COMMENTS
(1)	1 2 3 4	0	0	61	δ_{LONG} δ_{COLL} δ_{LAT} δ_{RUD}	• Familiarity • Out-of-ground effect • Stable with SAS-on
*(2)	5 6 7 8	14.08	-2.54	61	δ_{LONG} δ_{COLL} δ_{LAT} δ_{RUD}	• Familiarity • Out-of-ground effect • Stable with SAS-on
(3)	9 10 11 12	0	0	15.2	δ_{LONG} δ_{COLL} δ_{LAT} δ_{RUD}	• Replacement of VALT test point • In-ground effect • Stable with SAS-on
---	--	14.08	-2.54	15.2	---	• VALT test point • Unsafe maneuver (not recommended)
*(4)	13 14 15 16	20	-2.54	61	δ_{LONG} δ_{COLL} δ_{LAT} δ_{RUD}	• VALT test point • Stable with SAS-on • Additional inputs may be required to hold u or w fixed
(5)	17 18	40	0	97.5	δ_{LONG} & δ_{COLL} δ_{LAT} & δ_{RUD}	• Unstable with SAS-on • Pilot stabilization required • Additional inputs may be required for lateral decoupled response

*Conditions to be repeated: 13 additional maneuvers, total number of maneuvers = 49

TABLE 4.1 (Concluded)

FLIGHT TEST POINT	FLT. TEST SEQ. NO.	AIRSPEED (KTS)	VERTICAL SPEED (M/SEC)	ALTITUDE (M)	CONTROL INPUT	COMMENTS
*(6)	19 20	40	-2.54	97.5	δ_{LONG} & δ_{COLL} δ_{LAT} & δ_{RUD}	• VALT test point • Pilot stabilization required
(7)	21 22	40	-5.08	97.5	δ_{LONG} & δ_{COLL} δ_{LAT} & δ_{RUD}	• High descent rate • Pilot stabilization required
*(8)	23 24	60	-2.54	128	δ_{LONG}&δ_{COLL} δ_{LAT}&δ_{RUD}	• VALT test point • Most unstable condition
(9)	25 26 27 28	14.08	+2.54	15.2	δ_{LONG} δ_{COLL} δ_{LAT} δ_{RUD}	• VALT test point • Ascent condition
(10)	29 30	40	+2.54	97.5	δ_{LONG} & δ_{COLL} δ_{LAT} & δ_{RUD}	• VALT test point • Ascent condition
(11a)	31	Repeat (2) with v = +10 kts				• Right Lateral Flight
(11b)	32	Repeat (2) with v = -10 kts.....				• Left Lateral Flight
(11c)	33	Repeat (2) with -10 kts airspeed.....				• Rearward flight
*(12)	34 35	Repeat (8) with a one-minute turn				• VALT test point • Spiral descent condition • Pilot stabilization required

(4) differential cyclic for excitation of the primary yaw mode (δ_{RUD}).

Flight Test Point (2): Following flight test point (1), the pilot establishes a descent rate of 2.54 m/sec at 61 m altitude. This is achieved by flying to 30-60 m above the altitude test condition, and obtaining zero forward velocity and the specified descent rate at approximately 23 m above the altitude test point at which time one of the four uncoupled inputs are applied for approximately 15 sec. An altitude loss of approximately 125 ft will be encountered during the maneuver. The trim velocities can be established by radio ground link to the real time radar monitoring system of the VALT test facility. This procedure is repeated for each of the four inputs.

Flight Test Point (3): The next flight test point is for the evaluation of in-ground effect at hover. The VALT trajectory point most influenced by the in-ground effect is Point D of Figures 2.1, 2.2 and 2.3. The VALT test point is zero forward airspeed at 15.2 m with a descent rate of 2.54 m/sec. Since any complete maneuver would then be limited in time from the safety of flight constraint, this point is deleted from the test plan. Instead, flight test point (3) is at zero descent rate at 50 ft altitude. This test point will isolate in-ground effect and is stable with the SAS-on. All four uncoupled inputs--δ_{LONG}, δ_{COLL}, δ_{LAT}, δ_{RUD}--are tested at this point.

Flight Test Point (4): The next flight test point is at forward speed of 20 kts. This flight test point is a VALT trajectory point and the altitude is 61 m with a descent rate of 2.54 m/sec. This condition is stable with the SAS-on; however, it is also highly nonlinear. As discussed in preceding chapters, there is a strong effect of forward velocity on angle-of-attack stability (M_w) and vertical velocity on speed stability (M_u).

This nonlinear M_{uw} effect may require special inputs in order to provide only the linear derivatives which the objectives of this particular program require.

Flight Test Point (5): Flight test condition (5) is not a VALT trajectory point, but is one of three flight test points which are included to define CH-47 stability and control coefficients at the forward speed of 40 kts [the other points are (6) and (7)]. This forward speed is predicted to be unstable with the SAS-on and, thus, will require pilot stabilization as well as additional inputs for decoupled lateral response. Test point (5) is a zero velocity descent rate at 40 kts with two coupled inputs--δ_{LONG}-δ_{COLL} and δ_{LAT}-δ_{RUD}--at an altitude of 97.5 m.

Flight Test Point (6): This is a VALT trajectory point requiring pilot stabilization and is the same as the conditions of (5) except that the two coupled δ_{LONG}-δ_{COLL} and δ_{LAT}-δ_{RUD} inputs are performed at a descent rate of 2.54 m/sec.

Flight Test Point (7): This is not a VALT trajectory point but does complete the flight test data at 40 kts forward speed. The purpose of this point is to determine the effect of high descent rate and, thus, validate trends established by points (5) and (6).

Flight Test Point (8): This flight condition (airspeed = 60 kts, 500 FPM descent) is predicted to be the most unstable VALT trajectory point. At an altitude of 61 m, the δ_{LONG}-δ_{COLL} and δ_{LAT}-δ_{RUD} coordinated inputs are applied.

Flight test point (8) completes the hover and descent test conditions. The next two points are for the climb condition. The two climb conditions will provide basic information as to

the effect of climb rate (take-off) on stability and control coefficients.

Flight Test Point (9): This flight point is conducted at zero forward velocity and a climb rate of 2.54 m/sec at an altitude of 15.2 m. This is a VALT take-off tracjectory point. Four uncoupled inputs (δ_{LONG}, δ_{COLL}, δ_{LAT}, δ_{RUD}) are used. To achieve this point, the pilot may simply lift off the pad and attempt to establish the vertical rate as soon as possible. No safety of flight constraint is necessary for this powered takeoff. It is not necessary for the steady state vertical velocity to be established exactly at 15.2 m.

Flight Test Point (10): This flight condition is: 40 kt airspeed, 2.54 m/sec climb and 97.5 m altitude. This is an unstable point and requires the two coordinated inputs--δ_{LONG}-δ_{COLL} and δ_{LAT}-δ_{RUD}. This point completes the ascent phase.

The remaining test points are perturbations about the hover condition of test point (2) with commanded velocity calibration being established by ground-radio link. These three points are placed last because they require significant pilot attention.

Flight Test Point (11a): A sideslip is established by translating right laterally at 10 kts.

Flight Test Point (11b): Flight test point (11b) is the same as (11a) except the sideslip is established to the left with a lateral velocity of 10 kts.

Flight Test Point (11c): Flight test point (11c) is the same as flight test point (2) except the CH-47C is translating backward with a velocity of 10 kts.

Flight Test Point (12): Flight test point (12) is the same as flight test point (8) except a steady turn rate (one minute turn) is established.

These twelve points constitute the basic flight test requirements. It is further recommended that certain of these test points be repeated at least once. These VALT trajectory points are 2, 4, 6, 8, and 12.

4.2 FLIGHT TEST INPUTS

Three basic types of inputs are required to implement the flight test plans. These types are as follows:

(1) single axis inputs,

(2) coupled axis inputs, and

(3) pilot inputs required for stabilization or decoupling.

The application of these inputs is now discussed.

4.2.1 Single Axis Inputs* [(1), (2), (3), (4), (9), (11)]

Single axis inputs are defined relative to the fuselage reference axis about which they are applied. For example, differential collective (δ_{LONG}) is considered applied about the fuselage y axis, differential cyclic (δ_{RUD}) about the z axis, and collective cyclic (δ_{LAT}) about the x axis. Collective (δ_{COLL}) is applied almost along the z axis. These inputs are desirable because they can allow good excitation of the principal modes which are most affected by parameters of interest.

The flight test single axis inputs which are recommended for the test plan are used only at hover and low forward speed

*Note: Numbers in parentheses define effected flight test points.

(20 kts). These inputs are shown in Figure 4.1. The input consists of two parts--a rapid doublet followed by a slower, lower amplitude movement. For the longitudinal input, this slower stick movement is a doublet and for the lateral case, the slower stick movement is such as to return the rotorcraft to trim. The rapid doublet, in all inputs, excites the shorter period modes.

The amplitudes and frequency of these inputs are specifically chosen to minimize nonlinear rotorcraft response affects. All inputs are applied with the SAS-on.

4.2.2 Coupled Axis Inputs [(5), (6), (7), (8), (10), (12)]

Coupled axis inputs are those which are applied about two or more axes during the same maneuver. Such inputs optimize the information in cross-coupled derivatives.

The inputs designed for the unstable 40 kt and 60 kt points are shown in Figure 4.2. It should be noted that the δ_{LONG} input contains only the second ½-cycle of the low frequency input. This was established as a requirement in the previous chapter to prevent the response from diverging too rapidly because of the unstable pitch divergence root.

In addition to the specified inputs of Figures 4.1 and 4.2. there is another class of inputs. These are the inputs required from the pilot to stabilize or decouple the helicopter responses. Such inputs are themselves made in addition to the inputs specified above. Such inputs will provide useful identification data and can be treated accordingly in the post-flight data reduction phase to supplement results from the specified inputs.

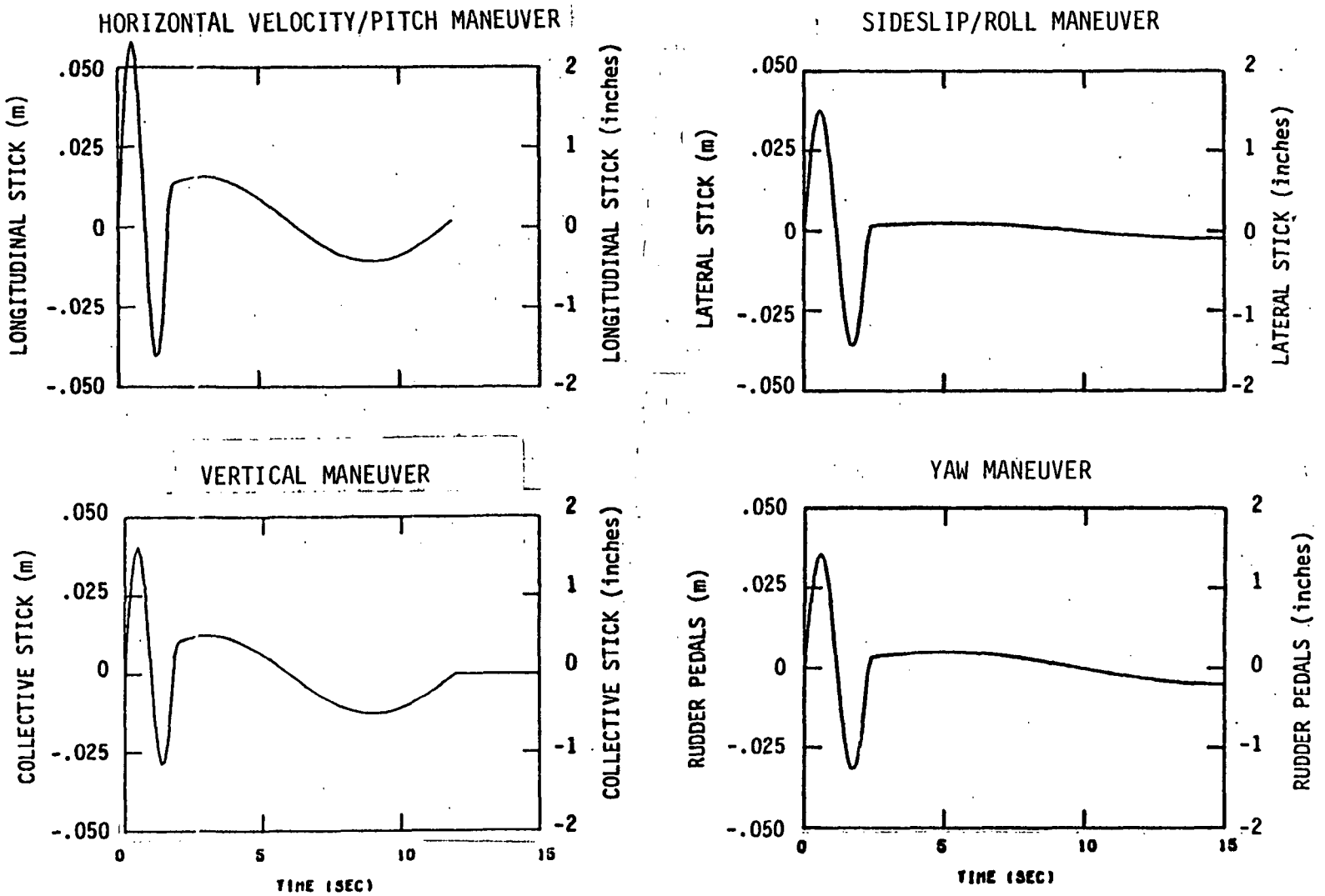

Figure 4.1 Flight Test Input Design, Hover and 20 Knots (4 Individual Maneuvers)

Control Input Design Summary

HOVER & 20 KNOT TEST POINTS	HIGH FREQ. INPUT		LOW FREQ. INPUT		T_o (SEC)	T_1 (SEC)	T_2 (SEC)
	A_1 (CM)	ω_1 (RAD/SEC)	A_2 (CM)	ω_2 (RAD/SEC)			
1. δ_{LONG}	5.08	3.43	.13	.525	0.0	1.825	12.0
2. δ_{COLL}	3.81*	3.43	.13	.525	0.0	1.825	12.0
3. δ_{LAT}	3.81	2.70	.25	.319	0.0	2.33	-
4. δ_{RUD}	3.56*	2.70	.50	.319	0.0	2.33	-

* Amplitude limited to prevent tags actuator rate saturation

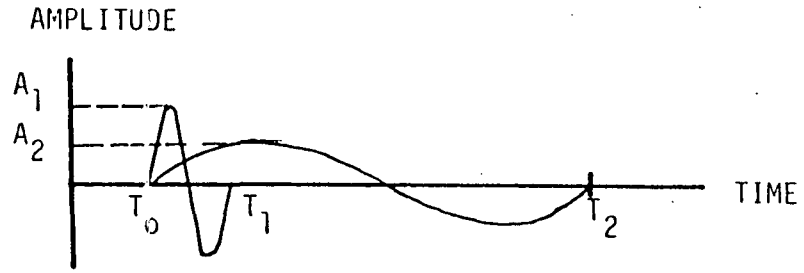

Figure 4.1 (Concluded)

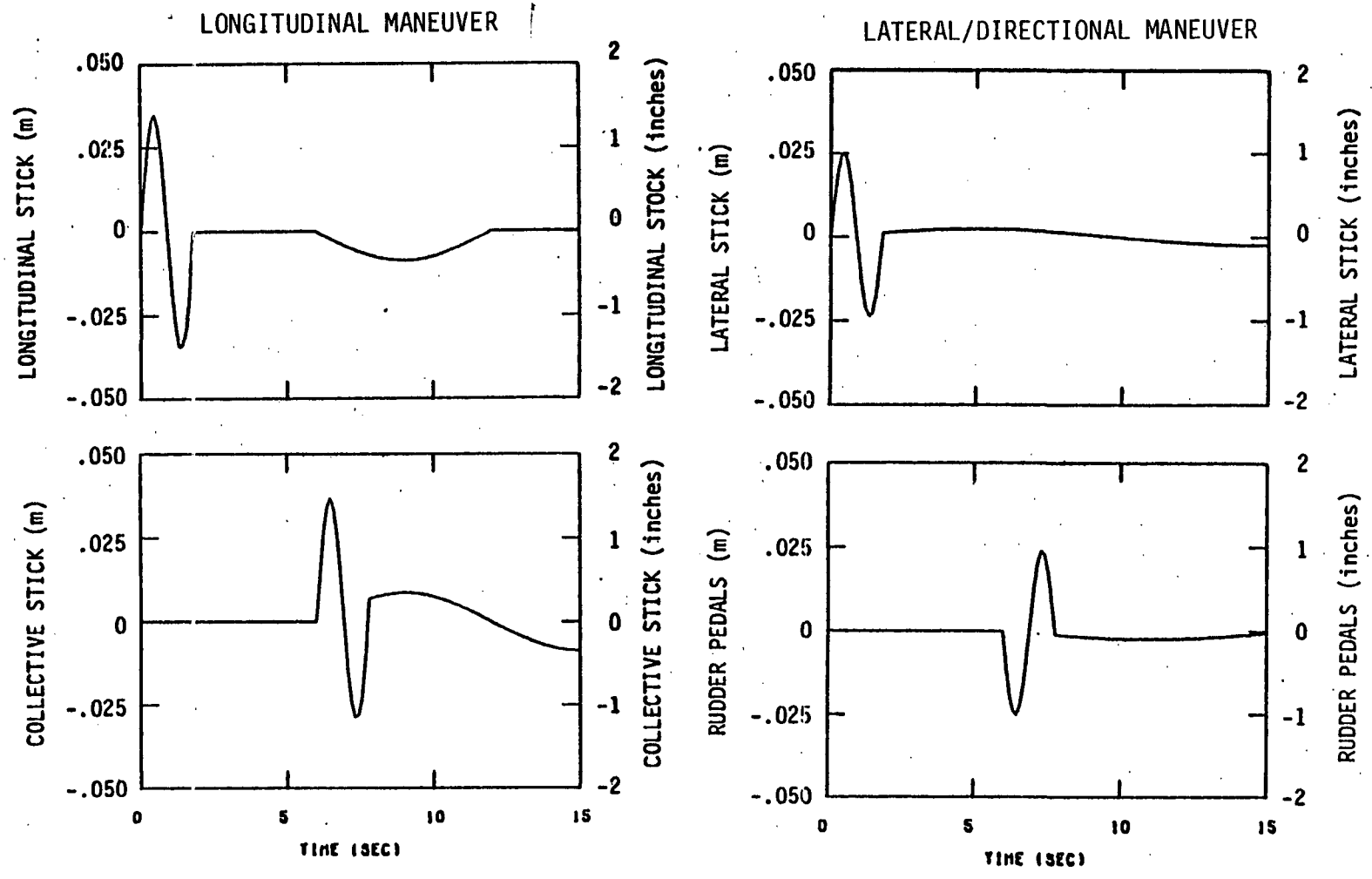

Figure 4.2 Flight Test Input Design, 40 Knots and 60 Knots (2 Individual Maneuvers)

Control Input Design Summary

40 & 60 KNOT TEST POINTS	HIGH FREQ. INPUT A_1 (CM)	HIGH FREQ. INPUT ω_1 (RAD/SEC)	LOW FREQ. INPUT A_2 (CM)	LOW FREQ. INPUT ω_2 (RAD/SEC)	T_o (SEC)	T_1 (SEC)	T_2 (SEC)
1. δ_{LONG}*	3.56	3.43	.90	.525	0.0	1.8	12.0
AND $\delta_{COLL.}$	3.56	3.43	.90	.525	6.0	7.8	-
2. δ_{LAT}	2.54	3.50	.25	.319	0.0	1.8	-
AND δ_{RUD}	-2.54	3.50	-.25	.319	6.0	7.8	-

* FIRST 1/2 CYCLE IS ZERO FOR δ_{LONG}

PILOT STABILIZATION REQUIRED:

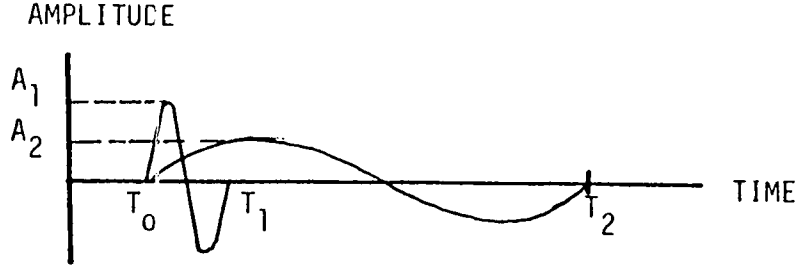

Figure 4.2 (Concluded)

V. CONCLUSIONS AND RECOMMENDATIONS

5.1 CONCLUSIONS

This investigation has studied the requirements for accurate flight test identification of the stability and control derivatives of the CH-47 VALT Research Aircraft. From the results of this simulation study, it is concluded that the linear quasi-static aerodynamic derivatives can be identified from flight data with excellent accuracy for many of the important derivatives. Furthermore, the results of this study have isolated and expanded upon specific areas of parameter identification of importance to the general rotorcraft identification problem. In addition, the results have led to specific conclusions pertinent to the overall VALT program system design studies.

The principal conclusions which have led to a flight test specification are as follows:

(1) Uncoupled longitudinal/lateral-directional linear models may be used to adequately describe the small perturbation responses of the CH-47 VALT helicopter about specific trim points. This assumes that the SAS is on and, therefore, longitudinal modes are decoupled from lateral modes. Rotor degrees of freedom have a minor influence on identification accuracy except for some high rate inputs which couple rotor/fuselage motions due to roll rate feedback.

(2) The representation of the landing trajectory by piecewise linear models is, in general, not valid for low-speed perturbations from nominal. For this reason, it is concluded that careful attention must be made of possible nonlinearities at such low speeds. This may be performed using model structure determination procedures and/or specifically designed inputs.

(3) Error characteristics of the CH-47 VALT instrumentation and LRC data acquisition systems are acceptable for the task of parameter identification.

(4) For the cases analyzed, it is concluded that multi-cycle inputs offer marginal improvement in estimate accuracy over simple single cycle inputs such as doublets. Hover and 20 kt conditions require independent excitation of longitudinal/pitch and vertical modes due to nonlinearities (SAS-on permits such decoupling). Higher speed inputs require simultaneous inputs about two axes.

(5) Wind gusts of root-mean-square (RMS) velocity 4.14 kts in forward and vertical directions tend to degrade accuracy. Below 1.78 kts RMS velocity, negligible parameter estimate accuracy degradation is predicted. A lateral gust of 5.92 kts may be encountered without affecting longitudinal identification accuracy, but lateral-directional identification accuracy is affected.

The results of this study have been based on a global, nonlinear helicopter analysis (C-81) and linear derivative models taken from Ref. 1. Thus, the results of the flight test program can be used to validate these computer simulations as well as the entire identification methodology upon which the flight plan is based. Twelve flight test points with a total of forty-nine maneuvers are specified for the flight plan. Such a flight test should produce a most valuable data base for not only the VALT program, but also for rotorcraft parameter identification research and development in general.

Although the emphasis in this work has been directed toward producing a detailed flight test specification for the CH-47, several issues have emerged which are of general interest to the overall VALT system design studies. These issues are:

(1) The linear 10 DOF rotor/fuselage derivative model derived from the C-81 nonlinear simulation program was found to predict rotor instability with high gain feedback of the CH-47 production SAS. The present CH-47 production SAS roll rate feedback gain (K_p = -5.0 in/rad/sec) was shown to reduce rotor damping by a factor of two. A roll rate feedback gain value of -20.0 was found to yield approximately 10% critical damping. (Actual flight tests of the CH-47 have shown that roll rate feedback of -17.17 produces 10% critical

damping.) It is concluded that the C-81 derived linear model is, thus, a valid and accurate tool for investigation of high gain feedback on rotor stability, and is useful for assessment of VALT program control system designs.

(2) Aerodynamic nonlinearities in the landing approach were found to be very important in this investigation. Perturbations in longitudinal or vertical velocity of 3.05 m/sec (10 ft/sec) from a nominal trim condition produced significant nonlinearity. As a result, linear theory used for navigation and control systems designs should only be used as preliminary to the final designs. More emphasis (than is currently used in rotorcraft control design) should be devoted to the nonlinear simulation for early evaluation (and redesign as required) of linear designs and may, in fact, be necessary to achieve adequate vehicle performance. A time-varying coefficient model with coefficients varying with airspeed is not acceptable for modeling the CH-47 in a landing approach since nonlinearity also occurs with vertical velocity perturbations. Linear designs based upon optimal techniques may, in fact, be far from optimal due to the significant nonlinear nature of helicopters in a landing approach.

(3) Random wind gust was found to produce significant response of the CH-47.

5.2 RECOMMENDATIONS

The techniques demonstrated for this effort can be extended to provide data for other VALT objectives. Specific items include:

(1) Evaluation of potential rotor stability problems of the VALT program adaptive control system design. The C-81 linear rotor/fuselage model has been shown to accurately duplicate the feedback gain values resulting in actual CH-47 rotor instability trends. The present CH-47 production SAS roll rate feedback gain value is shown to reduce rotor damping by a factor of two. It is, thus, recommended to evaluate the VALT program adaptive control system designs for potential rotor stability problems using the C-81 rotor/fuselage linear simulation model.

(2) Further analysis of wind shear effects on rotorcraft landing trajectories is a primary requirement. It is recognized that a logarithmic distribution is a realistic assumption about the low altitude atmospheric description. Since low-speed rotorcraft response is highly dependent on this distribution, further quantification of its effect would impact near terminal navigation, guidance, and display functions.

(3) Analysis of piloting techniques for parameter identification objectives has a more general application to development of piloting techniques for many types of VTOL aircraft. In particular, the results of this study have shown that the CH-47 aircraft is particularly sensitive to nonlinear responses at certain points on the landing trajectory. Such sensitivity can reduce safety-of-flight margins. Since commercial VTOL operation would rely on pilots of varying experience, a training procedure, based on the types of considerations discussed in this report, could enhance these margins.

REFERENCES

1. Ostroff, A.J.; Downing, D.R.; and Rood, W.J.: A Technique Using a Nonlinear Helicopter Model for Determining Trims and Derivatives. NASA TN D-8159, 1976.

2. Molusis, J.A.: Rotorcraft Derivative Identification from Analytical Models and Flight Test Data. AGARD CP-172, 1975.

3. Sorensen, J.A.; Mohr, R.L.; and Cline, T.B.: Instrumentation Requirements for Aircraft Parameter Identification with Application to the Helicopter. NASA CR-132675, 1975.

4. AGARD Conf. Proceedings No. 172: Methods for Aircraft State and Parameter Identification. AGARD CP-172, 1975.

5. Davis, J.M.: Rotorcraft Flight Simulation with Aeroelastic Rotor and Improved Aerodynamic Representation. Vol. I and Vol. II, USAAMRDL-TR-74-10A and 10B, June 1974.

6. Gupta, N.K.: Maximum Likelihood Estimation with Reduced Sensitivity Functions. Presented at IEEE Decision and Control Conference (Houston, Texas), Dec. 10-12, 1975.

7. Hall, W.E.; Gupta, N.K.; and Smith, R.G.: Identification of Aircraft Stability and Control Coefficients for the High Angle-of-Attack Regime. ONR Contract No. N00014-72-C-0328, March 1974.

8. Gupta, N.K.; and Hall, W.E., JR.: Input Design for Identification of Aircraft Stability and Control Derivatives. NASA CR-2493, 1975.

9. Creedon, J.F.; and Griffin, W.R.: Flight Control System Requirements for Advanced V/STOL Aircraft. Presented at 1972 Electronic and Aerospace Systems Conference (Washington, D.C.), Oct. 16-18, 1972.

10. CAE Electronics Ltd.: Tactical Aircraft Guidance System Advanced Development Program. USAAMRDL Tech. Rept. 71-57, U.S. Army, Feb. 1972 (Available from DDC as AD 894 999L).

11. Sikorsky Aircraft: XH-49A Accident Investigation Report, Vol. I and II. Prepared under Contract DAAJ02-72-C-0202, April 30, 1974.

12. Davis, J.M.: Stability and Control Analysis. No. 114-AD-603 (Contract DA23-204-AMC-04366(Y)), Vertol Div., Boeing Co., Nov. 28, 1966.

13. Albion, N.; Leet, J.R.; and Mollenkof, P.A.: Ground-Base Flight Simulation of the CH-47C Helicopter. USAAVLABS Tech. Rep. 69-71, U.S. Army, Oct. 1969.

14. Molusis, J.A.; and Hall, W.E.: Analysis of ACE Reentry Vehicle Aerodynamics by an Advanced System Identification Method (U). ONR Contract No. N00014-75-C-0076 (SECRET).

15. Molusis, J; and Briczinski, S.: Helicopter Derivative Identification from Analytic Models and Flight Test Data. NASA TN D-7647, April 1974.

16. Athans, M.; and Falb, P.L.: Optimal Control. McGraw Hill Book Co., 1966.

17. Hohenemser, K.H.: Hingeless Rotorcraft Flight Dynamics. AGARDograph No. 197, 1974.

18. Bryant, W.H.; and Hodge, W.F.: Effects of Flight Instrumentation Errors on the Estimation of Aircraft Stability and Control Derivatives. NASA TN D-7647, April 1974.

19. Hodge, W.F. and Bryant, W.H.: Monte Carlo Analysis of Inaccuracies in Estimated Aircraft Parameters Caused by Unmodeled Flight Instrumentation Errors. NASA TN D-7712, Feb. 1975.

20. AGARD Conference Proceedings No. 140: Flight in Turbulence. AGARD-CP-140, Nov. 1973.

21. Clegg, Peter: Energy for the Home. Garden Way Publishing, Charlotte, Vermont, 1975.

22. Glaser, J.J.: Data Requirements on Turbulence in the Earth's Atmospheric Shear Layer for STOL Design Criteria. Flight In Turbulence, AGARD-CP-140, Nov. 1973.

APPENDIX A

C-81 LINEAR DERIVATIVE MODELS (40 KTS)

The linear models employed in this report at the 40 kt condition were derived from the C-81 nonlinear simulation program. The development of the various models, state variable definitions, Stability Augmentation System (SAS), and usage of these models is presented in the second chapter of this report. The state variable representation is given here since this is the form used for identification, for time history simulations, and for computation of eigenvalues. The state variable form is given in Eq. (A.1) and the F and G matrices are presented in this appendix for each model. The following models are presented:

- 10 DOF rotor/fuselage model (SAS-off)
- First order rotor model (SAS-off)
- 6 DOF quasi-static model (SAS-off)
- 10 DOF rotor/fuselage model (with CH-47 production SAS)
- 6 DOF quasi-static model (with CH-47 production SAS)

$$\dot{x} = Fx + Gu \tag{A.1}$$

A.1 10 DOF ROTOR/FUSELAGE MODEL (SAS-OFF)

The state vector definition for the 10 DOF model is shown in Eq. (A.2) and the control vector is shown in Eq. (A.3).

$$X^T = [\theta \quad \phi \quad \psi \quad u \quad w \quad q \quad v \quad p \quad r \quad \dot{a}_{1_{MR}} \quad \dot{b}_{1_{MR}} \quad \dot{a}_{1_{TR}} \quad \dot{b}_{1_{TR}} \quad a_{1_{MR}} \quad b_{1_{MR}} \quad a_{1_{TR}} \quad b_{1_{TR}}] \tag{A.2}$$

$$u^T + [\delta_{COLL} \quad \delta_{LONG} \quad \delta_{LAT} \quad \delta_{RUD}] \tag{A.3}$$

The F-matrix of stability derivatives is shown in Table A.1 and the G-matrix of control derivatives is shown in Table A.2.

Table A.1
F-Matrix (10 DOF Model, SAS-Off)

	1	2	3	4	5	6	7	8	9
1	0.00000	0.00000	0.00000	0.00000	0.00000	1.00000	0.00000	0.00000	0.00000
2	0.00000	0.00000	0.00000	0.00000	0.00000	0.00000	0.00000	1.00000	0.00000
3	0.00000	0.00000	0.00000	0.00000	0.00000	0.00000	0.00000	0.00000	1.00000
4	-32.06200	0.00000	-0.06927	-0.00099	0.06872	-14.58400	0.00764	0.00970	-0.17362
5	-2.67600	0.06927	0.00000	-0.01191	-0.66346	70.22100	-0.04285	-0.07380	-0.47033
6	0.00000	0.00000	0.00000	-0.00301	0.00289	-1.15940	0.00144	0.14736	-0.18855
7	0.00000	32.06200	2.67600	0.00103	0.00272	-0.02234	-0.03601	13.97000	-68.01300
8	0.00000	0.00000	0.00000	0.00022	0.00216	-0.03725	-0.00353	0.00475	0.00618
9	0.00000	0.00000	0.00000	-0.00003	-0.00008	0.11857	-0.00041	0.04100	-0.02032
10	0.00000	0.00000	0.00000	0.04023	0.97566	-56.08500	-0.33053	-50.14100	-12.81400
11	0.00000	0.00000	0.00000	-0.23282	-0.20557	56.92000	-0.37892	-38.55100	-12.67800
12	0.00000	0.00000	0.00000	0.13727	0.94175	-19.79200	0.11981	51.05100	-0.87678
13	0.00000	0.00000	0.00000	-0.25110	-0.19747	50.91000	0.36920	40.04580	-4.14680
14	0.00000	0.00000	0.00000	0.00000	0.00000	0.00000	0.00000	0.00000	0.00000
15	0.00000	0.00000	0.00000	0.00000	0.00000	0.00000	0.00000	0.00000	0.00000
16	0.00000	0.00000	0.00000	0.00000	0.00000	0.00000	0.00000	0.00000	0.00000
17	0.00000	0.00000	0.00000	0.00000	0.00000	0.00000	0.00000	0.00000	0.00000

	10	11	12	13	14	15	16	17
1	0.00000	0.00000	0.00000	0.00000	0.00000	0.00000	0.00000	0.00000
2	0.00000	0.00000	0.00000	0.00000	0.00000	0.00000	0.00000	0.00000
3	0.00000	0.00000	0.00000	0.00000	0.00000	0.00000	0.00000	0.00000
4	0.01142	0.17427	0.01258	0.20277	-13.12300	-0.82123	-14.97800	-0.62435
5	0.03770	-0.54848	0.05659	-0.55953	2.21710	2.30340	3.86100	3.11020
6	-0.00338	0.05107	0.00379	-0.06467	0.98582	-0.21020	2.00440	0.32833
7	0.12898	0.03271	-0.20399	-0.02745	-0.99561	10.82800	1.02250	-13.09200
8	0.02633	0.00118	-0.06365	-0.00916	0.26286	6.93220	0.36128	-8.03230
9	0.03337	0.02084	-0.00641	-0.01704	-1.30750	1.58360	1.16900	0.76587
10	-36.61400	-49.52300	-0.00379	0.06467	-39.15100	-937.36000	-2.00440	-0.32833
11	51.61800	-36.23900	0.06387	0.01172	905.41000	-17.74000	-0.53970	7.81370
12	0.00338	-0.05107	-36.55100	-49.46500	-0.98582	0.21020	-43.51500	-934.47000
13	0.02859	0.00263	51.51700	-36.02100	0.17102	7.02590	898.25000	-15.55800
14	1.00000	0.00000	0.00000	0.00000	0.00000	0.00000	0.00000	0.00000
15	0.00000	1.00000	0.00000	0.00000	0.00000	0.00000	0.00000	0.00000
16	0.00000	0.00000	1.00000	0.00000	0.00000	0.00000	0.00000	0.00000
17	0.00000	0.00000	0.00000	0.00000	0.00000	0.00000	0.00000	0.00000

Table A.2
G-Matrix (10 DOF Model, SAS-Off)

	1	2	3	4
1	0.00000	0.00000	0.00000	0.00000
2	0.00000	0.00000	0.00000	0.00000
3	0.00000	0.00000	0.00000	0.00000
4	1.05360	-0.17740	-0.00113	0.07712
5	-11.35200	0.78872	0.00258	-0.29688
6	0.02863	-0.34946	0.01973	-0.00142
7	-0.11943	-0.12247	0.15600	-0.13777
8	-0.10513	-0.07688	-0.02340	-0.13063
9	0.01821	-0.03622	0.00851	0.02279
10	11.20500	4.01230	42.83500	71.08900
11	-7.23410	13.33200	0.86260	1.52850
12	0.64838	0.71489	-31.23800	52.84800
13	-8.44060	14.13500	0.37912	-0.43187
14	0.00000	0.00000	0.00000	0.00000
15	0.00000	0.00000	0.00000	0.00000
16	0.00000	0.00000	0.00000	0.00000
17	0.00000	0.00000	0.00000	0.00000

A.2 6 DOF QUASI-STATIC MODEL (SAS-OFF)

The state vector definition for the 6 DOF quasi-static model is shown in Eq. (A.4) and the control vector is shown in Eq. (A.5). This model is derived from the 10 DOF rotor/fuselage model and the development is presented in the second chapter.

$$X^T = [\theta \quad \phi \quad \psi \quad u \quad w \quad q \quad v \quad p \quad r]$$

$$u^T = [\delta_{COLL} \quad \delta_{LONG} \quad \delta_{LAT} \quad \delta_{RUD}]$$

The F-matrix of stability derivatives is shown in Table A.3 and the G-matrix of control derivatives is shown in Table A.4.

Table A.3

F-Matrix (6 DOF Quasi-Static Model, SAS-Off)

	1	2	3	4	5	6	7	8	9
1	0.00000	0.00000	0.00000	0.00000	0.00000	1.00000	0.00000	0.00000	0.00000
2	0.00000	0.00000	0.00000	0.00000	0.00000	0.00000	0.00000	1.00000	0.00000
3	0.00000	0.00000	0.00000	0.00000	0.00000	0.00000	0.00000	0.00000	1.00000
4	-32.06200	0.00000	-0.06927	-0.00869	0.06069	-12.84100	0.00855	0.13540	-0.41191
5	-2.67600	0.06927	0.00000	-0.11703	-0.65657	69.67300	-0.04391	-0.10234	-0.45820
6	0.00000	0.00000	0.00000	-0.00215	0.00370	-1.32970	0.00115	0.13047	-0.16296
7	0.00000	32.06200	2.67600	-0.00033	0.00082	-0.39209	-0.04274	12.54700	-68.16100
8	0.00000	0.00000	0.00000	-0.00046	0.00143	-0.32134	-0.00731	-0.83710	-0.07788
9	0.00000	0.00000	0.00000	0.00010	0.00226	0.03148	-0.00189	-0.10754	-0.05625

Table A.4

G-Matrix (6 DOF Quasi-Static Model, SAS-Off)

	1	2	3	4
1	0.00000	0.00000	0.00000	0.00000
2	0.00000	0.00000	0.00000	0.00000
3	0.00000	0.00000	0.00000	0.00000
4	0.79662	0.24571	-0.00052	-0.02440
5	-11.27000	0.71150	-0.00061	0.05546
6	0.05303	-0.39600	-0.00332	0.00225
7	0.00407	-0.09048	1.08590	-0.05503
8	-0.02129	-0.06444	0.56090	-0.05879
9	0.03689	-0.02651	0.05345	0.18811

A.3 10 DOF ROTOR/FUSELAGE MODEL (WITH CH-47 PRODUCTION SAS)

The state vector definition for the 10 DOF rotor/fuselage model with SAS is shown in Eq. (A.6) and the control vector is shown in Eq. (A.8). The development of this model is presented in the second chapter.

$$\underline{X}^T = [\underline{\theta} \quad \underline{\phi} \quad \underline{\psi} \quad \underline{u} \quad w \quad \underline{q} \quad v \quad \underline{p} \quad r \quad \underline{a1}_{MR} \quad \underline{b1}_{MR} \quad \underline{a1}_{TR} \quad \underline{b1}_{TR} \quad \dot{a}_{1MR} \quad \dot{b}_{1MR} \quad \dot{a}_{1TR} \quad \dot{b}_{1TR} \quad v_1 \quad v_2 \quad v_3 \quad v_4 \quad v_5 \quad v_6 \quad v_7 \quad v_8] \tag{A.6}$$

$$u^T = [\delta_{COLL} \quad \delta_{LONG} \quad \delta_{LAT} \quad \delta_{RUD}] \tag{A.7}$$

The F-matrix of stability derivatives is shown in Table A.5 and the G-matrix of control derivatives is shown in Table A.6.

The F-matrix presented in Table A.5 includes the CH-47 production SAS. The recommended SAS modification (discussed in the second chapter) is to divide the roll rate feedback gain by a factor of two. This change modifies the F-matrix element occurring in the 21st row and 8th column ($F_{21,8}$) from a value of -106.4 to -53.2.

A.4 6 DOF QUASI-STATIC MODEL (WITH CH-47 PRODUCTION SAS)

The state vector definition for the 6 DOF quasi-static model with SAS is shown in Eq. (A.8) and the control vector is shown in Eq. (A.9). The development of this model is presented in the second chapter.

$$X^T = [\theta \quad \phi \quad \psi \quad u \quad w \quad q \quad v \quad p \quad r \quad v_1 \quad v_2 \quad v_3 \quad v_4 \quad v_5 \quad v_6 \quad v_7 \quad v_8] \tag{A.8}$$

$$u^T = [\delta_{COLL} \quad \delta_{LONG} \quad \delta_{LAT} \quad \delta_{RUD}] \tag{A.9}$$

The F-matrix of stability derivatives is shown in Table A.7 and the G-matrix of control derivaties is shown in Table A.8.

The F-matrix presented in Table A.7 includes the CH-47 production SAS. The recommended SAS modification (discussed in the second chapter) is to divide the roll rate feedback gain by a factor of two. This change modifies the F-matrix element occurring in the 13th row and 8th column ($F_{13,8}$) from a value of -106.4 to -53.2.

Table A.5

F-Matrix (10 DOF Rotor/Fuselage Model with CH-47 Production SAS)

	1	2	3	4	5	6	7	8	9	10	11	12	13
1	0.00000	0.00000	0.00000	0.00000	0.00000	1.00000	0.00000	0.00000	0.00000	0.00000	0.00000	0.00000	0.00000
2	0.00000	0.00000	0.00000	0.00000	0.00000	0.00000	0.00000	1.00000	0.00000	0.00000	0.00000	0.00000	0.00000
3	0.00000	0.00000	0.00000	0.00000	0.00000	0.00000	0.00000	0.00000	1.00000	0.00000	0.00000	0.00000	0.00000
4	-32.06200	0.00000	-0.06927	0.00097	0.06872	-14.58400	0.00764	0.00970	-0.17362	0.01142	0.17427	0.01258	0.20277
5	-2.67600	0.06927	0.00000	-0.12793	-0.66346	70.22100	-0.04285	-0.07380	-0.47033	0.03770	-0.54848	0.05659	-0.55953
6	0.00000	0.00000	0.00000	0.00086	0.00289	-1.15940	0.00144	0.14736	-0.18855	-0.00338	0.05107	0.00379	-0.06467
7	0.00000	32.06200	2.67600	0.00239	0.00272	-0.02234	-0.03601	13.97000	-68.01300	0.12898	0.03271	-0.20399	-0.02745
8	0.00000	0.00000	0.00000	0.00107	0.00216	-0.03725	-0.00353	0.00475	0.00618	0.02633	0.00118	-0.06365	-0.00916
9	0.00000	0.00000	0.00000	0.00036	-0.00008	0.11857	-0.00041	0.04100	-0.02032	0.03379	0.02084	-0.00641	-0.01704
10	0.00000	0.00000	0.00000	-0.00430	0.97577	-56.08500	-0.33053	-50.14100	-12.81400	-36.61400	-49.52300	-0.00379	0.06467
11	0.00000	0.00000	0.00000	-0.38081	-0.20557	56.92000	-0.37892	-38.55100	-12.67800	51.61800	-36.23900	0.06387	0.01172
12	0.00000	0.00000	0.00000	0.12933	0.94175	-19.79200	0.11981	51.05100	-0.87678	0.00338	-0.05107	-36.55100	-49.46500
13	0.00000	0.00000	0.00000	-0.40800	-0.19747	50.91000	0.36920	40.45800	-4.14680	0.02859	0.00263	51.51700	-36.02100
14	0.00000	0.00000	0.00000	0.00000	0.00000	0.00000	0.00000	0.00000	0.00000	1.00000	0.00000	0.00000	0.00000
15	0.00000	0.00000	0.00000	0.00000	0.00000	0.00000	0.00000	0.00000	0.00000	0.00000	1.00000	0.00000	0.00000
16	0.00000	0.00000	0.00000	0.00000	0.00000	0.00000	0.00000	0.00000	0.00000	0.00000	0.00000	1.00000	0.00000
17	0.00000	0.00000	0.00000	0.00000	0.00000	0.00000	0.00000	0.00000	0.00000	0.00000	0.00000	0.00000	1.00000
18	0.00000	0.00000	0.00000	0.00000	0.00000	22.30000	0.00000	0.00000	0.00000	0.00000	0.00000	0.00000	0.00000
19	0.00000	0.00000	0.00000	0.00000	0.00000	-56.55000	0.00000	0.00000	0.00000	0.00000	0.00000	0.00000	0.00000
20	0.00000	0.00000	0.00000	0.00000	0.00000	153.73000	0.00000	0.00000	0.00000	0.00000	0.00000	0.00000	0.00000
21	0.00000	0.00000	0.00000	0.00000	0.00000	0.00000	0.00000	-106.40000	0.00000	0.00000	0.00000	0.00000	0.00000
22	0.00000	0.00000	0.00000	0.00000	0.00000	0.00000	0.00000	0.00000	-105.26000	0.00000	0.00000	0.00000	0.00000
23	0.00000	0.00000	0.00000	0.00000	0.00000	0.00000	0.00000	0.00000	1107.00000	0.00000	0.00000	0.00000	0.00000
24	0.00000	0.00000	0.00000	0.00000	0.00000	0.00000	0.00000	1.57540	0.00000	0.00000	0.00000	0.00000	0.00000
25	0.00000	0.00000	0.00000	0.00000	0.00000	0.00000	0.18745	0.00000	0.00000	0.00000	0.00000	0.00000	0.00000

Table A.5
(Concluded)

	14	15	16	17	18	19	20	21	22	23	24	25
1	0.00000	0.00000	0.00000	0.00000	0.00000	0.00000	0.00000	0.00000	0.00000	0.00000	0.00000	0.00000
2	0.00000	0.00000	0.00000	0.00000	0.00000	0.00000	0.00000	0.00000	0.00000	0.00000	0.00000	0.00000
3	0.00000	0.00000	0.00000	0.00000	0.00000	0.00000	0.00000	0.00000	0.00000	0.00000	0.00000	0.00000
4	-13.12300	-0.82123	-14.97800	-0.62435	-0.17740	0.00000	0.00000	-0.00113	0.07712	0.00000	0.07712	0.07712
5	2.25710	2.30340	3.86100	3.11020	0.78872	0.00000	0.00000	0.00258	-0.29688	0.00000	-0.29688	-0.29688
6	0.90582	-0.21020	2.00440	0.32833	-0.34946	0.00000	0.00000	0.01973	-0.00142	0.00000	-0.00142	-0.00142
7	-0.90561	10.82800	1.02250	-13.09200	-0.12247	0.00000	0.00000	0.15600	-0.13777	0.00000	-0.13777	-0.13777
8	0.26286	6.93220	0.36128	-8.03230	-0.07688	0.00000	0.00000	-0.02340	-0.13063	0.00000	-0.13063	-0.13063
9	-1.30750	1.58360	1.16900	0.76587	-0.03622	0.00000	0.00000	0.00851	0.02279	0.00000	0.02279	0.02279
10	-39.15100	-937.36000	-2.00440	-0.32833	4.01230	0.00000	0.00000	42.83500	71.08900	0.00000	71.08900	71.08900
11	905.41000	-17.74000	-0.53970	7.81370	13.33200	0.00000	0.00000	0.86260	1.52850	0.00000	1.52850	1.52850
12	-0.90582	0.21020	-43.51500	-934.47000	0.71489	0.00000	0.00000	-31.23800	52.84800	0.00000	52.84800	52.84800
13	0.17102	7.02590	898.25000	-15.55800	14.13500	0.00000	0.00000	0.37912	-0.43187	0.00000	-0.43187	-0.43187
14	0.00000	0.00000	0.00000	0.00000	0.00000	0.00000	0.00000	0.00000	0.00000	0.00000	0.00000	0.00000
15	0.00000	0.00000	0.00000	0.00000	0.00000	0.00000	0.00000	0.00000	0.00000	0.00000	0.00000	0.00000
16	0.00000	0.00000	0.00000	0.00000	0.00000	0.00000	0.00000	0.00000	0.00000	0.00000	0.00000	0.00000
17	0.00000	0.00000	0.00000	0.00000	0.00000	0.00000	0.00000	0.00000	0.00000	0.00000	0.00000	0.00000
18	0.00000	0.00000	0.00000	0.00000	0.00000	1.00000	0.00000	0.00000	0.00000	0.00000	0.00000	0.00000
19	0.00000	0.00000	0.00000	0.00000	0.00000	0.00000	1.00000	0.00000	0.00000	0.00000	0.00000	0.00000
20	0.00000	0.00000	0.00000	0.00000	-0.03640	-0.81790	-3.04100	0.00000	0.00000	0.00000	0.00000	0.00000
21	0.00000	0.00000	0.00000	0.00000	0.00000	0.00000	0.00000	-21.28000	0.00000	0.00000	0.00000	0.00000
22	0.00000	0.00000	0.00000	0.00000	0.00000	0.00000	0.00000	0.00000	0.00000	1.00000	0.00000	0.00000
23	0.00000	0.00000	0.00000	0.00000	0.00000	0.00000	0.00000	0.00000	-3.18900	-10.51700	0.00000	0.00000
24	0.00000	0.00000	0.00000	0.00000	0.00000	0.00000	0.00000	0.00000	0.00000	0.00000	-0.24350	0.00000
25	0.00000	0.00000	0.00000	0.00000	0.00000	0.00000	0.00000	0.00000	0.00000	0.00000	0.00000	-5.75000

Table A.6

G-Matrix (10 DOF Rotor/Fuselage Model with CH-47 Production SAS)

	1	2	3	4
1	0.00000	0.00000	0.00000	0.00000
2	0.00000	0.00000	0.00000	0.00000
3	0.00000	0.00000	0.00000	0.00000
4	1.05360	-0.17740	-0.00113	0.07712
5	-11.35200	0.78872	0.00258	-0.29688
6	0.02863	-0.34946	0.01973	-0.00142
7	-0.11943	-0.12247	0.15600	-0.13777
8	-0.10513	-0.07688	-0.02340	-0.13063
9	0.01821	-0.03622	0.00851	0.02279
10	11.20500	4.01230	42.83500	71.08900
11	-7.23410	13.33200	0.86260	1.52850
12	0.64838	0.71489	-31.23800	52.84800
13	-8.44060	14.13500	0.37912	-0.43187
14	0.00000	0.00000	0.00000	0.00000
15	0.00000	0.00000	0.00000	0.00000
16	0.00000	0.00000	0.00000	0.00000
17	0.00000	0.00000	0.00000	0.00000
18	0.00000	0.00000	0.00000	0.00000
19	0.00000	0.00000	0.00000	0.00000
20	0.00000	0.00000	0.00000	0.00000
21	0.00000	0.00000	0.00000	0.00000
22	0.00000	0.00000	0.00000	0.00000
23	0.00000	0.00000	0.00000	0.00000
24	0.00000	0.00000	0.00000	0.00000
25	0.00000	0.00000	0.00000	0.00000

The DOF models discussed in this report used in the simulation are generated from the F- abd G-matrices shown in Tables A.7 and A.8 by setting to zero all cross-coupled derivatives, thus yielding either a 3 DOF longitudinal model or 3 DOF lateral model with the corresponding SAS.

Table A.7

F-Matrix (6 DOF Quasi-Static Model with CH-47 Production SAS)

	1	2	3	4	5	6	7	8	9
1	0.00000	0.00000	0.00000	0.00000	0.00000	1.00000	0.00000	0.00000	0.00000
2	0.00000	0.00000	0.00000	0.00000	0.00000	0.00000	0.00000	1.00000	0.11590
3	0.00000	0.00000	0.00000	0.00000	0.00000	0.00000	0.00000	0.00000	1.00670
4	-32.20000	0.00000	0.00000	-0.01857	0.02894	-5.76930	-0.00127	-0.02869	-0.08620
5	-3.70650	0.00000	0.00000	0.02097	-0.25982	0.40010	0.00975	0.35800	0.43277
6	0.00000	0.00000	0.00000	0.01356	0.00285	-1.34220	0.00027	0.08761	0.01388
7	-3.70650	31.98500	0.00000	-0.00001	0.00244	0.00500	-0.13179	-0.10109	-0.18117
8	0.00000	0.00000	0.00000	-0.00005	0.00060	0.03561	-0.00623	-0.75473	-0.07538
9	0.00000	0.00000	0.00000	0.0002	0.00022	-0.14434	-0.00103	-0.05958	-0.04658
10	0.00000	0.00000	0.00000	0.00000	0.00000	22.30000	0.00000	0.00000	0.00000
11	0.00000	0.00000	0.00000	0.00000	0.00000	-56.55000	0.00000	0.00000	0.00000
12	0.00000	0.00000	0.00000	0.00000	0.00000	153.7300	0.00000	0.00000	0.00000
13	0.00000	0.00000	0.00000	0.00000	0.00000	0.00000	0.00000	-106.40000	0.00000
14	0.00000	0.00000	0.00000	0.00000	0.00000	0.00000	0.00000	0.00000	-105.26000
15	0.00000	0.00000	0.00000	0.00000	0.00000	0.00000	0.00000	0.00000	1107.00000
16	0.00000	0.00000	0.00000	0.00000	0.00000	0.00000	0.00000	1.57540	0.00000
17	0.00000	0.00000	0.00000	0.00000	0.00000	0.00000	0.00000	0.00000	0.00000

	10	11	12	13	14	15	16	17
1	0.00000	0.00000	0.00000	0.00000	0.00000	0.00000	0.00000	0.00000
2	0.00000	0.00000	0.00000	0.00000	0.00000	0.00000	0.00000	0.00000
3	0.00000	0.00000	0.00000	0.00000	0.00000	0.00000	0.00000	0.00000
4	-0.10910	0.00000	0.00000	0.00012	0.00007	0.00000	0.00007	0.00007
5	-0.03148	0.00000	0.00000	-0.00110	0.00005	0.00000	0.00005	0.00005
6	-0.31958	0.00000	0.00000	0.00000	0.00021	0.00000	0.00021	0.00021
7	*-0.01113*	*0.00000*	*0.00000*	*1.15720*	*-0.05506*	*0.00000*	*-0.05506*	*-0.05506*
8	0.00538	0.00000	0.00000	0.43174	-0.06077	0.00000	-0.06077	-0.06077
9	-0.04252	0.00000	0.00000	0.04229	0.19881	0.00000	0.19881	0.19881
10	0.00000	1.00000	0.00000	0.00000	0.00000	0.00000	0.00000	0.00000
11	0.00000	0.00000	1.00000	0.00000	0.00000	0.00000	0.00000	0.00000
12	-0.03640	-0.81790	-3.04100	0.00000	0.00000	0.00000	0.00000	0.00000
13	0.00000	0.00000	0.00000	-21.28000	0.00000	0.00000	0.00000	0.00000
14	0.00000	0.00000	0.00000	0.00000	0.00000	1.00000	0.00000	0.00000
15	0.00000	0.00000	0.00000	0.00000	-6.38700	-10.82900	0.00000	0.00000
16	0.00000	0.00000	0.00000	0.00000	0.00000	0.00000	-0.24350	0.00000
17	0.00000	0.00000	0.00000	0.00000	0.00000	0.00000	0.00000	-5.75000

Table A.8

G-Matrix (6 DOF Quasi-Static Model with CH-47 Production SAS)

	1	2	3	4
1	0.00000	0.00000	0.00000	0.00000
2	0.00000	0.00000	0.00000	0.00000
3	0.00000	0.00000	0.00000	0.00000
4	0.93711	-0.10910	0.00012	0.00007
5	-8.05100	-0.03148	-0.00110	0.00005
6	0.01764	-0.31958	0.00000	0.00021
7	0.05696	-0.01113	1.15720	-0.05506
8	-0.01442	0.00538	0.43174	-0.06077
9	-0.00059	-0.04252	0.04229	0.19881
10	0.00000	0.00000	0.00000	0.00000
11	0.00000	0.00000	0.00000	0.00000
12	0.00000	0.00000	0.00000	0.00000
13	0.00000	0.00000	0.00000	0.00000
14	0.00000	0.00000	0.00000	0.00000
15	0.00000	0.00000	0.00000	0.00000
16	0.00000	0.00000	0.00000	0.00000
17	0.00000	0.00000	0.00000	0.00000

APPENDIX B

DERIVATIVE MODELS FROM REF. 1 (HOVER)

The linear models employed in this report at the hover condition were supplied by LRC. Details of the simulation procedure employed using these models are presented in the second chapter. The numerical values of the state variable representations for the 6 DOF quasi-static models are presented in this appendix for both the SAS-off and SAS-on models. The following two models are presented:

- 6 DOF quasi-static model (SAS-off)
- 6 DOF quasi-static model (with CH-47 production SAS)

The state variable form used is shown in Eq. (B.1).

$$\dot{x} = Fx + Gu \ . \tag{B.1}$$

B.1 6 DOF QUASI-STATIC MODEL (SAS-OFF)

The state vector definition is shown in Eq. (B.2) and the control vector is shown in Eq. (B.3).

$$x^T = [\theta \quad \phi \quad \psi \quad u \quad w \quad q \quad v \quad p \quad r] \tag{B.2}$$

$$u^T = [\delta_{COLL} \quad \delta_{LONG} \quad \delta_{LAT} \quad \delta_{RUD}] \tag{B.3}$$

The F-matrix of stability derivatives is shown in Table B.1 and the G-matrix of control derivatives is shown in Table B.2.

Table B.1

F-Matrix (6 DOF Quasi-Static Model, SAS-Off)

	1	2	3	4	5	6	7	8	9
1	0.00000	0.00000	0.00000	0.00000	0.00000	1.00000	0.00000	0.00000	0.00000
2	0.00000	0.00000	0.00000	0.00000	0.00000	0.00000	0.00000	1.00000	0.11590
3	0.00000	0.00000	0.00000	0.00000	0.00000	0.00000	0.00000	0.00000	1.00670
4	-32.20000	0.00000	0.00000	-0.01857	0.02894	-5.76930	-0.00127	-0.02869	-0.08620
5	-3.70650	0.00000	0.00000	0.02097	-0.25982	0.40010	0.00975	0.35800	0.43277
6	0.00000	0.00000	0.00000	0.01356	0.00285	-1.34220	0.00027	0.08761	0.01388
7	-3.70650	31.98500	0.00000	-0.00001	0.00244	0.00500	-0.13179	-10.10900	-0.18117
8	0.00000	0.00000	0.00000	-0.00005	0.00060	0.03561	-0.00623	-0.75473	-0.07538
9	0.00000	0.00000	0.00000	0.00022	0.00022	-0.14434	-0.00103	-0.05985	-0.04658

Table B.2

G-Matrix (6 DOF Quasi-Static Model, SAS-Off)

	1	2	3	4
1	0.00000	0.00000	0.00000	0.00000
2	0.00000	0.00000	0.00000	0.00000
3	0.00000	0.00000	0.00000	0.00000
4	0.93710	-0.10910	0.00012	0.00007
5	-8.05100	-0.03148	-0.00110	0.00005
6	0.01764	-0.31958	0.00000	0.00021
7	0.05696	-0.01113	1.15720	-0.05506
8	-0.01442	0.00538	0.43174	-0.06077
9	-0.00059	-0.04252	0.04229	0.19881

B.2 6 DOF QUASI-STATIC MODEL (WITH CH-47 PRODUCTION SAS)

The state vector definition for the 6 DOF quasi-static model with SAS is shown in Eq. (B.4) and the control vector is shown in Eq. (B.5). The development of this model is presented in the second chapter.

$$X^T = [\theta \quad \phi \quad \psi \quad u \quad w \quad q \quad v \quad p \quad r \quad v_1 \quad v_2 \quad v_3 \quad v_4 \quad v_5 \quad v_6 \quad v_7 \quad v_8] \tag{B.4}$$

$$u^T = [\delta_{COLL} \quad \delta_{LONG} \quad \delta_{LAT} \quad \delta_{RUD}] \tag{B.5}$$

The F-matrix of stability derivatives is shown in Table B.3 and the G-matrix of control derivatives is shown in Table B.4.

The F-matrix presented in Table B.3 includes the CH-47 production SAS. The recommended SAS modifications (discussed in the second chapter) is to divide the roll rate feedback gain by a factor of two. This change modifies the F-matrix element occurring in the 13th row and 8th column ($F_{13,8}$) from a value of -106.4 to -53.2.

The 3 DOF models discussed in this report are generated from the F- and G-matrices shown above by setting to zero all cross-coupled derivatives, thus yielding a 3 DOF longitudinal model and a 3 DOF lateral model with the corresponding SAS.

Table B.3

F-Matrix (6 DOF Quasi-Static Model with CH-47 Production SAS)

	1	2	3	4	5	6	7	8	9
1	0.00000	0.00000	0.00000	0.00000	0.00000	1.00000	0.00000	0.00000	0.00000
2	0.00000	0.00000	0.00000	0.00000	0.00000	0.00000	0.00000	1.00000	0.00000
3	0.00000	0.00000	0.00000	0.00000	0.00000	0.00000	0.00000	0.00000	1.00000
4	-32.06200	0.00000	-0.06927	-0.01141	0.06069	-12.84100	0.00855	0.13540	-0.41191
5	-2.67600	0.06927	0.00000	-0.12440	-0.65657	69.67300	-0.04391	-0.10234	-0.45820
6	0.00000	0.00000	0.00000	0.00215	0.00370	-1.32970	0.00157	0.13047	-0.16296
7	0.00000	32.06200	2.67600	0.00066	0.00082	-0.39200	-0.04274	12.54700	-68.16100
8	0.00000	0.00000	0.00000	0.00025	0.00143	-0.32130	-0.00731	-0.83710	-0.07788
9	0.00000	0.00000	0.00000	0.00040	0.00226	0.03140	-0.00189	-0.10754	-0.05625
10	0.00000	0.00000	0.00000	0.00000	0.00000	22.30000	0.00000	0.00000	0.00000
11	0.00000	0.00000	0.00000	0.00000	0.00000	-56.55000	0.00000	0.00000	0.00000
12	0.00000	0.00000	0.00000	0.00000	0.00000	153.73000	0.00000	0.00000	0.00000
13	0.00000	0.00000	0.00000	0.00000	0.00000	0.00000	0.00000	-106.40000	0.00000
14	0.00000	0.00000	0.00000	0.00000	0.00000	0.00000	0.00000	0.00000	-105.26000
15	0.00000	0.00000	0.00000	0.00000	0.00000	0.00000	0.00000	0.00000	1107.00000
16	0.00000	0.00000	0.00000	0.00000	0.00000	0.00000	0.00000	1.57540	0.00000
17	0.00000	0.00000	0.00000	0.00000	0.00000	0.00000	0.18740	0.00000	0.00000

	10	11	12	13	14	15	16	17
1	0.00000	0.00000	0.00000	0.00000	0.00000	0.00000	0.00000	0.00000
2	0.00000	0.00000	0.00000	0.00000	0.00000	0.00000	0.00000	0.00000
3	0.00000	0.00000	0.00000	0.00000	0.00000	0.00000	0.00000	0.00000
4	0.24571	0.00000	0.00000	-0.00052	-0.02440	0.00000	-0.02440	-0.02440
5	0.71150	0.00000	0.00000	-0.00061	0.05546	0.00000	0.05546	0.05546
6	-0.39600	0.00000	0.00000	-0.00332	0.00225	0.00000	0.00225	0.00225
7	-0.09048	0.00000	0.00000	1.08590	-0.05503	0.00000	-0.05503	-0.05503
8	-0.06444	0.00000	0.00000	0.56090	-0.05880	0.00000	-0.05880	-0.05880
9	-0.02651	0.00000	0.00000	0.05345	0.18808	0.00000	0.18808	0.18808
10	0.00000	1.00000	0.00000	0.00000	0.00000	0.00000	0.00000	0.00000
11	0.00000	0.00000	1.00000	0.00000	0.00000	0.00000	0.00000	0.00000
12	-0.03640	-0.81790	-3.04100	0.00000	0.00000	0.00000	0.00000	0.00000
13	0.00000	0.00000	0.00000	-21.28000	0.00000	0.00000	0.00000	0.00000
14	0.00000	0.00000	0.00000	0.00000	0.00000	1.00000	0.00000	0.00000
15	0.00000	0.00000	0.00000	0.00000	-3.18900	-10.51700	0.00000	0.00000
16	0.00000	0.00000	0.00000	0.00000	0.00000	0.00000	-0.24350	0.00000
17	0.00000	0.00000	0.00000	0.00000	0.00000	0.00000	0.00000	-5.75000

Table B.4

G-Matrix (6 DOF Quasi-Static Model with CH-47 Production SAS)

	1	2	3	4
1	0.00000	0.00000	0.00000	0.00000
2	0.00000	0.00000	0.00000	0.00000
3	0.00000	0.00000	0.00000	0.00000
4	0.79662	0.24571	-0.00052	-0.02440
5	-11.27000	0.71150	-0.00061	0.05546
6	0.05303	-0.39600	-0.00332	0.00225
7	0.00407	-0.09048	1.08590	-0.05503
8	-0.02129	-0.06444	0.56090	-0.05880
9	0.03689	-0.02651	0.05345	0.18808
10	0.00000	0.00000	0.00000	0.00000
11	0.00000	0.00000	0.00000	0.00000
12	0.00000	0.00000	0.00000	0.00000
13	0.00000	0.00000	0.00000	0.00000
14	0.00000	0.00000	0.00000	0.00000
15	0.00000	0.00000	0.00000	0.00000
16	0.00000	0.00000	0.00000	0.00000
17	0.00000	0.00000	0.00000	0.00000

APPENDIX C

NONLINEAR SIMULATION MODEL

The nonlinear simulation model was derived by representing the fixed operating point linear derivative model by nonlinear polynomials. The polynomials were developed from tabular derivative data as a function of airspeed and descent rate, obtained from Ref. 1 (for the hover condition and from LRC (for the 60 kt spiral descent condition). The structure of the polynomials used in the curve fit are

$$f_i = k_1 + k_2 x_4 + k_3 x_4^2 + k_4 x_5 + k_5 x_5^2 + k_6 x_4 x_5 + k_7 x_4 x_5^2 + k_8 x_4^2 x_5 + k_9 x_4^2 x_5^2 \qquad \text{(C.1)}$$

where $x_4 = u$ and $x_5 = w$. The nonlinear simulation model (with SAS-off) is shown in Eq. (C.2).

Tables C.1 and C.2 present the numerical values of the polynomial coefficients for the hover and 60 kt spiral descent conditions, respectively.

$$
\begin{bmatrix} \dot{\theta} \\ \dot{\varphi} \\ \dot{\psi} \\ \dot{u} \\ \dot{w} \\ \dot{q} \\ \dot{v} \\ \dot{p} \\ \dot{r} \end{bmatrix} =
\begin{bmatrix}
0 & 0 & 0 & 0 & 0 & \cos\varphi_o & 0 & 0 & -\sin\varphi_o \\
0 & 0 & 0 & 0 & 0 & \sin\varphi_o \tan\theta_o & 0 & 1.0 & \cos\varphi_o \tan\theta_o \\
0 & 0 & 0 & 0 & 0 & \sin\varphi_o \sec\theta_o & 0 & 0 & \cos\varphi_o \sec\theta_o \\
-g\cos\theta_o & 0 & 0 & f_1 & f_3 & f_9 - w_o & f_2 + r_o & f_8 & f_{10} + v_o \\
-g\sin\theta_o & 0 & 0 & f_{21} & f_{23} & f_{29} + u_o & f_{22} & f_{28} & f_{30} \\
0 & 0 & 0 & f_{41} & f_{43} & f_{49} & f_{42} & f_{48} & f_{50} \\
-g\sin\theta_o \sin\varphi_o & g\cos\theta_o \cos\varphi_o & 0 & f_{11} - r_o & f_{13} & f_{19} & f_{12} & f_{18} + w_o & f_{20} - u_o \\
0 & 0 & 0 & (I_1 f_{31} + I_3 f_{51}) & (I_1 f_{33} + I_3 f_{53}) & (I_1 f_{39} + I_3 f_{59}) & (I_1 f_{32} + I_3 f_{52}) & (I_1 f_{38} + I_3 f_{58}) & (I_1 f_{40} + I_3 f_{60}) \\
0 & 0 & 0 & (I_2 f_{31} + I_1 f_{51}) & (I_2 f_{33} + I_1 f_{53}) & (I_2 f_{39} + I_1 f_{59}) & (I_2 f_{32} + I_1 f_{52}) & (I_2 f_{38} + I_1 f_{58}) & (I_2 f_{40} + I_1 f_{60})
\end{bmatrix}
\begin{bmatrix} \theta \\ \varphi \\ \psi \\ u \\ w \\ q \\ v \\ p \\ r \end{bmatrix}
$$

$$
+
\begin{bmatrix}
0 & 0 & 0 & 0 \\
0 & 0 & 0 & 0 \\
0 & 0 & 0 & 0 \\
f_5 & -f_4 & f_6 & f_7 \\
f_{25} & -f_{24} & f_{26} & f_{27} \\
f_{45} & -f_{44} & f_{46} & f_{47} \\
f_{15} & -f_{14} & f_{16} & f_{17} \\
(I_1 f_{35} + I_3 f_{55}) & -(I_1 f_{34} + I_3 f_{54}) & (I_1 f_{36} + I_3 f_{56}) & (I_1 f_{37} + I_3 f_{57}) \\
(I_2 f_{35} + I_1 f_{55}) & -(I_2 f_{34} + I_1 f_{54}) & (I_2 f_{36} + I_1 f_{56}) & (I_2 f_{37} + I_1 f_{57})
\end{bmatrix}
\begin{bmatrix} \delta_{COLL} \\ \delta_{LONG} \\ \delta_{LAT} \\ \delta_{PED} \end{bmatrix}
\qquad (C.2)
$$

Table C.1

Polynomial Coefficients Used for the Hover Nonlinear Simulation Model

f_i

i	K1	K2	K3	K4	K5	K6	K7	K8	K9
1	-.18570000-01	.67362344-03	-.25370513-05	.15401417-07	.54724370-05	.55863689-05	-.99119720-07	-.69673121-07	-.21130391-08
2	-.12700000-02	-.12581609-08	.21223440-06	-.10020401-03	-.59764783-05	.13144398-05	.85264366-07	.11568166-07	.11358488-08
3	.28940000-01	-.94730569-05	.31285918-05	-.48361935-03	-.54724381-05	.65544361-05	.72474667-07	.11042518-07	.75723149-09
4	.10910000+00	-.36264060-03	.70546680-05	-.67562708-03	-.93607395-05	.71938941-06	.16519977-06	.20270936-06	.44487501-08
5	.93710000+00	-.75787447-02	.98677672-05	-.52022018-03	.85038846-04	-.92632298-05	-.12928241-06	.78533458-06	-.26913314-07
6	.12000000-01	.88809947-06	-.17527125-07	.13200528-04	-.14401151-06	.88813497-07	.17837550-15	-.10516696-08	-.63102720-10
7	.70000000-04	.74008288-06	-.13145344-07	.90003599-05	-.72005760-07	.53268098-07	.36674352-15	-.52583479-09	-.42602297-17
8	-.28690000-01	.10152457-02	.91272508-05	-.72818912-02	.16532523-03	.19915932-03	-.25366148-06	.22610902-06	.20129767-07
9	.25707200+01	.88143940-03	-.69150445-04	.26095055-02	-.10447969-03	.13866452-03	.47886574-05	-.91258732-06	.22748464-07
10	-.86720000+01	.27260915-02	.15818217-05	.45523821-02	.26807744-03	-.39719172-03	-.22914799-05	.20349807-06	-.56098308-07
11	-.10000000-04	.40408525-04	-.11830809-06	.21600864-04	-.17956287-13	.11812195-05	.70935357-07	-.70987701-08	-.15775676-09
12	-.13179000+00	.25044403-03	.13162871-04	.45061796-03	-.22681820-04	.67675881-05	.57553722-07	.25765905-07	.37230732-08
13	.24000000-02	.19242155-04	-.28003401-06	.42001700-05	.25202017-05	.68616906-06	-.21316098-08	.19981723-07	.16096432-08
14	.11130000-01	.11262581-02	-.65288522-06	.59402375-04	.18001442-05	.34859297-04	.54036322-06	-.30761330-07	-.47327255-09
15	.56960000-01	.23978683-04	.23661621-05	-.99903998-03	-.25274026-04	-.44406735-06	-.27710787-07	.80452724-07	.91498957-08
16	.11571700+01	.24748348+03	-.55385677-05	.82804585-04	.16705650-04	.10835316-05	-.14919880-07	-.16143067-06	.16562109-08
17	-.85600000-01	.58510953-03	-.15818228-05	.13980557-03	-.79206862-06	.15897610-05	.94056849-07	.13408811-07	.28395252-09
18	-.16049600+01	.47616917-03	-.95010164-04	.17099484-01	.12442587-03	.76644036-05	-.53183488-06	-.16266702-05	-.13788135-07
19	.50000000-02	-.22177323-02	.15292410-05	-.87603504-04	-.22897831-04	-.12272209-03	-.29821219-05	.18667132-06	.58685498-08
20	-.18117000+00	.13425104-03	-.98458622-05	.16974678-02	.36362893-04	.95010334-06	.13354538-05	-.19639926-06	-.76038805-08
21	.20970000-01	-.55430129-02	.33476806-05	-.52622107-03	-.74165896-05	.55437382-04	.88888005-06	.20507608-07	.15775740-08
22	.97500000-02	.84698046-04	-.89388334-06	.11352454-02	.49683976-04	.43518615-05	.13429140-06	-.12810369-06	-.47327255-07
23	-.25982000+00	.66341033-03	-.29121320-04	.47845915-02	.59332701-04	.36679959-05	.19930521-06	-.17957262-06	-.16695900-07
24	.31480000-01	.39865305-02	-.10954378-06	.13800552-03	-.28801855-06	-.63324055-05	-.15550083-05	.42055522-07	.14198128-08
25	-.80509599+01	.12884293-02	-.51521053-04	-.53708113-02	-.80178523-03	-.53553816-05	-.55953432-06	.74739522-05	.25935552-06
26	-.11000000+02	-.12729426-04	-.14898656-06	-.11400458-01	-.18721495-05	.10657618-06	.21316064-08	.84133565-08	-.18930797-09
27	.50000000-04	.28123149-05	.30672469-07	-.60002400-05	.14401152-06	.34637264-06	.31974130-08	.18404218-08	.31551368-10
28	.35000000+00	.21653049-03	-.42958984-04	.51237854-01	.15965837-02	.78866386-03	-.15656668-04	-.24887761-05	-.28673870-06
29	.40010000+00	-.15191385-01	.20107993-04	-.55356214-02	-.16071678-03	-.13583136-02	-.46319870-04	.87498935-06	.30075881-07
30	.43277000+00	.27872558-01	.43112354-04	-.45397819-02	-.15607968-02	.36505811-02	.20319565-04	.79664273-07	.20194466-06
31	-.14000000+01	.13321492-04	-.35054288-07	.21000840-04	-.50404031-06	-.66610122-06	-.22381898-07	-.60471000-08	-.15775673-09
32	-.58300000-02	.16261812-05	.12707163-06	.29401179-04	-.72006634-07	-.35525372-07	.10658054-07	.47325129-08	-.25241004-09
33	.52000000-03	.63647128-05	.19710016-06	.90003598-05	.50404033-06	.38189803-06	.11723851-07	.81504389-08	.94654168-10
34	-.22130000+01	.36648904-03	-.15511506-05	.21300853-03	-.28082289-05	.92898916-05	.14706105-06	.29972876-07	.40172330-09
35	-.18190000-01	-.53730019-04	.14591332-05	-.97803912-04	-.94327568-05	-.10657619-05	-.72474716-07	.74142710-07	.28396213-08
36	.41500000+00	-.85553531-04	-.13408222-05	-.15600815-04	.43204317-05	-.33749441-06	-.63949722-08	-.41540710-07	-.56795670-09
37	-.13905000+00	.17525162-03	-.19279740-06	.27001010-04	-.19441764-05	.53287921-06	.25579357-07	.21033443-07	.25241905-09
38	-.73128000+00	.25843696-03	-.23127043-04	-.41509657-02	.25057986-04	-.13410823-05	.47961456-07	-.39674302-06	-.36391276-08
39	.92400000-01	-.10859976-02	.79003519-05	-.93543745-03	-.50402073-06	.34681671-04	-.85797307-06	.18272759-06	.36707116-09
40	-.57040000-01	.88810615-06	-.26904142-05	.47041681-03	.13249054-04	.13854903-05	.31547819-06	-.43644288-07	-.15776631-08
41	.13560000-01	.11841325-04	.30760106-05	.62342494-03	.12745022-04	-.79932140-06	.27710946-07	-.17037088-06	-.41647796-08
42	.27000000-03	.19242155-04	.43817819-07	.15600624-04	.43203459-06	.39877260-05	.73540520-07	-.34179255-08	-.15775671-09
43	.28500000+02	.28966044-03	-.12863355-06	.78603143-04	.20881675-05	.90412140-05	.22595064-06	-.24714228-07	-.63102646-09
44	.31958000+00	-.26790952-04	.77338432-05	-.13518540-02	-.21545823-04	-.49735818-06	-.17052640-07	.27593731-06	.80557784-08
45	.17640000-01	-.48579040-03	.18403481-05	-.20760831-03	-.46083657-05	.80811400-04	-.25014435-05	.72302258-07	.17353234-08
46	.00000000	-.14801657+06	.43817814-08	.00000000	.00000000	-.17762700+07	.16838309+16	-.26994693-17	-.63102700-10
47	.21000000-03	.26642984-05	-.26290688-07	.22800912-04	-.28802303-06	-.35525399-07	.21316097-08	-.15775044-08	-.36368301-16
48	.10030000-01	.20447010-02	.74577920-05	-.35395416-02	.45291626-04	.22658100-03	-.66037252-05	.22505731-06	-.33570635-07
49	-.12085500+01	.71040255-04	-.80002572-04	.54698180-02	-.37846242-03	-.98582848-05	-.36237330-06	.67306719-07	.71621542-07
50	.10040000-01	.11027235-03	-.24976152-06	.39343574-02	.25943675-03	.11412535-04	.14100596-05	-.17431422-06	-.47989603-07
51	.23000000-03	.34043813-05	-.30672469-07	.27001080-04	-.79206331-06	.88813493-07	.21316101-08	.63100178-08	.25241079-09
52	-.55000000-03	.55210183-04	.43817774-08	.72002880-05	-.14401168-06	.17762704-06	-.63948434-08	-.10516699-08	-.63102650-10
53	.18000000-01	-.29603315-05	.17527126-07	-.54002161-05	-.72005720-07	-.35525399-06	-.10658047-07	.52583468-09	-.35489492-17
54	.42940000-01	.25162807-05	-.29489391-05	.38701552-03	.55444447-05	.44406790-06	.85264193-08	-.65203505-07	-.94653585-09
55	.52000000-03	.85849613-04	-.15774412-06	.21000840-04	.36002879-06	.11190500-05	.95922441-07	-.10516696-07	-.12620528-09
56	.96000000-02	.34635879-04	-.14898049-06	.90003624-05	.72007318-07	-.34637264-05	.43271669-06	-.10621863-06	.12620541-07
57	.20049000+00	.38168249-04	-.99151872-06	.15600657-04	.28802349-05	-.17762751-06	-.21316924-08	-.28395108-07	-.31549732-09
58	-.14000000-02	.20426267-03	-.12181352-05	-.23100924-03	.51124089-05	.50712509-05	-.25899055-06	-.27084491-07	.72568059-09
59	-.14700000+00	.32859709-04	.14135627-04	.15372615-02	-.90727599-05	.95918558-06	-.10657873-07	.38964358-06	.32813438-08
60	-.40080000-01	.16281423-04	.41188722-06	.72602920-04	-.48243942-05	-.10657024-05	-.14921230-07	-.15775029-07	-.82033195-09

Table C.2

Polynomial Coefficients Used for the 60 KT Spiral Descent Nonlinear Simulation Model

f_i

i	K1	K2	K3	K4	K5	K6	K7	K8	K9
1	-.19100000E-01	-.2256731E-03	.1849116E-05	.1314052E-03	-.6480553E-06	-.2531184E-05	-.1598707E-07	.4390720E-07	.4101706E-09
2	-.1990000E-02	-.1007992E-03	.6879196E-06	-.4280331E-04	.6480518E-05	-.1509829E-06	-.3016227E-06	-.1761546E-07	.5000102E-08
3	.3950000E-01	-.6210696E-04	-.2357398E-05	.1818072E-03	.3600374E-06	.4016302E-05	-.1005805E-07	-.1577505E-07	.6310252E-10
4	.1240200E+00	.6296105E-03	.9331199E-06	-.2250098E-03	.2952238E-05	.8126033E-05	.5222455E-07	-.4916555E-07	-.1041199E-08
5	.4711400E+00	-.3122750E-02	-.1001019E-04	.4300371E-02	.5112421E-05	.4900929E-04	.3346623E-06	-.1850936E-06	-.7887859E-08
6	-.4030000E-02	-.2457075E-04	.3680969E-06	-.2526101E-03	-.1800144E-05	-.2691049E-05	-.6075087E-07	.9202107E-08	-.3470646E-09
7	-.5270000E-02	-.3478389E-04	.1183680E-06	-.2262090E-03	-.2160173E-06	-.3934037E-05	-.2238190E-07	-.1446045E-07	-.3155146E-10
8	-.8190000E-02	-.1376559E-03	.1770259E-05	-.3444137E-03	-.1156012E-04	-.2586249E-04	-.3960530E-05	-.6473026E-06	.7032009E-07
9	.2290720E+01	-.3465511E-02	.1600171E-04	-.5129605E-02	-.7915856E-05	-.6406119E-04	.3655681E-06	.1012228E-06	-.6152585E-08
10	.1880000E+01	.9968237E-03	.1220764E-04	.2540501E-02	-.9706376E-04	-.7745425E-04	.5756410E-05	.1568828E-05	-.1167084E-06
11	-.1370000E-02	-.1213735E-04	.8298145E-06	-.1104044E-03	-.1152092E-05	-.9856298E-06	.2877672E-07	.7624604E-08	-.8101672E-09
12	-.6990000E-01	-.3115749E-03	-.4203473E-05	.3828153E-03	-.4176357E-05	-.2486777E-05	-.3623753E-07	-.1577512E-08	.6310294E-09
13	.2750000E-02	-.3285967E-04	-.2453797E-06	-.3600144E-04	-.1444114E-06	-.1829558E-05	-.4689540E-07	.2524007E-07	-.8203355E-09
14	.5360000E-01	-.5236820E-03	-.2681649E-05	.5550222E-03	-.1080080E-05	-.1940574E-04	-.3335968E-06	.1348706E-06	.4070120E-08
15	.2640000E-01	-.1913654E-03	-.3286314E-06	-.1599004E-02	.2311385E-04	-.3676878E-05	-.4050051E-07	-.1319845E-06	-.9465440E-09
16	.1090200E+01	-.5113970E-03	.5302011E-06	-.1394456E-02	-.4752630E-05	-.1675909E-04	-.5648810E-07	-.6125996E-07	-.2839981E-09
17	-.6080000E-01	-.5244227E-03	.5696281E-07	-.9558382E-03	-.1080092E-05	-.1409470E-04	-.1598709E-07	.2708050E-07	.7256849E-09
18	-.2243090E+01	-.3103611E-02	.7207153E-04	-.2936877E-01	-.9360933E-05	-.3042751E-04	-.8142813E-06	-.1199428E-05	.2877040E-07
19	.7870000E-02	.3055802E-02	-.7815083E-05	-.1927277E-02	-.5962076E-04	-.6778246E-04	-.1246992E-05	-.4590537E-06	-.1943562E-07
20	-.2379000E+00	-.2537004E-03	.8750798E-05	-.3090723E-02	-.1706537E-04	-.7771182E-05	.1333322E-05	.3525721E-06	-.2817536E-07
21	-.7401000E-01	-.1386543E-02	-.9845862E-05	-.1224048E-02	-.3168273E-05	-.3782566E-04	-.5169156E-06	-.1930615E-06	-.1202107E-07
22	-.1939000E-01	-.6583777E-03	-.4570579E-05	-.7656308E-03	-.5098008E-04	-.1920147E-04	-.1732998E-05	-.1956104E-06	-.3420166E-07
23	-.5395500E+00	-.3047661E-02	-.1305778E-04	-.1649406E-02	-.9288841E-05	-.3208851E-04	-.4156794E-07	-.4198793E-06	-.3502214E-08
24	-.5131200E+00	-.1309798E-02	-.8499051E-04	-.6394455E-02	-.4053924E-04	-.3676878E-04	-.1359965E-05	-.1996342E-06	-.1703773E-07
25	-.9183500E+01	-.2075177E-01	-.8545945E-04	-.2350654E-01	-.1242797E-03	-.1884711E-03	-.4419918E-05	-.7069843E-06	-.6414413E-07
26	-.4180000E-01	-.5158377E-03	-.1034482E-05	-.3054722E-02	-.2088164E-05	-.4612084E-04	-.1038837E-06	-.1706334E-06	-.3154281E-10
27	-.1796000E-01	-.5654233E-04	-.1594968E-05	-.1143645E-02	-.1526521E-04	-.1122602E-04	-.1087121E-06	-.6678102E-07	-.1640671E-08
28	-.2523100E+00	-.8525902E-02	-.2967703E-04	-.6138245E-02	-.4555084E-03	-.5099670E-04	-.2478635E-04	-.1850938E-06	-.3093770E-06
29	-.1308100E+01	-.5644615E-02	-.1198855E-03	-.2644005E-01	-.7466981E-04	-.2673463E-03	-.2451308E-05	-.3358507E-05	-.3293970E-07
30	-.1023200E+01	-.1426293E-01	-.1168401E-03	-.1767310E-01	-.5877110E-03	-.7675528E-03	-.2470001E-04	-.1150342E-04	-.4344303E-06
31	-.3590000E-01	-.1480166E-06	-.1095445E-06	-.1560002E-04	-.2080230E-06	-.8881349E-07	-.1278965E-07	-.1577504E-08	-.1262053E-09
32	-.5220000E-02	-.6806782E-05	-.1402169E-06	-.2760110E-04	-.1440109E-06	-.7016207E-06	-.9592291E-08	-.9727941E-08	-.9465417E-10
33	-.1860000E-02	-.1774198E-05	-.3505426E-07	-.3780151E-04	-.3600288E-06	-.5506436E-06	-.1705287E-07	-.5784103E-08	-.2524110E-09
34	-.9111999E-02	-.9129962E-04	-.1651931E-05	-.7080783E-03	-.1755521E-11	-.2335795E-05	-.8653016E-07	-.1288295E-07	-.7256783E-09
35	-.6550000E-02	-.6066679E-04	-.1516693E-05	-.3828153E-03	-.5472435E-05	-.8881348E-06	-.1838694E-07	-.7519437E-07	-.5670246E-09
36	-.3988400E+00	-.1111804E-03	-.1533015E-06	-.3324132E-03	-.8641063E-06	-.3810099E-05	-.1598700E-07	-.1498647E-07	-.1577658E-09
37	-.1346000E+00	-.9491520E-04	-.1752737E-07	-.1386054E-03	-.1656161E-05	-.2495659E-05	-.1172386E-07	-.1288291E-07	-.9466803E-10
38	-.8753300E+00	-.7069272E-03	-.1847130E-04	-.7818312E-02	-.1296079E-04	-.2675054E-04	-.2608700E-06	-.2618655E-06	-.7420666E-08
39	-.1952000E+01	-.1311827E-03	-.6768507E-05	-.2947317E-02	-.1771342E-04	-.1190989E-04	-.3954135E-06	-.9202105E-08	-.4574944E-08
40	-.7440000E-01	-.8906694E-04	-.6519525E-05	-.9430377E-03	-.9720775E-05	-.2673207E-05	-.5467578E-06	-.1033265E-06	-.1012708E-07
41	-.4990000E-02	-.3197154E-04	-.1498569E-05	-.1110044E-03	-.1080086E-05	-.2202574E-05	-.8313276E-07	-.5258349E-08	-.1577566E-08
42	-.5340000E-02	-.9635879E-04	-.6616489E-06	-.1752070E-03	-.9504754E-05	-.6172538E-05	-.3783606E-06	-.1101623E-06	-.7666977E-08
43	-.1856000E-01	-.4992125E-04	-.1007088E-05	-.1356055E-03	-.7200378E-07	-.4307454E-05	-.3303997E-07	-.5284619E-07	-.8618867E-09
44	-.3929000E+00	-.1006740E-02	-.4938271E-05	-.3426137E-03	-.9720089E-05	-.6714298E-05	-.1620026E-06	-.1919297E-06	-.6941583E-09
45	-.1650000E+00	-.1192421E-02	-.2276773E-04	-.1794671E-02	-.2066568E-04	-.4822574E-05	-.5147831E-06	-.5439760E-06	-.1987736E-08
46	-.3190000E-02	-.1494967E-04	-.1621259E-06	-.6300251E-04	-.6480525E-06	-.8970163E-06	-.5329020E-08	-.6572933E-08	-.3155144E-10
47	-.1026000E-01	-.1107164E-03	-.5959222E-06	-.7086203E-03	-.2068168E-05	-.9600739E-05	-.4796122E-07	-.1288295E-07	-.9465491E-10
48	-.4296000E-01	-.8346654E-03	-.8331673E-05	-.1484658E-02	-.6417472E-04	-.7378625E-04	-.6028190E-05	-.1372954E-05	-.1199582E-06
49	-.1700000E+01	-.2145029E-02	-.2056863E-04	-.3070922E-02	-.2736236E-04	-.9458038E-04	-.6799815E-06	-.1482848E-06	-.8613975E-08
50	-.5155000E-01	-.5294552E-03	-.1353470E-05	-.4740168E-04	-.1671253E-03	-.4957569E-04	-.1014859E-04	-.1397666E-05	-.2088699E-06
51	.3600000E-03	-.1480165E-05	-.8134493E-07	-.1260050E-04	-.3600288E-06	-.4480674E-07	-.5324022E-08	-.4495430E-08	-.3155137E-10
52	-.9000000E-04	-.1050917E-04	-.2190490E-07	-.1260050E-04	-.7200577E-07	-.2930845E-06	-.3197415E-08	-.7887520E-09	-.3155133E-10
53	-.6700000E-03	-.2510281E-05	-.1095445E-06	-.3960158E-04	-.4320346E-06	-.2220337E-06	-.5329022E-08	-.2366256E-08	-.9465403E-10
54	-.1989000E-01	-.2107756E-03	-.1691367E-05	-.9402376E-03	-.1080084E-05	-.5497555E-05	-.2451360E-07	-.4916555E-07	-.9788915E-09
55	-.1780000E-02	-.1006512E-04	-.1209371E-05	-.4758190E-03	-.7128570E-05	-.3916675E-05	-.2025029E-07	-.9701651E-07	-.1735324E-08
56	-.8480000E-02	-.3685012E-04	-.3067243E-07	-.6000240E-04	-.1440125E-06	-.1030236E-05	-.2131628E-08	-.1051669E-08	-.6311022E-10
57	-.1935000E+00	-.8718171E-04	-.5696236E-07	-.1962078E-03	-.2520201E-05	-.2131525E-05	-.1705254E-07	-.1156832E-07	-.9212647E-10
58	-.8930000E-02	-.1184132E-04	-.1402169E-06	-.6552202E-03	-.3024243E-05	-.2939726E-05	-.4796123E-07	-.3707135E-07	-.5363731E-09
59	-.4302000E-01	-.8767021E-03	-.7862021E-05	-.4066962E-02	-.7304586E-05	-.1618181E-04	-.1278935E-07	-.2406108E-06	-.2776511E-08
60	-.3395000E-01	-.3041207E-04	-.7010051E-06	-.3720148E-03	-.6336505E-05	-.5595252E-06	-.1524099E-06	-.2077046E-07	-.7256792E-09

APPENDIX D

NONLINEAR DERIVATIVE MODEL

Input design studies were based on linear derivative models for simulation of the CH-47. The evaluation of derivative nonlinearity was limited to a qualitative assessment of the importance of nonlinearity on derivative identification accuracy. This qualitative assessment was based upon examination of the primary speed dependent derivatives and the nature of their variations about the trim condition. The specific conclusions reached, based upon this qualitative assessment, are that: (1) for airspeeds of 20 kts and below, longitudinal maneuvers should be designed to independently excite airspeed while holding descent rate near its trim value, and the reverse procedure (constant airspeed, variable descent rate); and (2) for airspeed of 40 kts and above, nonlinearity is not significant and both u and w can be excited during one maneuver. The present discussion is aimed at validating this assumption and quantifying the resulting derivative identification accuracy using a nonlinear simulation model.

The nonlinear simulation model used throughout this analysis is derived from linear derivatives obtained at various trim speeds and descent rates from the LRC CH-47 nonlinear simulation program HELICOP Ref. [1]. A polynomial is selected to represent the variation in the derivative values as a function of u and w and a least square curve fit is used to determine the coefficients of the polynomial. Equation (D.1) shows the polynomial form selected for representing the derivative variation with u and w. This is a second-order polynomial with all possible cross terms between u and w. This model was selected based upon examination of the variation in the derivatives with u and w and is valid for airspeed changes of ± 20 kts and vertical speed changes of ± 500 FPM.

$$f_i = k_1 + k_2 u + k_3 u^2 + k_4 w + k_5 w^2 + k_6 uw$$
$$+ k_7 uw^2 + k_8 u^2 w + k_9 u^2 w^2 \qquad (D.1)$$

where $i = 1,2,3,\ldots,60$ represents a different set of coefficients k_i for each stability derivative, and u and w are deviations from a reference trim (values for K_j's may be found in Appendix C).

As an example, Figure 2.5 shows the derivatives M_u and M_w as a function of airspeed and descent rate. The polynomial of Eq. (D.1) for M_u at the hover condition is derived by selecting nine numerical values of the derivative M_u corresponding to the nine values of (u,w) coordinates (see Figure 2.5). This establishes nine equations of the form of Eq. (D.1) in nine unknowns (the K's). The equations are solved for the unknown K's and the resulting polynomial fit passes uniquely through the nine points used in the fit.

The structure of the nonlinear simulation used throughout this analysis is shown in Eq. (D.2).

$$\begin{bmatrix} \dot{\underline{x}} \\ \dot{\underline{v}} \end{bmatrix} = \begin{bmatrix} F(u,w) & G(u,w) \\ B_c K_c & A_c \end{bmatrix} \begin{bmatrix} \underline{x} \\ \underline{v} \end{bmatrix} + \begin{bmatrix} G(u,w) \\ 0 \end{bmatrix} \begin{bmatrix} \underline{u} \end{bmatrix} \qquad (D.2)$$

where the $\underline{x}$ vector represents the rigid body state and the $\underline{v}$ vector represents the SAS state variables previously defined. The F and G matrices are nonlinear polynomial functions of the state variables u and w. An alternate way of viewing Eq. (D.2) is to consider the F and G matrices as functions of time, since both u and w are, in fact, time functions. The computer simulation allows monitoring the time variation of F and G along with the time history response of the state variables.

The full nonlinear model used at LRC from which the polynomial representation was derived is more accurate since the external force-moment components are nonlinear with the other state variables v, q, p, r, and control inputs. However, over the $\pm$20 kt airspeed about a reference trim, the significant nonlinearity is due to u and w and thus Eq. (D.2) provides an accurate representation of the Ref. 1 simulation data.

To further the understanding of the nonlinear polynomial simulation, a time history simulation is presented and discussed. It was previously found that changes in w must be kept small in order to identify the linear derivative M_u; otherwise, nonlinearity would be significant. Thus, at hover a longitudinal input δ_{LONG} was used to excite u, q, and θ states while w remained near its trim value. This maneuver is repeated here using the nonlinear simulation and is shown in Figure D.1. The linear simulation is also shown by the solid line superimposed upon the nonlinear response. The nonlinear time response of u, q, and θ shows excellent comparion to that of the linear model except near the end of the data record where $t > 13$ sec. Also, it is seen that w shows much larger discrepancy between linear and nonlinear response indicating the possibility of nonlinearity in the Z-force equation. Although the response comparison of Figure D.1 gives a quantitative measure of the degree of nonlinearity, it provides little information as to the actual variation in the derivatives.

The variation with time of the stability and control derivatives are an output from the nonlinear C-81 simulation. Figure D.2 shows this variation for the longitudinal stability and control derivatives for this maneuver. This figure permits immediate interpretation of the nonlinear behavior of the system. It is emphasized that at this condition (hover), the δ_{LONG} input was chosen to retain linearity in the important derivative

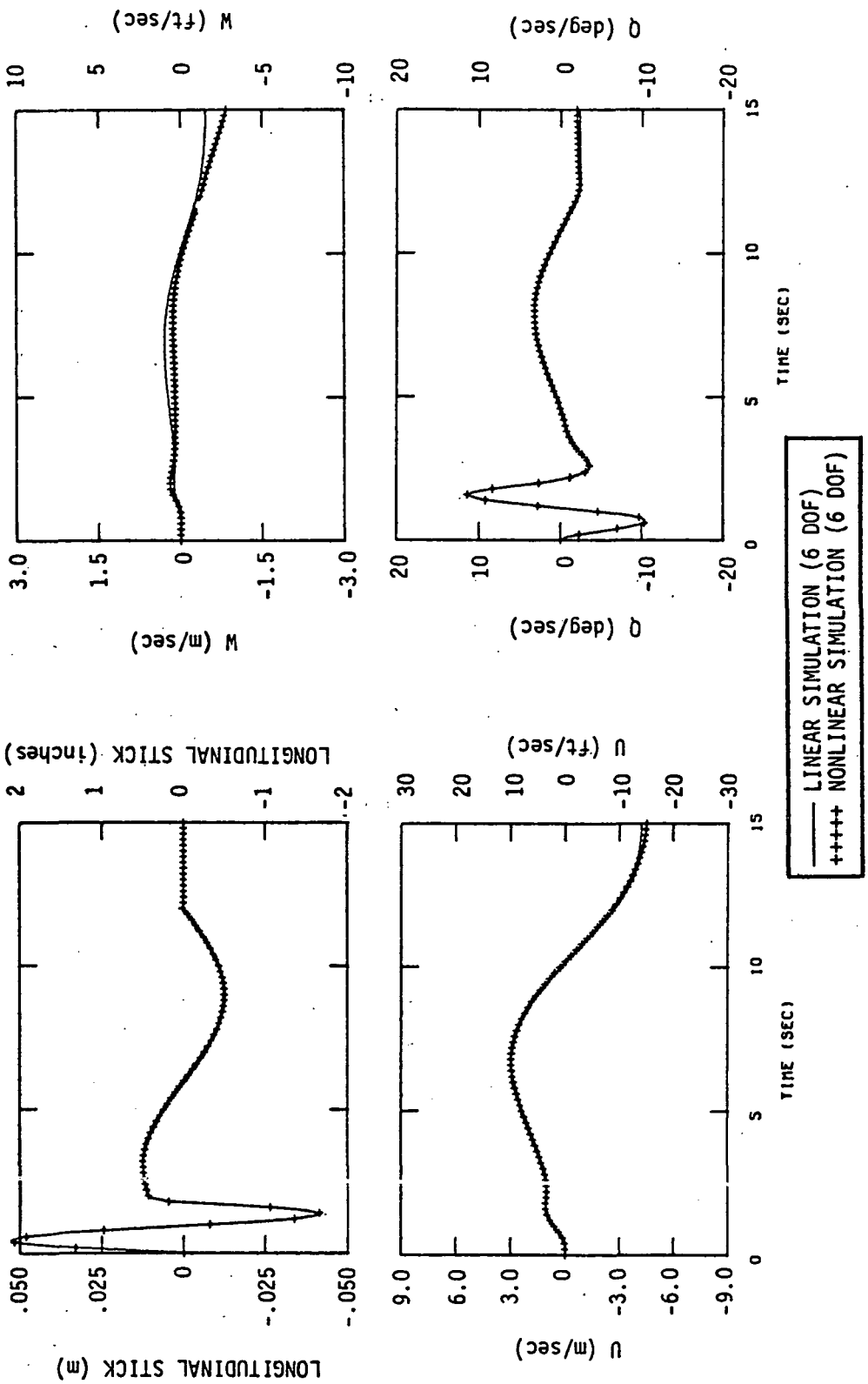

Figure D.1 Time History Comparison of the 6 DOF Nonlinear and Linear Simulation for the δ_{LONG} Input Maneuver (Hover, SAS-On)

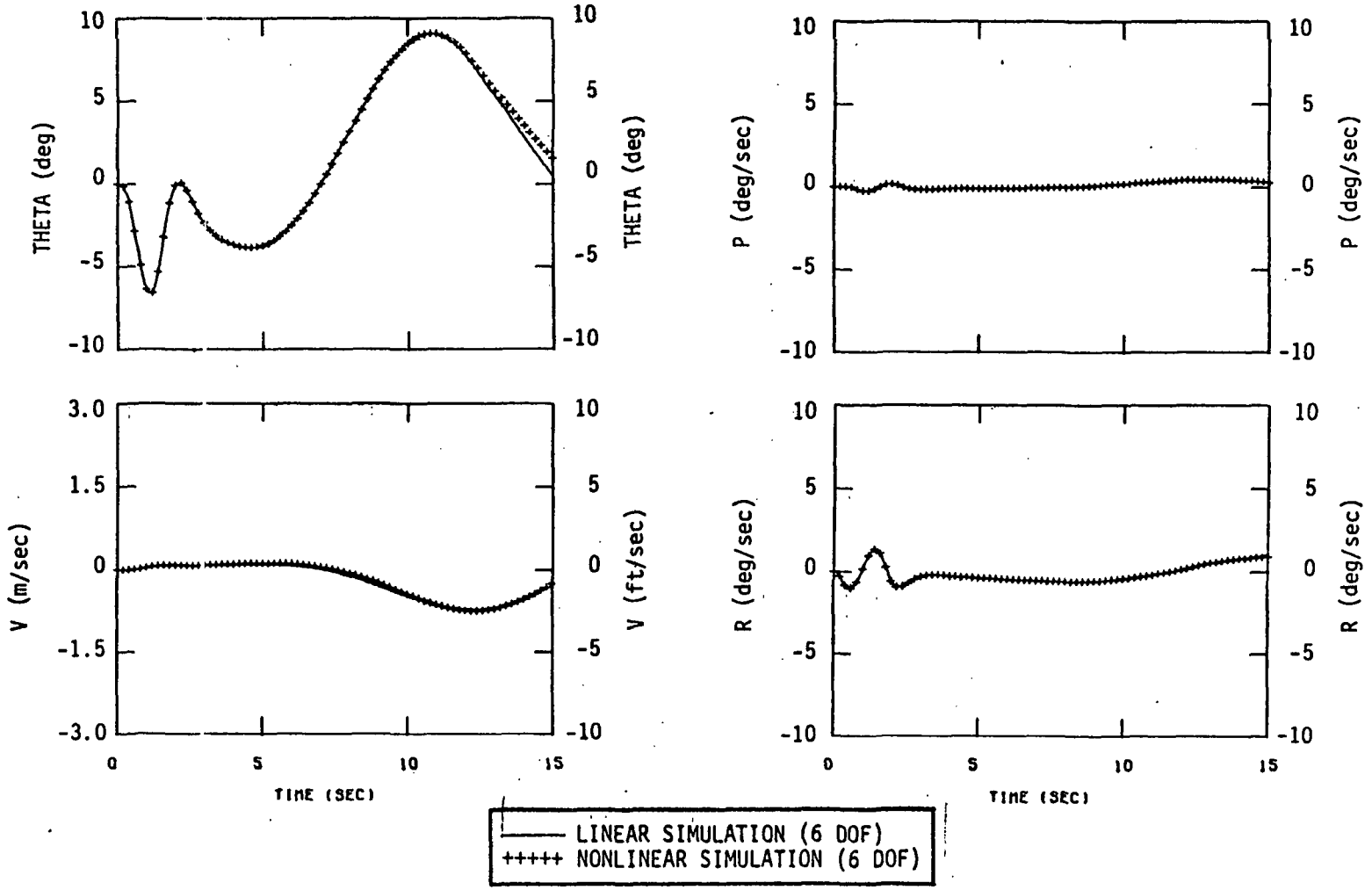

Figure D.1 (Concluded)

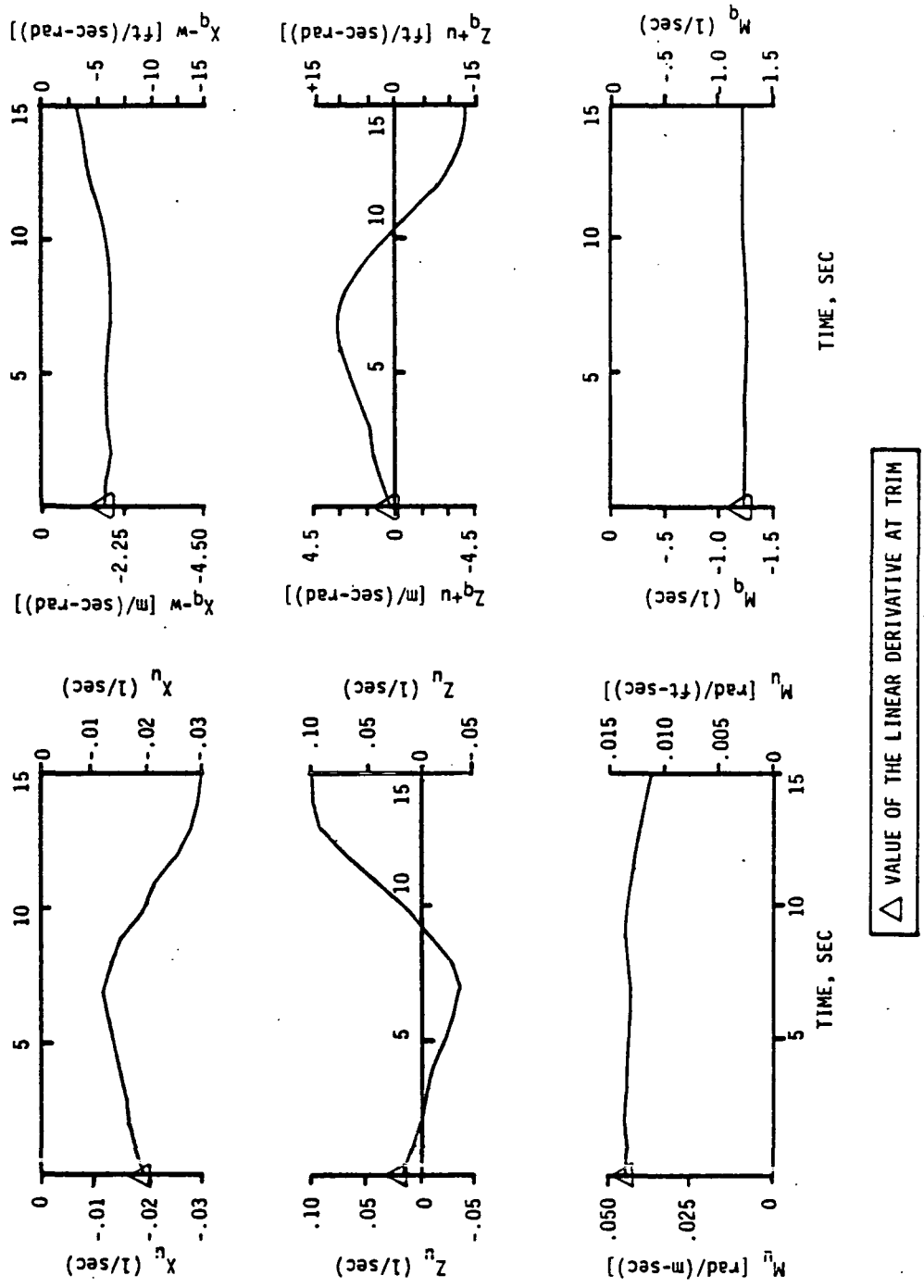

Figure D.2 Time Variation of Longitudinal Derivatives for the δ_{LONG} Input Maneuver (Nonlinear Simulation, Hover)

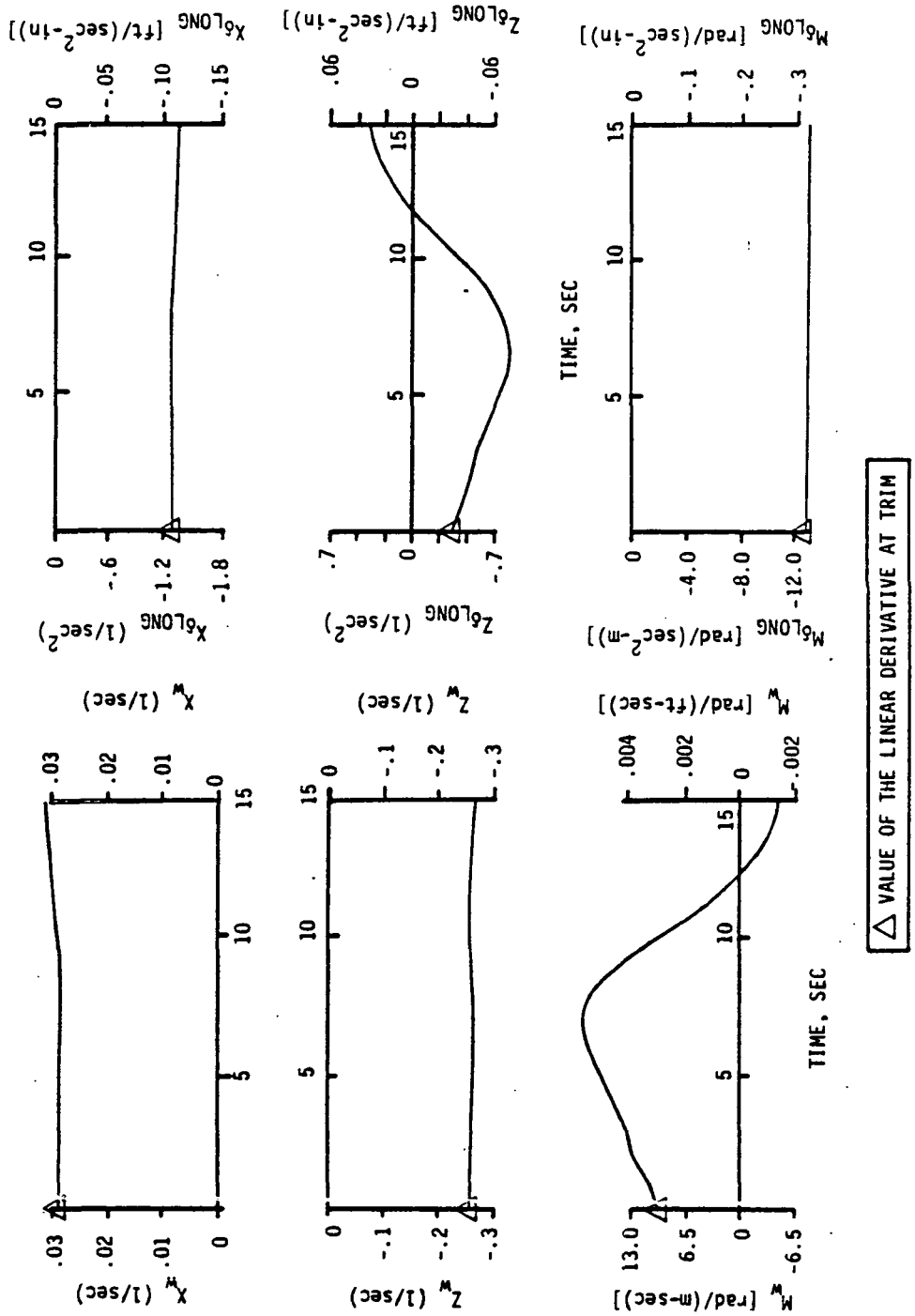

Figure D.2 (Concluded)

M_u. M_w is highly nonlinear with u and its effect in the response is not significant since w is maintained near trim. The derivatives M_u, M_q and $M_{\delta_{LONG}}$ are nearly constant and equal to their trim value. The derivatives X_u, Z_u and $Z_{\delta_{LONG}}$ are significantly nonlinear. The source of nonlinearity is mainly attributed to large excursions in u.

The problem of trying to identify stability derivatives for a linear model when the derivatives are a function of time can sometimes be approached by reducing the data sample period. To illustrate this point, a second derivative identification run was made in which the data length was reduced to 12 sec thereby keeping airspeed constant. The original data length used was 15 sec and a reduction to 12 sec resulted in a 10 ft/sec maximum value for u. This improved identification accuracy considerably. The results are shown in Table D.1.

Table D.1

The Effect of Nonlinearity on Identification Results Using the Nonlinear Simulation for the δ_{LONG} Input Maneuver (Hover)

PARAMETER	TRUE PARAMETER VALUE	IDENTIFIED PARAMETER VALUE USING:		
		LINEAR SIMULATION (15 SEC)	NONLINEAR SIMULATION (15 SEC)	NONLINEAR SIMULATION (12 SEC)*
X_u	-.01857	-.0158	.00448	-.01905
M_u	.04449	.04968	.004619	.04944
Z_w	-.2598	-.0692	-.7056	-.2046
M_q	-1.3422	-1.522	-1.424	-1.476
$X_{\delta_{LONG}}$	-1.3092	-1.1160	-.5988	-1.11588
$Z_{\delta_{LONG}}$	-.37776	-.5352	-.5976	-.54036
$M_{\delta_{LONG}}$	-12.58189	-12.1535	-12.9606	-12.3071

*Reduction of data length to 12 sec removed major nonlinearity due to u.

Figure D.3 shows the time history match of the identified derivative model and the 6 DOF nonlinear simulation using only 12 sec of data in the identification. The simulation data contains random noise, bias, and scale factor errors as previously employed in the last chapter. The reduction of data length to 12 sec completely eliminated degradation in identified derivatives due to nonlinearity as shown in Table D.1 and Figure D.3.

The results just presented demonstrate that accurate linear derivatives can be identified from a nonlinear simulation with noise contamination in the form of random errors, bias, and scale factor errors representative of flight test data.

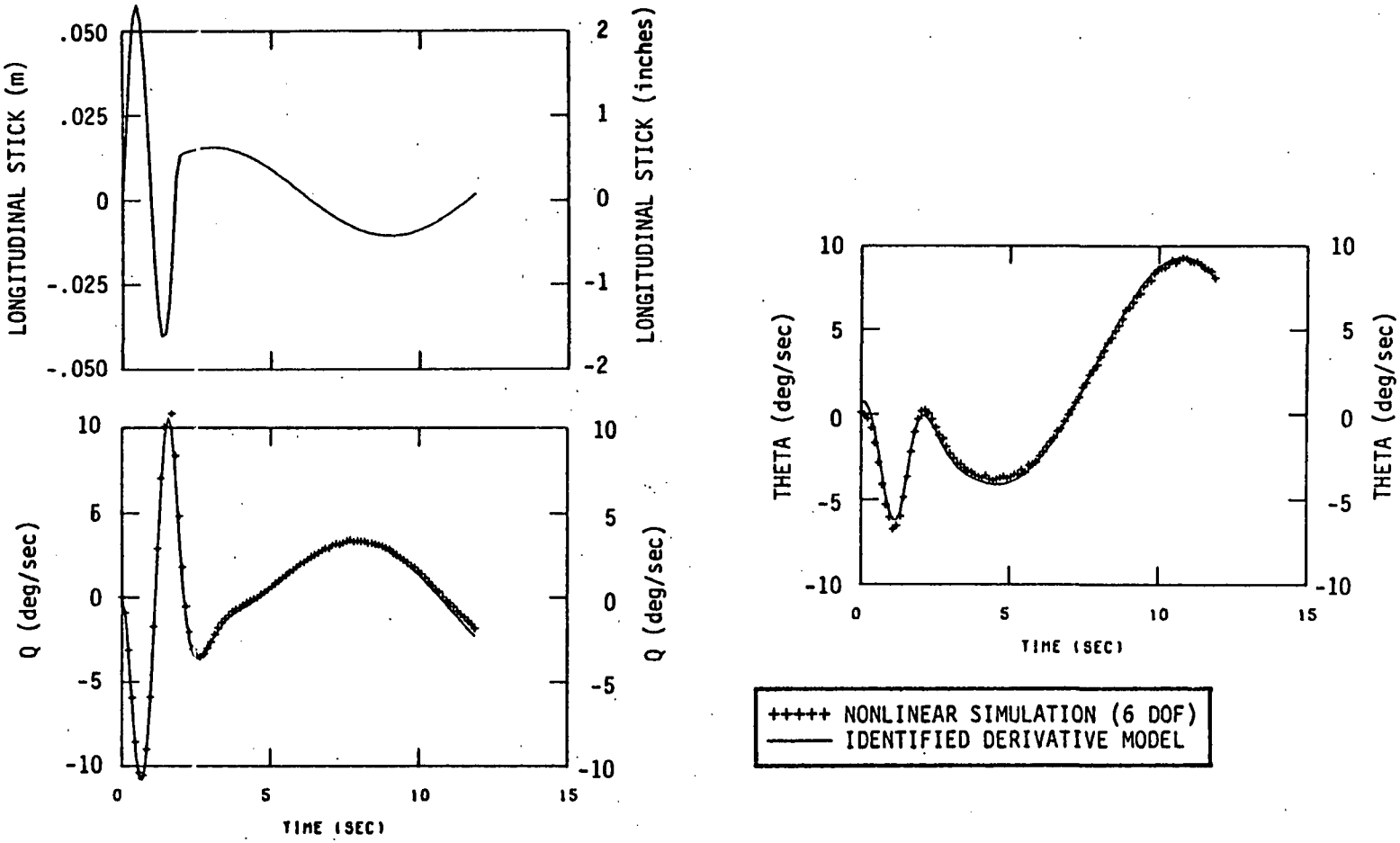

Figure D.3 Longitudinal Time History Match of Identified Derivative Model and 6 DOF Nonlinear Noise Contaminated Simulation Data Using 12 Sec of Data (Hover, δ_{LONG} Input, Random Noise, Bias, and Scale Factor Errors)

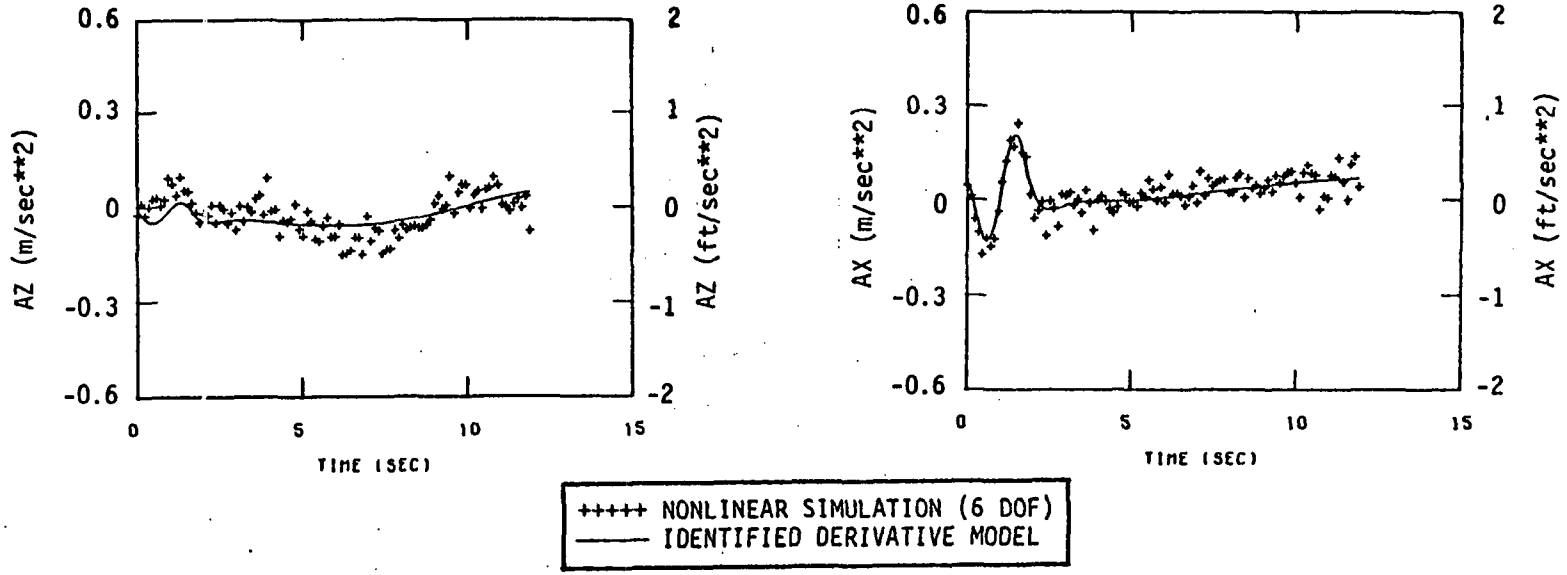

Figure D.3 (Concluded)

NASA Contractor Report 158948
Distribution List
NAS1-14010

	No. of Copies
NASA Langley Research Center Hampton, VA 23665 Attn: Report & Manuscript Control Office, Mail Stop 180A Ward F. Hodge, Mail Stop 494	1 25
NASA Ames Research Center Moffett Field, CA 94035 Attn: Library, Mail Stop 202-3	1
NASA Dryden Flight Research Center P. O. Box 273 Edwards, CA 93523 Attn: Library	1
NASA Goddard Space Flight Center Greenbelt, MD 20771 Attn: Library	1
NASA Lyndon B. Johnson Space Center 2101 Webster Seabrook Road Houston, TX 77058 Attn: JM6/Library	1
NASA Marshall Space Flight Center Marshall Space Flight Center, AL 35812 Attn: Library, AS61L	1
Jet Propulsion Laboratory 4800 Oak Grove Drive Pasadena, CA 91103 Attn: Library, Mail 111-113	1
NASA Lewis Research Center 21000 Brookpark Road Cleveland, OH 44135 Attn: Library, Mail Stop 60-3	1
NASA John F. Kennedy Space Center Kennedy Space Center, FL 32899 Attn: Library, NWSI-D	1
National Aeronautics and Space Administration Washington, DC 20546 Attn: RE-4	1

	No. of Copies
NASA Scientific and Technical Information Facility 6571 Elkridge Landing Road Linthicum Heights, MD 21090	30 plus original